Jacek F. Gieras
Izabella A. Gieras

ELECTRICAL ENERGY UTILISATION

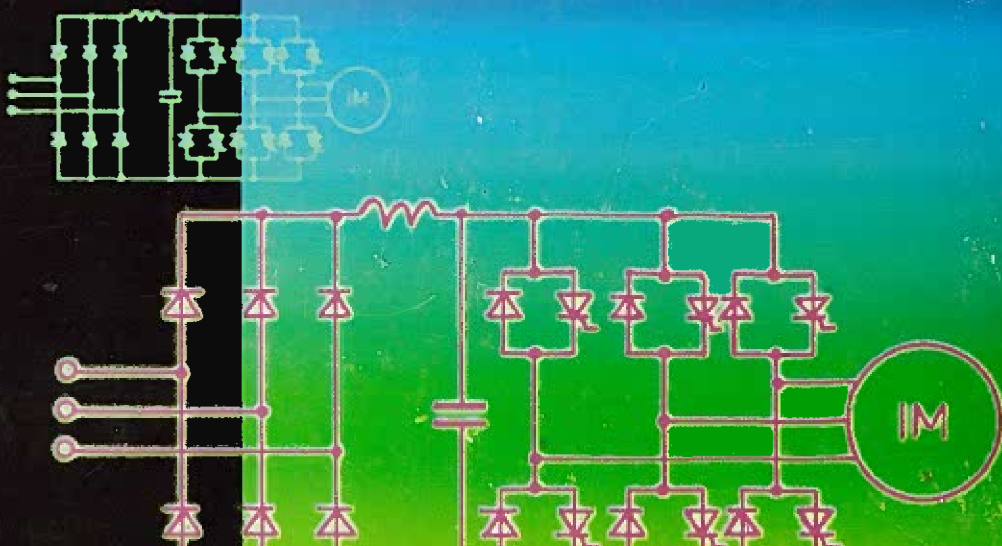

wydawnictwo
adam marszałek

Jacek F. Gieras
Izabella A.Gieras

Electrical Energy Utilisation

Wydawnictwo Adam Marszalek

Jacek F. Gieras
Izabella A. Gieras

ELECTRICAL ENERGY UTILISATION

wydawnictwo
adam marszałek

COVER DESIGN
Zbigniew Raplewicz

Poland, Toruń 1998

ISBN 83-7174-199-5

PUBLISHING HOUSE ADAM MARSZAŁEK
Poland, 87-100 Toruń, Przy Kaszowniku 37 St., phone/fax (48-56)322-38, (0-601)20-98-10
Printed by MADO, Poland, 87-148 Łysomice, Warszawska St., phone (0-601)20-98-10
DTP: BOWrtm, (48-56)645-51-32

Contents

Preface

This text evolved from notes used in teaching an undergraduate course *Energy Utilisation* at the University of Cape Town. As the curricula of electrical engineering programmes became more and more overcrowded, many electrical engineering departments decided to limit the number of compulsory courses in heavy current electrical engineering. As a result, the number of lectures in electrical machines and related subjects have been reduced. Under such circumstances students need a concise textbook which covers electrical motors with emphasis on their performance, selection and applications, characteristics of modern electrical drives including variable-speed drives and the use of electrical energy in households.

This textbook deals with fundamentals of electrical motors, drives, electrical traction and domestic use of electrical energy. It is intended to serve third year students taking a one semester course in energy utilisation or electric power engineering. Transformers and electromechanical generators have been omitted as transformation and generation of electric power is usually covered by a parallel course in power systems.

The textbook consists of seven chapters: 1. *Energy and drives*, 2. *D.c. motors*, 3. *Three-phase induction motors*, 4. *Synchronous motors*, 5. *Variable-speed drives*, 6. *Electrical traction* and 7. *Domestic use of electrical energy*. Chapter 7 also contains principles of illumination. For a one semester course and two lectures per week the authors recommend the first four chapters. For four lectures per week the authors recommend all seven chapters. Students using this textbook should have taken courses in circuit theory and electromagnetism as prerequisites.

It would have been impossible to publish this textbook without a generous financial support from the Foundation for Research Development (FRD) and *Eskom* of South Africa.

February, 1998

Jacek F. Gieras
Izabella A. Gieras

1

ENERGY AND DRIVES

1.1 Electrical energy

Electrical energy may be produced from a variety of primary energy sources. The present mix of electrical energy sources in the world as percentage is shown in Table 1.1.

Table 1.1. Sources of world-wide electrical energy

Source	Percent.
Coal	42%
Hydro	19%
Nuclear	17%
Gas	12%
Oil	10%
Renewables	fraction

Electrical energy is consumed by three main sectors: industry, trade and services, and households. This consumption is distributed as shown in Table 1.2:

Table 1.2. Major consumers of world-wide electrical energy

Consumer	Percent.
industry	33%
trade and services	31%
households	29%
transport	5%
public lighting	1%
agriculture	1%

Once produced, electrical energy is directed into *loads*, where it performs useful functions for mankind. The main types of loads that use electrical energy are:

- electrical drives
- illumination
- electric traction
- electric heating
- electric welding
- electrochemistry
- households

The study of the *utilisation of electrical energy* is a branch of electrical engineering that deals with the applications of electric motor drives, lights, heaters, welders, and other electrical appliances, covers their proper maintenance, and aims towards the efficient use of electrical energy.

Today **in an industrialized country more than 65% of the generated electrical energy is consumed by electrical drives**. This means that our modern life can function only with the help of a large number of electric motors.

1.2 Conservation of electrical energy

The contemporary world faces three major problems that threaten to develop into crises in the near future:

- the division of the world into rich and poor countries,
- an enormous increase in energy consumption,
- the drastic pollution of our planet.

The reduction of both energy consumption and pollution is in the hands of scientists and engineers (see Table 1.3. World statistics show that 26 million tons of oil equivalent (MTOE) of primary energy is consumed per day by mankind. Of this primary energy, 7.6 MTOE is used for generating electricity [53]. The growth in total energy consumption is projected to be 1.5% per annum in the coming decades. Thus, by 2010 the consumption of primary energy will be about 30% higher than it is today [53].

World electricity consumption is estimated at 10 000 TWh per annum [53], and the industrial sector in developed countries accounts for over 30% of this figure. More than 65% of total electrical energy consumption is consumed by electric motor drives. More than five billion electrical drives, ranging in size from micromotors to large synchronous machines, are produced *per annum*. This will give some idea of the enormous number of electrical drives presently in use on the planet.

The increasing electrical energy demand is causing tremendous concern for environmental pollution (see Table 1.3) both from *acid rain* and through the *greenhouse effect*. Power plants that use fossil and nuclear fuel are cause for particular concern about such pollution of the air. There is no doubt that energy savings can improve these side effects considerably, and it has been estimated that in developed industrialized countries roughly 20% of electrical energy could be saved by using more efficient control strategies for electrical drives.

Electrical machines have an enormous potential influence on the reduction of energy consumption. Electrical energy consumption can be saved in one of the following ways [39]:

Table 1.3. Population, energy consumption and pollution growth in the world

Year	Population billions	Primary energy consumption billion tons of oil equivalent	CO_2 and NO_x emission billion tons
1990	5.3	7.7	25.0
2000	6.2	9.1	22.6
2010	7.1	11.6	31.9

- good housekeeping;
- the use of variable-speed drives;
- construction of electric motors with better efficiency.

Good housekeeping measures are cheap, quick and easy to implement. The simplest way to save energy costs is to switch idling motors off. Motors can be switched off manually or automatically, and devices exist that use either the input current to the motor or limit switches to detect an idling motor. When larger motors are being switched off and on, the high starting current drawn by the motor could cause supply interference or mechanical problems with couplings, gearboxes, belts, and the like, which deteriorate from repeated starting. These problems can be avoided by using electronic *soft starters* with solid-state devices.

Fan and pump drives employ over 50% of the motors that are used in industry. Most fans and pumps use some form of flow control in an attempt to match supply with demand. Traditionally, mechanical means have been used to restrict the flow, such as a damper on a fan or a throttle valve on a pump. However, such methods waste energy by increasing the resistance to flow and by running the fan or pump away from its most efficient point. A much better method of flow control is to use a variable-speed drive to alter the speed of the motor. For centrifugal fans and pumps the power input is proportional to the cube of the speed, while the flow is proportional to the speed itself. Hence, reduction to 80% of maximum speed (i.e. to 80% of the flow rate) would give about a 50% reduction in power consumption.

The use of permanent magnets (PMs) in electrical machines improves their efficiency by eliminating excitation losses. Since the application of PMs in electrical machines increases the magnetic flux density in the airgap, the machine can achieve a greater output power with the same physical dimensions.

Most energy consumption is by three-phase induction motors rated at below 10 kW. Consider a small three-phase, 1.5 kW four-pole, 50 Hz cage induction motor. The full-load efficiency of such a motor is usually 74%. By replacing such a motor with a rare-earth PM synchronous motor, the efficiency can be increased up to 88%. This means that the three-phase PM synchronous motor would draw only 1705 W from the mains, instead of the 2027 W that was drawn by the three-phase cage induction motor. Hence, the power saving is 322 W for one motor. If in a country, say, a million similar motors were installed, the reduction in power consumption would be 322 MW. This would enable one quite big turboalternator to be disconnected from the power system. If the energy that was saved had been generated by a thermal power plant, the saving would thus have helped towards the reduction of CO_2 and NO_x emissions into the atmosphere.

1.3 Classification of electric motors

Many nations have contributed to the invention, construction, and development of electrical machines. M. Faraday's principle of conversion of electric energy into mechanical energy, formulated in 1822, was the beginning of electric motor design. In 1834 a Russian scientist, B. Jacobi, designed a prototype of the modern d.c. motor. His battery-powered electric motor boat with 16 passengers could travel along the Neva River even against the current. The first self-starting single-phase a.c. commutatorless motor was demonstrated by an Italian professor, G. Ferraris, in 1885. The polyphase induction motor was invented by the Yugoslavian inventor N. Tesla in 1887. The three-phase cage induction motor was built in 1889 by M. Dolivo-Dobrowolsky, a Polish engineer working in Germany. He had also developed a double-cage three-phase induction motor by 1893. The first rotary-current synchronous generator was built in 1887 by F.A. Haselwander. The first solid cylindrical-rotor synchronous generator was built by C. Brown in 1901 at the Maschinenfabrik Oerlikon (Switzerland).

Electric motors can be classified according to their principle of operation:

- d.c. motors (commutator and PM brushless motors);
- induction motors (cage rotor motors, wound rotor motors, electromagnetically excited a.c. commutator motors);
- synchronous motors (electromagnetically excited motors, PM synchronous motors, hysteresis motors, reluctance motors, stepping motors).

Other classifications are used, such as the one given below:

Alternating current (a.c.) motors, which are driven on the single-phase or three-phase commercial network at 50 or 60 Hz.

Direct current (d.c.) commutator motors, which are driven on the commercial network via rectifiers, or which are fed with d.c. generators or batteries.

Electronically-commutated motors — the major members of this category are brushless PM motors, switched-reluctance motors and stepping motors (for position control).

The *rated duty* of an electrical motor is the set of operating conditions for which it has been designed by the manufacturer. The rated duty is characterized by values given on the motor's name plate, which are termed *rated values.* These might include, for instance: *rated output, rated voltage, rated current, rated speed*, etc. According to their rated output, motors may be divided into:

- micro-motors — less than 100 W;
- fractional horsepower motors — from 100 W to 1 kW;
- low-power motors — from 1 kW to 10 kW;
- medium-power motors — from 10 kW to 100 kW;
- high-power motors — from 100 kW to 1 MW;
- very high-power motors — over 1 MW.

Similarly, motors can be classified according to the magnitude of their rated voltage, in which case they are generally distinguished as follows:

- Very low-voltage — below 100 V;
- Low-voltage — from 100 to 500 V;
- High voltage — above 500 V.

According to their speed, motors are frequently classified into the following groups:

- Low-speed — below 250 rpm;
- Medium-speed — from 250 to 3000 rpm;
- High speed — above 3000 rpm.

1.4 Applications of electric motor drives

The possible applications of electrical motor drives are very numerous. A representative sampling is given in the list which follows and in the illustrations of this section.

- Industry (Figs 1.1 to 1.4):
  industrial drives (pumps, blowers, compressors, mills, handling systems);
  machine tools;
  servo drives;
  automation processes;
  internal transportation systems;
  robots;

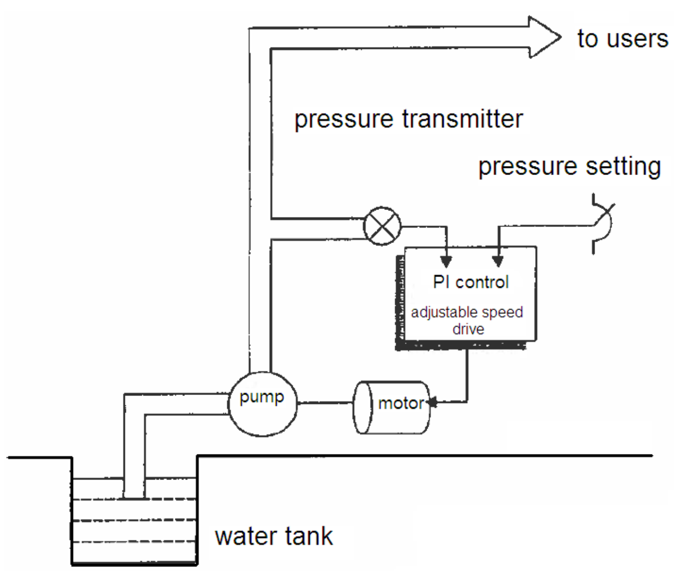

Fig. 1.1. An electric motor driven pump.

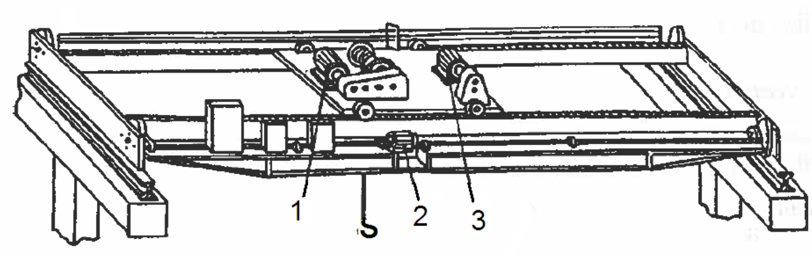

Fig. 1.2. A gantry crane: 1 - hoist motor, 2 - motor for bridge propulsion, 3 - motor for crab propulsion.

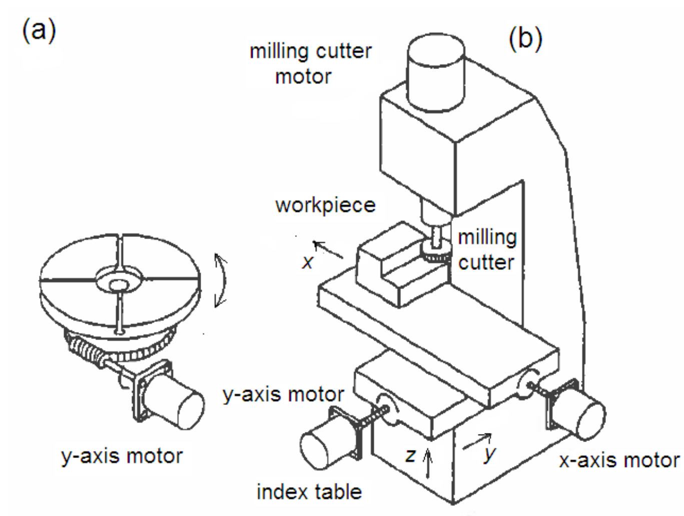

Fig. 1.3. Small and medium-sized motors in machine tools: (a) index table, (b) milling machine.

- Instruments and control systems;
- Defense;
  tanks;
  missiles;
  radar systems;
  submarines;
  torpedos;
- Aerospace:
  rockets;
  space shuttles;
  satellites;
- Medical and healthcare equipment:
  dentists' drills;
  air compressors;

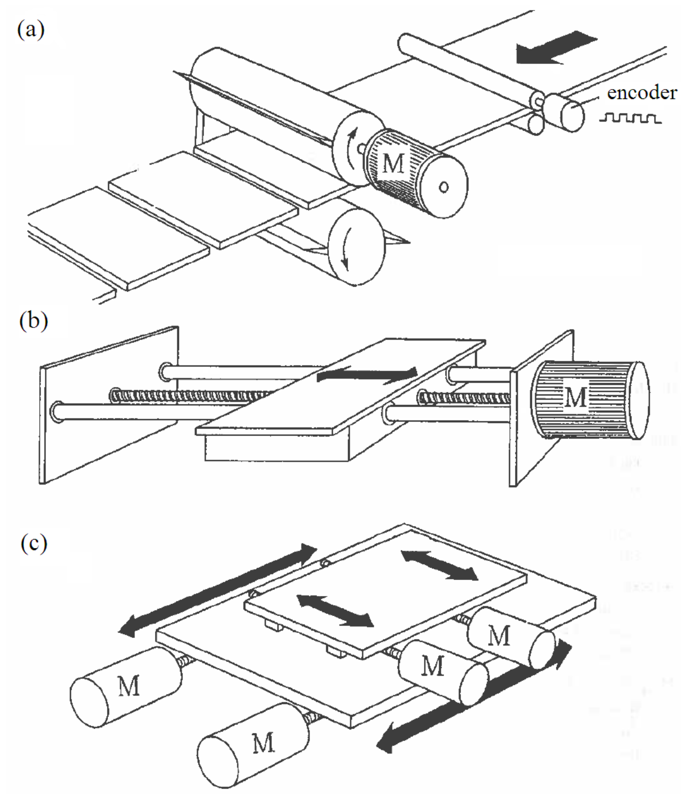

Fig. 1.4. Industrial servo drives: (a) rotary-knife cut-off system, (b) positioning drive (leadscrew table), (c) synchronized motion control (dual leadscrew tables). M — electric motor.

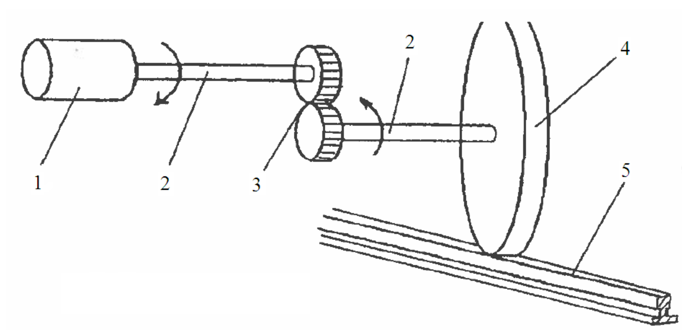

Fig. 1.5. Principle of operation of an electric train drive system: 1 — electric motor, 2 — shaft, 3 — gears, 4 — driving wheel, 5 — rail.

hand-held surgical tools
artificial heart motors;
electric wheelchairs;
trotters,
rehabilitation equipment;

- Transportation (Figs 1.5 and 1.7):
  road vehicles;
  electric trains;
  streetcars (trams);
  electric cars;
  auxiliary equipment for aircraft;
  ships;

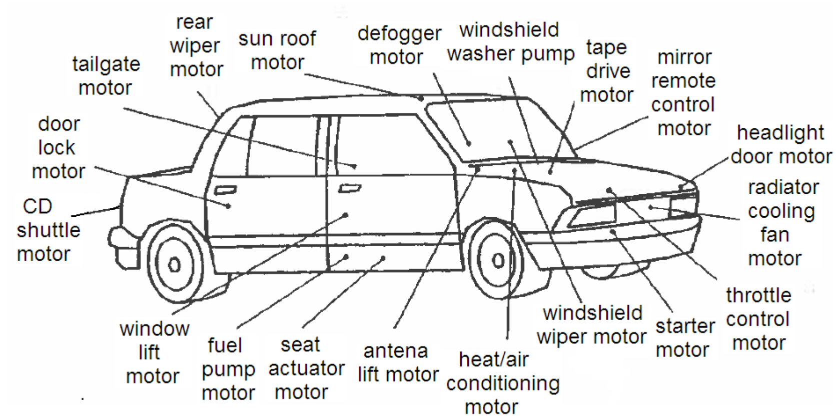

Fig. 1.6. Small motors installed in a car.

- Information and office equipment (Figs 1.8):
  computers;
  printers;
  plotters;
  scanners;
  facsimile machines;
  photocopiers;
  audiovisual aids;

- Public life (Figs 1.9 and 1.10):
  elevators and escalators;
  heat transfer and air-handling systems;
  catering equipment (canteen kitchens, restaurants, hotels, hospitals, etc.);
  coin laundry machines;

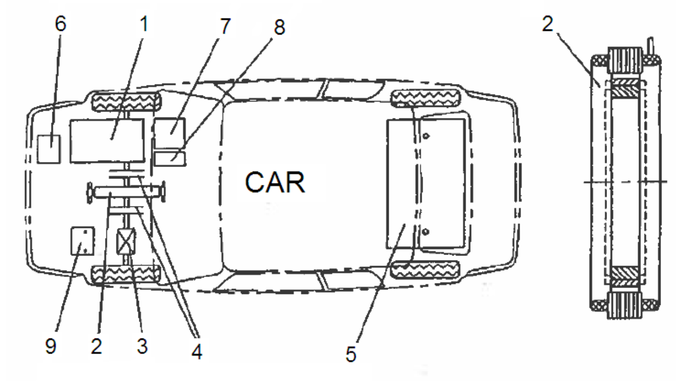

Fig. 1.7. VW *Golf* with a single-shaft hybrid drive: 1 — combustion engine, 2 — permanent magnet disc synchronous motor (flywheel), 3 — gearbox, 4 — clutches, 5 — traction battery, 6 — battery charger, 7 — power electronics, 8 — control electronics, 9 — standard 12 V battery. Courtesy of *Robert Bosch GmbH*, Stuttgart, Germany.

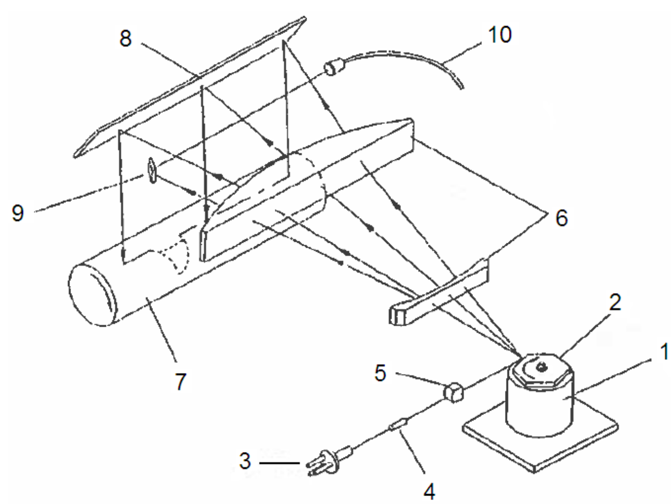

Fig. 1.8. A brushless motor turns the polygonal mirror in a laser printer: 1 — brushless motor, 2 — scanner mirror, 3 — semiconductor laser, 4 — collimator lens, 5 — cylindrical lens, 6 — focusing lenses, 7 — photosensitive drum, 8 — mirror, 9 — beam detect mirror, 10 — optical fiber.

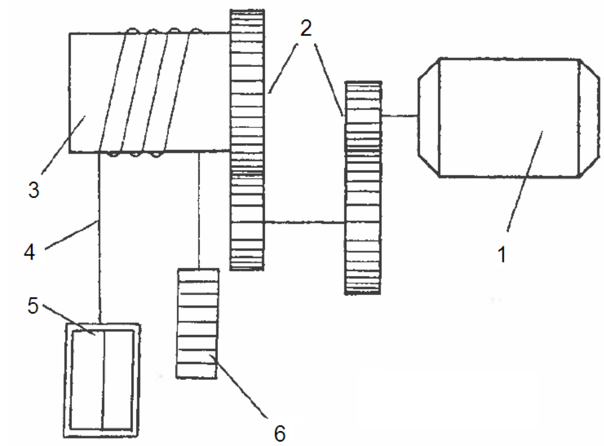

Fig. 1.9. Principle of operation of an elevator drive system: 1 — electric motor, 2 — gears, 3 — drum, 4 — rope, 5 — car, 6 — counterweight.

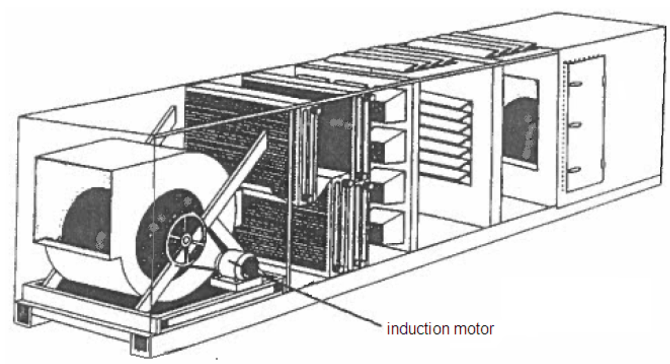

Fig. 1.10. An air-handling unit.

automatic vending machines;
cash dispensers;
money-changing machines;
ticketing machines;
clocks;
amusement park equipment;

- Domestic life:
  kitchen equipment (refrigerators, microwave ovens, dishwashers, mixers, electric knives, etc.);
  bathroom equipment (shavers, toothbrushes, hair dryers, etc.);
  washing machines and clothes dryers;
  vacuum cleaners;
  electric toys;
  vision and sound equipment;

hand power tools (drills, hammers, grinders, polishers, saws, sanders, etc.);
security systems (automatic garage doors, automatic gates, etc.);

- Renewable energy systems Fig. 1.11.

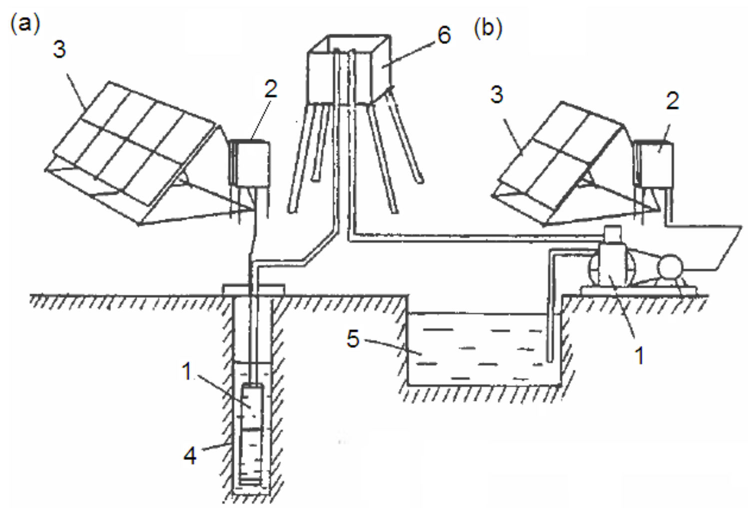

Fig. 1.11. Photovoltaic water pumping systems: (a) submerged system, (b) surface system. 1 — electric motor–pump unit, 2 — inverter, 3 — solar panels, 4 — well, 5 — water reservoir, 6 — water storage tank.

1.5 Trends in the electric-motor and drives industry

The electrical drives family has a very large share of the entire world market in electrical and electronic goods, which is depicted by region in Fig. 1.12. Table 1.4 reflects current and projected trends in the variable speed drives market in Europe [54]. Notice how fast the demand for a.c. motor drives is increasing in comparison with the relatively slow expansion of the market for d.c. commutator motors. The d.c. motor is more costly than comparable a.c. motors and its maintenance costs are also higher. A similar tendency is seen in comparing brushless PM motor drives with d.c. PM commutator motor drives.

As a result of recent progress in the development of solid-state devices, there is now also a huge market for the power electronics that are used in the control of electrical drives.

1.6 How many motors are used in affluent homes ?

Table 1.5 gives an account of the number of electric motors that may be in use in a typical affluent home.

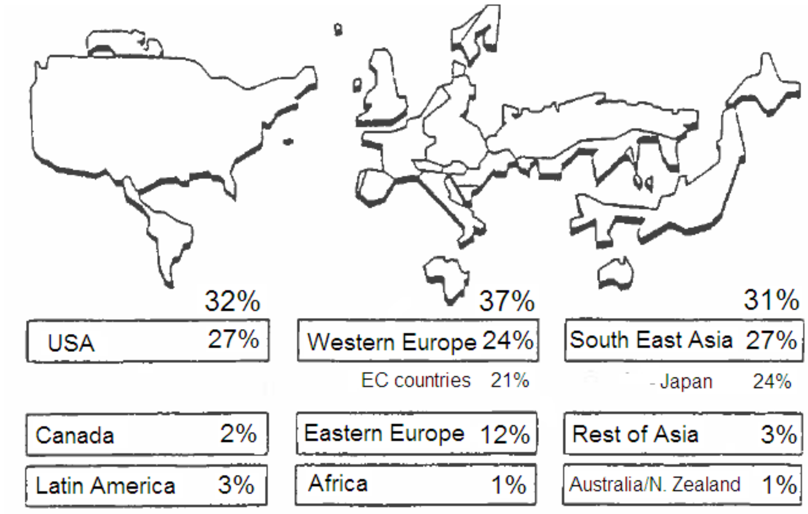

Fig. 1.12. The world's electrical and electronics market by region.

Table 1.4. The Variable-speed drives market in Europe (US$ million)

Type of drives	1994	1995	1996	1997	1998
Electrical d.c. commutator motor drives	468.5	469.9	474.0	482.5	491.4
Electrical a.c. motor drives	761.1	779.7	808.3	846.4	886.3
Mechanical drives	181.3	182.3	183.4	185.7	188.0
Hydraulic drives	113.7	117.1	120.9	125.3	130.1
Total	1 524.6	1 549.0	1 586.6	1 639.9	1 695.8

1.7 Fundamentals of mechanics of machines

1.7.1 Torque and power

The shaft torque T as a function of mechanical power P is expressed as

$$T = F\frac{D}{2} = \frac{P}{\Omega} = \frac{P}{2\pi n} \tag{1.1}$$

where $\Omega = 2\pi n$ is the angular speed and n is the rotational speed in rev/s.

1.7.2 Simple gear trains

In the simple trains shown in Fig. 1.13, let n_1, n_2 = speeds of 1 and 2, N_1 and N_2 = numbers of teeth on 1 and 2, D_1, D_2 = pitch circle diameters of 1 and 2.

Table 1.5. Motors used in a typical affluent household excluding cars

(1) LIVING		(3) AMUSEMENTS/HOBBIES	
Refrigerator	1	Record player	1
Coffee mill	1	Cassette recorder (2)	4
Food processor	1	Walkman	1
Electric knife	1	CD player (2)	6
Dishwasher	1	Video recorder	3
Vacuum cleaner	1	Still cameras (2)	2
Hair-drier	1	Video camera	3
Electric shaver	1	Toys (3)	3
Electric meter	1	Power tools (3)	3
Fans (2)	2	(4) PERSONAL COMPUTER	
Gardening trimmer	1	Floppy disk drive	2
		Hard drive	2
		CD ROM	3
(2) CLOTHES		Fan	1
Sewing machine	1	Printer	4
Washing machine	2 or 3		
Drier	2	(5) TIMEPIECES	
		Clocks (2)	2
		Quartz watches (3)	3
		Total	60

Table 1.6. Basic formulae for linear and rotational motions

Linear motion			Rotational motion		
Quantity	Formula	Unit	Quantity	Formula	Unit
Linear displacement	$s = \theta r$	m	Angular displacement	θ	rad
Linear velocity	$v = ds/dt$ $v = \Omega r$	m/s	Angular velocity	$\Omega = d\theta/dt$	rad/s or 1/s
Linear acceleration	$a = dv/dt$ $a_t = \alpha_r$ $a_r = \Omega^2 r$	m/s^2	Angular acceleration	$\alpha = d\Omega/dt$	rad/s^2 or 1/s^2
Mass	m	kg	Moment of inertia	J	kgm^2
Force	$F = ma$	N	Torque	$T = J\alpha$	Nm
Work	$dW = Fds$	Nm	Work	$dW = Td\theta$	Nm
Kinetic energy	$E_k = 0.5mv^2$	J or Nm	Kinetic energy	$E_k = 0.5J\Omega^2$	J
Power	$P = dW/dt$ $= Fv$	W	Power	$P = dW/dt$ $= T\Omega$	W

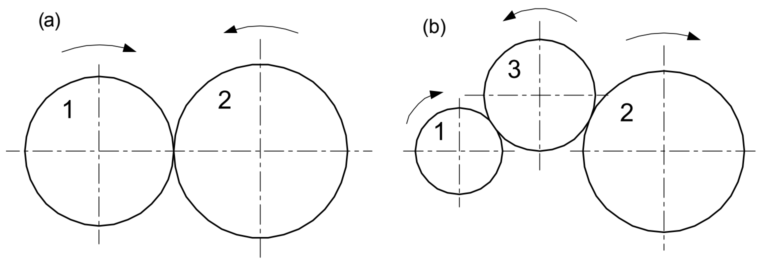

Fig. 1.13. Simple trains

- in train according to Fig. 1.13a

$$\gamma = \frac{n_1}{n_2} = -\frac{N_2}{N_1} = -\frac{D_2}{D_1} \tag{1.2}$$

- in train according to Fig. 1.13b

$$\gamma = \frac{n_1}{n_2} = \frac{N_2}{N_1} = \frac{D_2}{D_1} \tag{1.3}$$

The negative sign signifies that 1 and 2 rotate in opposite directions. The idler, 3, Fig. 1.13b, does not affect the velocity ratio of 1 to 2 but decides on the directions of 2. The ratio $\gamma = N_2/N_1$ is called the *gear ratio*.

1.7.3 Efficiency of a gear train

Allowing for friction, the efficiency of a gear train is

$$\eta = \frac{\text{output power}}{\text{input power}} \tag{1.4}$$

Thus,

$$\eta = \frac{P_2}{P_1} = \frac{T_2(2\pi n_2)}{T_1(2\pi n_1)} = \frac{T_2 n_2}{T_1 n_1} \tag{1.5}$$

According to eqn (1.2) $n_2/n_1 = |N_1/N_2|$ so that eqn (1.5) becomes

$$\frac{T_2 n_2}{T_1 n_1} = \frac{T_2 N_1}{T_1 N_2}$$

The torque on 1

$$T_1 = T_2 \frac{N_1}{N_2} \frac{1}{\eta} \tag{1.6}$$

1.7.4 Equivalent moment of inertia

In the simple trains shown in Fig. 1.13a, let J_1, J_2 = moments of inertia of rotating masses of 1 and 2, Ω_1 and Ω_2 = angular speed of 1 and 2, D_1, D_2 = pitch circle diameters of 1 and 2, $0.5J_1\Omega_1^2$, $0.5J_2\Omega_2^2$ = kinetic energy of 1 and 2, respectively.

The net energy supplied to a system in unit time is equal to the rate of change of its kinetic energy E_k (Table 1.6), i.e.

$$P = \frac{dE_k}{dt} = T\Omega_1$$

$$T\Omega_1 = \frac{d}{dt}[0.5J_1\Omega_1^2 + 0.5J_2\Omega_2^2] = 0.5\left(J_1 + \frac{\Omega_2^2}{\Omega_1^2}J_2\right) \times \frac{d}{dt}\Omega_1^2 \tag{1.7}$$

$$= 0.5\left(J_1 + \frac{\Omega_2^2}{\Omega_1^2}J_2\right) \times 2\Omega_1\frac{d\Omega_1}{dt} \tag{1.8}$$

The quantity $J_1 + (\Omega_2/\Omega_1)^2 J_2$ may be regarded as the equivalent moment of inertia of the gears referred to wheel 1. The moments of inertia of the various gears may be reduced to an equivalent moment of inertia of the motor shaft, i.e.

$$T = \left(J_1 + \frac{\Omega_2^2}{\Omega_1^2}J_2\right)\frac{d\Omega_1}{dt} = \left(J_1 + \frac{N_1^2}{N_1^2}J_2\right)\frac{d\Omega_1}{dt} \tag{1.9}$$

The equivalent moment of inertia is equal to the moment of inertia of each wheel in the train being multiplied by the square of its gear ratio relative to the reference wheel.

Example 1.1

Find the steady-state torque, output power, and shaft moment of inertia of an electric motor which is propelling a rolling mill as shown in Fig. 1.14. The speed of the motor is $n = 950$ rpm. The flywheel and rollers are made of steel of density $\rho = 7\ 800$ kg/m^3.

Solid steel flywheel 1: diameter $D_1 = 1.5$ m, thickness $l_1 = 0.15$ m;

First roller 2: diameter $D_2 = 0.4$ m, length $l_2 = 0.9$ m, circumferential force $F_2 = 20$ kN, number of teeth of the first gear $N_1 = 15$, $N_2 = 35$, efficiency of the first gear $\eta_1 = 0.88$;

Second roller 3: diameter $D_3 = 0.5$ m, length $l_3 = 1.3$ m, circumferential force $F_3 = 14$ kN, number of teeth of the second gear $N_3 = 20$, $N_4 = 45$, efficiency of the second gear $\eta_2 = 0.86$;

Solution

The shaft torque

$$T = F_2\frac{D_2}{2}\frac{N_1}{N_2}\frac{1}{\eta_1} + F_3\frac{D_3}{2}\frac{N_1}{N_2}\frac{N_3}{N_4}\frac{1}{\eta_1}\frac{1}{\eta_2}$$

$$= 20\frac{0.4}{2}\frac{15}{35}\frac{1}{0.88} + 14\frac{0.5}{2}\frac{15}{35}\frac{20}{45}\frac{1}{0.88}\frac{1}{0.86} = 2.829 \text{ kNm}$$

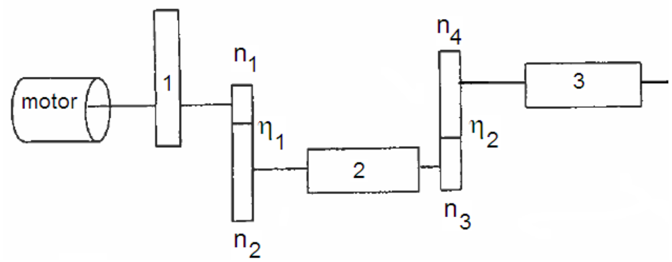

Fig. 1.14. Electric motor driven rolling mill.

The motor output power

$$P_{out} = T(2\pi n) = 2.829\left(2\pi \times \frac{950}{60}\right) = 281.4 \text{ kW}$$

The mass of the flywheel

$$m_1 = \rho\frac{\pi D_1^2}{4}l_1 = 7800\frac{\pi \times 1.5^2}{4}0.15 = 2067.6 \text{ kg}$$

The mass of the first roller

$$m_2 = \rho\frac{\pi D_2^2}{4}l_2 = 7800\frac{\pi \times 0.4^2}{4}0.9 = 882.2 \text{ kg}$$

The mass of the second roller

$$m_3 = \rho\frac{\pi D_3^2}{4}l_3 = 7800\frac{\pi \times 0.5^2}{4}1.3 = 1991 \text{ kg}$$

The moment of inertia of the flywheel

$$J_1 = m_1\frac{D_1^2}{8} = 2067.6\frac{1.5^2}{8} = 581.5 \text{ kgm}^2$$

Note that the moment of inertia of a hoop is $J = mr^2$ and the moment of inertia of a solid cylinder is $J = 0.5mr^2$.

The moment of inertia of the first roller

$$J_2 = m_2\frac{D_2^2}{8} = 882.2\frac{0.4^2}{8} = 17.6 \text{ kgm}^2$$

The moment of inertia of the second roller

$$J_3 = m_3\frac{D_3^2}{8} = 1991\frac{0.5^2}{8} = 62.2 \text{ kgm}^2$$

The total moment of inertia of the system with respect to the motor shaft (see eqns 1.2 and 1.8)

$$J = J_1 + J_2\left(\frac{N_1}{N_2}\right)^2 + J_3\left(\frac{N_1N_3}{N_2N_4}\right)^2$$

$$= 581.5 + 17.6\left(\frac{15}{35}\right)^2 + 62.2\left(\frac{15}{35}\frac{20}{45}\right)^2 = 587 \text{ kgm}^2$$

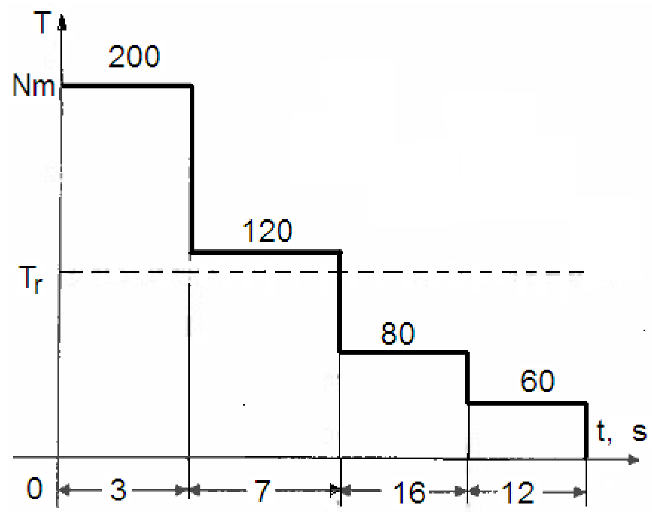

Fig. 1.15. Torque profile of the electric motor referred to in Example 1.2.

Example 1.2

A 12-kW, 1000-rpm electric motor operates with almost constant speed and with the torque profile given in Fig. 1.15. The overload capacity factor $T_{max}/T_r = 2$. Find the thermal utilization coefficient of the motor.

Solution

The rated shaft torque

$$T_r = \frac{P_{out}}{2\pi n} = \frac{12000}{2\pi \times (1000/60)} = 114.6 \text{ Nm}$$

The *rms* torque based on the given duty cycle

$$T_{rms}^2(t_1 + t_2 + t_3 + ... + t_n) = T_1^2 t_1 + T_2^2 t_2 + T_3^2 t_3 + ... + T_n^2 t_n$$

$$T_{rms}^2 \sum t_i = \sum T_i^2 t_i$$

$$T_{rms} = \sqrt{\frac{\sum T_i^2 t_i}{\sum t_i}} = \sqrt{\frac{200^2 \times 3 + 120^2 \times 7 + 80^2 \times 16 + 60^2 \times 12}{3 + 7 + 16 + 12}} = 95.5 \text{ Nm}$$

Note that in electric circuits the *rms* or effective current is

$$I_{rms} = \sqrt{\frac{1}{T}\int_0^T i^2 dt}$$

since the average power delivered to the resisitor is

$$P = \frac{1}{T}\int_0^T i^2 R dt = R\frac{1}{T}\int_0^T i^2 dt = RI_{rms}^2$$

The coefficient of thermal utilization of the motor

$$\frac{T_{rms}}{T_r} \times 100\% = \frac{95.5}{114.6} \times 100\% = 83.3\%$$

1.8 Torque equation

In a typical electromechanical system a motor drives a load (machine) through a gear system. The load speed may be different from that of the motor. Thus, the motor–load system is represented by an equivalent rotational system. For a constant moment of inertia ($dJ/dt = 0$), the motor–load system can be described by the following fundamental torque equation:

$$J\frac{d\Omega}{dt} = T_d - T \tag{1.10}$$

where J is the moment of inertia of motor–load system referred to the motor shaft, Ω is the instantaneous angular velocity of the motor shaft, T_d is the instantaneous torque developed by the motor and T is the instantaneous external load torque (resisting). The sign of T_d is positive for motoring and negative for braking mode. The torque T oposes T_d for the resisting external load and it is positive for the driving external torque. The sign of $Jd\Omega/dt$ is positive for acceleration and negative for deceleration.

The time taken to change the speed from Ω_1 to Ω_2 is

$$t = J\int_{\Omega_1}^{\Omega_2} \frac{d\Omega}{T_d(\Omega) - T(\Omega)} \tag{1.11}$$

It is very difficult to express the dynamic torque $T_{dyn}(\Omega) = T_d(\Omega) - T(\Omega)$ by analytical equations. In simplified calculations the dynamic torque can be replaced by a constant torque equal to the average dynamic torque T_{dynav} the action of which is equivalent to the practical dynamic torque within the speed interval $\Omega_1 \le \Omega \le \Omega_2$. Thus, the time to accelerate the motor from $\Omega_1 = 0$ to the steady state speed $\Omega_2 = \Omega$ is

$$t_a = J\int_0^{\Omega} \frac{d\Omega}{T_{dyn}(\Omega)} = J\frac{1}{T_{dyn}(\Omega)}\int_0^{\Omega} d\Omega \approx J\frac{\Omega}{T_{dynav}} \tag{1.12}$$

The time of breaking that is needed to bring the motor from the steady-state speed Ω to $\Omega = 0$ is

$$t_b = J\int_{\Omega}^{0} \frac{d\Omega}{T_{dynb}} \tag{1.13}$$

where T_{dynb} is the dynamic breaking torque.

Example 1.3

An electric motor rated at 7.5 kW and 1450 rpm runs without any load. The no-load speed is $n_0 = 1480$ rpm, the rotor's moment of inertia $J = 0.041$ kgm^2, the rotational (friction) losses $\Delta P_{rot} = 110$ W (measured at $n = n_0$) and the average starting torque can be expressed as $T_{stav} = 2.25T_r$ where T_r is the rated shaft torque. The motor is started by switching the supply voltage on. The motor decelerates to zero speed due to switching the supply voltage off. Find the time of acceleration t_a and the time t_b to bring the motor to zero speed.

Solution

The rated angular speed is $\Omega_r = 2\pi n_r = 2\pi \times (1450/60) = 151.8$ rad/s and the no-load angular speed is $\Omega_0 = 2\pi n_0 = 2\pi \times (1480/60) = 155$ rad/s. The rated shaft torque is

$$T_r = \frac{7500}{151.8} = 49.4 \text{ Nm}$$

The average starting torque is $T_{stav} = 2.25T_r = 2.25 \times 49.4 = 111.15$ Nm. The motor runs without any load so that the external load torque is $T = 0$. Thus, the average dynamic torque

$$T_{dynav} = T_{stav} - T = 111.15 - 0 = 111.15 \text{ Nm}$$

Since the steady state speed is equal to the no-load speed Ω_0, the calculated time of acceleration from zero speed to 155 rad/s is

$$t_a = J\frac{\Omega_0}{T_{dynav}} = 0.041\frac{155}{111.15} = 0.057 \text{ s}$$

In practice, the time of acceleration is longer due to transient effects.

When the supply voltage is cut off, the motor is retarded by the breaking dynamic torque T_{dynb} produced by rotational losses ΔP_{rot}, i.e.

$$T_{dynb} = \frac{\Delta P_{rot}}{\Omega_0} = \frac{110}{155} = 0.7 \text{ Nm}$$

The time necessary to obtain zero speed is

$$t_b = J\frac{\Omega_0}{T_{dynb}} = 0.041\frac{155}{0.7} = 9.08 \text{ s}$$

1.9 Mechanical characteristics of machines

In general, the mechanical characteristic $T = f(\Omega)$ of a machine driven by an electric motor can be described by the following equation:

$$T = T_r\left(\frac{\Omega}{\Omega_r}\right)^{\beta} \tag{1.14}$$

where T_r is the resisting torque of the machine at rated angular speed Ω_r, $\beta = 0$ for hoists, belt conveyors, rotating machines and vehicles (constant torque machines), $\beta = 1$ for mills, callanders, paper machines and textile machines, $\beta = 2$ for rotary pumps, fans, turbocompressors and blowers.

Example 1.4

A 10 kW, 1450 rpm electric motor has been used to drive the following machines: (a) a hoist ($\beta = 0$), (b) a mill ($\beta = 1$) and (c) a fan ($\beta = 2$). The load torque in each case is 60 Nm. Find the drop in mechanical power if the speed is reduced to $n = 1200$ rpm.

Solution

The output power delivered by the motor at $T_r = 60$ Nm and $n_r = 1450$ rpm

$$P_{outr} = T_r \Omega_r = T_r(2\pi n_r) = 60(2\pi \frac{1450}{60}) = 9111 \text{ kW}$$

As the speed is reduced to $n = 1200$ rpm, the load torque is subject to a change according to eqn (1.14), i.e.

(a) for the hoist

$$T = 60 \left(\frac{1200}{1450}\right)^0 = 60 \text{ Nm}$$

$$P_{out} = T(2\pi n) = 60 \times \left(2\pi \frac{1200}{60}\right) = 7540 \text{ W}$$

(b) for the mill

$$T = 60 \left(\frac{1200}{1450}\right)^1 = 49.7 \text{ Nm}$$

$$P_{out} = T(2\pi n) = 49.7 \times \left(2\pi \frac{1200}{60}\right) = 6245 \text{ W}$$

(c) for the fan

$$T = 60 \left(\frac{1200}{1450}\right)^2 = 41.1 \text{ Nm}$$

$$P_{out} = T(2\pi n) = 41.1 \times \left(2\pi \frac{1200}{60}\right) = 5165 \text{ W}$$

The mechanical power at reduced speed and referred to the rated power is

(a) for the hoist

$$\frac{7540}{9111} \times 10\% = 82.7\%$$

(b) for the mill

$$\frac{6245}{9111} \times 10\% = 68.5\%$$

(c) for the fan

$$\frac{5165}{9111} \times 10\% = 56.7\%$$

Problems

1. A flywheel rotates with the speed $n = 300$ rpm. Its diameter is $d = 1.2$ m, thickness $l = 0.1$ m and density $\rho = 7700$ kg/m^3. Find: (a) the moment of inertia, (b) the kinetic energy and (c) the necessary external torque to achieve the steady-state speed in $\Delta t = 8$s.

   Answer: (a) $J = 156.7$ kgm^2, $E_k = 77\ 328.3$ J, (c) 615.4 Nm.
2. An elevator drive consists of a three-phase electric motor, gears and a rope which is wound on a drum (see Fig. 1.9). One end of the rope is tied to the car and the other end to the counterweight. The mass of the car is $m_c = 300$ kg, the maximum mass of the load (passengers or materials) is $m = 1100$ kg, the mass of the counterweight is $m_0 = 650$ kg, the steady-state linear speed is $v = 1.5$ m/s, the steady state motor speed is $n = 950$ rpm and the efficiency of the whole gear system is $\eta = 0.86$. Find: (a) the steady state torque where the car is lifted up and dropped down, (b) the moment of inertia of both the car and counterweight as seen from the motor's shaft. The moment of inertia of the drum and gears can be neglected.

   Answer: (a) 129 Nm (up), 95.4 Nm (down), (b) $J = 0.4662$ kgm^2.
3. For the elevator drive of Example 1.2. select the electric motor for continuous operation and find the moment of inertia of the car, drum and counterweight as seen from the motor's shaft. The moment of inertia of the drum is 2.2 kgm^2 and the drum diameter is 0.5 m.

   Answer: 13 kW, 950 rpm; 0.4742 kgm^2.
4. The required torque profile of an industrial machine is described as follows: 75 Nm for $0 \le t_1 \le 40$ s, 40 Nm for $40 \le t_2 \le 90$ s, 90 Nm for $90 \le t_3 \le 135$ s, 0 Nm for $135 \le t_4 \le 160$ s, 105 Nm for $160 \le t_5 \le 190$ s, 0 Nm for $190 \le t_6 \le 200$ s, 75 Nm for $0 \le t_1 \le 40$ s, ... The required speed is $950 \pm 1\%$ rpm. Select the electric motor for continuous operation.

   Answer: $T_{rms} = 70.7$ Nm, $P \approx 7034$ W, motor rated at 7.5 kW.
5. An electric motor rated at 55 kW and 975 rpm runs without any load. The no-load speed is $n_0 = 990$ rpm, the rotor's moment of inertia $J = 3.1$ kgm^2, the rotational (friction) losses $\Delta P_{rot} = 440$ W (measured at $n = n_0$) and the average starting torque can be expressed as $T_{stav} = 2.52 T_r$ where T_r is the rated shaft torque. The motor is started by switching the supply voltage on. The motor decelerates to zero speed due to switching the supply voltage off. Find the time of acceleration t_a and the time t_b to obtain zero speed.

   Answer: $t_a = 0.237$ s, $t_b = 75.76$ s.
6. A three-phase, 50 Hz motor draws 65 kVA at $\cos\phi = 0.75$ lagging power factor from a 380 V (line-to-line) source. It is desired to improve the power factor to 0.92 lagging by connecting a capacitor bank across the terminals of the motor. Calculate: (a) the line current before and after the addition of the capacitor bank and (b) the required rating of the capacitor bank.

   Answer: (a) 98.76 A before, 80.5 A after (b) $Q_C = 22.13$ kVAR, $C = 487.8\ \mu$F for star-connected capacitors, $C = 162.6\ \mu$F for delta-connected capacitors.

2

D.C. MOTORS

2.1 Construction

Fig. 2.1 shows the longitudinal and cross sections of a typical *d.c. commutator motor* with its electromagnetic excitation system and interpoles. The electromagnetic torque developed by this type of motor is created by two main windings: the *armature winding*, in which the EMF is induced, and the *field winding*, which produces the exciting magnetic flux. In typical designs, the armature winding is inserted into slots of a laminated rotor core while the field winding is located on salient stator poles.

The armature coils are interconnected through the *commutator*, which consists of a number of insulated copper segments. The commutator is located on the same shaft as the armature (rotor) and rotates together with the armature winding. In d.c. *motors*, the commutator serves as a mechanical inverter, converting d.c. line current into a.c. armature current. The armature (rotor) core must be laminated to reduce the core losses that may arise due to the flow of a.c. current. In d.c. *generators*, the commutator serves as a mechanical rectifier. Current is fed to the commutator with the aid of *brushes*, often made of carbon. The brushes are held in *brush holders*, and they must be free to move radially in order to maintain contact with the commutator as they wear away. The current is conducted from the brush to the *brush stud* by means of a *brush pigtail*.

The *main pole* consists of a pole core with a concentrated-parameter coil and a pole shoe. The pole shoes should also be laminated to reduce the additional iron losses due to any variable airgap reluctance caused by the rotor slots. The pole cores can be made either solid or laminated. The higher the voltage for a given diameter of armature, the fewer is the number of main poles, to provide space for the larger number of commutator segments. High-current motors require a large number of poles in order to carry currents which sometimes exceed 1 kA per brush set.

There are smaller poles, which are called *interpoles* or *commutating poles* between the main poles. The *interpole winding* may be called the *commutating winding*, and it is connected in series with the armature winding. Interpoles produce an MMF in opposition to that of the armature winding in order to achieve commutation with reduced sparking at the brushes and to reduce the demagnetizing effect of the quadrature axis armature reaction MMF. Interpoles are generally omitted in small d.c. machines, such as fractional-horsepower motors.

In motors subject to heavy duties, the quadrature armature reaction is neutralized by means of a *compensating winding* embedded in the pole-shoe slots of the main poles. Like the interpole winding, the compensating winding is connected in series with the armature winding.

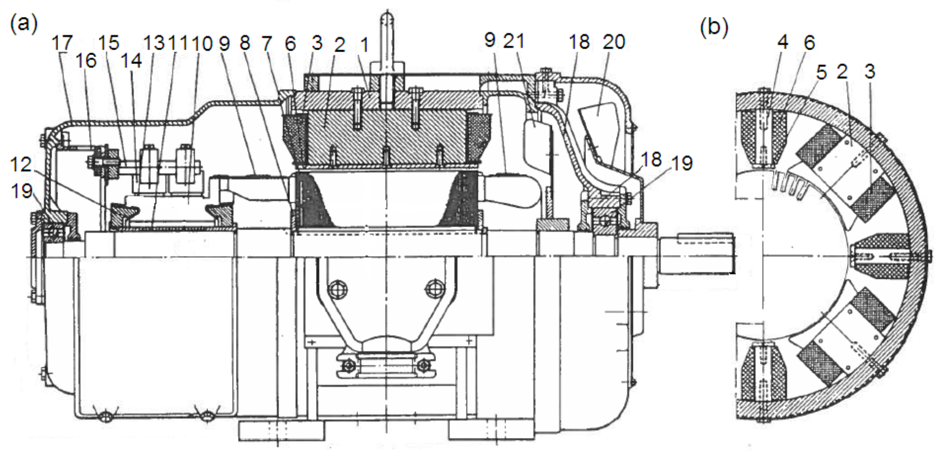

Fig. 2.1. A d.c. motor : (a) longitudinal section, (b) cross section. 1 — frame, 2 — main pole core, 3 — field excitation winding, 4 — interpole core, 5 — interpole shoe, 6 — interpole coil, 7 — armature core, 8 — clamping rings, 9 — bands securing the end connections, 10 — commutator segment, 11 — commutator steel cylinder, 12 — commutator clamping cone, 13 — brush, 14 — brush holder, 15 — brush stud.

D.c motors may be classified according to their armature and field winding connections as follows:

(a) *separately-excited motors*, in which the field winding is fed from a source which is separate to that of the armature winding;
(b) *shunt motors*, in which the armature and field windings are connected in parallel;
(c) *series motors*, in which the armature and field windings are connected in series;
(d) *compound motors* with two field windings, i.e. series and shunt (parallel).

2.2 Fundamental equations

2.2.1 Terminal voltage

From Kirchhoff's voltage law, the terminal (input) voltage of a d.c. motor is

$$V = E + I_a \sum R_a + \Delta V_{br} \tag{2.1}$$

where E is the voltage induced in the armature winding (called the EMF), I_a is the armature current, and ΔV_{br} is the brush voltage drop. The brush voltage drop is approximately constant, and for the majority of typical d.c. motors is practically independent of the armature current. For carbon brushes, $\Delta V_{br} \approx 2$ V. The armature circuit resistance is, in general:

$$\sum R_a = R_a + R_{int} + R_{comp} + R_{se} \tag{2.2}$$

where R_a is the resistance of the armature winding, R_{int} is the resistance of the commutation winding located on the interpoles, R_{comp} is the resistance of the compensating winding, and R_{se} is the resistance of the series winding. For small and medium-power shunt d.c. motors $\sum R_a = R_a + R_{int}$.

2.2.2 Armature winding EMF

The EMF induced in the armature winding by the main flux Φ is

$$E = \frac{N}{a} pn\Phi = c_E n\Phi \tag{2.3}$$

where N is the number of the armature conductors, a is the number of pairs of armature current parallel paths, p is the number of pole pairs, Φ is the main (useful) magnetic flux, and c_E is the so-called *armature constant*, which can be expressed as

$$c_E = \frac{Np}{a} \tag{2.4}$$

The following relationship exists between the number of armature conductors N and the number of commutator segments C:

$$N = 2CN_c \tag{2.5}$$

where N_c is the number of turns per one armature coil.

2.2.3 Magnetic flux

The magnetic flux in the airgap is

$$\Phi = b_p L_i B_g = \alpha_i \tau L_i B_g \tag{2.6}$$

where b_p is the pole shoe width, L_i is the effective length of the armature stack, B_g is the airgap magnetic flux density, $\alpha_i = b_p/\tau = 0.55 \ldots 0.75$ is the effective pole arc coefficient and $\tau = \pi D/(2p)$ is the pole pitch defined as the armature circumference πD divided by the number of poles $2p$.

2.2.4 Electromagnetic (developed) torque

The electromagnetic torque developed by the motor is

$$T_d = \frac{EI_a}{2\pi n} = \frac{VI_a - I_a^2 \sum R_a - \Delta V_{br} I_a}{2\pi n}$$

$$= \frac{N}{a}\frac{p}{2\pi} I_a \Phi = c_T \Phi I_a \tag{2.7}$$

where

$$c_T = \frac{Np}{2\pi a} = \frac{c_E}{2\pi} \tag{2.8}$$

is the *torque constant*. Note that the electromagnetic torque is proportional to the armature current.

2.2.5 Electromagnetic power

The electromagnetic power developed by the motor is

$$P_g = \Omega T_d \tag{2.9}$$

where the rotor angular speed is

$$\Omega = 2\pi n \tag{2.10}$$

On the other hand, the electromagnetic power may also be written as

$$P_g = E I_a \tag{2.11}$$

2.2.6 Rotor and commutator linear speed

The rotor (armature) linear speed is

$$v = \pi D n \tag{2.12}$$

where D is the external diameter of the rotor. Similarly, the commutator linear speed is

$$v_C = \pi D_C n \tag{2.13}$$

where D_C is the external diameter of the commutator.

2.2.7 Input and output power

A motor converts an electrical input power

$$P_{in} = V I_a \tag{2.14}$$

into a mechanical output power that is expressible as

$$P_{out} = \Omega T = \eta P_{in} \tag{2.15}$$

where T is the shaft (output) torque, and η is the efficiency.

2.2.8 Losses

The d.c. motor losses are

$$\sum \Delta P = \Delta P_a + \Delta P_f + \Delta P_{se} + \Delta P_{Fe} + \Delta P_{br} + \Delta P_{rot} + \Delta P_{str} \tag{2.16}$$

where each component of the total power loss is listed below:

- the armature winding losses:

$$\Delta P_a = I_a^2 \sum R_a \tag{2.17}$$

- the shunt-field winding loss:

$$\Delta P_f = I_f^2 R_f \tag{2.18}$$

- the series-field winding loss:

$$\Delta P_{se} = I_{se}^2 R_{se} \tag{2.19}$$

- the armature core loss:

$$\Delta P_{Fe} = \Delta P_{ht} + \Delta P_{et} + \Delta P_{hy} + \Delta P_{ey} \tag{2.20}$$

- the brush-drop loss:

$$\Delta P_{br} = I_a \Delta V_{br} \approx 2 I_a \tag{2.21}$$

- the rotational losses:

$$\Delta P_{rot} = \Delta P_{fr} + \Delta P_{wind} + \Delta P_{vent} \tag{2.22}$$

- the stray load losses:

$$\Delta P_{str} \approx 0.01 P_{out} \tag{2.23}$$

In the above equations, I_f is the shunt-field current, I_{se} is the series-field current, $\Delta P_{ht} \propto f B_t^2$ are the hysteresis losses in the armature teeth, $\Delta P_{et} \propto f^2 B_t^2$ are the eddy-current losses in the armature teeth, $\Delta P_{hy} \propto f B_y^2$ are the hysteresis losses in the armature yoke, $\Delta P_{ey} \propto f^2 B_y^2$ are the eddy-current losses in the armature yoke, f is the frequency of the armature flux (current), B_t is the magnetic flux density in the armature teeth, B_y is the magnetic flux density in the armature yoke, ΔP_{fr} are the friction losses (due to the bearings and commutator–brushes), ΔP_{wind} are the windage losses, and ΔP_{vent} are the ventilation losses.

The frequency of the armature current is

$$f = pn \tag{2.24}$$

It is sometimes convenient to express the motor losses as a function of the motor's efficiency. Thus,

$$\sum \Delta P = P_{in} - P_{out} = \frac{P_{out}}{\eta} - P_{out} = P_{out}\frac{1-\eta}{\eta} \tag{2.25}$$

2.2.9 Armature line current density

The *armature line current density*

$$A = \frac{NI_a}{2a\pi D_a} \tag{2.26}$$

expresses the *armature electric loading*.

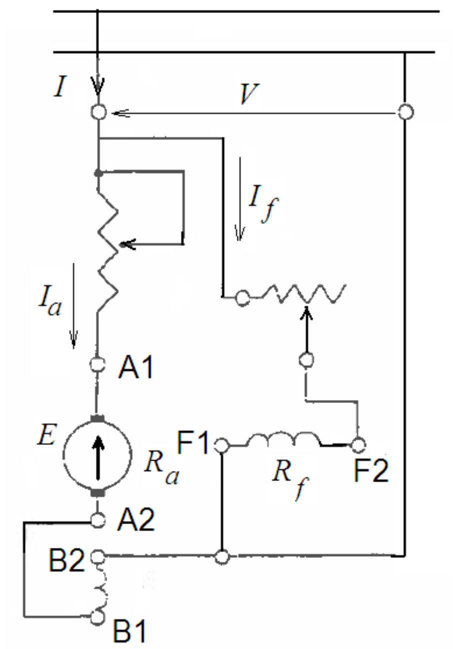

Fig. 2.2. Circuit diagram of a d.c. shunt motor.

2.3 D.c. shunt motor

In the d.c. shunt motor, the shunt field windings are connected in parallel with the armature winding (note that 'shunt' is an early word that designated a parallel connection).

The circuit diagram of a shunt d.c. motor is shown in Fig. 2.2. The total line current, I, is given by

$$I = I_a + I_f \tag{2.27}$$

where I_a is the armature current and I_f is the shunt-field current.

The speed of the motor, as a function of the terminal voltage V, the magnetic flux Φ and the armature current I_a, can be expressed as follows:

$$n = \frac{E}{c_E\Phi} = \frac{V - I_a \sum R_a - \Delta V_{br}}{c_E\Phi} = \frac{V}{c_E\Phi} - \frac{\sum R_a}{c_E\Phi} I_a - \frac{\Delta V_{br}}{c_E\Phi} \tag{2.28}$$

If the shaft torque is zero, then $I_a \approx 0$ and the no-load speed is

$$n_o \approx \frac{V - \Delta V_{br}}{c_E\Phi} \tag{2.29}$$

Neglecting the armature reaction ($\Phi = const$) and neglecting any temperature fluctuation ($\sum R_a = const$), the speed equation can be brought to the simple form:

$$n = n_o - c_a I_a \tag{2.30}$$

in which $c_a = \sum R_a/(c_E\Phi)$ is a constant (if $\Phi = const$). Since $I_a = T_d/(c_T\Phi)$, the speed can be expressed as a function of the electromagnetic torque, i.e.:

$$n = n_o - K_a T_d \tag{2.31}$$

where $K_a = \sum R_a/(c_E c_T \Phi^2)$ is also a constant (again, if $\Phi = const$).

The speed–torque characteristics are shown in Fig. 2.3. The curves in Fig. 2.3 are affected by the direct axis armature reaction (magnetizing or demagnetizing action). In general, the action of the armature MMF on the main MMF is termed the *armature reaction*.

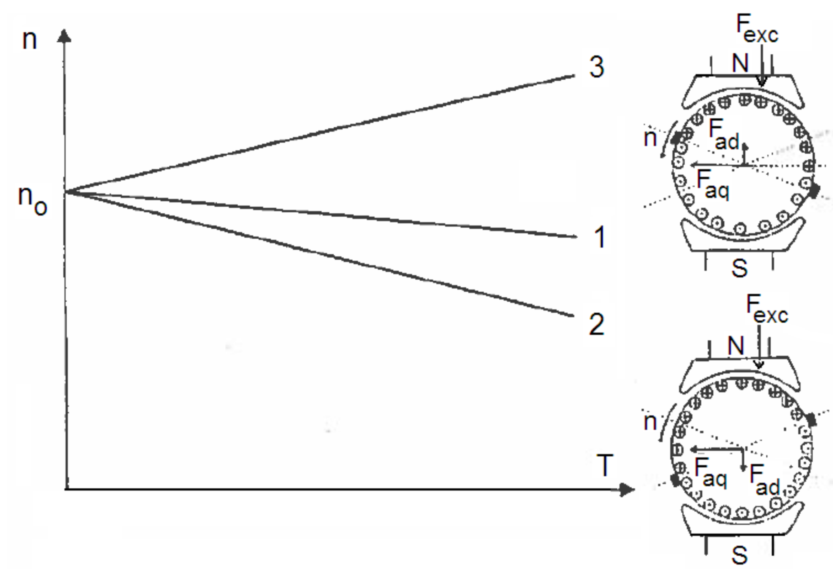

Fig. 2.3. Speed-torque characteristics of a d.c. shunt motor: 1 — brushes are on the geometrical neutral line, 2 — brushes are shifted ahead from the neutral line, 3 — brushes are shifted back from the neutral line.

2.4 D.c. series motor

In a d.c. series motor, the armature and series field windings are connected in series (see Fig. 2.4). The armature current and the field current are therefore the same:

$$I = I_a = I_f \tag{2.32}$$

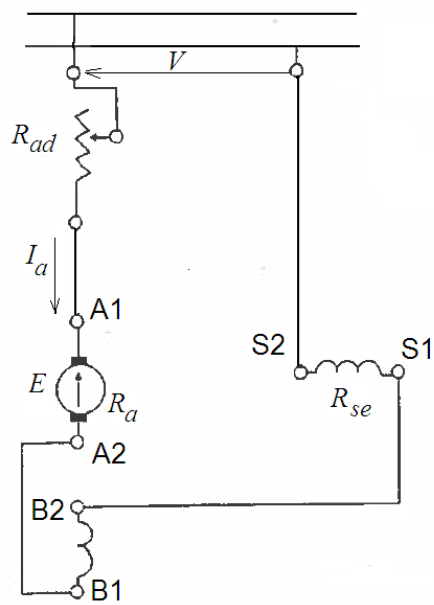

Fig. 2.4. Circuit diagram of a d.c. series motor.

If the magnetic circuit is unsaturated, the magnetic flux $\Phi \propto I_a$ and

$$\Phi = c_I I_a \tag{2.33}$$

The electromagnetic torque of an unsaturated motor is proportional to the square of the armature current:

$$T_d = c_T \Phi I_a \approx c_T c_I I_a^2 \tag{2.34}$$

The speed equation for such a motor is

$$n = \frac{E}{c_E \Phi} = \frac{V - I_a \sum R_a - \Delta V_{br}}{c_E c_I I_a} \approx \frac{V - \Delta V_{br}}{c_E c_I I_a} - \frac{\sum R_a}{c_E c_I} = \frac{A}{I_a} - B \tag{2.35}$$

where

$$A = \frac{V - \Delta V_{br}}{c_E c_I}; \qquad B = \frac{\sum R_a}{c_E c_I} \tag{2.36}$$

At no load ($\Phi \approx 0$, $I_a \approx 0$), the speed becomes very high. This is dangerous because mechanical damage will eventually ensue, such as rupture of the bandings, or damage to the armature winding, the commutator, or other important components. For this reason a series motor should be operated so as to exclude the possibility of starting it without a load (by means of a permanent coupling, toothed gear, worm gear, etc.)

Since $T_d = c_T c_I I_a^2$, the armature current can be expressed as a function of the torque:

$$I_a = \sqrt{\frac{T_d}{c_T c_I}} = c\sqrt{T_d} \tag{2.37}$$

where $c = 1/\sqrt{c_T c_I}$.

The speed-torque curve shown in Fig. 2.5b has a similar shape to the speed current relationship shown in Fig. 2.5a, and so the speed-torque relationship can be approximated by the equation

$$n = \frac{A}{I_a} - B = \frac{A}{c\sqrt{T_d}} - B = \frac{K}{\sqrt{T_d}} - B \tag{2.38}$$

where $K = A/c$.

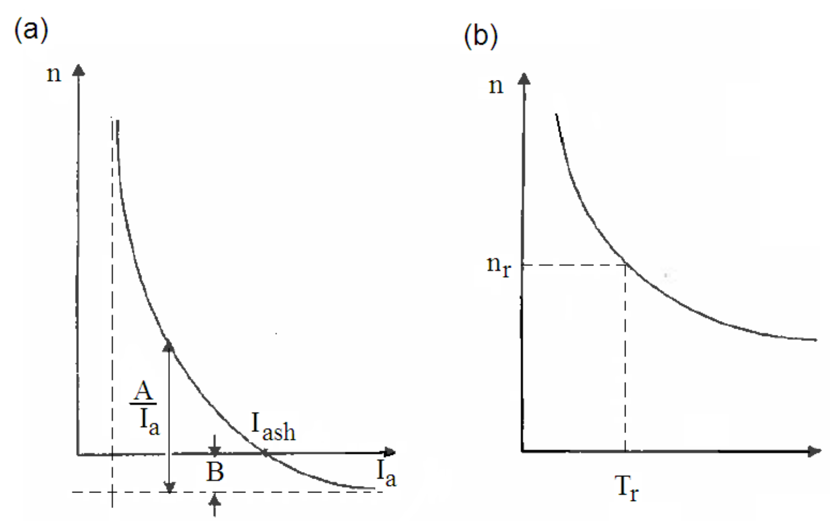

Fig. 2.5. Characteristics of a d.c. series motor: (a) speed–armature current, (b) speed–torque.

2.5 Compound-wound motor

A compound-wound d.c. motor has two field windings: a shunt field winding and a series field winding (see Fig. 2.6). When the field windings are *cumulatively com-*

pounded, their magnetizing forces are added, increasing the flux. When the field windings are *differentially connected*, the series field winding opposes the shunt winding. The resultant exciting flux is

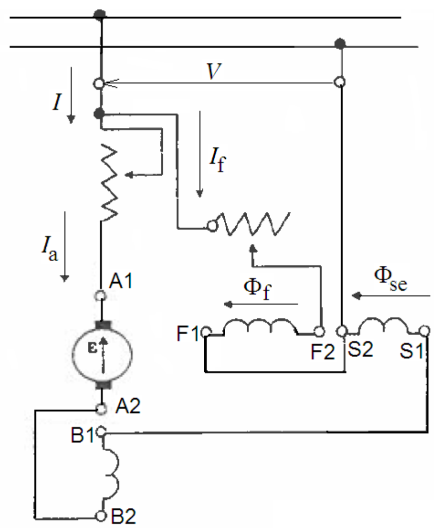

Fig. 2.6. Circuit diagram of a d.c. compound-wound motor: $\Phi = \Phi_f + \Phi_{se}$ for cumulative compound, $\Phi = \Phi_f - \Phi_{se}$ for differential compound.

$$\sum \Phi = \Phi_f \pm \Phi_{se} \tag{2.39}$$

where the '+' sign is for a cumulative compound motor and the '–' sign is for the differential case (which is almost never used). The load current is similar to that of a shunt motor and given by eqn (2.27). The speed of the compound-wound motor,

$$n = \frac{V - I_a \sum R_a - \Delta V_{br}}{c_E(\Phi_f \pm \Phi_{se})} \tag{2.40}$$

is inversely proportional to the total excitation flux.

Cumulative compound motors have characteristics resembling those of a series motor. The flux–armature current characteristic and the torque–armature current characteristic for a d.c. cumulative compound motor are shown in Fig. 2.7a. The shunt field winding limits the excessive speed increase when the load is removed, since in this case the flux Φ_f remains, and hence sets a limit on the no-load speed $n_o \approx (V - \Delta V_{br})/(c_E\Phi_f)$ (Fig. 2.7b).

2.6 Starting

To decrease the current inrush when starting a motor, a starting rheostat is inserted into the armature circuit (as in Fig. 2.8). By combining eqn (2.1), in which $\sum R_a =$

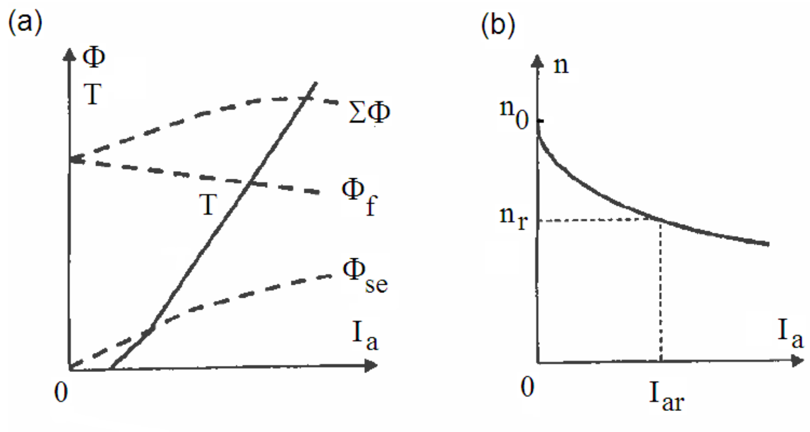

Fig. 2.7. Characteristics of a d.c. cumulative compound motor: (a) flux–armature current and torque–armature current curves, (b) speed–torque curve.

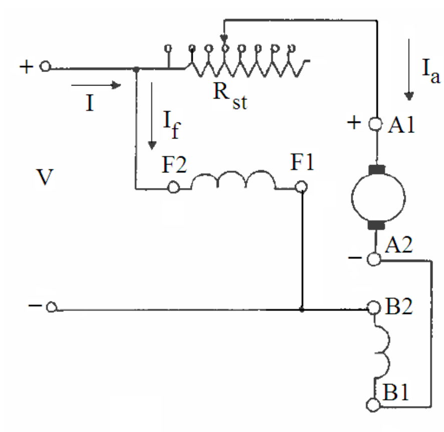

Fig. 2.8. Circuit diagram of a d.c. shunt motor with a starting rheostat R_{st}.

$\sum R_a + R_{st}$ (where R_{st} is the variable resistance of the starting rheostat) with eqn (2.3), the armature current can be expressed as a function of speed. Thus

$$I_a = \frac{V - \Delta V_{br} - c_E n \Phi}{\sum R_a + R_{st}} \tag{2.41}$$

Suppose now that $R_{st} = 0$. At the first instant of starting the motor, the speed $n = 0$ and the EMF $E = 0$. Hence, at this instant, the starting current is equal to the blocked-rotor (short-circuit) current:

$$I_{ash} = \frac{V - \Delta V_{br}}{\sum R_a} \gg I_{ar} \tag{2.42}$$

where I_{ar} is the rated armature current. To reduce the starting current I_{ash}, a starting rheostat is connected in series with the armature winding so that the resultant resistance of the armature circuit is $\sum R_a + R_{st}$. Note that the resistance R_{st} is greatest at the instant when the motor is started. Thereafter, the blocked-rotor armature current I_{ash} drops to the value of

$$I_{amax} = \frac{V - \Delta V_{br}}{\sum R_a + R_{st}} \tag{2.43}$$

As the speed increases from 0 to n', the EMF increases too, and

$$I_{amin} = \frac{V - E' - \Delta V_{br}}{\sum R_a + R_{st}} \tag{2.44}$$

where $E' = c_E n' \Phi < E$. When the speed reaches its rated value n_r, the starting rheostat can be removed, since at that instant

$$I_a = I_{ar} = \frac{V - c_E n_r \Phi - \Delta V_{br}}{\sum R_a} \tag{2.45}$$

2.7 Speed control of d.c. motors

The relationship

$$n = \frac{1}{c_E \Phi}[V - I_a(\sum R_a + R_{rhe}) - \Delta V_{br}] \tag{2.46}$$

summarises all the important contributions to the speed of a d.c. motor. In particular, the eqn (2.46) shows that the speed of a d.c. motor can be controlled by changing:

- the supply mains voltage V;
- the armature-cirucit resistance $\sum R_a + R_{rhe}$ where R_{rhe} is the speed control rheostat;
- the field flux Φ.

Example 2.1

A 4 kW, 220 V, 20.6 A, 1200 rpm separately-excited d.c. motor has an armature circuit resistance $\sum R_a = 0.3\Omega$ and efficiency $\eta = 85.5$ %. If the terminal voltage is reduced to 50% of the rated voltage but the field excitation current is constant and the shaft torque is $T = 20$ Nm = *const* find:

(a) the speed n;
(b) the speed n' with additional armature series resistance $R_{rhe} = 5\Omega$;
(c) the speed–torque characteristics for $\sum R_a = 0.3\Omega$ and $\sum R_a + R_{rhe} = 5.35\Omega$.

The armature reaction is neglected and the brush voltage drop is $\Delta V_{br} = 2$ V.

Solution

The rated EMF

$$E = V - I_a \sum R_a - \Delta V_{br} = 220.0 - 20.6 \times 0.3 - 2.0 = 211.82 \text{ V}$$

The rated angular speed

$$\Omega_r = 2\pi n = 2\pi \frac{1200}{60} = 125.6 \text{ rad/s}$$

The armature constant

$$c_E \Phi = \frac{E}{n} = \frac{211.82 \times 60}{1200} = 10.591 \text{ Vs}$$

The rated shaft torque

$$T_r = \frac{P_{out}}{\Omega_r} = \frac{4000}{125.6} = 31.85 \text{ Nm}$$

The rated developed torque

$$T_{dr} = \frac{c_E \Phi}{2\pi} I_a = \frac{10.591}{2\pi} 20.6 = 34.72 \text{ Nm}$$

The torque corresponding to the rotational losses at no load

$$T_0 = T_{dr} - T_r = 34.72 - 31.85 = 2.87 \text{ Nm}$$

The electromagnetic torque developed by the motor at $T = 20$ Nm

$$T_{d20} = T_0 + T = 2.87 + 20.0 = 22.87 \text{ Nm}$$

The armature current at shaft torque $T = 20$ Nm

$$I_{a20} = \frac{T_{d20}}{c_E \Phi} 2\pi = \frac{22.87}{10.591} 2\pi = 13.57 \text{ A}$$

The speed at $V = 110\,\text{V}$ and $T = 20$ Nm

$$n = \frac{1}{c_E \Phi}(0.5V - I_{a20} \sum R_a - \Delta V_{br})$$

$$= \frac{1}{10.591}(110.0 - 13.57 \times 0.3 - 2.0) = 9.81 \text{ rev/s} = 588 \text{ rpm}$$

The corresponding angular speed

$$\Omega = 2\pi n = 2\pi \times 9.81 = 61.64 \text{ rad/s}$$

The speed at $V = 110$ V, $T = 20$ Nm and armature resistance $R_{rhe} = 5\ \Omega$

$$n' = \frac{1}{c_E \Phi}[0.5V - I_{a20}(\sum R_a + R_{rhe}) - \Delta V_{br})]$$

$$= \frac{1}{10.591}[110.0 - 13.57(0.3 + 5.0) - 2.0] = 3.4 \text{ rev/s} = 204.4 \text{ rpm}$$

The corresponding angular speed

$$\Omega' = 2\pi n' = 2\pi \times 3.4 = 21.36 \text{ rad/s}$$

The no-load speed at $V = 220$ V

$$n_0 = \frac{1}{c_E\Phi}(V - \Delta V_{br}) = \frac{1}{10.591}(220 - 2) = 20.58 \text{ rev/s} = 1235 \text{ rpm}$$

The no-load speed at $V = 110$ V

$$n_0' = \frac{1}{c_E\Phi}(0.5V - \Delta V_{br}) = \frac{1}{10.591}(110 - 2) = 10.20 \text{ rev/s} = 611.8 \text{ rpm}$$

The characteristics are plotted in Fig. 2.9.

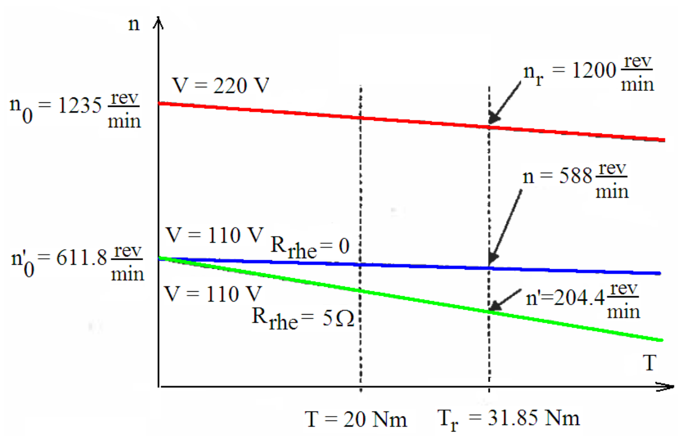

Fig. 2.9. Speed–torque characteristics for $V = 220$ V ($R_{rhe} = 0$), $V = 110$ V ($R_{rhe} = 0$), and $V = 110$ V and with the armature circuit rheostat $R_{rhe} = 5.0\Omega$.

2.8 Braking

In some duties that require rapid retardation, it is necessary to brake a motor during the operating period. A speed reduction from Ω_1 to Ω_2 during braking time $0 \leq t \leq t_b$ of a system of inertia J requires a braking power P_b (see Table 1.6). These quantities may be related by the equation

$$E_k = \int_0^{t_b} P_b dt = \frac{1}{2}J(\Omega_1^2 - \Omega_2^2) \tag{2.47}$$

In practice the braking time t_b is shortened by rotational losses and by the presence of any load torque.

The three electrical braking methods which are now considered in terms of shunt and series d.c. motors are:

- rheostatic braking;
- counter current braking (plugging);
- regenerative braking.

2.8.1 Braking a shunt d.c. motor

Rheostatic braking.

The armature is disconnected from the supply and then connected across a resistor R_b. The machine then acts as a generator, driven by its stored kinetic energy and dissipating power in its armature circuit resistance. Since $V = 0$ and $E < 0$, the armature current is reversed, and

$$I_a = \frac{-E}{\sum R_a + R_b} < 0 \tag{2.48}$$

The brush voltage drop ΔV_{br} has been neglected.

Counter-current braking.

The armature terminal connections are reversed so that the supply voltage, now augmented by the rotational EMF, imposes a large current and a strong braking torque. To intensify the braking, the resistance $\sum R_a + R_b$ is reduced by changing R_b. The braking current is very high (since $E < 0$), and is written as

$$I_a = \frac{-V - E}{\sum R_a + R_b} \tag{2.49}$$

Regenerative braking

If the rotational EMF is greater than the applied voltage (that is, if $V < E$), then the machine generates electrical energy and produces a braking torque by current reversal where

$$I_a = \frac{V - E}{\sum R_a + R_b} \tag{2.50}$$

This is maintained down to the speed at which the EMF and voltage balance. The speed of a shunt motor must be higher than the no-load speed n_o. A motor undergoes regenerative braking if forced by the driven machine to run at a speed exceeding n_o. Visualise, for example, a train riding down-hill.

2.8.2 Braking a series d.c. motor

Rheostatic braking.

The field and armature windings, being connected in series, are cut off from the power circuit and closed on a load resistance R_b.

Counter-current braking.

This type of braking can be accomplished in two ways: (a) when the driven machine forces the motor to rotate in the opposite direction to the developed torque, and (b) by reversing both the armature current and the direction of rotation.

Regenerative braking.

The field and armature windings must be connected in parallel or separately excited.

2.9 Permanent magnet d.c. commutator motors

2.9.1 Permanent magnet materials

A permanent magnet (PM) material is described by the *demagnetization curve* which is a portion of the full B—H hysteresis loop located in the second quadrant in the magnetic flux density B versus magnetic field intensity H coordinate system. The *coercive force* H_c corresponds to $B = 0$ and the *remanent magnetic flux density* B_r corresponds to $H = 0$.

There are three classes of PM materials that are used for electric motors. These are listed below, and their demagnetization curves are given in Fig. 2.10:

- Alnicos (Ni, Al, Fe, Co, Cu, Ti);
- ceramics (ferrites), e.g. barium ferrite $BaO \times 6Fe_2O_3$;
- rare-earth materials, e.g. samarium–cobalt SmCo and neodymium–iron–boron NdFeB.

The main advantages of *Alnico* are its high magnetic remanent flux density and low temperature coefficients for B_r and H_c. These advantages permit a high airgap flux density and high operating temperatures. Unfortunately, the demagnetization curve is extremely nonlinear and the coercive force is very low. Therefore it is very easy not only to magnetize but also to demagnetize Alnico. Alnico is used in PM disc commutator motors, where the airgap is relatively large. This results in a negligible armature reaction. Sometimes, the Alnico PMs are protected from the armature field, and consequently from demagnetization, by means of additional soft-iron pole shoes. Alnico magnets are still used in motors having ratings in the range 500 W to 150 kW.

A *ferrite* has a higher coercive force than that of Alnico, but at the same time has a lower remanent magnetic flux density. The temperature coefficient of the remanent flux density is relatively high. The main advantages of ferrites are their low cost and their very high resistance which means that no eddy-current losses are suffered in the PM volume. Ferrite magnets are most economical when used in fractional horsepower motors and they tend to have an economic advantage over Alnico up to about 7.5 kW.

During the last two decades great progress in improving the available energy density $(BH)_{max}$ has been achieved with the development of the *rare-earth* PMs. The rare-earth elements are (in general) not rare at all, but their natural minerals are usually mixed compounds. To produce a given rare-earth metal, several others,

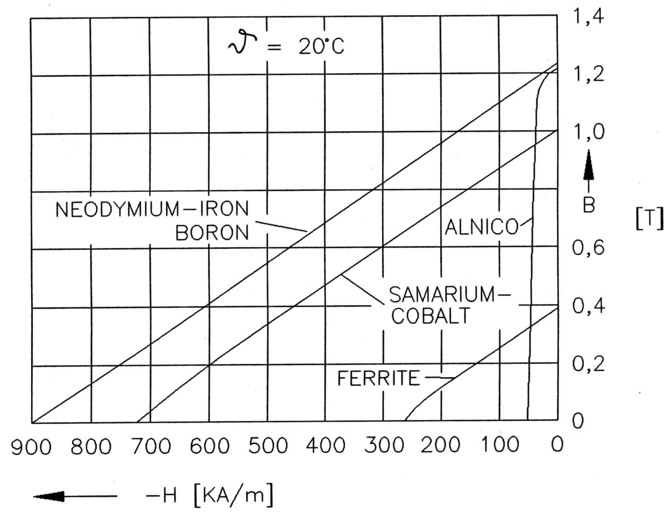

Fig. 2.10. Demagnetization curves for different PM materials.

for which no commercial application exists, may also have to be refined from the available ore, and this limits the availability of such metals. The first generation of these new alloys was based on the composition $SmCo_5$ (samarium-cobalt), and has been in commercial production since the early 1970s. Today it is a well-established magnetic material. SmCo has the advantage of having high remanent flux density, high coercive force, a high energy product, a linear demagnetization curve and a low temperature coefficient. It is very suitable for building motors that have low volume, and which consequently display high specific powers and low moments of inertia. The cost is the only drawback. Both Sm and Co are relatively expensive due to their restricted supply.

With the discovery in the early 1980s of a second generation of rare-earth magnets based on the inexpensive metals Fe and Nd (neodymium) — a much more abundant rare-earth element than Sm — remarkable progress in lowering of raw material costs has been achieved. The NdFeB magnets, which are now produced in increasing quantities, have better magnetic properties than those of SmCo, but unfortunately only at room temperature. Several of their properties, and particularly the coercive force, are strongly temperature dependent (Curie temperature = 310^0C). However, the manufacturers of PMs promise NdFeB products that will have lower temperature coefficients and even lower cost in due course. Although NdFeB is unfortunately susceptible to corrosion, NdFeB magnets have a great potential for a considerably improved *performance–to–cost* ratio for many applications. For this reason they will have a major impact on the development and application of PM equipment in the future.

The rare-earth magnet materials are costly, but are the best economic choice in small motors. They might have a cost advantage in very large motors (ship propulsion), as well.

2.9.2 Construction of d.c. permanent magnet motors

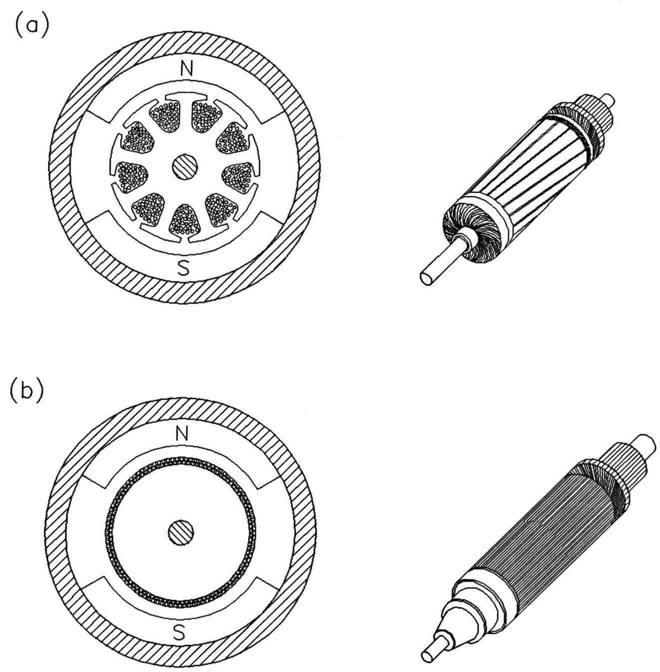

Fig. 2.11. Construction of d.c. PM commutator motors with laminated-core rotors: (a) slotted rotor, (b) slotless rotor.

PMs mounted on the stator (Fig. 2.11) produce a constant field flux Φ. Furthermore, the developed torque, T_d, and the armature EMF, E, are:

$$T_d = k_T I_a \qquad \text{and} \qquad E = k_E n \tag{2.51}$$

where $k_T = c_T \Phi$ and $k_E = c_E \Phi$. From the above equations and eqn (2.1) it is possible to obtain the steady-state speed n as a function of T_d for a given V, to arrive at

$$n = \frac{1}{k_E} (V - \Delta V_{br}) - \frac{\sum R_a}{k_E k_T} T_d \tag{2.52}$$

The family of curves $n = f(T_d)$ generated by eqn (2.52) are plotted in Fig. 2.12. As the torque is increased, the speed–torque characteristic at any given V is essentially horizontal, except for the drop due to the voltage drop $I_a \sum R_a$ across the armature-circuit resistance, to the brush voltage drop ΔV_{br}, and to the armature reaction. The speed–torque characteristics in Fig. 2.12 can be shifted vertically by controlling the applied terminal voltage V. Therefore, the speed of a load with an arbitrary speed–torque characteristic can be controlled by controlling V (with $\Phi = const$).

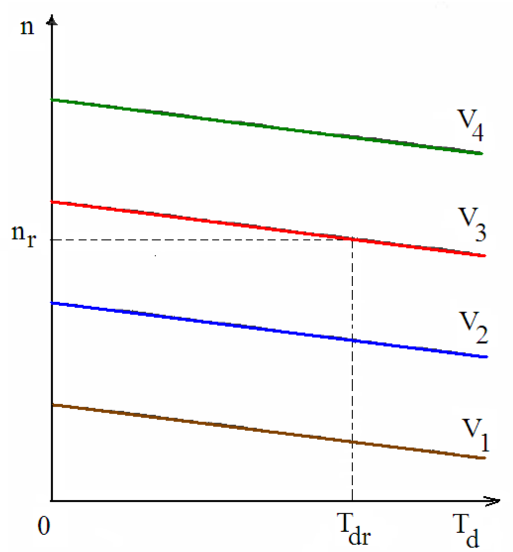

Fig. 2.12. Speed-torque curves at $V_1 < V_2 < V_3 < V_4$ for a d.c. PM commutator motor.

Magnetic circuit configurations of cylindrical-rotor PM motors for different types of PMs are shown in Fig. 2.13. Note the four fundamental armature (rotor) structures shown in Figs 2.11, 2.14 and 2.15. These are listed below:

- the conventional slotted rotor (Fig.2.11a);
- the slotless (surface wound) rotor (Fig.2.11b);
- the moving-coil cylindrical rotor (Fig.2.14a, Fig.2.15);
- the moving-coil disk (pancake) rotor (Fig.2.14b,c).

The *slotted-rotor* and *slotless-rotor* PM commutator motors have their armature winding fixed to the laminated core. Hence, the armature winding, the armature core, the commutator and the shaft comprise one integral part.

The *moving-coil d.c. motor* has its armature winding fixed to an insulating cylinder or disc which rotates between PMs or between PMs and a laminated core. Note that the moment of inertia of the rotor is very small, and that since in a moving-coil motor all iron cores are stationary (i.e. they do not move in the magnetic flux), no eddy-currents or hysteresis losses are produced in them. The efficiency of a moving-coil motor is thus better than that of a slotted rotor motor.

The mechanical time constant

$$T_m = \frac{2\pi n_0 J}{T_{dst}} = \frac{2\pi n_0 J}{c_T \Phi I_{ast}} = \frac{2\pi n_0 J}{k_T I_{ast}} \tag{2.53}$$

of moving-coil motors is much smaller than that of iron-core armature motors. In the above equation J is the moment of inertia of the rotor, n_0 is the no-load speed, T_{dst} is the starting electromagnetic torque, c_T is the torque constant, Phi is the magnetic flux and I_{ast} is the starting armature current.

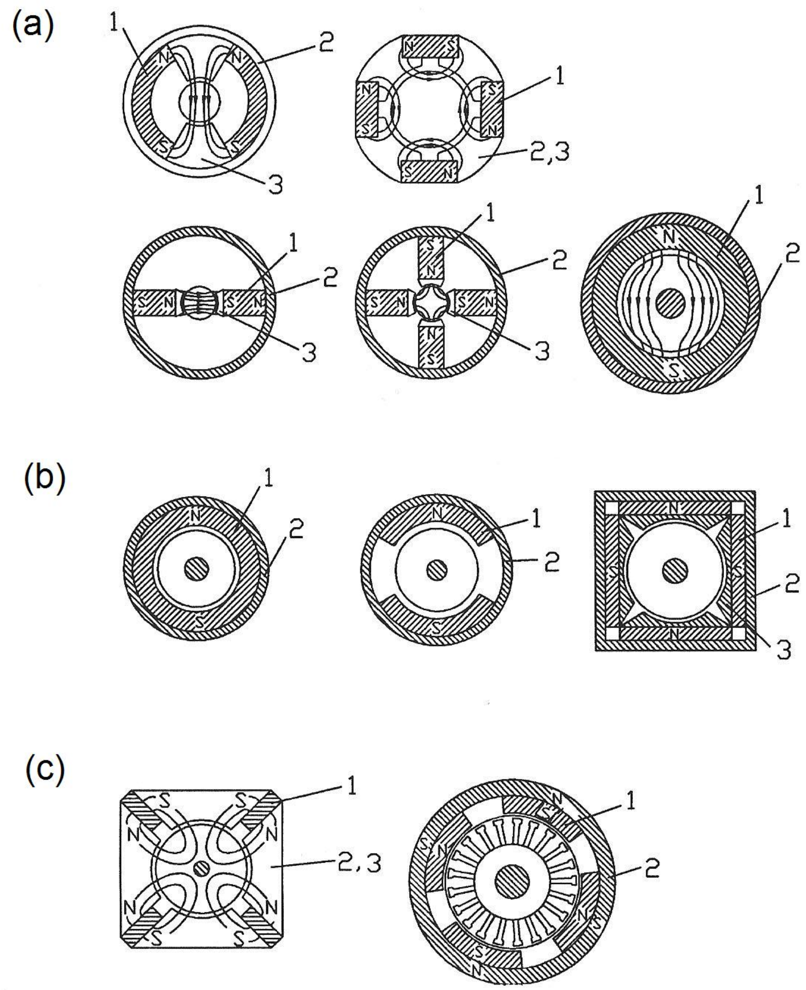

Fig. 2.13. Excitation systems of commutator motors with laminated-core rotors using different types of PMs: (a) Alnico; (b) ferrites; (c) rare-earth. 1 — PM, 2 — mild steel yoke, 3 — pole shoe.

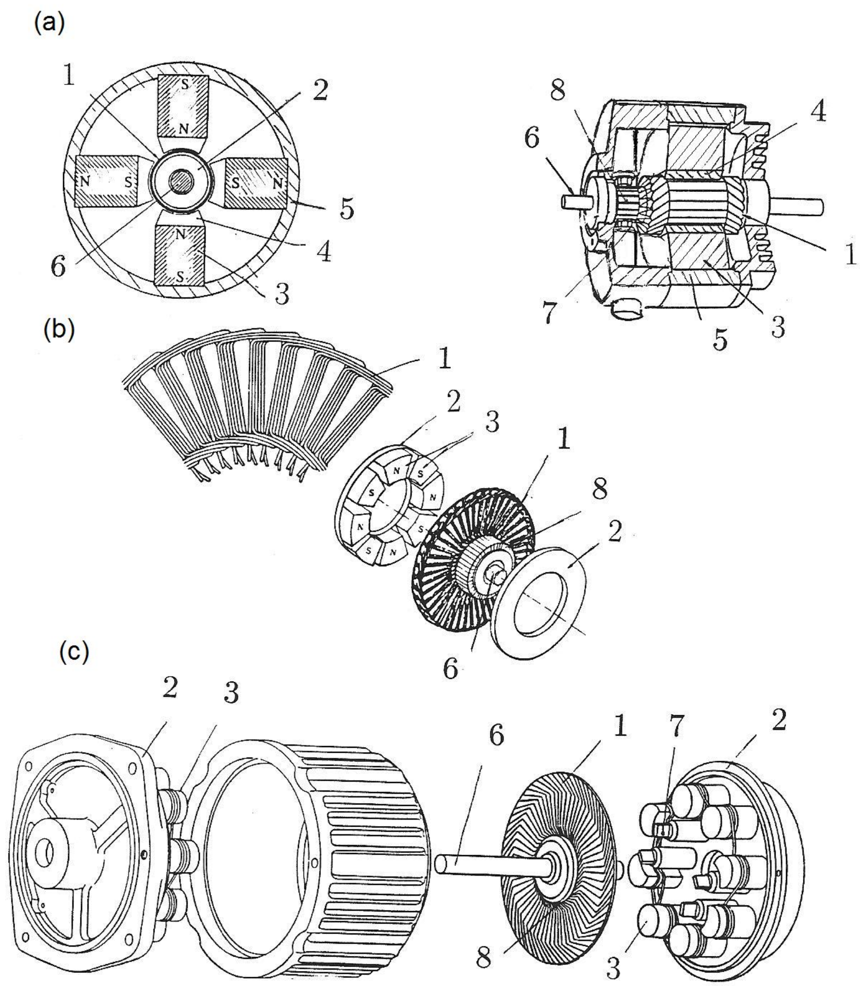

Fig. 2.14. Outside-field type moving coil PM commutator motors: (a) cylindrical motor; (b) disc motor with wound rotor; (c) disc motor with printed rotor winding. 1 — moving coil armature winding, 2 — mild steel yoke, 3 — PM, 4 — pole shoe, 5 — mild steel frame, 6 — shaft, 7 — brush, 8 — commutator.

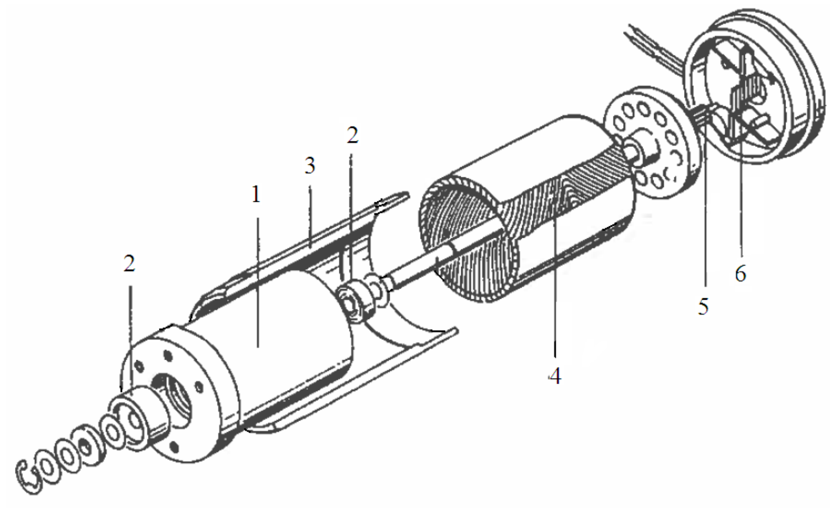

Fig. 2.15. Inside-field type cylindrical moving coil motor: 1 — PM, 2 — sleeve bearing, 3 — steel frame (magnetic circuit), 4 — armature winding, 5 — commutator, 6 — precious metal brushes.

2.9.3 Slotted-rotor PM d.c. motors

The core of a slotted rotor is made from laminated silicon steel sheet or carbon steel sheet, and the rotor windings are located in slots cut into the core. In the slotted rotor, the torque acts directly on the solid iron core, and not on the fragile coils alone. The slotted rotor is mechanically much more durable than a moving coil motor. A core having many slots is usually desirable because the greater the number of slots, the less the torque ripple (called *cogging*) and the less the electromagnetic noise. Cores having even numbers of slots are often used for the motors manufactured by an automated mass-production process, because of their relative ease of production. However, cores with odd numbers of slots are often preferred because they exhibit lower cogging torque.

Twisting the rotor laminations (*skewing*, as depicted in Fig. 2.11a) reduces the cogging and detent torque that is produced by the interaction between the rotor teeth and the pole shoes.

2.9.4 Slotless rotor PM motors

Extremely low cogging torque can be produced by fixing the windings on a cylindrical iron core without using slots (as in Fig. 2.11b). In this case the torque is exerted directly on the conductors in accordance with Fleming's left-hand rule (Appendix A). However, it is likely that the flux will decrease since the gap between the rotor core and the pole shoes is large. Therefore, rare-earth magnets or large Alnico magnets must be used to ensure sufficient magnetic flux.

2.9.5 Moving-coil cylindrical motors

Cylindrical outside-field type.

This type of motor (Fig. 2.14a) has the smallest electromechanical time constant. In order to obtain a small T_m, the ratio Φ/J must be as large as possible. One way to achieve this is to use an anisotropic Alnico magnet, which will produce more flux because it has a high remanence, B_r, and a low coercive force, H_c. Since Alnico magnets are easy to demagnetize, a long magnet, magnetized lengthwise, is used in order to avoid demagnetization. Some of the motors in which Alnico magnets are employed in this way can have a mechanical time constant of less than 1 ms.

Cylindrical inside-field type.

Moving-coil motors of the inner-field type, which are also known as coreless motors, are often used for applications of less than 10 W, but one also sometimes finds motors in this class with outputs near 30 W. This type of motor has a PM inside the moving-coil armature. Though the moment of inertia of this rotor is small, the electromechanical time constant is not always low, because little magnetic flux is obtained from the magnet which must be placed inside the armature and which is therefore necessarily of limited size. However, coreless motors are much used for driving the capstans of audio casette players and video tape recorders, the zoom lenses of cameras, etc. because: (a) they have very small size and high efficiency; and (b) they exhibit low cogging.

The inside-field type cylindrical moving coil motor is shown in Fig. 2.15. The different armature windings are classified as follows: (a) honeycomb winding; (b) rhombic winding; (c) bell winding; (d) ball winding [30].

2.9.6 Disc motors

There are two main types of disc (pancake) commutator motors: the wound-rotor motor and the printed armature winding motor.

In the *pancake wound-rotor motor* [8] the winding is usually made of magnetic wires and moulded with resin (as in Fig. 2.14b). The type of commutator is identical to the conventional type. Motors of this type can often be found, for example, in radiator fans.

The *disc-type printed armature winding motor* is shown in Fig. 2.14c. The coils are stamped from pieces of sheet copper and then welded, forming a wave winding. When this motor was invented by J. H. Baudot [3], the armature was made using a similar method to that by which printed boards are manufactured. Hence this is called a printed motor. The magnetic flux of the printed motor can be produced using either Alnico or ferrite magnets.

Exanple 2.2.

A two-pole, 380 W, 180 V, 1950 rpm, $\eta = 0.84$ d.c. commutator motor with segmental PMs has $N = 920$ armature conductors and armature circuit resistance

$\sum R_a = 5.84\ \Omega$. The effective length of the armature core $L_i = 0.064$ m, the armature diameter $D = 0.12$ m, the efefctive pole arc coefficient $\alpha_i = 0.75$, the number of pairs of armature parallel paths $a = 1$ and the brush voltage drop $\Delta V_{br} \approx 2$ V. Find: (a) the armature constant k_E and torque constant k_T, (b) the magnetic flux Φ and airgap magnetic flux density B_g, (c) the mechanical time constant T_m and (d) speed at 40% of the rated voltage and rated torque. The armature reaction is neglected.

Solution

(a) The armature constant and torque constant

The rated armature current

$$I_a = \frac{P_{out}}{V\eta} = \frac{380}{180 \times 0.84} = 2.51 \text{ A}$$

The EMF

$$E = V - I_a \sum R_a - \Delta V_{br}$$

$$= 180 - 2.51 \times 5.84 - 2 = 163.34 \text{ V}$$

The armature constant

$$k_E = \frac{E}{n} = \frac{163.34}{1950/60} = 5.026 \text{ Vs}$$

The torque constant

$$k_T = \frac{k_E}{2\pi} = \frac{5.026}{2\pi} = 0.8 \text{ Nm/A}$$

(b) The magnetic flux and airgap magnetic flux density

Since

$$k_T = \frac{N}{a}\frac{p}{2\pi}\Phi$$

the airgap magnetic flux density is

$$\Phi = \frac{2\pi a k_T}{Np} = \frac{2\pi \times 1 \times 0.8}{920 \times 1} = 0.00546 \text{ Wb}$$

The pole pitch

$$\tau = \frac{\pi D}{2p} = \frac{\pi \times 0.12}{2} = 0.1885 \text{ m}$$

The airgap magnetic flux density

$$B_g = \frac{\Phi}{\alpha_i \tau L_i} = \frac{0.00546}{0.75 \times 0.1885 \times 0.064} = 0.6 \text{ T}$$

(c) The mechanical time constant

The mass of the armature (rotor)

$$m_a = 1.1\rho\frac{\pi D^2}{4}L_i = 1.1 \times 8000\frac{\pi \times 0.12^2}{4} \times 0.064 \approx 6.37 \text{ kg}$$

It has been assumed that the average mass of the armature is $\rho = 8000$ kg/m^3 and 10% has been allowed for the commutator and shaft.

The moment of inertia of the armature

$$J = m_a\frac{D^2}{8} = 6.37\frac{0.12^2}{8} = 0.01147 \text{ kgm}^2$$

The speed at no load

$$n_0 \approx \frac{V}{k_E} = \frac{180}{5.026} = 35.8 \text{ rev/s} = 2149 \text{ rpm}$$

The starting current ($E = 0$)

$$I_{ast} = \frac{V - \Delta V_{br}}{\sum R_a} = \frac{180 - 2}{5.84} = 30.48 \text{ A}$$

The mechanical time constant

$$T_m = \frac{2\pi n_0 J}{k_T I_{ast}} = \frac{2\pi 35.8 \times 0.01147}{0.8 \times 30.48} \approx 0.1 \text{ s}$$

(d) The speed at 40% rated voltage and rated torque

The speed–torque equation

$$n = \frac{1}{5.026}(V - \Delta V_{br}) - \frac{5.84}{0.8 \times 5.026}T_d = 0.199(V - \Delta V_{br}) - 1.452T_d$$

For $V = 180$ V and $T_d = 2$ Nm the speed is $n = 35.422 - 2.904 = 32.5$ rev/s $= 1951$ rpm. For $V' = 0.4V = 0.4 \times 180 = 72$ V and $T_d = 2$ Nm the speed is

$$n' = 0.199(72 - 2) - 1.452 \times 2 = 13.93 - 2.904 = 11.03 \text{ rev/s} \approx 662 \text{ rpm}$$

Problems

1. On no-load, the speed of a d.c. motor is $n_0 = 950$ rpm. Calculate the speed when the load is such that the armature current is $I_a = 25$ A. The terminal voltage is $V = 400$ V $= const$, the armature circuit resistance is $\sum R_a = 0.15\ \Omega$, the brush voltage drop is $\Delta V_{br} = 2$ V, and the armature reaction is to be neglected.

   Answer: $n = 941$ rpm

2. A 25 kW d.c. shunt motor has the following rated parameters: $V_r = 220$ V, $I_r = 127$ A, $n_r = 1800$ rpm, $I_{fr} = 2.1$ A. The no-load speed is $n_o = 1850$ rpm. Find: (a) the resistance R_{st} of a starting rheostat to obtain the starting current $I_{st} = 2I_r$ and (b) the starting torque corresponding to R_{st} if the voltage across the shunt-field winding terminals is $V_f = V_r = 220$ V.
   Assumptions: (i) the open circuit characteristic (magnetization curve) $E = f(I_f)$ is linear; (ii) the armature reaction is neglected; (c) the brush contact voltage drop is neglected.

   Answer: (a) $R_{st} = 0.827\ \Omega$, (b) $T_{st} = 2.01T_r$
3. A 5.5 kW d.c. separately excited motor has a terminal voltage $V_r = 220$ V at rated current $I_{ar} = 30.5$ A and rated speed $n_r = 750$ rpm. The resistance of the armature circuit is $\sum R_a = 0.4\ \Omega$. Find: (a) the armature current at the first instant when the terminal voltage drops from $V_r = 220$ V down to $V' = 200$ V and (b) the steady-state speed n' at $V' = 200$ V.
   The armature reaction, brush contact voltage drop and armature winding inductance are neglected.

   Answer: (a) $I_a(t = 0) = -19.5$ A $(E > V)$, (b) $n' = 678$ rpm
4. A 13 kW, 220 V, 71 A, 600 rpm d.c. shunt motor has armature circuit resistance $\sum R_a = 0.25\ \Omega$ and shunt field resistance $R_f = 110\ \Omega$. The motor is loaded with the rated torque at rated voltage. Find: (a) the resistance of an armature rheostat needed to obtain the speed $n' = 200$ rpm and (b) the output power P'_{out} and input power P'_{in} required to obtain the speed $n' = 200$ rpm.
   The armature reaction and brush contact voltage drop are neglected.

   Answer: (a) $R_{rhe} = 1.96\ \Omega$, (b) $P'_{out} = 4.33$ kW, $P'_{in} = 15.6$ kW
5. A 22 kW, 220 V, 111 A, 1200 rpm d.c. separately excited motor has armature circuit resistance $\sum R_a = 0.1\ \Omega$. The rated field excitation current is $I_{fr} = 2$ A and the rated voltage across the excitation winding is $V_{fr} = 220$ V. Find: (a) the input voltage V' at the rated field current, rated torque and speed $n' = 0.5n_r$ and (b) the input and output power under the conditions given above.
   The armature reaction and brush contact voltage drop are neglected.

   Answer: (a) $V' = 115.45$ V, (b) $P'_{out} = 11$ kW, $P'_{in} = 13.1$ kW
6. A 36 kW, 600 V, 860 rpm, 73 A d.c. series motor has armature circuit resistance $\sum R_a = 0.35\ \Omega$ (including the series-field resistance R_{se}). The motor has been cut off from the power supply and closed on a load resistance $R_{rhe} = 8\ \Omega$ (this is dynamic braking). The open circuit characteristic (also called the magnetization curve) in relative units is given below:

E/E_r	0.058	0.87	1.16	1.28	1.40
I_a/I_{ar}	0	0.50	1.0	1.25	1.60

   Find the armature current I_{ab} and braking torque T_b if the rotor speed is $n_b = 1000$ rpm.
   Assumptions: (i) the nonlinearity of the magnetization curve is to be included; (b) the armature reaction is neglected, (c) the brush contact voltage drop is neglected.

   Answer: (a) $I_{ab} = 86.0$ A; (b) $T_b = 555.6$ Nm

7. A 30 kW, 220 V, 153 A, 3000 rpm d.c. shunt motor has the armature circuit resistance $\sum R_a = 0.07\ \Omega$ and the field excitation current $I_f = 2$ A. The motor had worked under rated conditions. At an instant $t = 0$ the armature terminal connections were reversed and a resistance R_b was inserted in the armature circuit (counter-current braking). Find: (a) the resistance R_b if the braking torque at $t = 0$ is $T_b = 2T_r$, (b) the input power and power dissipated in the resistance R_b at $t = 0$ and (c) the energy dissipated in the resistance R_b during braking, if the speed changes with time according to equation $n_b = n(1 - t/\tau)$ for $0 \leq t \leq \tau$ and $\tau = 10$ s. At $t = \tau$ the machine was switched off.
   Assumptions: (i) the characteristics $E = f(I_f)$ of the magnetic circuit is linear, (ii) the armature reaction is neglected, (c) the inductance of the armature winding is negligible, (d) the brush contact voltage drop is neglected.

   Answer: (a) $R_b = 1.63\ \Omega$, (b) $P_{inb}(t = 0) = 66.7$ kW, $P_b(t = 0) = 12.3$ kW, (c) 0.203 kWh
8. A two-pole, 750 W, 220 V, 1200 rpm, $\eta = 0.85$ d.c. commutator motor with segmental PMs has the armature circuit resistance $\sum R_a = 4.06\ \Omega$. The airgap magnetic flux density is $B_g = 0.63$ T, the effective length of the armature core $L_i = 0.084$ m, the armature diameter $D = 0.12$ m, the effective pole arc coefficient $\alpha_i = 0.8$, the number of pairs of armature parallel paths $a = 1$ and the brush voltage drop $\Delta V_{br} \approx 2$ V. Find: (a) the armature constant k_E and torque constant k_T, (b) the developed torque T_d and shaft torque T, (c) the number of armature conductors N, (d) the armature electric loading A and (e) the speed at 60% of the rated voltage and shaft torque $T = 2.5$ Nm. The armature reaction is neglected.

   Answer: (a) $k_E = 10.09$ Vs, $k_T = 1.6$ Nm/A, (b) $T_d = 6.4$ Nm, $T = 5.97$ Nm, (c) $N = 1260$, (d) $A = 6684.5$ A/m, (e) $n' \approx 729$ rpm.

3

THREE-PHASE INDUCTION MOTORS

3.1 Construction

Typical three-phase induction motors are shown in Fig. 3.1. Fig. 3.1a shows a low-power, three-phase *cage induction motor*, while Fig. 3.1b shows a medium-power, three-phase *induction motor with a wound rotor* (or *slip-ring rotor*).

The stator consists of a laminated core with a three-phase winding embedded in slots (Appendix B). This winding, when energized by a three-phase source of power, provides a *rotating magnetic field* (Appendix C).

The rotor windings are also contained in slots in a laminated core which is mounted on the shaft. In small motors, the rotor-lamination stack is pressed directly on the shaft. In larger machines, the core is mechanically connected to the shaft through a set of spokes called a 'spider'.

Cage–rotor windings consist of solid bars of conducting material which are positioned in the rotor slots. These *rotor bars* are shorted together at the two ends of the rotor by *end rings*. In large machines, the rotor bars may be made of copper alloy, which is driven into the slots and then brazed to the end rings. Rotors up to about 0.5 m in diameter usually have die cast aluminium cage windings. The core laminations for such rotors are stacked in a mould, which is then filled with molten aluminium. In this industrial process, the rotor bars, the end rings and the cooling-fan blades are all cast at the same time (Fig. 3.1a).

Cage induction motors are cheaper and more reliable than comparable wound–rotor motors.

The winding of a wound rotor is a polyphase winding, consisting of coils. It is almost always a three-phase Y-connected winding. The three terminal leads are connected to *slip rings*, mounted on the shaft. Carbon brushes riding on these slip rings are shorted together for normal operation. External resistances are inserted into the rotor circuit, via the brushes, which improves the motor's starting characteristics. As the motor accelerates, the external resistances are gradually reduced to zero. Another external resistance can also be used to control the speed (in a continuous duty cycle).

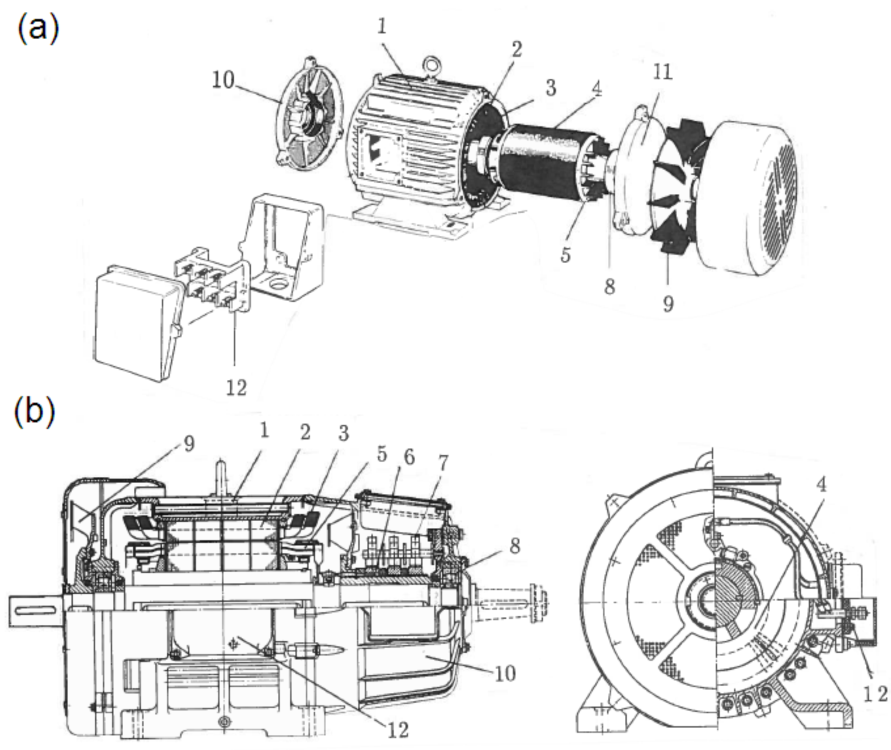

Fig. 3.1. Three-phase rotary induction motors: (a) with cage rotor, (b) with wound (slip-ring) rotor. 1 — frame, 2 — stator core, 3 — stator winding, 4 — rotor core, 5 — rotor winding, 6 — slip rings, 7 — brushes, 8 — bearing, 9 — cooling fan, 10 — end bell, 11 — cowl, 12 — terminal board.

3.2 Fundamental relationships

3.2.1 Slip

The *slip* (per unit) is the ratio of the *slip speed* $(n_s - n)$ to the synchronous speed n_s of the rotating magnetic field, i.e.

$$s = \frac{n_s - n}{n_s} = 1 - \frac{n}{n_s} \tag{3.1}$$

where $n_s = f/p$ is the *synchronous speed* in rev/s, f is the input frequency, p is the number of pole pairs, and n is the rotor speed. The slip speed $(n_s - n)$ expresses the speed of the rotor relative to the rotating field of the stator.

3.2.2 Rotor speed

According to eqn (3.1), the *rotor speed* is a function of the input frequency f, the number of pole pairs p, and the slip s. Thus:

$$n = n_s(1 - s) = \frac{f}{p}(1 - s) \tag{3.2}$$

The current in the rotor creates its own magnetic field rotating with a speed that is given by

$$n_{rot} = sf/p = sn_s \tag{3.3}$$

Since $n_s(1 - s) + n_{rot} = n_s$, the stator and rotor magnetic fields rotate with the same speed.

3.2.3 Input power

The electrical *input active power* delivered to the motor is

$$P_{in} = m_1 V_1 I_1 \cos\phi \tag{3.4}$$

where m_1 is the number of stator phases, V_1 is the input phase voltage, I_1 is the input phase current, $\cos\phi$ is the power factor, and ϕ is the phase angle between voltage and current.

3.2.4 Electromagnetic power

The *electromagnetic power* (or airgap power) is the active power crossing the airgap from the stator to the rotor, written

$$P_g = P_{in} - \Delta P_{1w} - \Delta P_{1Fe} \tag{3.5}$$

where the *stator winding* (or copper) *losses* are

$$\Delta P_{1w} = m_1 I_1^2 R_1 \tag{3.6}$$

and the *stator core losses* (comprising hysteresis ΔP_{1h} and eddy–current losses ΔP_{1e}) are

$$\Delta P_{1Fe} = \Delta P_{1h} + \Delta P_{1e} \tag{3.7}$$

In the above equations R_1 is the a.c. stator winding resistance, hysteresis losses ΔP_{1h} are proportional to fB^2 and eddy–current losses ΔP_{1e} are proportional to f^2B^2, where B is the magnetic flux density in the stator core's teeth or yoke.

3.2.5 Electromagnetic (developed) torque

The *electromagnetic torque* developed by the motor is

$$T_d = \frac{P_g}{\Omega_s} = \frac{P_g}{2\pi n_s} \tag{3.8}$$

where $\Omega_s = 2\pi n_s$ is the *synchronous angular speed*. Another quantity, the *stator angular frequency*, is written as $\omega_s = 2\pi f$).

The following relationship exists between the synchronous angular speed Ω_s and the *stator angular frequency* ω_s:

$$\Omega_s = 2\pi n_s = 2\pi \frac{f}{p} = \frac{\omega_s}{p} \tag{3.9}$$

3.2.6 Mechanical power

The developed *mechanical power* is obtained by subtracting the rotor losses from the electromagnetic (airgap) power, to obtain

$$P_m = P_g - \Delta P_{2w} - \Delta P_{2Fe} \approx P_g - \Delta P_{2w} \tag{3.10}$$

since the rotor hysteresis losses $\Delta P_{2h} \propto sf$, eddy current losses in the rotor core $\Delta P_{2e} \propto s^2 f^2$, and the rotor total core losses $P_{2Fe} \propto s(f + sf^2)$ are all negligible (except in the case of inverter-fed motors). In terms of the developed torque, T_d,

$$P_m = T_d \Omega = 2\pi n T_d \tag{3.11}$$

where $\Omega = 2\pi n = \Omega_s(1 - s)$ is the *rotor angular speed.*

Combining eqns (3.8) and (3.11) leads to

$$\frac{P_g}{P_m} = \frac{n_s}{n} = \frac{1}{1 - s} \tag{3.12}$$

and thus

$$P_m = P_g(1 - s) \tag{3.13}$$

3.2.7 Rotor winding losses

The *rotor winding losses* are calculated in the same way as those in the stator winding, namely as

$$\Delta P_{2w} = m_2 I_2^2 R_2 = m_1 (I_2')^2 R_2' \tag{3.14}$$

where m_2 is the number of rotor phases, I_2 is the rotor current, I_2' is the rotor current referred to the stator winding, R_2 is the a.c. rotor resistance and R_2' is the rotor a.c. resistance referred to the stator winding.

3.2.8 Voltage induced in the stator winding

The *voltage induced* (or EMF) per phase in the stator winding is given by the equation

$$E_1 = 4\sigma_f f N_1 k_{w1} \Phi \tag{3.15}$$

where σ_f is the *form factor* of the induced voltage (i.e. the ratio of its *rms* value to average value), f is the input frequency, N_1 is the number of stator turns per phase, k_{w1} is the stator winding factor (Appendix D), and Φ is the magnetic flux. For sinusoids, $\sigma_f = \pi\sqrt{2}/4 \approx 1.11$ and the stator winding EMF is then expressed as

$$E_1 = \pi\sqrt{2} f N_1 k_{w1} \Phi = 4.44 f N_1 k_{w1} \Phi \tag{3.16}$$

The *magnetic flux* is

$$\Phi = \alpha_i \tau L_i B_{mg} \tag{3.17}$$

where α_i is the ratio of the *average to the peak value* of the airgap magnetic flux density, $\tau = \pi D/(2p)$ is the stator pole pitch, D is the stator core inner diameter, L_i is the effective length of the stator core and B_{mg} is the peak value of the airgap magnetic flux density. Once again, for sinusoids, $\alpha_i = 2/\pi \approx 0.637$ and so the flux is

$$\Phi = \frac{2}{\pi} \tau L_i B_{mg} \tag{3.18}$$

The last eqn (3.18) can be obtained by integrating the sinusoidal distribution of magnetic flux density in the airgap over one pole pitch τ, i.e.

$$\Phi = L_i \int_0^\tau B_{mg} \sin\left(\frac{\pi}{\tau} x\right) dx = \frac{2}{\pi} \tau L_i B_{mg}$$

3.2.9 Stator winding factor

For chorded coils, with chord pitch $w_c < \tau$, the *stator winding factor* is the product of the stator distribution factor k_{d1} (expressing the distribution of the stator coils in the slots) and the stator pitch factor k_{p1} (Appendix D). Hence

$$k_{w1} = k_{d1} k_{p1} \tag{3.19}$$

The stator winding *distribution factor* is calculated as

$$k_{d1} = \frac{\sin[\pi/(2m_1)]}{q_1 \sin[\pi/(2m_1 q_1)]} \tag{3.20}$$

while the stator *pitch factor* is given by

$$k_{p1} = \sin \frac{w_c}{\tau} \frac{\pi}{2} \tag{3.21}$$

These formulae require knowledge of the number of slots per pole per phase , which is

$$q_1 = \frac{s_1}{2pm_1} \tag{3.22}$$

where s_1 is the number of stator slots.

3.2.10 Voltage induced in the rotor winding

The slip-dependent *voltage* (EMF) that is *induced in the rotor winding* per phase is

$$E_2(s) = 4\sigma_f sf N_2 k_{w2} \Phi \tag{3.23}$$

where sf is the *slip frequency* (i.e. the frequency of the rotor current), N_2 is the number of rotor turns per phase, and k_{w2} is the rotor winding factor which can be calculated in the same way as shown in Appendix D for the stator winding. For a cage winding $N_2 = 0.5$ and $k_{w2} = 1$. The above eqn (3.23) can also be written in the form

$$E_2(s) = sE_{2o} \tag{3.24}$$

where

$$E_{2o} = 4\sigma_f f N_2 k_{w2} \Phi \tag{3.25}$$

is the induced rotor voltage at $n = 0$ ($s = 1$).

3.2.11 Induced rotor voltage referred to the stator system

Using the *turns ratio* $(N_1 k_{w1})/(N_2 k_{w2})$, the induced rotor voltage referred to the stator winding is

$$sE'_{2o} = sE_{2o} \frac{N_1 k_{w1}}{N_2 k_{w2}} = sE_1 \tag{3.26}$$

For a transformer, the turns ratio is simply N_1/N_2. However, an a.c. electrical machine has its windings distributed in slots (Appendix B) with coil pitch $w_c \leq \tau$ and the turns ratio contains the 'effective' number of turns in the stator and rotor, $N_1 k_{w1}$ and $N_2 k_{w2}$, respectively.

3.2.12 Rotor current referred to the stator system

The *rotor current* can be referred to the stator (primary) system in a similar way to finding the secondary current of a transformer:

$$I'_2 = \frac{m_2 N_2 k_{w2}}{m_1 N_1 k_{w1}} I_2 \tag{3.27}$$

where m_1 is the number of stator phases, m_2 is the number of rotor phases, N_1 is the number of stator turns per phase, N_2 is the number of rotor turns per phase, k_{w1} is the stator winding factor, k_{w2} is the rotor winding factor, and I_2 is the current in the rotor conductors (bars). Eqn (3.27) has been derived by equating the stator and rotor MMFs for $s = 1$, effectively neglecting the magnetizing MMF, or else by equating the apparent internal powers and setting $m_1 E'_2 I'_2 = m_2 E_2 I_2$. For a cage rotor, $m_2 = s_2$ (the number of rotor slots), $N_2 = 0.5$ and $k_{w2} = 1$.

3.2.13 Rotor impedance

The slip-dependent *rotor impedance* is

$$\mathbf{Z}_2(s) = R_2 + jX_2(s) = R_2 + j2\pi sfL_2 = R_2 + jsX_2 \quad (3.28)$$

where L_2 is the rotor winding inductance, and

$$X_2 = 2\pi fL_2 \quad (3.29)$$

is the rotor inductance for $s = 1$.

The voltage across $\mathbf{Z}_2(s)$ is sE_2. Each phase of the rotor circuit can also be replaced with the impedance

$$\mathbf{Z}_2 = \frac{\mathbf{Z}_2(s)}{s} = \frac{R_2}{s} + jX_2 \quad (3.30)$$

for the induced voltage E_2.

3.2.14 Rotor impedance referred to the stator system

The rotor impedance, resistance and reactance referred to the stator winding are:

$$\mathbf{Z}_2' = R_2' + jX_2' = \frac{m_1(N_1k_{w1})^2}{m_2(N_2k_{w2})^2}\mathbf{Z}_2 \quad (3.31)$$

$$R_2' = \frac{m_1(N_1k_{w1})^2}{m_2(N_2k_{w2})^2}R_2 \quad (3.32)$$

$$X_2' = \frac{m_1(N_1k_{w1})^2}{m_2(N_2k_{w2})^2}X_2 \quad (3.33)$$

Eqn (3.32) is obtained by equating the rotor winding active losses $m_2I_2^2R_2$ and $m_1(I_2')^2R_2'$ and then applying eqn (3.27). Similarly, eqn (3.33) is obtained by equating the rotor *reactive* losses.

3.2.15 Output power

The mechanical *output power* (or shaft power) is

$$P_{out} = P_{in} - \Delta P_{1w} - \Delta P_{1Fe} - \Delta P_{2w} - \Delta P_{rot} - \Delta P_{str} = P_m - \Delta P_{rot} - \Delta P_{str} \quad (3.34)$$

The rotor core losses ΔP_{2Fe} are very small and can be neglected at the rated speed, since the frequency of magnetic flux in the rotor, sf (the slip frequency), is very low.

3.2.16 Rotational (mechanical) losses

The speed-dependent *rotational losses* are

$$\Delta P_{rot} = \Delta P_{fr} + \Delta P_{wind} + \Delta P_{vent} \quad (3.35)$$

where ΔP_{fr} is the frictional loss (in the bearings and between the slip rings and brushes), ΔP_{wind} is the windage loss and ΔP_{vent} represents the ventilation losses.

3.2.17 Stray losses

Stray load losses ΔP_{str} (sometimes called *additional losses*) are due to higher harmonics and are equal to 0.5% of the input power according to IEC (International Electrotechnical Commission) standards. According to NEMA (National Electrotechnical Manufacturer's Association of the USA) standards, stray load losses are equal to 1.2% of P_{out} if $P_{out} < 2500$ hp (1865 kW) and to 0.9% of P_{out} if $P_{out} \geq 2500$ hp.

3.2.18 Slip, electromagnetic power, and mechanical power

The slip can also be defined as

$$s = \frac{P_g - P_m}{P_g} = \frac{2\pi n_s T_d - 2\pi n T_d}{2\pi n_s T_d} = \frac{n_s - n}{n_s} \tag{3.36}$$

Since

$$P_g - P_m \approx P_{2w},$$

the electromagnetic power is equal to the rotor winding losses divided by the slip, or

$$P_g = \frac{P_{2w}}{s} \tag{3.37}$$

Similarly, the mechanical power may be approximated as

$$P_m = P_g(1-s) = P_{2w}\frac{1-s}{s} \tag{3.38}$$

3.2.19 Efficiency

The *efficiency* is the ratio of the output P_{out} to input power P_{in}. Since $P_{out} < P_m$ and $P_{in} > P_g$, this useful approximation to the efficiency (see Fig. 3.2) can be deduced:

$$\eta = \frac{P_{out}}{P_{in}} \approx \frac{P_m}{P_g} = 1 - s \tag{3.39}$$

Eqn (3.39) is only valid for medium and large-power induction motors. The output power as a function of efficiency and *power factor* $\cos\phi$ is

$$P_{out} = \eta P_{in} = m_1 V_1 I_1 \eta \cos\phi \tag{3.40}$$

3.2.20 Shaft torque

The *shaft torque* is the output power divided by the rotor angular speed $\Omega = 2\pi n$, i.e.

$$T = \frac{P_{out}}{\Omega} = \frac{P_{out}}{2\pi n} \tag{3.41}$$

where n is the shaft rotational speed.

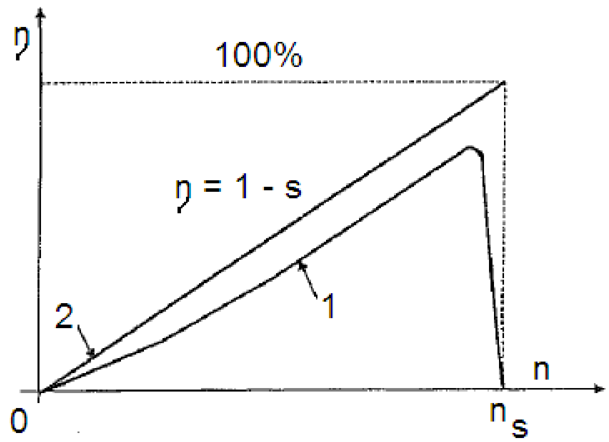

Fig. 3.2. Actual and approximated efficiency *versus* speed: 1 — actual, 2 — approximated ($\eta \approx 1 - s$.

3.3 Equivalent circuit

The T-type *equivalent circuit* per phase of an induction motor and the corresponding *phasor diagram* are shown in Fig. 3.3.

From Kirchhoff's current law, the *stator current* is

$$\mathbf{I}_1 = \mathbf{I}_{exc} + \mathbf{I}_2' \tag{3.42}$$

and the *exciting current* (in the vertical branch) is

$$\mathbf{I}_{exc} = I_{Fe} + jI_{\Phi} \tag{3.43}$$

where I_{Fe} is the *core loss current* (the active component of I_{exc}), and I_{Φ} is the *magnetizing current* (the reactive component of I_{exc}). The stator core losses can be calculated as

$$\Delta P_{Fe} = m_1 I_{Fe}^2 R_{Fe} = m_1 \frac{E_1^2}{R_{Fe}} \tag{3.44}$$

where R_{Fe} is the *resistance representing the stator core losses* (or core loss resistance).

The *rms* line stator current at $V_1 = 380$ V can be evaluated by the following *rule of thumb*: $I_1 \approx 2.2 P_{out}$ at $V_1 = 380$ V and with $2p = 2$, where P_{out} is in kilowatts and I_1 is in amps.

Then, from Kirchhoff's voltage law

$$\mathbf{V}_1 = \mathbf{I}_1(R_1 + jX_1) + \mathbf{E}_1 \tag{3.45}$$

and

$$\mathbf{E}_1 = \mathbf{E}_2' = \mathbf{I}_2' \left(\frac{R_2'}{s} + jX_2' \right) \tag{3.46}$$

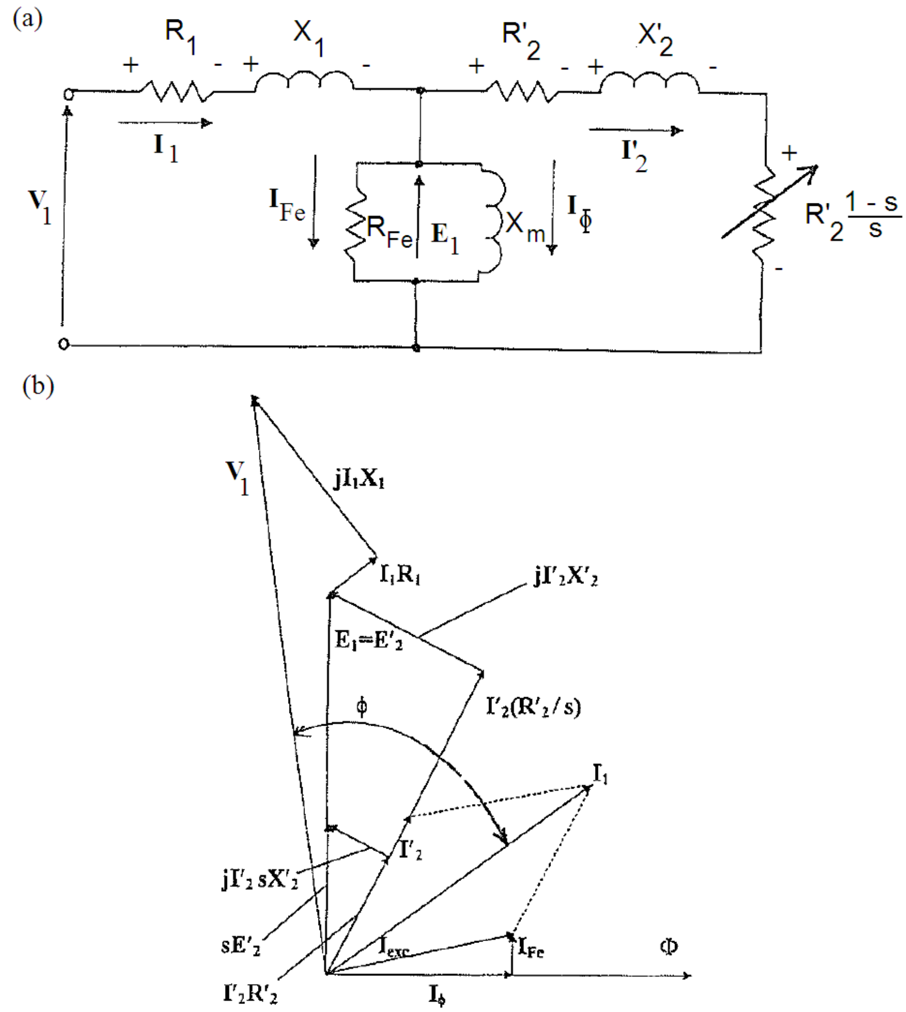

Fig. 3.3. Circuital model and phasor diagram of an induction motor: (a) equivalent circuit per phase; (b) phasor diagram. R_1 = stator winding resistance, X_1 = stator winding leakage reactance, R_2' = rotor winding resistance referred to the stator system, X_2' = rotor winding leakage reactance referred to the stator system, R_{Fe} = core-loss resistance, X_m = mutual reactance, $\mathbf{V}_1$ = input phase voltage, $\mathbf{I}_1$ = input (stator) phase current, $\mathbf{I}_2'$ = rotor current referred to the stator winding, $\mathbf{I}_{exc}$ = exciting current, I_{Fe} = core loss current, I_{Φ} = magnetizing current.

so

$$\mathbf{E}_2' = \mathbf{I}_2'(R_2' + jX_2') + \mathbf{I}_2' R_2' \frac{1-s}{s} \tag{3.47}$$

since

$$\frac{R_2'}{s} = R_2' + R_2' \frac{1-s}{s} \tag{3.48}$$

3.4 No-load and blocked-rotor tests

The resistances and reactances of the equivalent circuit can be determined from the results of a no-load test, blocked-rotor test and from measurement of the d.c. stator winding resistance.

3.4.1 No-load test

The *no-load test* on an induction motor is similar to the open-circuit test on a transformer. In this test the motor runs without any load. The input voltage V_1, input phase current I_{10}, input power P_{in0}, no-load speed n_0, stator winding resistance per phase R_1, rotor winding resistance R_2 per phase (only for a slip ring motor) are measured. The no-load parameters are found from the following equations:

- The no-load power factor

$$\cos\phi_0 = \frac{P_{in0}}{m_1 I_{10} V_1} \tag{3.49}$$

- The no-load stator winding losses

$$\Delta P_{1w0} = m_1 I_{10}^2 R_1 \tag{3.50}$$

- The no-load reactance

$$X_1 + X_m = \frac{Q_{in0}}{m_1 I_{10}^2} = \frac{\sqrt{(m_1 I_{10} V_1)^2 - P_{in0}^2}}{m_1 I_{10}^2} \tag{3.51}$$

- The no-load losses (core losses and rotational losses)

$$\Delta P_0 = P_{in0} - \Delta P_{1w0} \tag{3.52}$$

3.4.2 Blocked-rotor test

The *blocked rotor test* on an induction motor corresponds to the short-circuit test on a transformer. In this test the rotor is blocked ($n = 0$, $s = 1$) and a reduced voltage V_{1sh} is applied to the motor to obtain the rated current I_{1r} in the stator winding. The reduced input voltage V_{1sh}, input current I_{1r} and input power P_{insh} are measured. The blocked-rotor parameters are calculated as follows:

- The blocked-rotor power factor

$$\cos\phi_{sh} = \frac{P_{insh}}{m_1 I_{1r} V_{1sh}} \tag{3.53}$$

- The stator winding losses

$$\Delta P_{1w} = m_1 I_{1r}^2 R_1 \tag{3.54}$$

- The blocked-rotor impedance

$$\mid Z_{sh} \mid = \sqrt{R_{sh}^2 + Z_{sh}^2} = \frac{V_{1sh}}{I_{1r}} \tag{3.55}$$

- The blocked rotor resistance

$$R_{sh} = \frac{P_{insh}}{m_1 I_{1r}^2} \tag{3.56}$$

- The rotor resistance referred to the stator winding

$$R_2' = R_{sh} - R_1 \tag{3.57}$$

- The blocked rotor reactance

$$X_{sh} = \sqrt{Z_{sh}^2 - R_{sh}^2} \tag{3.58}$$

- The stator and rotor leakage reactances

$$X_1 \approx 0.5 X_{sh}, \qquad X_2' \approx 0.5 X_{sh} \tag{3.59}$$

- The developed torque at $s = 1$ and rated current

$$T_{dsh} \approx \frac{m_1 I_{1r}^2 R_2'}{2\pi n_s} \tag{3.60}$$

Example 3.1

No-load and blocked-rotor tests have been performed on a three-phase, four-pole, 60-Hz, 10 kW, Y-connected, 208 V (line-to-line) cage induction motor, with the following results:

No-load test: input frequency $f = 60$ Hz, input voltage (line-to-line) $V_{10L-L} = 208$ V, no-load current $I_{10} = 6.49$ A, no-load power $P_{in0} = 332$ W, stator winding resistance per phase $R_1 = 0.25\ \Omega$.

Blocked-rotor test (s=1): input frequency $f = 60$ Hz, input voltage (line-to-line) $V_{1shL-L} = 78.5$ V, input current $I_{1r} = 42$ A, input active power $P_{insh} = 2116.8$ W.

Solution

Calculations on the basis of the no-load test:

$$V_1 = \frac{208}{\sqrt{3}} = 120 \text{ V}$$

$$\cos\phi_0 = \frac{P_{in0}}{m_1 I_{10} V_1} = \frac{332}{3 \times 6.49 \times 120} = 0.142, \qquad \phi_0 = 81.8^0$$

$$\Delta P_{1w0} = m_1 I_{10}^2 R_1 = 3 \times 6.49^2 \times 0.25 = 31.6 \text{ W}$$

$$X_1 + X_m = \frac{\sqrt{(m_1 I_{10} V_1)^2 - P_{in0}^2}}{m_1 I_{10}^2} = \frac{\sqrt{(3 \times 6.49 \times 120)^2 - 332^2}}{3 \times 6.49^2} = 18.3 \ \Omega$$

$$\Delta P_0 = P_{in0} - \Delta P_{1w0} = 332 - 31.6 = 300.4 \text{ W}$$

Calculations on the basis of the blocked-rotor test:

$$V_{1sh} = \frac{78.5}{\sqrt{3}} = 45.3 \text{ V}$$

$$\cos\phi_{sh} = \frac{P_{insh}}{m_1 I_{1r} V_{1sh}} = \frac{2116.8}{3 \times 42 \times 45.3} = 0.37, \qquad \phi_{sh} = 68.23^0$$

$$\Delta P_{1w} = m_1 I_{1r}^2 R_1 = 3 \times 42^2 \times 0.25 = 1323 \text{ W}$$

$$| Z_{sh} | = \frac{V_{1sh}}{I_{1r}} = \frac{45.3}{42} = 1.078 \ \Omega$$

$$R_{sh} = \frac{P_{insh}}{m_1 I_{1r}^2} = \frac{2116.8}{3 \times 42^2} = 0.4 \ \Omega$$

$$R_2' = R_{sh} - R_1 = 0.4 - 0.25 = 0.15 \ \Omega$$

$$X_{sh} = \sqrt{Z_{sh}^2 - R_{sh}^2} = \sqrt{1.078^2 - 0.4^2} = 1 \ \Omega$$

$$X_1 \approx 0.5 X_{sh} = 0.5 \times 1 = 0.5 \ \Omega, \qquad X_2' \approx 0.5 X_{sh} = 0.5 \times 1 = 0.5 \ \Omega$$

$$n_s = \frac{60}{2} = 30 \text{ rev/s}$$

$$T_{dsh} \approx \frac{m_1 I_{1r}^2 R_2'}{2\pi n_s} = \frac{3 \times 42^2 \times 0.15}{2\pi \times 30} = 4.21 \text{ Nm}$$

3.5 Torque-speed characteristics

The rotor current may now be written

$$\mathbf{I}_2' = \frac{sE_1}{R_2' + jsX_2'} = \frac{E_1}{R_2'/s + jX_2'} \tag{3.61}$$

and the stator EMF is

$$\mathbf{E}_1 = \frac{\mathbf{V}_1}{\mathbf{Z}_1 + \mathbf{Z}_o\mathbf{Z}_2'/(\mathbf{Z}_o + \mathbf{Z}_2')}\frac{\mathbf{Z}_o\mathbf{Z}_2'}{\mathbf{Z}_o + \mathbf{Z}_2'} = \frac{\mathbf{V}_1\mathbf{Z}_o\mathbf{Z}_2'}{\mathbf{Z}_1\mathbf{Z}_o + \mathbf{Z}_1\mathbf{Z}_2' + \mathbf{Z}_o\mathbf{Z}_2'}$$

$$= \frac{\mathbf{V}_1\mathbf{Z}_2'}{\mathbf{Z}_1 + \mathbf{Z}_2' + \mathbf{Z}_2'\mathbf{Z}_1/\mathbf{Z}_o}$$

where the impedances are given by:

$$\mathbf{Z}_1 = R_1 + jX_1 \tag{3.62}$$

$$\mathbf{Z}_2' = \frac{R_2'}{s} + jX_2' \tag{3.63}$$

$$\mathbf{Z}_o = R_o + jX_o = \frac{jR_{Fe}X_m}{R_{Fe} + jX_m} \tag{3.64}$$

The denominator of the fraction expressing $\mathbf{E_1}$ can be brought to the form

$$\mathbf{Z}_1 + \mathbf{Z}_2' + \mathbf{Z}_2'\frac{\mathbf{Z}_1}{\mathbf{Z}_o} = \mathbf{Z}_1 + \mathbf{Z}_2'(1 + \frac{\mathbf{Z}_1}{\mathbf{Z}_o}) = \mathbf{Z}_1 + \mathbf{Z}_2'(1 + \tau_1) \tag{3.65}$$

where *Heyland's coefficient* for the stator is

$$\tau_1 = \frac{\mathbf{Z}_1}{\mathbf{Z}_o} \approx \frac{X_1}{X_m} \tag{3.66}$$

Thus, the rotor current can be expressed as

$$\mathbf{I}_2' = \frac{\mathbf{V}_1}{R_1 + jX_1 + (R_2'/s + jX_2')(1 + \tau_1)}$$

$$= \frac{\mathbf{V}_1}{R_1 + (R_2'/s)(1 + \tau_1) + j[X_1 + X_2'(1 + \tau_1)]} \tag{3.67}$$

or

$$I_2' = \frac{V_1}{\sqrt{[R_1 + (R_2'/s)(1 + \tau_1)]^2 + [X_1 + X_2'(1 + \tau_1)]^2}} \tag{3.68}$$

For $s \to \pm\infty$, the rotor current is obviously at its maximum, so

$$I_{2max}' = \lim_{s\to\pm\infty} I_2' = \frac{V_1}{\sqrt{R_1^2 + [X_1 + X_2'(1 + \tau_1)]^2}} \tag{3.69}$$

The stator and rotor current – speed characteristics are plotted in Fig. 3.4.

The developed torque, first given by eqn (3.8), may now be expressed in terms of the equivalent circuit parameters as

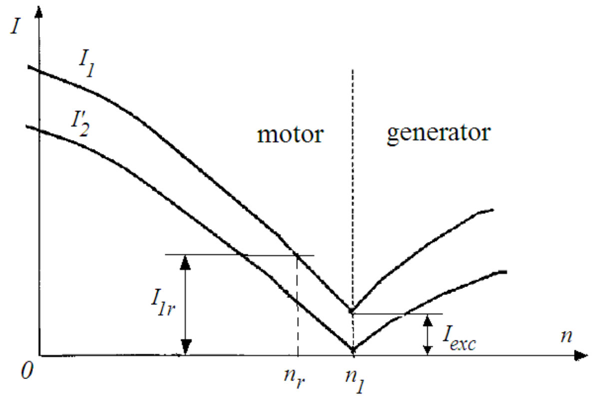

Fig. 3.4. Stator and rotor current versus speed.

$$T_d = \frac{P_g}{2\pi n_s} = \frac{m_1}{2\pi n_s}(I_2')^2\frac{R_2'}{s}$$

$$= \frac{m_1}{2\pi n_s}\frac{V_1^2(R_2'/s)}{[R_1 + (R_2'/s)(1+\tau_1)]^2 + [X_1 + X_2'(1+\tau_1)]^2} \qquad (3.70)$$

To find the critical value of slip $s = s_{cr}$ which corresponds to the maximum (pull-out) developed torque T_{dmax}, we take the derivative of T_d with respect to s and equate it to zero (in other words, the first derivative test for maxima and minima is applied):

$$\frac{dT_d}{ds} = 0 \qquad (3.71)$$

The critical value of the slip is found to be

$$s_{cr} = \pm\frac{R_2'(1+\tau_1)}{\sqrt{R_1^2 + [X_1 + X_2'(1+\tau_1)]^2}} \qquad (3.72)$$

The '+' sign signifies a machine in motor mode and the '–' sign denotes generator mode.

In conventional induction machines, R_1 is considerably less than $X_1+X_2'(1+\tau_1)$. For this reason, $R_1^2 \ll [X_1 + X_2'(1+\tau_1)]^2$ and may therefore be disregarded. Thus

$$s_{cr} \approx \pm\frac{R_2'(1+\tau_1)}{X_1 + X_2'(1+\tau_1)} \approx \pm\frac{R_2'}{X_1 + X_2'} \qquad (3.73)$$

The *maximum (pull-out) torque* is now found by re-substitution:

$$T_{dmax} = T_d(s = s_{cr}) = \pm\frac{m_1 V_1^2}{4\pi n_s(1+\tau_1)}\frac{1}{\left\{\sqrt{R_1^2 + [X_1 + X_2'(1+\tau_1)]^2} \pm R_1\right\}}$$

$$\approx \pm\frac{m_1 V_1^2}{4\pi n_s(1+\tau_1)}\frac{1}{X_1 + X_2'(1+\tau_1)} \qquad (3.74)$$

In the denominator, '$+R_1$' is for $s_{cr} > 0$ (signifying a motor or brake) and '$-R_1$' is for $s_{cr} < 0$ (denoting a generator). The absolute value of maximum torque is slightly higher for the generator mode than for the motor mode, if the stator winding resistance is taken into account. In practice, only the leakage reactances X_1 and X_2 affect the maximum torque T_{dmax}.

The *starting torque* is for the slip value $s = 1$, and so:

$$T_{dst} = T_d(s=1) = \frac{m_1 V_1^2}{2\pi n_s} \frac{R_2'}{[R_1 + R_2'(1+\tau_1)]^2 + [X_1 + X_2'(1+\tau_1)]^2} \tag{3.75}$$

The torque – speed characteristic of an induction motor is plotted in Fig. 3.5a, where it can be seen that the maximum torque T_{dmax} for a generator is higher than that for a machine in motor mode. The developed torque of an induction machine depends, as do the maximum and starting torques, on the voltage squared (see Fig. 3.6).

The maximum torque according to eqn (3.74) is independent of both the stator and rotor circuit resistances (Fig. 3.7). However, the critical slip is directly proportional to the rotor resistance, R_2'. Thus, if R_2' increases then s_{cr} increases too, while $T_{dmax} = const$ (Fig. 3.7). The ratio

$$OCF = \frac{T_{dmax}}{T_{dr}} \tag{3.76}$$

where T_{dr} is the rated developed torque, is called the *overload capacity factor* and the ratio

$$STR = \frac{T_{dst}}{T_{dr}} \tag{3.77}$$

is called the *starting torque ratio*. Similarly, the ratio

$$SCR = \frac{I_{1st}}{I_{1r}} \tag{3.78}$$

where I_{1r} is the rated input current, is called the *starting current ratio*.

The values of the ratios OCF, STR and SCR are given for various different motors in Table 5.1.

Table 3.1. The OCF, STR, and SCR for single-cage, double-cage, and deep-bar induction motors

Motor	$OCF = T_{dmax}/T_{dr}$	$STR = T_{dst}/T_{dr}$	$SCR = I_{1st}/I_{1r}$
single-cage	1.6 to 1.8	1.0 to 1.5	4.0 to 7.0
double-cage	1.6 to 3.2	1.0 to 2.0	3.0 to 5.0
deep-bar	1.6 to 3.2	0.2 to 1.0	3.0 to 5.0

Finally, the ratio of any torque T_d to the pull-out torque T_{dmax} is expressed by Kloss' formula:

$$\frac{T_d}{T_{dmax}} \approx \frac{2}{s_{cr}/s + s/s_{cr}} \tag{3.79}$$

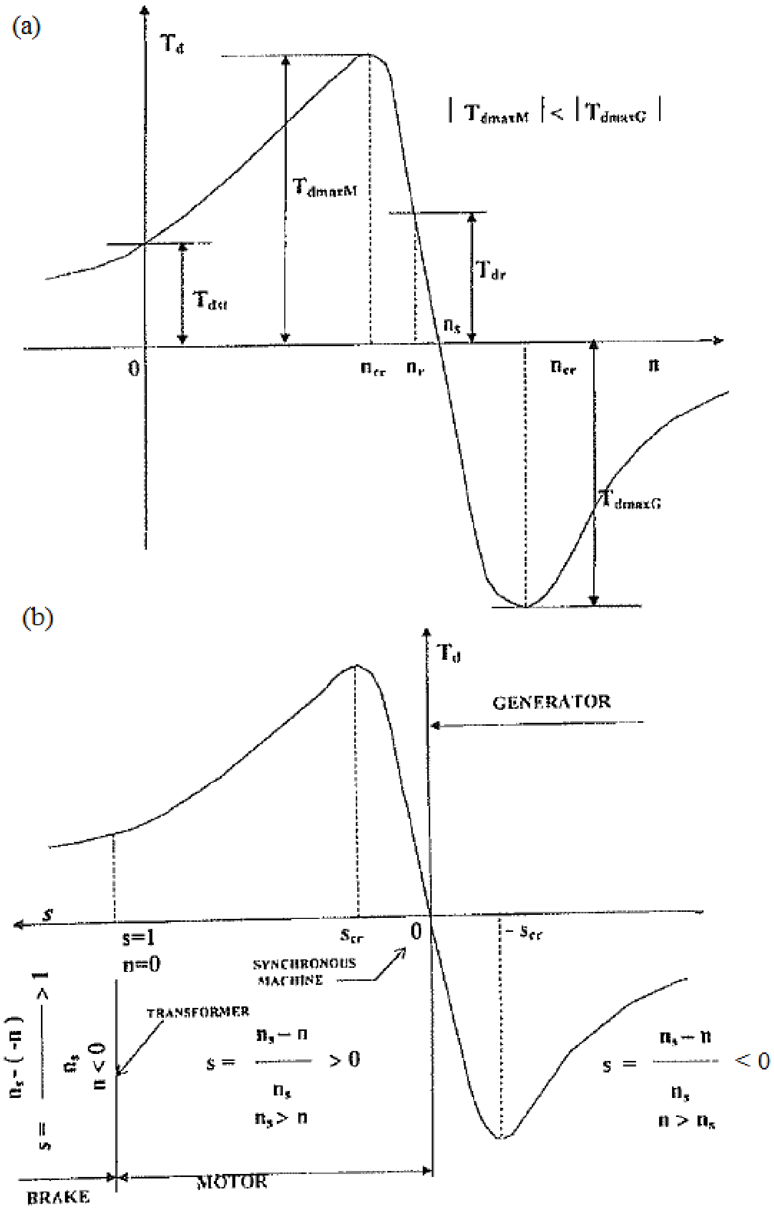

Fig. 3.5. Mechanical characteristics of an induction machine: (a) torque–speed, (b) torque–slip.

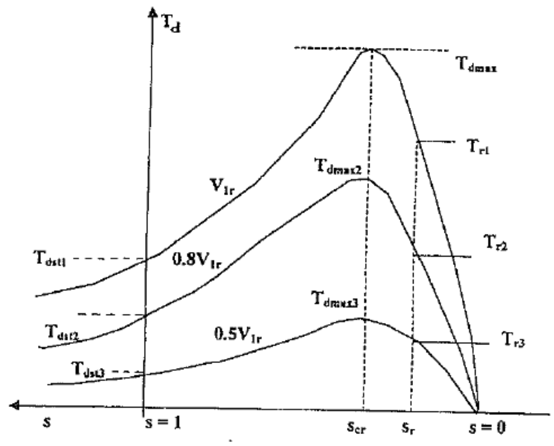

Fig. 3.6. The influence of the input voltage on the torque–slip characteristic of an induction machine.

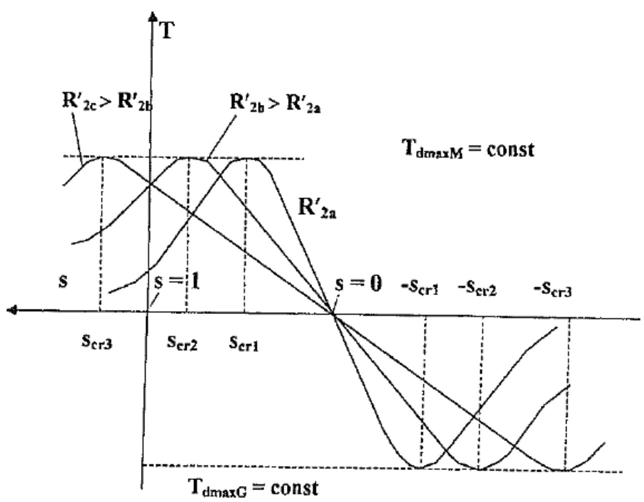

Fig. 3.7. The influence of the rotor circuit resistance on the torque–slip characteristic of an induction machine.

Note that eqn (3.79) can be derived with the aid of eqns (3.70), (3.73), and (3.74).

Example 3.2

A three-phase, 12-pole ($2p = 12$), 420 V (line-to-line), Y-connected, 5.5 kW, 50 Hz cage induction motor has the following equivalent circuit parameters: $R_1 = 0.833\ \Omega$, $X_1 = 1.864\ \Omega$, $R_2' = 0.833\ \Omega$, $X_2' = 1.864\ \Omega$, $X_m = 36.25\ \Omega$. The machine operates with a slip of 0.03. The rotational loss is $\Delta P_{rot} = 250$ W and the stray loss is $\Delta P_{str} = 60$ W.

For an input frequency of 60 Hz, rated input voltage of 420 V, and rated slip of 0.03 find: (a) the rotor speed, (b) the stator and rotor currents at slip 0.03, (c) the mechanical power and the output power, assuming that the rotational loss is $\Delta P_{rot} = 250$ W and the stray loss is $\Delta P_{str} = 60$ W, (d) the input power, efficiency and power factor, (e) the stator and rotor winding losses, (f) the electromagnetic (airgap) power and electromagnetic (developed) torque, (g) the starting torque T_{dst} and starting torque ratio STR, (h) the pull-out torque T_{dmax}, the critical slip s_{cr}, and the overload capacity factor OCF.

Assumptions: The core-losses are neglected ($R_{Fe} = 0$) and the skin effect in the rotor bars is also negligible.

Solution

The rotor speed

- Synchronous speed
  At 50 Hz, $n_s = f/p = 50/6 = 8.33 \times 60 = 500$ rpm
  At 60 Hz, $n_s = f/p = 60/6 = 10.0 \times 60 = 600$ rpm

- Rotor speed
  At 50 Hz, $n = 500(1 - 0.03) = 485$ rpm
  At 60 Hz, $n = 600(1 - 0.03) = 582$ rpm

The stator and rotor rated currents

- Reactances at 60 Hz

$$X_1 = X_2' = \frac{60}{50}1.864 = 2.237\ \Omega$$

$$X_m = \frac{60}{50}36.25 = 43.5\ \Omega$$

- The impedances of the vertical and rotor branches for the rated slip

$$\frac{(R_2'/s + jX_2')jX_m}{R_2'/s + j(X_2' + X_m)} = \frac{(0.833/0.03 + j2.237)j43.5}{0.833/0.03 + j(2.237 + 43.5)} = (18.353 + j13.269)\ \Omega$$

- The stator (input) current

$$\mathbf{I}_1 = \frac{V_1}{R_1 + 18.353 + j(X_1 + 13.269)} = \frac{420/\sqrt{3}}{0.833 + 18.353 + j(2.237 + 13.269)}$$

$$= \frac{242.5}{19.186 + j15.506} = (7.645 - j6.179)\ \mathrm{A}$$

$$\mid \mathbf{I}_1 \mid = I_1 = \frac{242.5}{\sqrt{19.186^2 + 15.506^2}} = 9.83\ \mathrm{A}$$

- Heyland's coefficient

$$\tau_1 = \frac{X_1}{X_m} = \frac{2.237}{43.5} = 0.0514$$

- The rotor current referred to the stator system

$$I_2' = \frac{242.5}{\sqrt{\left(0.833 + \frac{0.833}{0.03}1.0514\right)^2 + (2.237 + 2.237 \times 1.0514)^2}} = 7.98\ \mathrm{A}$$

The stator and rotor winding losses

- Stator winding losses

$$\Delta P_{1w} = 3I_1^2 R_1 = 3 \times 9.83^2 \times 0.833 = 241\ \mathrm{W}$$

- Rotor winding losses

$$\Delta P_{2w} = 3(I_2')^2 R_2' = 3 \times 7.98^2 \times 0.833 = 159.1\ \mathrm{W}$$

The electromagnetic (airgap) power and developed torque

- Electromagnetic power crossing the airgap

$$P_g = \frac{3(I_2')^2 R_2'}{s} = \frac{\Delta P_{2w}}{s} = \frac{159.1}{0.03} = 5.303\ \mathrm{kW}$$

- Developed torque

$$T_d = \frac{P_g}{2\pi n_s} = \frac{5303.3}{2\pi 10} = 84.4\ \mathrm{Nm}$$

The mechanical power and output power

- The rotational loss is $\Delta P_{rot} = 250$ W and the stray loss is $\Delta P_{str} = 60$ W.

- Mechanical power

$$P_m = (1 - s)P_g = (1 - 0.03)5303.3 = 5.144 \text{ kW}$$

- Output (shaft) power

$$P_{out} = P_m - \varDelta P_{rot} - \varDelta P_{str} = 5144.2 - 250 - 60 = 4.834 \text{ kW}$$

The input power, efficiency and power factor

- The input current was found above to be

$$\mathbf{I}_1 = (7.645 - j6.179) \text{ A} \qquad \text{so} \qquad |\,\mathbf{I}_1\,| = I_1 = \sqrt{7.645^2 + 6.179^2} = 9.83 \text{ A}$$

- Apparent input power

$$S_{in} = 3V_1 I_1 = 3 \times \frac{420}{\sqrt{3}} \times 9.83 = 7150.95 \text{ VA}$$

- Active input power

$$P_{in} = 3V_1 \times 7.636 = 3 \times \frac{420}{\sqrt{3}} \times 7.636 = 5.555 \text{ kW}$$

or

$$P_{in} = P_{out} + \varDelta P_{rot} + \varDelta P_{str} + \varDelta P_{2w} + \varDelta P_{1w} =$$

$$4834.2 + 250.0 + 60.0 + 241.5 + 159.1 = 5.545 \text{ kW}$$

- Efficiency

$$\eta = \frac{P_{out}}{P_{in}} = \frac{4834.20}{5554.89} = 0.87$$

- Power factor

$$cos\phi = \frac{P_{in}}{S_{in}} = \frac{5554.89}{7150.95} = 0.777$$

The starting torque and starting torque ratio (STR)

- Starting torque (s=1)

$$T_{dst} = \frac{3V_1^2}{2\pi n_s} \frac{R_2'}{\left[R_1 + R_2'(1+\tau_1)\right]^2 + \left[X_1 + X_2'(1+\tau_1)\right]^2}$$

$$= \frac{3(420/\sqrt{3})^2}{2\pi \times 10} \frac{0.833}{(0.833 + 0.833 \times 1.0514)^2 + (2.237 + 2.237 \times 1.0514)^2}$$

$$= 95.97 \text{ Nm}$$

- Starting torque ratio

$$STR = \frac{T_{dst}}{T_{dr}} = \frac{95.97}{84.40} = 1.137$$

The pull-out torque, critical slip, and overload capacity factor (OCF)

- Critical slip

$$s_{cr} = +\frac{R_2'(1+\tau_1)}{\sqrt{R_1^2 + [X_1 + X_2'(1+\tau_1)]^2}}$$

$$\frac{0.833 \times 1.0514}{\sqrt{0.833^2 + (2.237 + 2.237 \times 1.0514)^2}} = 0.1877$$

- Kloss' formula

$$\frac{T_{dr}}{T_{dmax}} \approx \frac{2}{s_{cr}/s + s/s_{cr}} = \frac{2}{0.1877/0.03 + 0.03/0.1877} = 0.312$$

- Maximum torque

$$T_{dmax} = \frac{T_{dr}}{0.312} = \frac{84.4}{0.312} = 270.9 \text{ Nm}$$

- Overload capacity factor (OCF)

$$OCF = \frac{270.9}{84.4} = 3.21$$

3.6 Starting

3.6.1 Slip–ring motors

An induction motor with slip rings is started by connecting the stator to the power line, with some additional resistance R_{st} being fully cut-in in the rotor circuit, in the form of a starting rheostat (Fig. 3.8). The developed torque T_d according to eqn (3.70) must be the same for $s = 1$ and $R_{st} > 0$ as it is for $0 < s < 1$ and $R_{st} = 0$. So,

$$\frac{(R_2'/s)}{[R_1 + (R_2'/s)(1+\tau_1)]^2 + [X_1 + X_2'(1+\tau_1)]^2}$$

$$= \frac{R_2' + R_{st}'}{[R_1 + (R_2' + R_{2st}')(1+\tau_1)]^2 + [X_1 + X_2'(1+\tau_1)]^2}$$

where R_{st}' is the rotor starting resistance referred to the stator winding. Thus

$$\frac{R_2'}{s} = R_2' + R_{st}' \qquad \text{and} \qquad R_1 + \frac{R_2'}{s}(1+\tau_1) = R_1 + (R_2' + R_{st}')(1+\tau_1)$$

or

$$\frac{R_2}{s} = R_2 + R_{st}$$

The starting rheostat resistance

$$R_{st} = \frac{R_2}{s} - R_2 = R_2 \frac{1-s}{s} \tag{3.80}$$

gives the necessary starting torque and small starting current (as shown in Fig. 3.9). For example, if the rotor resistance is $R_2 = 0.1\Omega$ and the rotor rated speed is $n = 975$ rpm, then the corresponding slip is $s = (1000 - 975)/1000 = 0.025$ and the starting rheostat resistance should be $R_{st} = 0.1(1 - 0.025)/0.025 = 3.9\Omega$. After switching on the stator windings, the rheostat is gradually cut-out until the rotor winding is short-circuited.

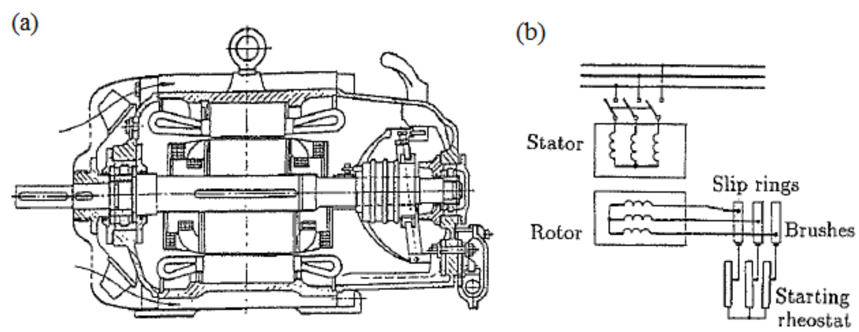

Fig. 3.8. A slip-ring induction motor: (a) longitudinal section, (b) connection diagram.

Starting rheostats are usually made of metal and have oil or liquid cooling. To reduce the rotor circuit resistance and in order to decrease the friction losses of the brushes on the slip rings, wound-rotor induction motors are frequently provided with devices for short-circuiting the rings whilst running and for further lifting the brushes (Fig. 3.8a).

3.6.2 Cage–rotor motors

Direct switching

. A small cage induction motor may be switched 'direct-on-line', meaning that it is switched directly onto normal voltage, momentarily taking several times the full-load current at a low power factor. Direct switching may be the subject of Supply Authority regulations. However, there is usually no restriction on small induction motors up to 5.5 kW.

Star–delta switching

. For star–delta ($Y - \Delta$) switching (see Fig. 3.10), a motor must be built with a Δ-connected stator winding. Let V_{1L} be the line voltage, and let V_{1Y} and $V_{1\Delta}$ be the

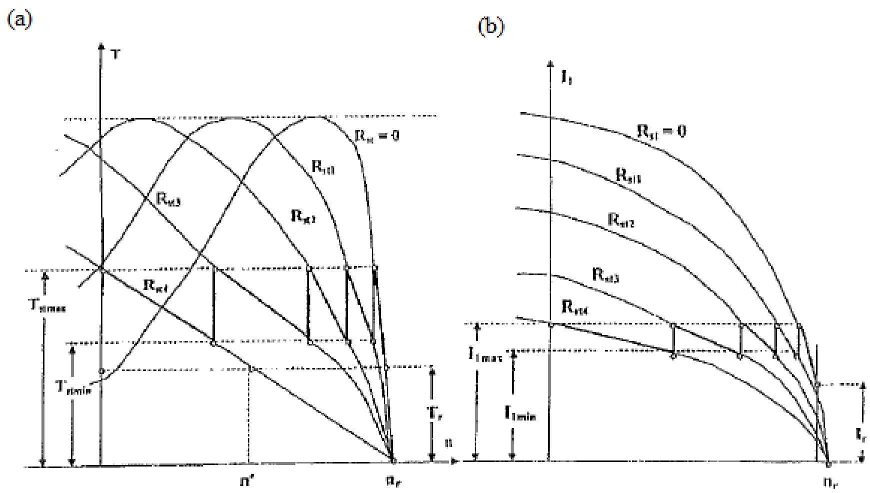

Fig. 3.9. Characteristics of a slip-ring induction motor with starting rheostat: (a) starting torque–speed curve, (b) starting input current–speed curve.

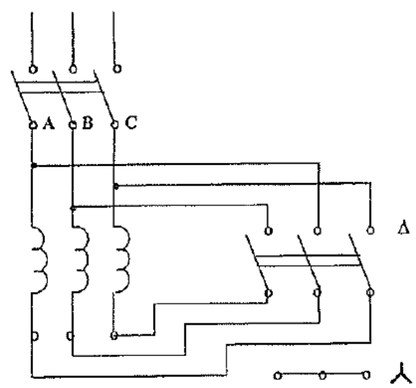

Fig. 3.10. Star–delta switching.

voltages per phase for Y and $\varDelta$ connection of the windings. Next let I_{1stLY}, $I_{1stL\varDelta}$, I_{1stY}, and $I_{1st\varDelta}$ represent the starting current in the line and in the phases of the stator winding when it is Y- and $\varDelta$-connected, respectively. Finally, $\mid \mathbf{Z}_{sh} \mid = Z_{sh}$ is the blocked-rotor (short-circuit) impedance for $s = 1$ of the motor, per phase. Then, in the case of the $Y-$connection,

$$I_{1stLY} = I_{1stY} = \frac{V_{1Y}}{Z_{sh}} = \frac{V_{1L}}{\sqrt{3}Z_{sh}} \tag{3.81}$$

and for the motor with its stator winding $\varDelta$-connected

$$I_{1stL\Delta} = \sqrt{3}I_{1st\Delta} = \frac{\sqrt{3}V_{1\Delta}}{Z_{sh}} = \frac{\sqrt{3}V_{1L}}{Z_{sh}} \tag{3.82}$$

By comparing the above two equations, it is seen that

$$\frac{I_{1stLY}}{I_{1stL\Delta}} = \frac{1}{3} \tag{3.83}$$

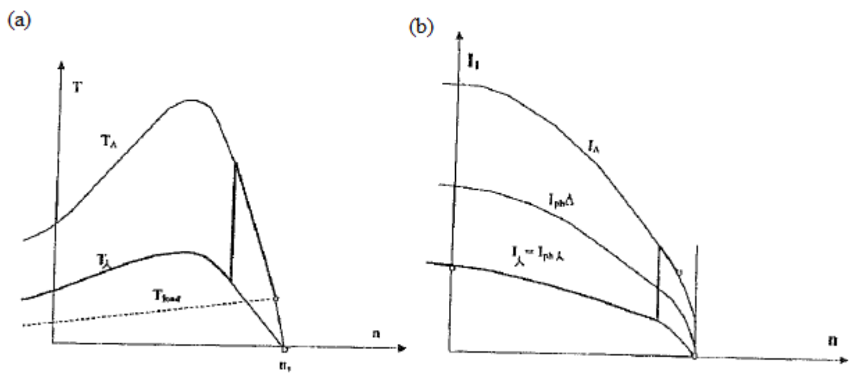

Fig. 3.11. Characteristics of $Y - \Delta$ switching: (a) torque–speed curve, (b) stator current–speed curves.

Thus, *the starting current when the stator winding is Y-connected is one-third of that when it is Δ-connected*. Meanwhile, *the starting torque T_{st} also decreases by a factor of three*. Hence:

$$T_{stY} \propto V_{1Y}^2 = \frac{1}{3}V_{1L}^2 \qquad \text{and} \qquad T_{st\Delta} \propto V_{1\Delta}^2 = V_{1L}^2$$

Combining these expressions now gives

$$\frac{T_{stY}}{T_{st\Delta}} = \frac{1}{3} \tag{3.84}$$

The characteristics of an induction motor for $Y - \Delta$ switching are shown in Fig. 3.11.

Stator impedance starting

. The inclusion of a resistor or of an inductive reactor (see Fig. 3.12) in each of the stator input lines reduces the stator terminal voltage. Suppose that the starting current in the external circuit of a Y-connected motor is limited to I_{1stL}, so we can write

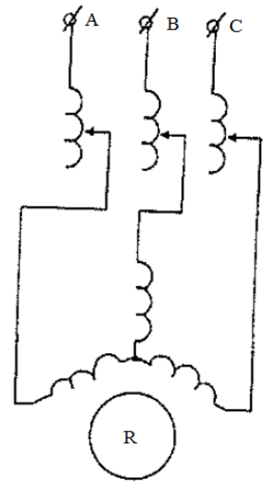

Fig. 3.12. Reactor starting.

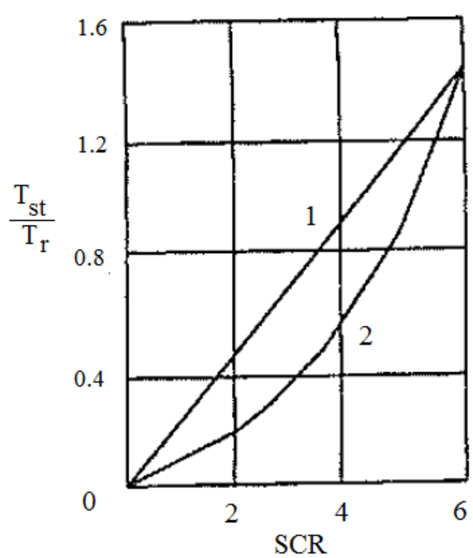

Fig. 3.13. Relation $T_{st}/T_r = f(SCR)$ for starting by means of autotransformer (1) and reactor (2).

$$I_{1stL} = SCR \times I_{1r} \tag{3.85}$$

where SCR is the permissible starting current ratio and I_{1r} is the input rated current. Assuming $I_1 \approx I_2'$, the starting torque is then

$$T_{st} \approx \frac{m_1 I_{1stL}^2 R_2'}{2\pi n_s} = SCR^2 \frac{m_1 I_{1r}^2 R_2'}{2\pi n_s} \propto SCR^2 \tag{3.86}$$

In other words, when starting an induction motor with a reactor, the starting torque depends on the square of the value of SCR. The rated torque is

$$T_r \approx \frac{m_1 I_{1r}^2 R_2'}{2\pi n_s} \frac{1}{s_r} \tag{3.87}$$

where s_r is the rated slip. Consequently

$$\frac{T_{st}}{T_r} = SCR^2 s_r \tag{3.88}$$

The relation $T_{st}/T_r = f(SCR)$ is plotted in Fig. 3.13.

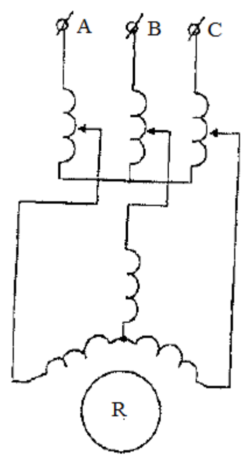

Fig. 3.14. Autotransformer starting.

Autotransformer starting

. Suppose that the autotransformer in Fig. 3.14 is used to reduce the stator applied voltage. If ϑ is the voltage ratio of the autotransformer and if Z_{sh} is the impedance of one motor phase for $s = 1$, then, neglecting for simplicity the autotransformer impedance, the starting voltage V_{1LY} across the motor input terminals and the starting motor current I_{1stY} are: *

$$V_{1LY} = \frac{1}{\vartheta} V_{1L} \qquad \text{and} \qquad I_{1stY} = \frac{V_{1LY}}{Z_{sh}} = \frac{V_{1L}}{\vartheta Z_{sh}} \tag{3.89}$$

where V_{1L} is the line voltage of the external circuit. The starting line current in the autotransformer winding (external circuit) is

$$I_{1L} = \frac{1}{\vartheta} I_{1stY} = \frac{1}{\vartheta^2}\frac{V_{1L}}{Z_{sh}} = \frac{1}{\vartheta^2} I_{1sh} \tag{3.90}$$

where $I_{1sh} = V_{1L}/Z_{sh}$ is the short-circuit current of the motor at rated voltage. As compared with the stator impedance starting that was described in the previous subsection, this method of starting has a considerable advantage with respect to the starting torque. Indeed,

$$T_{st} = \frac{m_1 I_{1stY}^2 R_2'}{2\pi n_s} = \frac{m_1 (I_{1L}\vartheta)^2 R_2'}{2\pi n_s} \tag{3.91}$$

and the rated torque is given by eqn (3.87). Consequently, in this case,

$$\frac{T_{st}}{T_r} = \frac{I_{1L}^2 \vartheta^2}{I_{1r}^2} s_r = \frac{I_{1L}}{I_{1r}} \frac{\vartheta^2 I_{1L}}{I_{1r}} s_r = SCR \frac{\vartheta^2 I_{1L}}{I_{1r}} s_r \tag{3.92}$$

where SCR is the starting current ratio in the external circuit. Now, according to eqn (3.90),

$$\vartheta^2 = \frac{I_{1sh}}{I_{1L}}$$

and so

$$\frac{T_{st}}{T_r} = SCR \frac{I_{1sh}}{I_{1r}} s_r \tag{3.93}$$

In this case, therefore, the relation $T_{st}/T_r = f(SCR)$ is a straight line, since for given values of I_{1sh}/I_{1r} and s_r the torque $T_{st} \propto SCR$ (see Fig. 3.13).

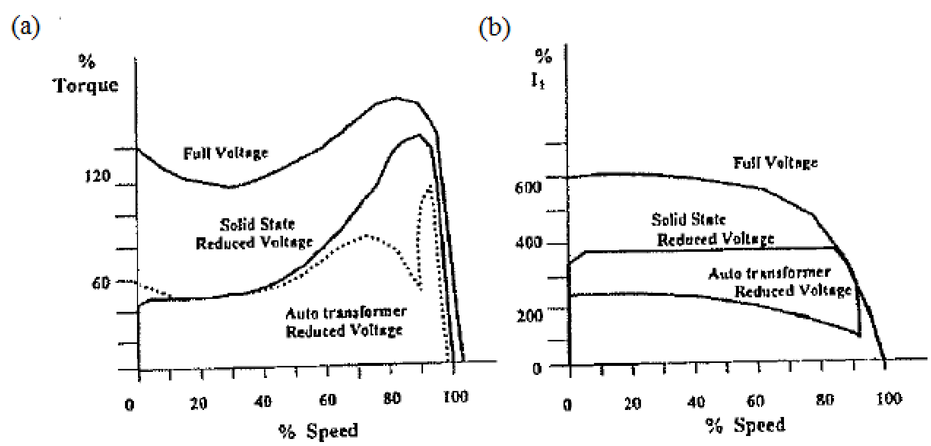

Fig. 3.15. Comparison of the characteristics of full voltage, autotransformer reduced voltage, and solid state reduced voltage starters: (a) torque, (b) line current.

Solid state soft starters

. A typical induction motor, designed according to IEC standards, produces approximately 140% of its normal full-load torque almost instantly when full voltage is applied. The same motor draws about six times its full load current at start-up. As has been emphasized, substantial damage to the motor and auxiliary equipment can occur as a result of this. Reducing the voltage at start-up reduces the starting torque, current surge, electrodynamic forces on the motor windings, and also the mechanical and electrical shock transmitted to the equipment.

The voltage at the first instant of starting can be smoothly reduced with the aid of semiconductor devices, using the so-called *solid state soft starter*. The power circuit of a solid state soft starter is similar to that shown in Fig. 5.12a (Chapter 5). At the heart of a soft starter one usually finds a microprocessor, which provides the control logic for the starting process. The load characteristics of an induction motor with and without the soft starter are shown in Fig. 3.15.

3.7 Induction motors that use skin effect in the rotor winding

3.7.1 Double-cage motors

The double-cage induction motor was first suggested by M. Dolivo-Dobrovolsky, and it is one of the variations of the cage induction motor that uses the skin-effect phenomenon in the rotor winding to improve the starting properties. The stator of such a motor does not differ from that of a conventional a.c. motor, but its rotor consists of two cages (see Fig. 3.16). The upper cage nearer to the airgap, called the *starting cage,* is made of a somewhat resistive material such as brass, aluminium, bronze, *etc.*, while the lower cage, called the *operating cage,* is made of copper. In small induction motors both of the two cages, together with the end rings, are made of aluminium alloy.

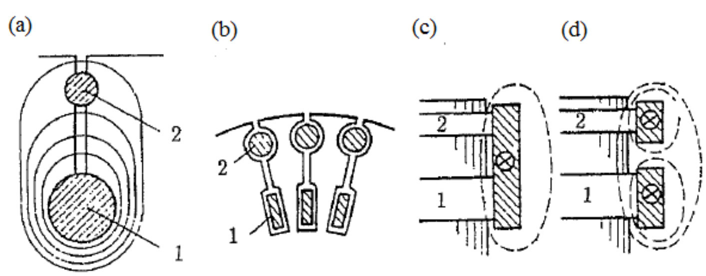

Fig. 3.16. Design of rotor windings of a double-cage motor: 1 — operating cage, 2 — starting cage.

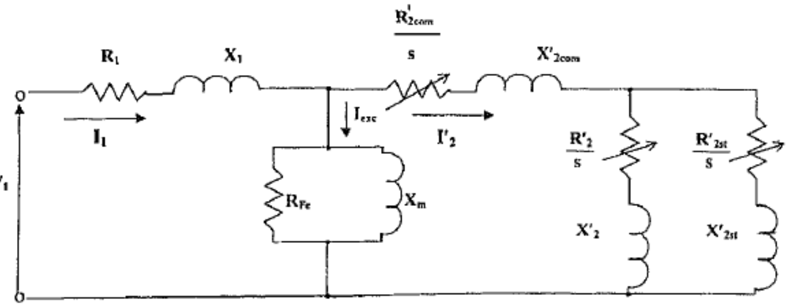

Fig. 3.17. Equivalent circuit per phase of a double-cage induction motor: R'_2, X'_2 — resistance and leakage reactance of the operating cage, R'_{2st}, X'_{2st} — resistance and leakage reactance of the starting cage, R'_{2com}, X'_{2com} — common resistance and reactance. All other symbols are according to Fig. 3.3.

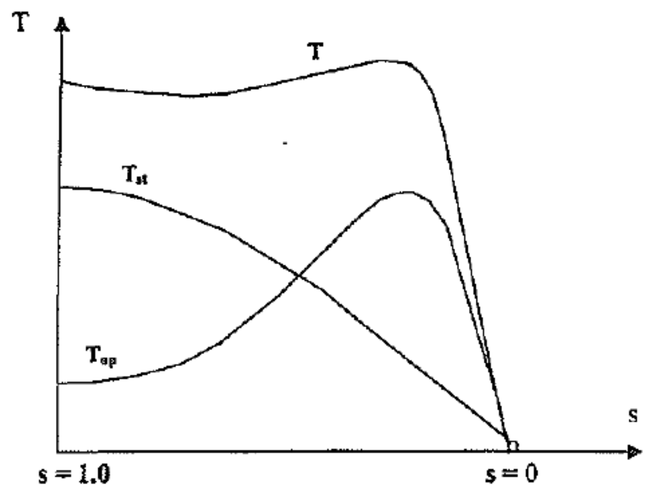

Fig. 3.18. Torque–speed curves for a double-cage motor: T_{op} is the torque produced by the operating (lower) cage, T_{st} is the torque produced by the starting (upper) cage and T is the resultant torque.

At starting, the frequency of the rotor current is high and equal to the frequency of the source. The current amplitude is distributed between the upper and lower windings in inverse proportion to their impedances. Since the lower cage has a very high inductive reactance, its impedance is several times that of the upper cage, whose reactance is practically zero. The current in the lower cage is thus appreciably smaller than that in the upper cage. Furthermore, owing to the high leakage inductive reactance of the lower cage, the current in it lags by a large angle behind the EMF induced by the mutual inductance flux, and the winding consequently produces a small torque. Conversely, the current in the upper cage at starting is not only of considerable magnitude, but is also nearly in phase with the mutual inductance EMF because of the negligible inductive inductance and high resistance of the cage, owing to which this winding produces a very high torque. The torque during the starting period is hence developed mainly by the upper cage, which, in consequence, is referred to as the starting cage.

As the motor speed increases, the frequency in the rotor winding begins to decrease. This results in a reduction of the inductive reactance and an increase in the current in the lower cage, accompanied by a corresponding decrease in the phase angle between the current and the voltage. Consequently, this cage gradually begins to develop a greater and greater torque. When the motor reaches full speed and has a very small slip s, the inductive reactance of the lower cage becomes negligible in comparison with its resistance. The total working current of the whole rotor winding will be divided between two cage windings in inverse proportion to their resistances, and, since the upper cage winding has a resistance which is 5 to 6 times that of the lower cage winding, the current in the upper cage becomes considerably smaller than that in the lower cage. Hence the torque is mainly developed by the lower cage, which is often called the operating cage.

The equivalent circuit per phase of a double-cage induction motor is shown in Fig. 3.17. The common resistance R'_{2com} exists only if the double-cage winding has common end rings. The common reactance X'_{2com} represents the linkage flux between the upper and lower cages.

Fig. 3.18 shows approximate torque curves for the upper and lower cages, as well as the total torque curve of both cage windings considered together.

3.7.2 Deep bar motors

Principle of operation.

The deep bar motor is similar to the double-cage motor and has better starting characteristics compared with the conventional single-cage motor. The shape of the slots of a deep bar motor, with one of the most widely used methods of connecting the bars to the short-circuiting end rings, is shown in Fig. 3.19a. Bars with cross sections that are other than rectangular are also used, examples being trapezoidal or bottle-shaped. In further discussion only bars with a rectangular cross section will be considered, since they are the main ones and of the simplest shape with respect to design and manufacture.

In deep bar motors, use is made of the *skin-effect* that is induced in the rotor winding bars by the slot leakage fluxes.

Let us first consider the phenomena at starting. At the initial instant, when $s = 1$, the frequency in the rotor is equal to the input (stator) frequency. The slot

(a)

(b)

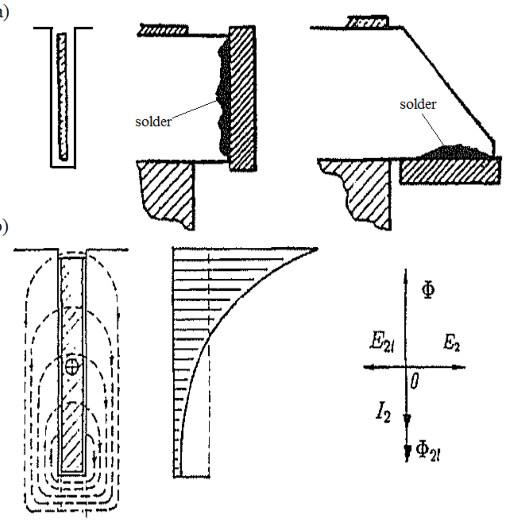

Fig. 3.19. Deep bar rotor induction motor: (a) details of design, (b) leakage flux in rotor slot of a deep bar motor and distribution of current density in rotor conductor.

leakage flux paths within the rotor under these conditions are depicted in Fig. 3.19b. Bar portions of different height are linked by different numbers of leakage flux lines: the lower parts by the greatest number of flux lines, and the upper parts by the least number. For this reason, the maximum leakage EMFs are induced in the lower parts of the bars, and the minimum EMFs in the upper parts.

It can therefore be seen that the rotor leakage flux EMF, E_{2l}, is directed oppositely to the rotor main EMF, E_2, but, in accordance with the previous discussion, it is greater in the lower parts of the conductor than in its upper parts. Consequently, less current should flow through the lower parts than through the upper ones; in other words, the current is forced to the outside of the conductor (producing a skin effect). Hence the current density is distributed along the conductor height as shown in Fig. 3.19b.

The skin effect takes place in all types of motors. With the usual conductor height being 10 to 12 mm and the fundamental harmonic of input frequency being 50 to 60 Hz, however, it is almost unnoticeable. Nevertheless, in deep bars that are 20 to 50 mm high, the skin effect is very strong and appreciably changes the rotor parameters.

Rotor resistance and inductive reactance.

For all practical purposes, the skin effect takes place only in that part of the conductor which lies in the slot, and is absent in the end connections of the winding. Therefore, the resistance R_2' and inductive reactance X_2' of the rotor winding can be expressed as follows:

$$R_2' = k_R R_{2sl}' + R_{2e}' \qquad \text{and} \qquad X_2' = k_X X_{2sl}' + X_{2e}' \tag{3.94}$$

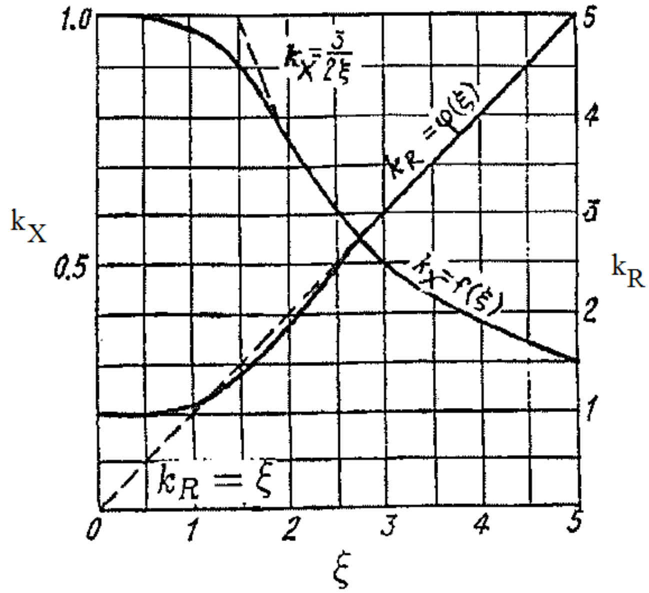

Fig. 3.20. Coefficients k_R and k_X versus ξ.

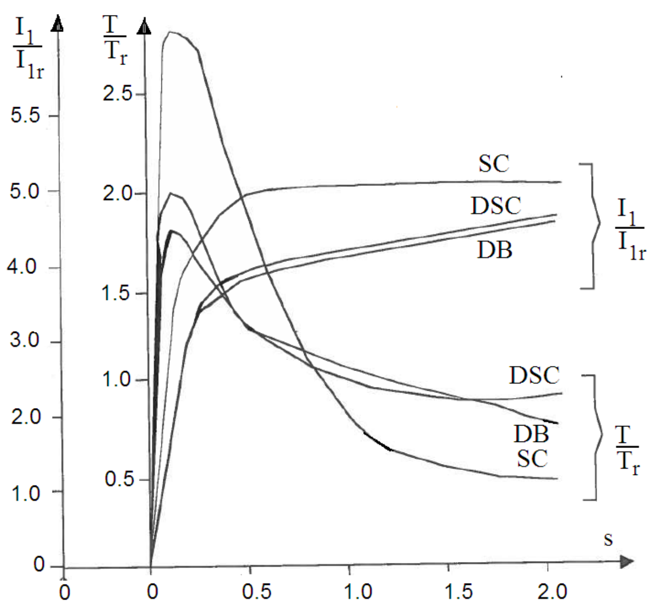

Fig. 3.21. Torque and current versus slip for double-cage induction motor (DSC), deep bar (DB), and ordinary single-cage motor (SC).

where R'_{2sl} is the resistance of the slot part of the rotor winding assuming a uniform current distribution along the conductor cross section, k_R is the factor allowing for the increase of the resistance R'_{2sl} due to the skin effect, R'_{2e} is the constant-value resistance of the rotor end connections, X'_{2sl} and X'_{2e} are the leakage inductive reactances of the slot and end connections of the rotor winding with uniform current distribution over the conductor cross section and with a frequency f $(s = 1)$, and k_X is the factor allowing for the decrease of the inductive reactance X'_{2sl} due to the skin effect. Analysis of this problem shows that

$$k_R = \xi \frac{\sinh 2\xi + \sin 2\xi}{\cosh 2\xi - \cos 2\xi} \tag{3.95}$$

and

$$k_X = \frac{3}{2\xi} \frac{\sinh 2\xi - \sin 2\xi}{\cosh 2\xi - \cos 2\xi} \tag{3.96}$$

where

$$\xi = h_{2b} \sqrt{\pi \mu_0 s f \sigma_2 \frac{b_{2b}}{b_2}} \tag{3.97}$$

and where h_{2b} is the height of the rotor bar, $\mu_0 = 0.4\pi \times 10^{-6}$ H/m is the magnetic permeability of free space, sf is the rotor slip frequency, σ_2 is the conductivity of the rotor winding, b_{2b} is the width of the rotor bar, and b_2 is the width of the rotor slot. Knowing ξ, it is possible to determine the factors k_R and k_X (see Fig. 3.20). For values of $\xi > 2$, the skin-effect coefficients can be simply expressed as:

$$k_R = \xi \qquad \text{and} \qquad k_X = \frac{3}{2\xi} \tag{3.98}$$

3.7.3 Comparison of torque–slip and input-current curves of cage induction motors.

Fig. 3.21 combines the characteristics of the torque and the input current for an ordinary cage induction motor, a double-cage motor with a high value of the starting torque, and a deep-bar motor, each as a function of the slip s. The highest starting current I_{1st} $(s = 1)$ and the highest pull-out torque T_{dmax} $(s = s_{cr})$ are found in the ordinary single-cage motor. Induction motors using the skin effect in their rotor have lower starting currents and higher starting torques than ordinary single-cage motors.

3.8 Speed control

Eqn (3.2) provides the basis for several methods of speed control for induction motors, which can be grouped under the headings of changing:

- the input frequency f;
- the number of stator pole pairs p;
- the slip s, i.e. by adjusting the rotor circuit resistance of wound-rotor induction motors or the input voltage of cage induction motors.

3.8.1 Frequency changing for speed control

An excellent way to control the speed of an induction motor is to vary the input frequency using solid–state converters. Assuming $R_1 \ll X_1+X_2'(1+\tau_1)$ and $1+\tau_1 \approx 1$, the pull out torque according to eqn (3.74) is

$$T_{dmax} \approx \pm \frac{m_1 V_1^2}{4\pi n_s} \frac{1}{2\pi f(L_1 + L_2')} = \pm \frac{m_1 p}{8\pi^2} \frac{1}{L_1 + L_2'} \left(\frac{V_1}{f}\right)^2 \tag{3.99}$$

where $L_1 = X_1/(2\pi f)$ and $L_2' = X_2'/(2\pi f)$ are, respectively, the stator winding inductance and the rotor winding inductance (referred to the stator winding).

The critical slip according to eqn (3.73) is

$$s_{cr} \approx \pm \frac{R_2'}{2\pi f(L_1 + L_2')} \tag{3.100}$$

Note that *both the pull-out torque and critical slip are inversely proportional to the input frequency*. Hence, if the input frequency f decreases while V_1 =const, the speed will decrease too (via an increase in slip), and the overload capacity factor OCF will increase according to eqn (3.76) (see Fig. 3.22a). The magnetic flux Φ will also increase, since the stator EMF $E_1 \approx V_1$ is expressed by eqns (3.15) and (3.16). The product $f\Phi$ must be constant at V_1 =const. Obviously, at a reduced input frequency the stator core losses increase due to an increase in the magnetic flux density. Changing the input frequency, the speed is usually controlled by keeping V_1/f=const (see Fig. 3.23). This ensures approximately constant magnetic flux density $\Phi = const$ in the airgap.

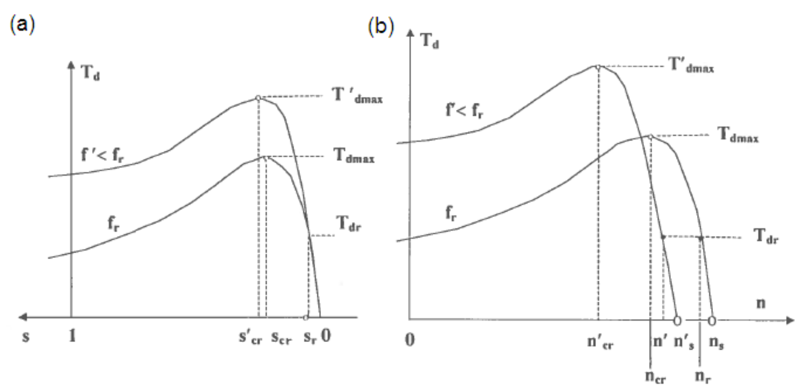

Fig. 3.22. Influence of the input frequency on the characteristics: (a) torque–slip, (b) torque-speed.

A schematic power circuit diagram of a solid–state converter is shown in Fig. 3.24. It consists of a *rectifier* (a.c. to d.c. converter), an *intermediate circuit* (filter), and an *inverter* (d.c. to a.c. converter, Fig. 3.25a) each of which employs thyristors or other power semiconductor devices (for more detail, see Chapter 5).

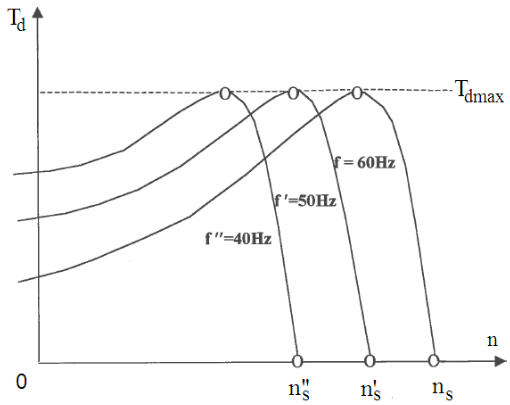

Fig. 3.23. Torque–speed characteristics of an induction motor for various input frequencies at $V_1/f = const.$

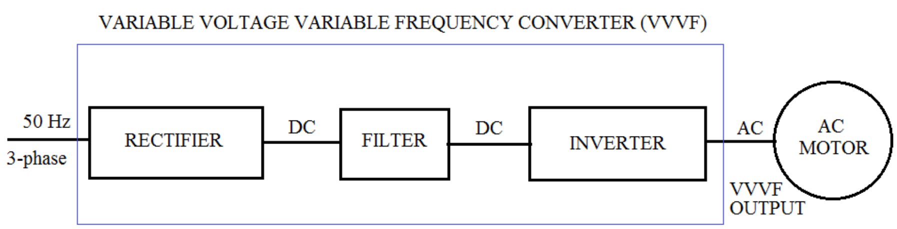

Fig. 3.24. Frequency conversion circuitry.

A thyristor with triggering facilities enables the frequency to be controlled. The principle of switching the thyristor so that it ceases to conduct is termed *commutation*. This can be *natural commutation*, where the thyristor ceases to conduct due to a natural decrease of current to zero, or it can be *forced commutation*, which is obtained by connecting a charged capacitor in parallel with the thyristor, thereby applying a reverse voltage across it (Fig. 3.25b). An auxiliary d.c. supply may be provided to combat the dependence of the capacitor charge upon the load current.

The sequence of the firing pulses that are sent as inputs to the inverter circuit can be controlled by a pulse generator in any desired manner, and the thyristors are generally fired in diagonal pairs, resulting in a stepped waveform such as the one shown in Fig. 3.26a. The fundamental of this waveform is the frequency that defines the speed at which the induction motor being driven by the circuit will operate. An alternative type of output from an inverter circuit is obtained by *high frequency chopping*, which results in a stepped PWM (*pulse width modulation*) waveform (as in Fig. 3.26b). Again, the fundamental frequency imposes the synchronous speed.

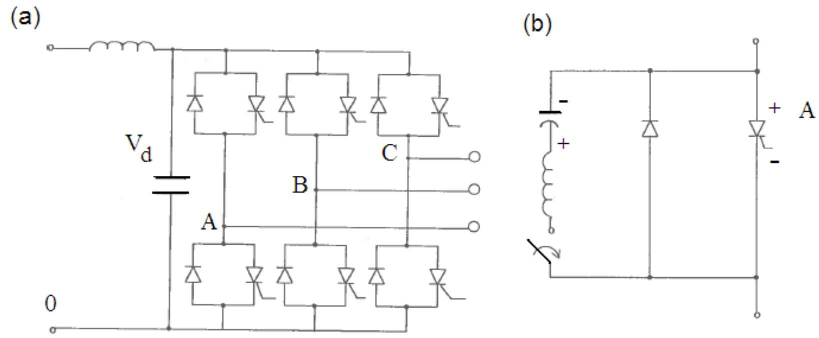

Fig. 3.25. Basic inverter circuit: (a) three-phase bridge, (b) forced commutation.

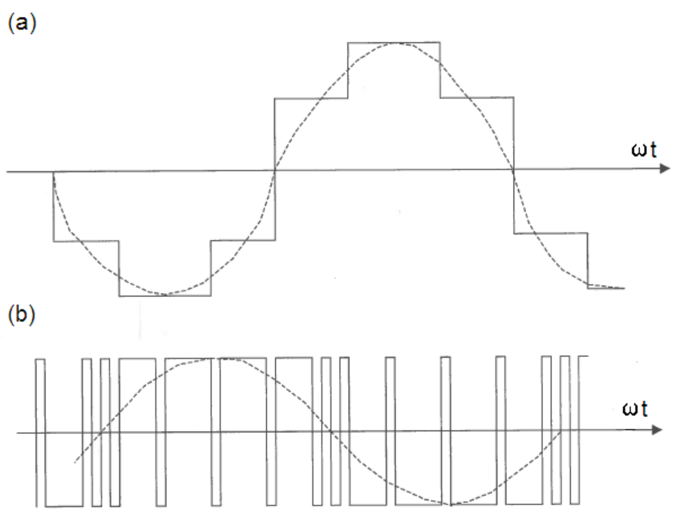

Fig. 3.26. Inverter output voltage waveforms: (a) six-pulse square-wave, (b) PWM waveform.

3.8.2 Pole changing for speed control

The number of pole pairs in the stator can be changed as follows:

- by placing one winding on the stator and changing the number of poles by successively reconnecting the parts of this winding;
- by placing two independent windings on the stator;
- by providing two independent stator windings, each with reconnection of the poles.

Double-speed motors are usually made with one winding on the stator, the number of poles being changeable in the ratio 1:2. Three- and four-speed motors are provided with two windings on the stator, one or both of which can have the number of its poles changed. So, for example, if it is desired to obtain a motor for four synchronous speeds, such as 1500, 1000, 750, and 500 rpm, two windings should be placed on the stator, one of which gives $p = 2$ and $p = 4$ pole pairs, the other $p = 3$ and $p = 6$.

If the motor has a wound rotor, the number of pole pairs must be changed simultaneously on the stator and rotor. This complicates the design of the rotor. Therefore, motors with a changing number of poles usually have a short-circuited rotor with a cage winding. Such a rotor can operate without any reconnection and with any number of stator poles.

There exist several methods of switching over the pole pairs of a winding. The one most frequently used is the method of changing the direction of the current in the separate halves of each phase winding or, more simply, in the half-windings. Schematic diagrams of the half-winding commutation which changes the number of poles in the ratio of 2:1 are given in Fig. 3.27a. When the number of poles is changed, the airgap flux density changes, and so do the torque – speed curves (Fig. 3.27b).

3.8.3 Speed control by voltage variation

The speed of an induction motor may be continuously controlled by controlling the input voltage applied to the stator winding: the electromagnetic torque is then proportional to the square of the input voltage. This method of speed control changes the output (shaft) torque, and hence the efficiency falls off drastically with the reduction in speed, making the method unsuitable for most applications.

3.8.4 Changing the resistance in the rotor circuit

In motors with slip rings the speed can be controlled with the aid of a rheostat in the rotor circuit. The control diagram does not differ from the ordinary diagram of an induction motor with a wound rotor (see Fig. 3.9). In practice, the control rheostats are similar to starting rheostats, but are bigger and are designed for continuous operation. The torque-speed characteristics are shown in Fig. 3.28.

3.9 Braking

Simple friction brakes may serve for hoists, lifts and cranes but electrical methods are adopted for more sophisticated drives, especially where precision in braking time or load positioning is called for. However, these electrical methods may impose severe duty cycles and may involve both thermal and mechanical stresses.

3.9.1 Direct current injection (dynamic) braking

In this method, the stator winding, immediately after its disconnection from the 3-phase supply, is excited with direct current from a rectifier and (in the case of slip-ring machines) a resistance is introduced into the rotor circuit. The d.c. excitation establishes a stationary gap flux, the magnitude and position of which depends

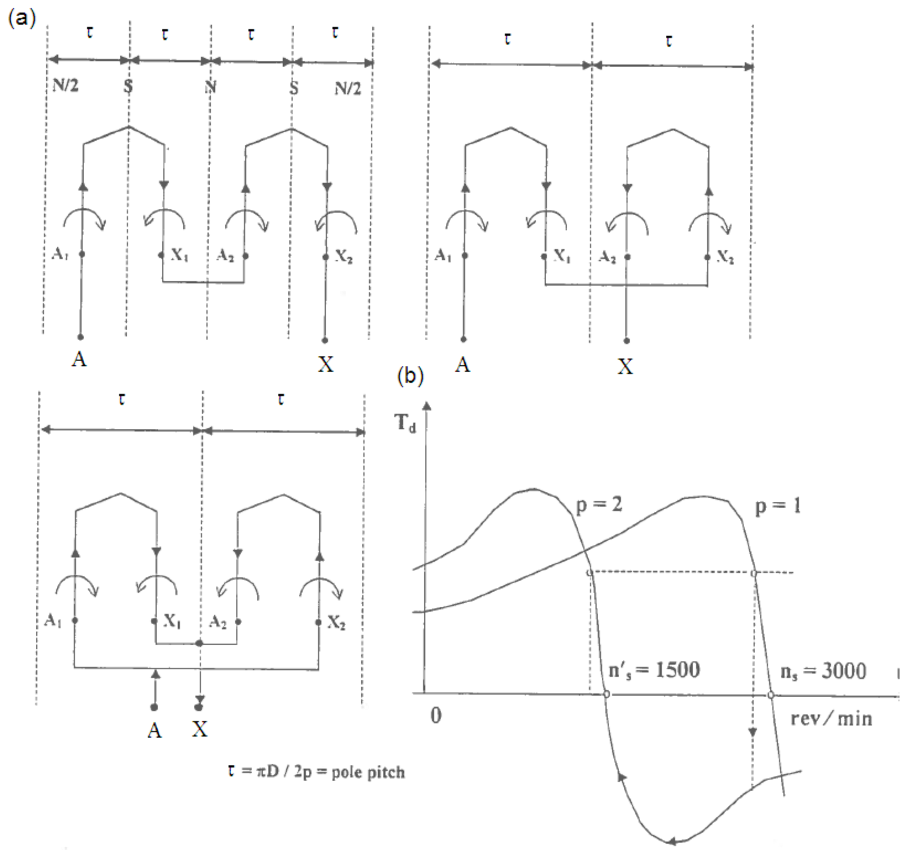

Fig. 3.27. Pole changing for speed control: (a) diagrams, (b) torque–speed characteristics.

on the resultant combined MMF of the d.c. stator and induced rotor currents. A rotor EMF, E_2, proportional to the flux and to the speed, is generated in the rotor winding, the braking effect being the result of the $I_2^2R_2$ loss. A typical connection diagram is given in Fig. 3.29a. The torque-speed characteristics are shown in Fig. 3.29b.

3.9.2 Plugging

Braking is obtained by reversal of the stator connections while the motor is running, so reversing the direction of the rotating-wave airgap field. The slip s is then greater than unity, and the machine develops a braking (i.e. reversed) torque. The stator and rotor currents are both large. Cage motors up to 20 kW are plugged direct, using the star connection if a Y–Δ switch is provided. Larger cage motors require stator resistors, and slip-ring motors employ rotor resistance for current limitation. Some speed-torque characteristics obtained for plugging are shown in Fig. 3.30.

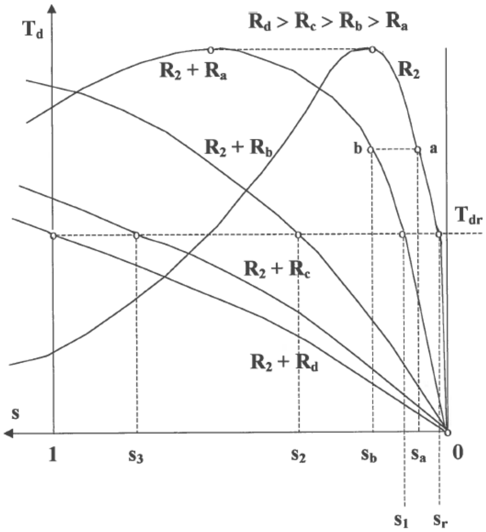

Fig. 3.28. Speed control by changing the slip (external rheostat resistance) of a wound-rotor motor.

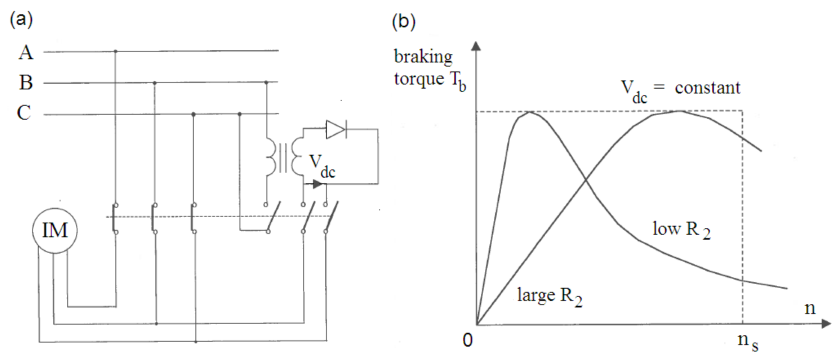

Fig. 3.29. Direct current injection braking: (a) circuit diagram, (b) braking characteristics.

3.9.3 Regenerative braking

The motor, overdriven by the load into a hypersynchronous speed (so that it exhibits negative slip), becomes an induction generator. In a slip-ring machine, braking can be maintained by a moderate rotor external resistance while useful energy is still returned to the supply. The relevant speed-torque characteristics are shown in Fig. 3.31.

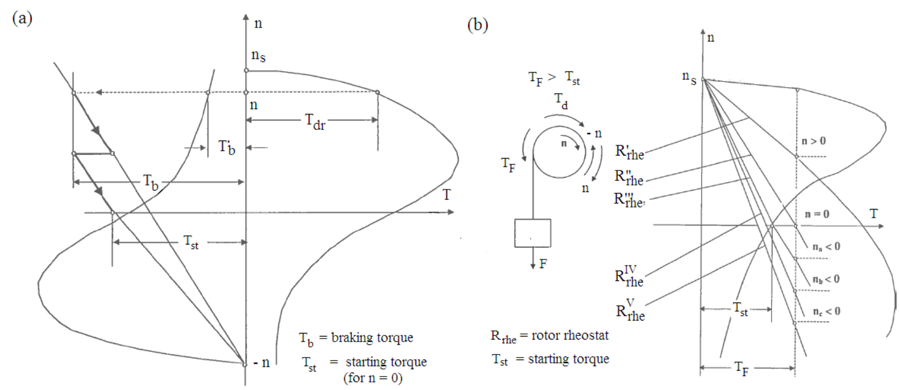

Fig. 3.30. Speed–torque characteristics for plugging obtained: (a) by reversal of two stator terminals, and (b) by lifting a mass, when $T_{st} < T_F$ and the rotor resistance is large.

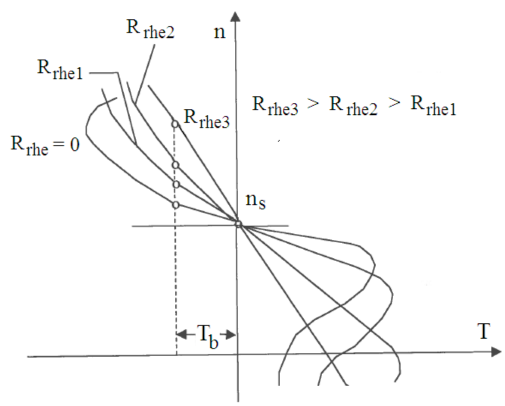

Fig. 3.31. Speed–torque charactersitics for regenerative braking.

3.10 Connection of a three-phase motor to a single-phase power supply

Typical induction motors with symmetrical three-phase windings can work when connected to a single-phase power supply. To obtain a starting torque, appropriate winding connections with additional elements R, L or C are necessary (see Fig. 3.32). The output power of a three-phase induction motor fed from single-phase mains is *always lower* than that of a motor fed with three-phase mains, and it is equal to between 55% and 70% of the rated power of a three-phase motor.

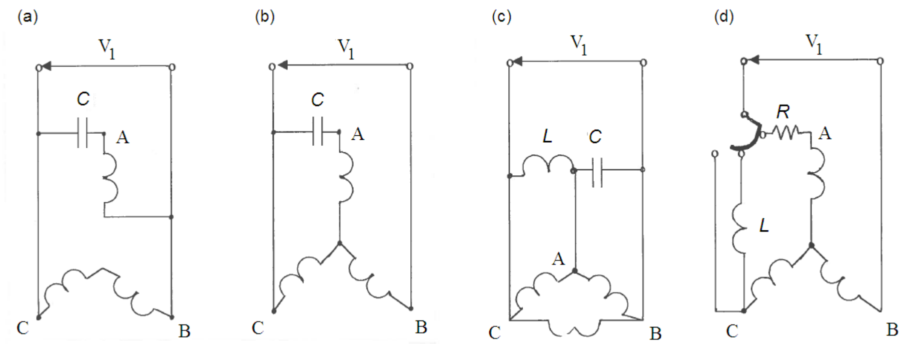

Fig. 3.32. Stator windings connection of a three-phase induction motor fed from single-phase mains.

3.11 Abnormal operating conditions

3.11.1 Increase in voltage, $P_{out} = const$

1. Rotor and stator currents dependent on the load fall almost inversely with voltage — see eqn (3.4);
2. Magnetizing current, flux density, saturation of the magnetic circuit and core losses rise. The temperature rise in the stator core due to the increased core losses and the quickly-rising magnetizing current limit the voltage increase;
3. The starting current rises at about the same rate;
4. The starting and pull-out torques increase as the square of the voltage;
5. At the same output, the power factor decreases due to the increased magnetizing current and the smaller active current;
6. The temperature rise in the rotor windings is reduced. The overall heating effect on the motor depends on whether the effect of the temperature rise in the core or in the windings is predominant. For normal voltage fluctuations it will hardly vary;
7. Efficiency will change little, rising or falling with the change in winding or core losses respectively;
8. Owing to the lower rotor losses, the speed will rise slightly.

3.11.2 Decrease in voltage $P_{out} = const$

1. Both the stator and rotor currents increase — see eqn (3.4);
2. Magnetizing current, flux density, core losses, and hence the temperature rise in the core, all fall;
3. The starting current drops approximately in proportion;
4. The starting and pull-out torques fall as the square of the voltage;
5. The power factor improves;
6. The rotor winding losses and in general the stator losses also increase, and as a rule heating increases;
7. Efficiency is hardly affected;
8. Speed drops off a little.

3.11.3 Change in frequency

A change in frequency results in proportional change in speed. Both the critical slip (eqn 3.73) and pull out torque (eqn 3.74) are inversely proportional to the input frequency. The power changes approximately in proportion to the frequency, although at lower frequencies it falls at a greater rate due to the deterioration in cooling.

Problems

1. The following data is read on the name plate of a three-phase cage induction motor: output power $P_{out} = 3$ kW, input frequency $f = 50$ Hz, speed $n = 2800$ rpm, voltage $V_1 = 380$ V (line-to-line), efficiency $\eta = 80\%$, power factor $\cos\phi = 0.92$. If the stator windings are Y-connected, find: (a) the number of poles $2p$, and the slip s, (b) the input current I_1, and input power P_{in}, (c) the mechanical power P_m and electromagnetic power P_g, given rotational losses $\Delta P_{rot} = 120$ W, (d) the shaft torque T and the developed torque T_d.

   Answer: (a) $2p = 2$, $s = 0.0666$, (b) $I_1 = 6.18$ A, $P_{in} = 3750$ W, (c) $P_m = 3120$ W, $P_g = 3343$ W, (d) $T = 10.23$ Nm, $T_d = 10.64$ Nm.
2. An induction motor, operating from a 60-Hz line, develops the output (shaft) power $P_{out} = 7.5$ kW at 1745 rev/min. At what speed will it run if the load torque is reduced to one-half ? What will be the output power at half torque ?

   Answer: $n = 1772.5$ rpm, $P_{out} \approx 3.8$ kW
3. A three-phase, six-pole (2p=6), 3000 V, 250 kW, 50 Hz induction motor has $s_1 = 90$ stator slots, and $s_2 = 80$ rotor slots. The number of stator turns per phase is $N_1 = 210$, and each coil has a span of 12 slots. The squirrel-cage rotor resistance is $R_2 = 13.6 \times 10^{-5}\,\Omega$ and the leakage reactance is $X_2 = 51.0 \times 10^{-5}\,\Omega$. Find the rotor impedance referred to the stator winding for $s = 1$.

   Answer: $\mathbf{Z}_2' = (0.75 + j2.8)\Omega$
4. Determine the stator rated current I_1, voltage drop across the stator winding impedance for rated operating conditions, blocked-rotor current I_2' and voltage drop across the rotor impedance assuming $s = 1$ for the motor of Problem 3 ($P_{out} = 250$ kW, $V_{1L} = 3000$ V, $m_1 = 3$, $f = 50$ Hz, Y connection, $R_1 = 0.72\ \Omega$, $R_2' = 0.75\ \Omega$, $X_1 = 2.78\ \Omega$, $X_2' = 2.8\ \Omega$, $\cos\phi = 0.9$ lagging, $\eta = 0.89$).

   Answer: $I_1 = 60$ A, $I_1 Z_1 = 172.3$ V, $I_2' \approx 561$ A at $s = 1$, $I_2' Z_2' = 1626.3$ V at $s = 1$
5. A four-pole induction motor draws 25 A from a 460 V (line-to-line), 50 Hz, three-phase line at a power factor of 0.85, lagging. The stator winding loss is $\Delta P_{1w} = 1000$ W, and the rotor winding loss is $\Delta P_{2w} = 500$ W. The rotational losses are $\Delta P_{rot} = 250$ W, core loss $\Delta P_{Fe} = 800$ W, and stray load loss $\Delta P_{str} = 200$ W. Calculate:
   (a) the electromagnetic (airgap) power, P_g;

(b) the mechanical power, P_m;
(c) the output power, P_{out};
(d) the efficiency, η;
(e) the slip, s, and operating speed, n;
(f) the developed torque, T_d;
(g) the shaft (output) torque, T.

Answer: (a) $P_g = 15\ 131$ W, (b) $P_m = 14\ 631$ W, (c) $P_{out} = 14\ 181$ W, (d) $\eta = 0.838$, (e) $s = 0.033$, $n \approx 1450$ rpm, (f) $T_d = 96.3$ Nm, (g) $T = 93.4$ Nm.

6. No-load and blocked-rotor tests have been performed on a three-phase, 500 kW, 50 Hz, Y-connected, 6 kV (line-to-line), 57 A, 980 rpm cage induction motor, with the following results:

   No-load test: input frequency $f = 50$ Hz, input voltage (line-to-line) $V_{10L-L} = 6$ kV, no-load current $I_{10} \approx I_{1exc} = 17$ A, no-load losses $\Delta P_0 = 14$ kW, rotational losses $\Delta P_{rot} = 3.5$ kW.

   Blocked-rotor test (s=1): input frequency $f = 50$ Hz, input voltage (line-to-line) $V_{1shL-L} = 380$ V, line current $I_{1sh} = 15$ A, input active power $P_{insh} = 1$ kW, stator winding resistance per phase $R_1 = 0.8\ \Omega$.

   Find the equivalent circuit resistances and reactances.

   Answer: $X_1 \approx X_2' = 7.3\ \Omega$, $R_{Fe} = 3670\ \Omega$, $X_m = 205\ \Omega$.

7. Find the overload capacity factor and starting torque ratio for the following cage induction motor: $m_1 = 3$, $P_{out} = 250$ kW, $V_{1L} = 3000$ V, $f = 50$ Hz, Y connection, $2p = 6$, $n = 972$ rev/min, $R_1 = 0.72\ \Omega$, $R_2' = 0.75\ \Omega$, $X_1 = 2.78\ \Omega$, $X_2' = 2.8\ \Omega$.

   Answer: $OCF \approx 2.3$, $STR = 0.662$.

8. A three-phase, four-pole, 210 kW, 50 Hz, 500 V (line-to-line), Y-connected cage induction motor is operating at its rated speed of $n_r = 1485$ rpm, rated voltage, and rated frequency. The critical slip corresponding to the pull-out torque is $s_{cr} = 0.044$. Find: (a) the starting torque T_{st} and (b) the starting current ratio SCR.

   Assumption: The no-load (exciting) current, Heyland's coefficient, and the stator winding resistance have all been neglected.

   Answer: $T_{st} = 274.13$ Nm, $SCR = 4.5$.

9. A three-phase, 50 Hz, 75 kW, 380 V (line-to-line) Y-connected, 1460 rpm, wound-rotor induction motor is operating at rated speed, rated voltage, and rated frequency with a three-phase rotor rheostat $R_{rhe} = 0.5\ \Omega$. The critical slip for $R_{rhe} = 0$ is $s_{cr} = 0.13$ and the rotor resistance is $R_2 = 0.05\ \Omega$. Find: (a) the starting torque T_{st} and (b) the starting current ratio SCR.

Assumption: The no-load (exciting) current, Heyland's coefficient, and stator winding resistance are neglected.

Answer: $T_{st} = 1170$ Nm, $SCR = 2.85$.

10. A three-phase, six-pole, 50 Hz, 2.8 kW, 220 V, Δ-connected, 950 rpm, cage induction motor has the overload capacity factor $OCF = 1.9$. This motor is connected to a three-phase, 50 Hz, 220 V line using a $Y - \Delta$ switch. The external shaft torque is $T = 0.15T_r$ where T_r is the rated torque. Find: (a) the starting current I_{1stY} and starting torque T_{stY} when the stator windings are Y-connected, (b) the steady-state speed n_Y and current I_{1Y} when the stator windings are Y-connected and (c) the developed torque $T^*_{d\Delta}$ and current $I^*_{1\Delta}$ when the speed $n^*_{\Delta} = n_Y$ and the stator windings are Δ-connected.

    Assumption: The no-load (exciting) current, Heyland's coefficient, and stator winding resistance are neglected.

    Answer: (a) $I_{1stY} = 9.65$ A, $T_{stY} = 6.08$ Nm, (b) $n_Y = 978.1$ rpm, $I_{1Y} = 1.17$ A, (c) $I^*_{1\Delta} = 2.03$ A, $T^*_{d\Delta} = 12.69$ Nm.

4

SYNCHRONOUS MOTORS

4.1 Construction

A *synchronous motor* operates at a constant speed in absolute synchronism with the line frequency. This means that the rotor speed is the same as that of the rotating magnetic field excited by the stator (or armature) a.c. winding.

There is no essential difference between the stators of polyphase synchronous and induction motors of comparable rating. The stator is made of stacked-up electrotechnical steel laminations, and the stator slots accommodate a three-phase distributed winding that sets up a rotating magnetic field.

The most common design of synchronous motor is the *salient-pole design* with concentrated rotor windings (see Fig. 4.1a). Synchronous motors are classified into the following groups, according to the design, construction, and material constitution of their rotors:

- electromagnetically-excited motors;
- permanent magnet (PM) motors;
- reluctance motors;
- hysteresis motors.

The rotor winding of an electromagnetically–excited synchronous motor is fed with d.c. current and requires only two slip rings. A significant feature of the electromagnetically–excited synchronous motor is the *controllability of its power factor* up to unity or leading values. To avoid the need for slip rings and brushes, almost all modern electromagnetically–excited motors are provided with *brushless excitation*, i.e. a small a.c. generator (exciter) is mounted on the rotor shaft, the output of which is rectified by shaft-mounted rectifiers rotating with the rotor. A cage winding is frequently mounted on salient-pole rotors that acts as a so-called *damper*, damping the oscillations under transient conditions. This winding is also necessary to start the motor (asynchronous starting).

A PM motor does not have the rotor excitation winding and thus field losses are eliminated. The use of PMs may also reduce the volume of a synchronous motor, and thereby produce a higher *output power-to-mass ratio*.

Synchronous motors can operate with higher efficiency than induction motors and can keep constant speed even under load variation and voltage fluctuation. They are most suitable for industrial drives such as compressors, blowers, pumps, fans, mills, crushers and motor-generator sets. Overexcited synchronous motors draw leading reactive current and can be used to compensate for a large number of induction motors that draw lagging reactive power. Synchronous motors are more expensive than their induction counterparts.

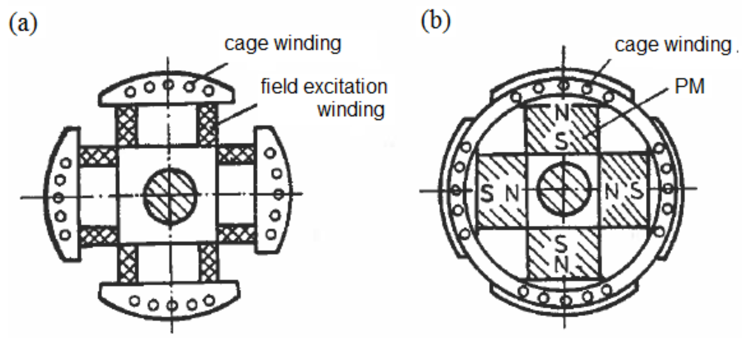

Fig. 4.1. Salient-pole synchronous motors with: (a) electromagnetic excitation, (b) permanent magnets.

4.2 Fundamental relationships

4.2.1 Speed

In the steady-state range, the *rotor speed* is given by the ratio of the *input frequency to the number of pole pairs*, as below:

$$n_s = \frac{f}{p} \tag{4.1}$$

This was also the case with the rotating magnetic field of an induction motor — compare eqn (3.2).

4.2.2 Induced voltage

The *rms* voltage (EMF) induced in one phase of the stator winding by the d.c. magnetic excitation flux Φ_f of the rotor is

$$E_f = \pi\sqrt{2} f N_1 k_{w1} \Phi_f \tag{4.2}$$

where N_1 is the number of stator turns per phase and k_{w1} is the stator winding coefficient (Appendix D).

Similarly, the voltage E_{ad} induced by the d-axis armature reaction flux Φ_{ad}, and the voltage E_{aq} induced by the q-axis flux Φ_{aq} are, respectively:

$$E_{ad} = \pi\sqrt{2} f N_1 k_{w1} \Phi_{ad} \tag{4.3}$$

and

$$E_{aq} = \pi\sqrt{2} f N_1 k_{w1} \Phi_{aq} \tag{4.4}$$

As shown in Fig. 4.1, the *direct* or d-axis is the centre axis of the magnetic pole, while the *quadrature* or q-axis is the axis of the highest airgap.

The EMFs per phase E_f, E_{ad}, and E_{aq}, and the magnetic fluxes Φ_f, Φ_{ad}, and Φ_{aq} are used in the construction of phasor diagrams and equivalent circuits.

4.2.3 Electromagnetic power

For an m_1-phase salient pole synchronous motor, the *electromagnetic power* (or airgap power) is expressed as

$$P_g = m_1 \left[\frac{V_1 E_f}{X_{sd}} \sin\delta + \frac{V_1^2}{2} \left(\frac{1}{X_{sq}} - \frac{1}{X_{sd}} \right) \sin 2\delta \right] \tag{4.5}$$

where V_1 is the input (terminal) phase voltage, E_f is the EMF induced by the d.c. magnetic excitation flux (without armature reaction), δ is the *power angle* (the angle between V_1 and E_f), X_{sd} is the synchronous reactance in the direct axis (called the d-axis synchronous reactance), and X_{sq} is the synchronous reactance in the quadrature axis (called the q-axis synchronous reactance).

4.2.4 Synchronous reactance

For a salient pole synchronous motor the d-axis and q-axis synchronous reactances are

$$X_{sd} = X_1 + X_{ad} \qquad \text{and} \qquad X_{sq} = X_1 + X_{aq} \tag{4.6}$$

where $X_1 = 2\pi f L_1$ is the stator winding leakage reactance, L_1 is the stator leakage inductance, X_{ad} is the d-axis armature reaction reactance, and X_{aq} is the q-axis armature reaction reactance. The armature reaction reactances X_{ad} and X_{aq} correspond to the mutual (airgap) reactance X_m of an induction motor. Usually, $X_{sd} > X_{sq}$, except in the case of some PM synchronous machines.

4.2.5 Electromagnetic (developed) torque

The *electromagnetic torque* developed by a synchronous motor is determined by the airgap power P_g and also by the angular synchronous speed $\Omega_s = 2\pi n_s$, which is equal to the mechanical angular speed of the rotor. These relationships may be written as follows:

$$T_d = \frac{P_g}{2\pi n_s} = \frac{m_1}{2\pi n_s} \left[\frac{V_1 E_f}{X_{sd}} \sin\delta + \frac{V_1^2}{2} \left(\frac{1}{X_{sq}} - \frac{1}{X_{sd}} \right) \sin 2\delta \right] \tag{4.7}$$

In a salient-pole synchronous motor, the electromagnetic torque has two components (see Fig. 4.2):

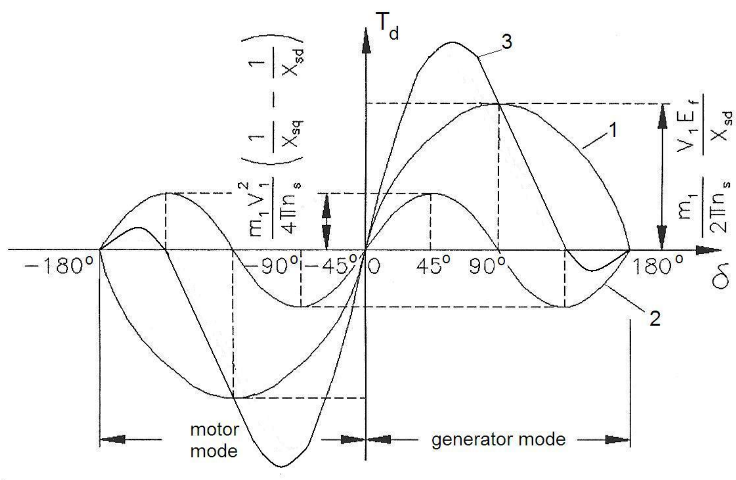

Fig. 4.2. Torque-angle characteristics of a salient-pole synchronous machine: 1 — synchronous torque T_{dsyn}, 2 — reluctance torque T_{drel}, 3 — resultant torque T_d.

$$T_d = T_{dsyn} + T_{drel} \tag{4.8}$$

where the fundamental part of the torque is written

$$T_{dsyn} = \frac{m_1}{2\pi n_s} \frac{V_1 E_f}{X_{sd}} \sin\delta \tag{4.9}$$

and is seen to be a function both of the input voltage V_1 and of the excitation EMF E_f. Meanwhile, the additional part of the torque is expressed as

$$T_{drel} = \frac{m_1 V_1^2}{4\pi n_s}\left(\frac{1}{X_{sq}} - \frac{1}{X_{sd}}\right)\sin 2\delta \tag{4.10}$$

and so depends *only* on the voltage V_1, and thus may exist in an unexcited machine (where $E_f = 0$). The torque T_{dsyn} is called the *synchronous torque* and the torque T_{drel} is called the *reluctance torque*.

In the particular case of synchronous machines with cylindrical rotors, $X_{sd} = X_{sq}$ and hence

$$T_d = T_{dsyn} = \frac{m_1}{2\pi n_s} \frac{V_1 E_f}{X_{sd}} \sin\delta \tag{4.11}$$

4.3 Phasor diagram

When drawing phasor diagrams of synchronous machines, two arrow systems are used:

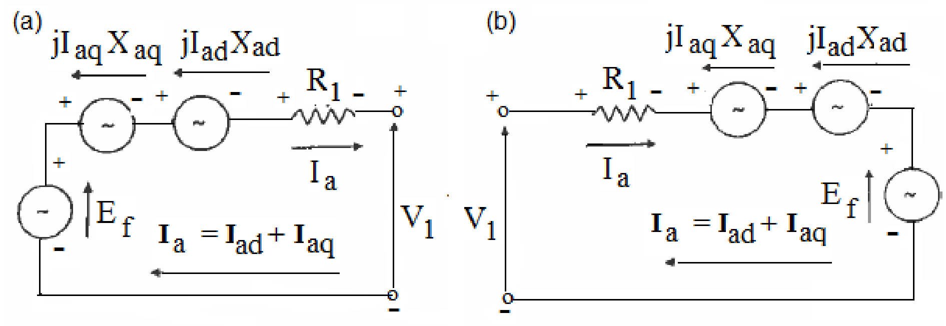

Fig. 4.3. Equivalent circuits of salient-pole synchronous machines: (a) generator arrow system, (b) consumer (motor) arrow system.

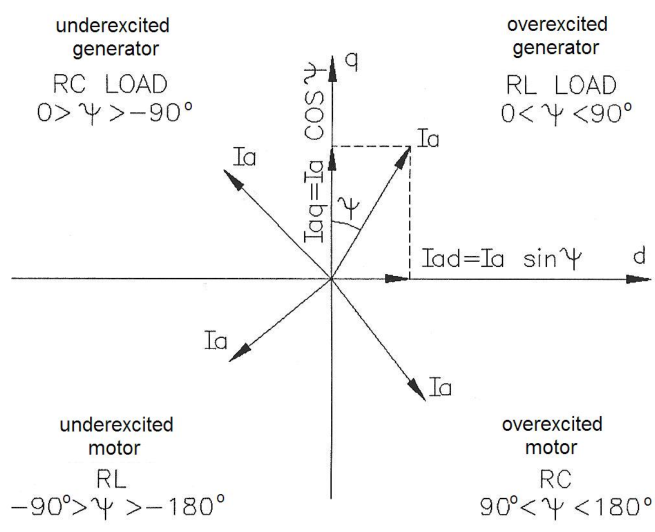

Fig. 4.4. Location of the armature current $\mathbf{I}_a$ in d–q coordinate system.

(a) the generator arrow system (see Fig. 4.3a), where

$$\mathbf{E}_f = \mathbf{V}_1 + \mathbf{I}_a R_1 + j\mathbf{I}_{ad} X_{sd} + j\mathbf{I}_{aq} X_{sq}$$

$$= \mathbf{V}_1 + \mathbf{I}_{ad}(R_1 + jX_{sd}) + \mathbf{I}_{aq}(R_1 + jX_{sq}) \tag{4.12}$$

(b) the consumer (motor) arrow system (see Fig. 4.3b), in which

$$\mathbf{V}_1 = \mathbf{E}_f + \mathbf{I}_a R_1 + j\mathbf{I}_{ad} X_{sd} + j\mathbf{I}_{aq} X_{sq}$$

$$= \mathbf{E}_f + \mathbf{I}_{ad}(R_1 + jX_{sd}) + \mathbf{I}_{aq}(R_1 + jX_{sq}) \tag{4.13}$$

where

$$\mathbf{I}_a = \mathbf{I}_{ad} + \mathbf{I}_{aq} \tag{4.14}$$

and

$$I_{ad} = I_a \sin\Psi \qquad\qquad I_{aq} = I_a \cos\Psi \tag{4.15}$$

where $\Psi = \phi \pm \delta$ is the angle between the excitation voltage E_f (the q-axis) and the armature current I_a (called the internal power factor angle). Note that if current arrows are drawn in opposite directions, this represents the rotation of the phasors (such as $\mathbf{I}_a$, $\mathbf{I}_{ad}$ or $\mathbf{I}_{aq}$) by 180^0, and it also means that voltage drops are represented in the opposite directions.

The location of the armature current $\mathbf{I}_a$ with respect to the d- and q-axes for generator and motor mode is shown in Fig. 4.4.

Phasor diagrams for synchronous generators are constructed using the generator arrow system. The same system can be used for motors. Fig. 4.5a shows a phasor diagram for a loaded synchronous motor, in which the load current, $\mathbf{I}_a$, lags behind the phasor of the applied voltage, $\mathbf{V}_1$, by the angle ϕ. At this angle the motor is *underexcited*, and an inductive current component, $I_a \sin\phi$, is induced with respect to the voltage $\mathbf{V}_1$. An underexcited motor thus draws an inductive current and hence also draws the corresponding reactive power from the line. Fig. 4.5b shows the phasor diagram for an underexcited motor, this time using the consumer arrow system. For synchronous motors, the consumer arrow system is more popular than the generator arrow system as a method of illustrating the current and voltage relationships within the motor. Fig. 4.5c is a phasor diagram that uses the consumer arrow system to show a load current $\mathbf{I}_a$ that *leads* the vector $\mathbf{V}_1$ by the angle ϕ. By contrast with the previous example, this motor is *overexcited* and thus induces, with respect to the line voltage $\mathbf{V}_1$, a capacitive current component $I_a \sin\phi$. An overexcited motor, consequently, draws a leading current from the circuit and delivers reactive power to it.

The input voltage V_1 projections on the d and q axes are

$$V_1 \sin\delta = I_{aq} X_{sq} - I_{ad} R_1$$

$$V_1 \cos\delta = E_f + I_{ad} X_{sd} + I_{aq} R_1 \tag{4.16}$$

The currents

$$I_{ad} = \frac{V_1(X_{sq}\cos\delta - R_1 \sin\delta) - E_f X_{sq}}{X_{sd} X_{sq} + R_1^2} \tag{4.17}$$

$$I_{aq} = \frac{V_1(R_1 \cos\delta + X_{sd}\sin\delta) - E_f R_1}{X_{sd} X_{sq} + R_1^2} \tag{4.18}$$

are obtained by solving the set of eqns (4.16).

In the phasor diagrams of Fig. 4.5, stator core losses have been neglected. This assumption is justified only for medium-power and large synchronous motors.

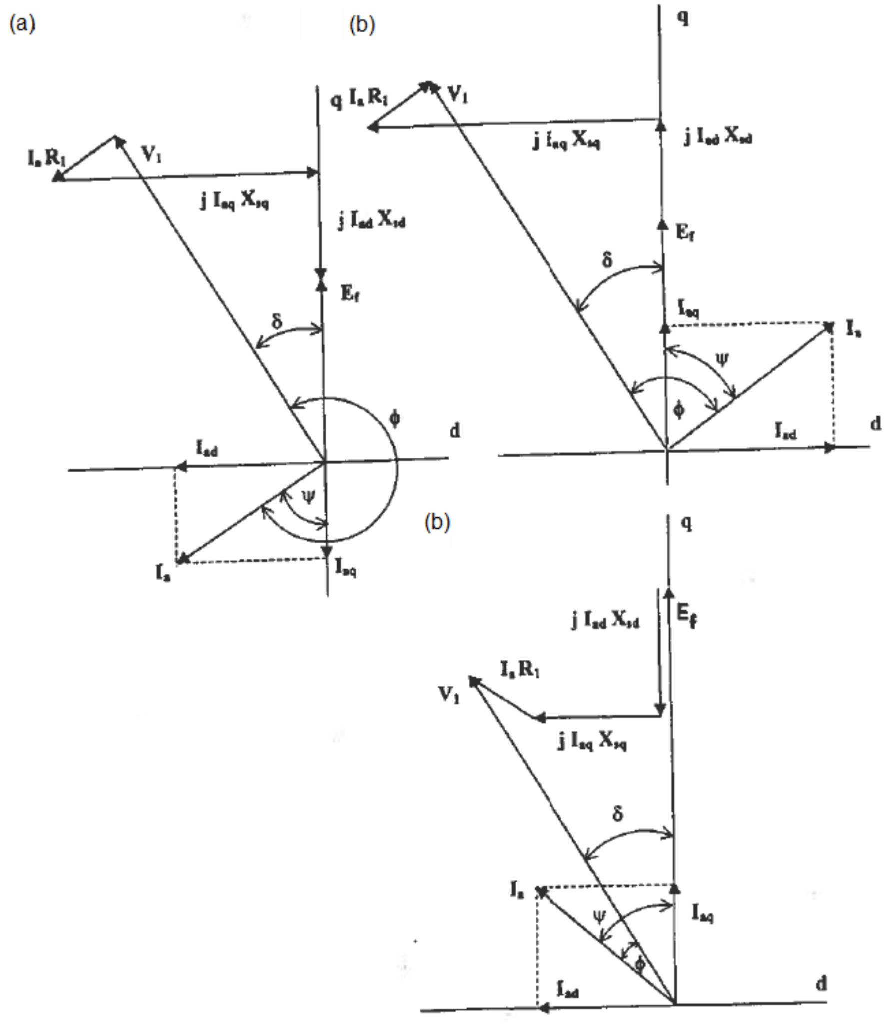

Fig. 4.5. Phasor diagrams of some salient-pole synchronous motors with electromagnetic excitation: (a) generator arrow system — underexcited motor, (b) consumer arrow system — underexcited motor, (c) consumer arrow system — overexcited motor.

Example 4.1

A three-phase, four-pole, 500 kW, 3.3 kV (line-to-line), 50 Hz, $\cos\phi = 0.8$ (lagging), $\eta = 0.94$, star-connected, salient pole synchronous motors has the d-axis synchronous reactance $X_{sd} = 10.0\ \Omega$ and the q-axis synchronous reactance $X_{sq} = 6.0\ \Omega$. The stator resistance can be neglected (large synchronous motor). Find the electromagnetic power, developed torque, maximum developed synchronous torque and maximum developed reluctance torque.

Solution

The number of pole pairs is $p = 2$. The synchronous speed according to eqn (4.1)

$$n_s = \frac{50}{2} = 25 \text{ rev/s} = 1500 \text{ rpm}$$

The phase voltage $V_1 = 3300/\sqrt{3} = 1905.25$ V. The armature current

$$I_a = \frac{P_{out}}{3V_1\eta\cos\phi} = \frac{500\times 10^3}{3\times 1905.25\times 0.94\times 0.8} = 116.33 \text{ A}$$

If $R_1 = 0$, according to the first eqn (4.16) $V_1\sin\delta \approx I_{aq}X_{sq} = I_aX_{sq}\cos(\phi\pm\delta)$ where $\cos(\phi\pm\delta) = \cos\phi\cos\delta \mp \sin\phi\sin\delta$. Thus

$$\tan\delta \approx \frac{I_aX_{sq}\cos\phi}{V_1 \pm I_aX_{sq}\sin\phi}$$

where the '+' sign is used when $\Psi = \phi + \delta$ and the '−' sign is used when $\Psi = \phi - \delta$. For given rated conditions

$$\tan\delta \approx \frac{116.33\times 6.0\times 0.8}{1905.25 - 116.33\times 6.0\times 0.6} = 0.3756$$

where $\sin\phi = 0.6$, i.e. $\cos\phi = 0.8$. The rated power angle $\delta = 20.59^0$, $\sin\delta = 0.3517$ and $\cos\delta = 0.9361$.

The q-axis armature current can be found on the basis of the first eqn (4.16) in which $R_1 = 0$, i.e.

$$I_{aq} \approx \frac{V_1\sin\delta}{X_{sq}} = \frac{1905.25\times 0.3517}{6.0} = 111.67 \text{ A}$$

The d-axis armature current

$$I_{ad} = \sqrt{I_a^2 - I_{aq}^2} = \sqrt{116.33^2 - 111.67^2} = 32.59 \text{ A}$$

The EMF E_f excited by the rotor flux can be found on the basis of the second eqn (4.16) in which $R_1 = 0$, i.e.

$$E_f \approx V_1\cos\delta - I_{ad}X_{sd} = 1905.25\times 0.9361 - 32.59\times 10.0 = 1457.64 \text{ V}$$

The electromagnetic power according to eqn (4.5)

$$P_g = 3\left[\frac{1905.25 \times 1457.64}{10.0}\sin(20.59^0) + \frac{1905.25^2}{2}\left(\frac{1}{6.0} - \frac{1}{10.0}\right)\sin(2 \times 20.59^0)\right]$$

$$= 531\ 997.7 \text{ W}$$

Since the stator winding resistance and the stator core losses have been neglected, the calculated electromagnetic power P_g is too high and equal to the input power P_{in}.

The electromagnetic torque according to eqn (4.7)

$$T_d = \frac{531\ 997.7}{2\pi \times 25} = 3386.8 \text{ Nm}$$

The maximum synchronous torque is for $\delta = 90^0$ or $\sin\delta = 1$, i.e.

$$T_{dsynmax} = \frac{3}{2\pi n_s}\frac{V_1 E_f}{X_{sd}} = \frac{3}{2\pi \times 25}\frac{1905.25 \times 1457.64}{10.0} = 5304 \text{ Nm}$$

The maximum reluctance torque si for $\delta = 45^0$ or $\sin 2\delta = 1$, i.e.

$$T_{drelmax} = \frac{3V_1^2}{4\pi n_s}\left(\frac{1}{X_{sq}} - \frac{1}{X_{sd}}\right) = \frac{3 \times 1905.25^2}{4\pi \times 25}\left(\frac{1}{6.0} - \frac{1}{10.0}\right) = 2310.91 \text{ Nm}$$

4.4 Characteristics

The most important characteristics of a synchronous motor are its torque—angle characteristic $T_d = f(\delta)$ (Fig. 4.2) and its armature current—field current characteristics (V-curves) $I_a = f(I_f)$ at $P_{out} = const$ or at $T = const$ (see Fig. 4.6).

Any change in the exciting current at $P_{out} = const$ results in a change in both the armature current and the power factor. The characteristic curves for $I_a = f(I_f)$ are limited on the left-hand side by stability restrictions, and on the right-hand side by maximum currents allowable in the windings. Minimum armature current is obtained when $\cos\phi = 1$. The motor operates at a lagging power factor, corresponding to an underexcited motor (or RL load), if its operating point is to the left of the unity power factor line, and conversely, the power factor is leading, corresponding to an overexcited motor (or RC load), if the operating point is to the right of the unity power factor line.

The most important advantage of synchronous motors with an electromagnetic excitation is the possibility of controlling the power factor by changing the excitation current. Since an overexcited motor behaves like an RC load, it can compensate for the reactive power consumed, for example, by nearby induction motors or underloaded transformers.

4.5 Starting

4.5.1 Starting by means of an auxiliary motor

The synchronous motor has an auxiliary starting motor on its shaft, capable of bringing it up to the synchronous speed at which synchronizing with the power

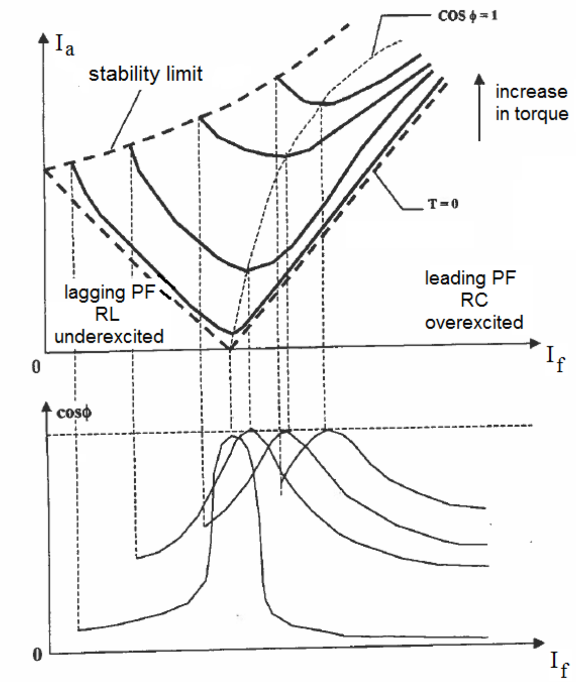

Fig. 4.6. V-curves $I_a = f(I_f)$ at T =const and $\cos\phi = f(I_f)$ for a synchronous motor.

circuit is possible. This auxiliary motor is commonly an induction motor. At start-up, the unexcited synchronous motor is accelerated almost to synchronous speed using the induction motor. At first, the synchronous motor is connected to the mains with an additional resistance across its rotor slip rings. The value of this resistance is about ten times that of the resistance of the field winding itself. If the latter were left open when the motor was started, such a high voltage would be induced across its terminals (owing to the great number of turns in the winding) that there would be a real danger of a breakdown of the insulation. Once the speed is close to the synchronous speed, the additional field winding resistance is removed and a d.c. excitation field current is supplied. The synchronous motor is then pulled into synchronism.

The disadvantage of this method is that it is impossible to start the motor under load. Larger auxiliary motors and very costly installation would be involved, and this is generally completely impractical.

4.5.2 Frequency-change starting

In this method, the frequency of the voltage applied to the motor is smoothly changed from zero up to the rated value. The motor runs synchronously during the entire starting period. Semiconductor inverters are commonly used to achieve this.

4.5.3 Asynchronous starting

A synchronous motor which has a cage winding on its rotor can be started as a cage induction motor. The starting torque is produced as a result of the interaction between the stator rotating magnetic field and the rotor winding currents. In small synchronous motors with solid steel salient poles, the cage winding is not necessary since the eddy currents induced in the solid steel pole shoes can interact with the stator magnetic field.

At the first instant of starting, using the asynchronous starting method, the field winding of the synchronous motor should be short-circuited or else closed via a resistance.

4.6 Comparison with induction motors

Table 4.1. Comparison between electromagnetically-excited synchronous and induction motors

Quantity	Electromagnetically-excited synchronous motor	Induction motor
Speed	Constant, independent of the load	As the load increases, the speed decreases slightly
$\cos\phi$	Adjustable $\cos\phi$ Operation at $\cos\phi = 1$ is possible	Impossible to change $\cos\phi$ (except for inverter-fed motors) $\cos\phi \approx 0.8...0.9$ at rated load $\cos\phi = 0.1$ at no load
Airgap	Large, from a few millimeters up to centimeters	Small, from less than 1 mm to maximum of 3 mm
Torque-voltage characteristic	Torque directly proportional to the input voltage. Better starting performance than that of an induction motor	Torque directly proportional to the square of the input voltage
Price	Expensive machine	Relatively cheap machine

Table 4.1 gives a comparison of the speed, power factor ($\cos\phi$), airgap, torque-voltage characteristic, and price of electromagnetically excited synchronous motors and induction motors. The large airgap in synchronous motors, which actually makes them much more reliable than induction motors, is also a practical requirement which minimises the effect of the armature reaction, minimises the synchronous reactance and improves stability.

4.7 Permanent magnet synchronous motors

Recent developments in rare-earth PM materials and in power electronics have opened new prospects for the design, construction and applications of PM motors. Servo drives with PM motors fed from solid-state converters are becoming commercially available on an increasing scale, and the continuous power of PM servo drives now reaches about 15 kW at 1500 rpm.

Rare earth PMs have also recently been used in prototypes of large power motors rated in the range of a few MWs. The applications of these large PM motors include both low-speed drives (such as for ship propulsion) and high-speed drives (in pumps and compressors).

The application of rare-earth PMs to large synchronous motors not only eliminates the need for an exciter and for sliding contacts (brushes and slip rings), but also offers much lower motor volume, limited maintenance, high efficiency over a broad range of loads, very good dynamic performance and reduced noise. On the other hand, each motor requires quite a large quantity of rare-earth PM material, and this results in higher motor prices.

PM synchronous motors are usually built with one of the following rotor configurations:

(a) classical (see Fig. 4.7a);
(b) interior-magnet rotor (Fig. 4.7b);
(c) surface-magnet rotor (Fig. 4.7c);
(d) inset-magnet rotor (Fig. 4.7d);
(e) rotor with buried-magnets symetrically distributed (Fig. 4.7e);
(f) rotor with buried magnets asymetrically distributed (Fig. 4.7f).

In the *classical PM rotor* (Fig. 4.7a), the magnets are magnetized radially and a cage winding is placed in laminated pole shoes so as to provide an internal torque in the course of asynchronous starting.

The *interior-magnet rotor* of Fig. 4.7b has radially magnetized and alternately-poled magnets. Because the magnet pole area is smaller than the pole area at the rotor surface, the airgap flux density on open circuit is less than the flux density in the magnet.

The *surface magnet rotor* can have magnets magnetized radially (as in Fig. 4.7c) or circumferentially. An external copper cylinder is sometimes used. It protects the PMs against the demagnetizing action of the armature reaction, provides an asynchronous starting torque, and acts as a damper. The *inset-type PM rotor* shown in Fig. 4.7d is very similar to the surface-magnet rotor.

The *buried-magnet rotor* has circumferentially magnetized PMs (Fig. 4.7e). An asynchronous starting torque is produced with the aid either of a cage winding (if the core of the motor is laminated) or of salient poles (in the case of a motor with a solid steel core). If the motor shaft is ferromagnetic, however, a large amount of useless magnetic flux will be directed through it. To increase the linkage flux, therefore, a buried-magnet rotor should always be equipped with a nonferromagnetic shaft.

An alternative construction involves a rotor with *asymmetrically distributed buried magnets* (Fig. 4.7f), in which the magnets are magnetized radially.

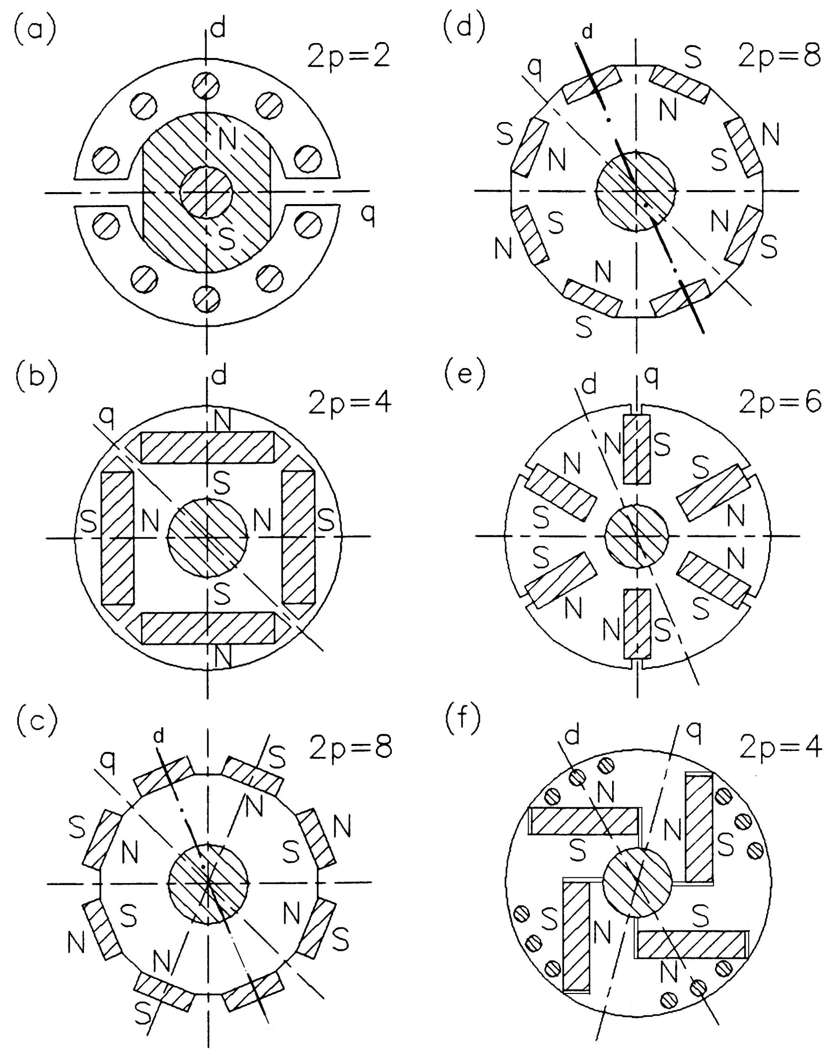

Fig. 4.7. Rotor configurations for PM synchronous motors: (a) classical configuration, (b) interior-magnet rotor, (c) surface-magnet rotor, (d) inset-magnet rotor, (e) rotor with buried-magnets symetrically distributed, (f) rotor with buried magnets asymetrically distributed.

Table 4.2. Comparison between permanent magnet synchronous motors with surface and buried magnets symetrically distributed

Surface magnets	Buried magnets
Airgap magnetic flux density is smaller than B_r	Airgap magnetic flux density can be greater than B_r (with more than four poles)
Simple motor construction	Relatively complicated motor construction (a nonferromagnetic shaft is common)
Small armature reaction flux	Higher armature reaction flux, consequently more expensive converter
Permanent magnets not protected against armature fields	Permanent magnets protected against armature fields
Eddy-current losses in permanent magnets (when their conductivity is greater than zero)	No eddy-current losses in permanent magnets

Example 4.2

A three-phase, 4-pole, 50 Hz, 1.5 kW, 380 V (line-to-line), star-connected synchronous motor with a buried-type permanent magnet rotor has the stator winding resistance per phase $R_1 = 4.98\ \Omega$, d-axis synchronous reactance $X_{sd} = 18.5\ \Omega$ and q-axis synchronous reactance $X_{sq} = 40.5\ \Omega$ (in a typical buried magnet motor $X_{sd} < X_{sq}$). The number of turns per phase $N_1 = 240$, the winding factor $k_{w1} = 0.96$, the effective length of the stator core $L_i = 0.103$ m and the inner stator core diameter $D = 0.0825$ m. At the power angle $\delta = 45^0$, the airgap magnetic flux density $B_{mg} = 0.685$ T, the rotational losses $\Delta P_{rot} = 40$ W, the stray losses $\Delta P_{str} = 0.05 P_{out}$ and the stator core losses can be neglected. Find the armature current, developed torque T_d, output power P_{out}, efficiency η and power factor $\cos\phi$.

Solution

The number of pole pairs is $p = 2$. The synchronous speed according to eqn (4.1)

$$n_s = \frac{50}{2} = 25 \text{ rev/s} = 1500 \text{ rpm}$$

The phase voltage $V_1 = 380/\sqrt{3} = 219.4$ V.

The pole pitch

$$\tau = \frac{\pi D}{2p} = \frac{\pi \times 0.0825}{4} = 0.0648 \text{ m}$$

The magnetic flux (fundamental space harmonic) produced by the rotor

$$\Phi_f = \frac{2}{\pi}\tau L_i B_{mg} = \frac{2}{\pi}0.0648 \times 0.103 \times 0.685 = 0.00291 \text{ Wb}$$

The EMF per phase induced in the stator winding by the rotor flux Φ_f according to eqn (4.2)

$$E_f = \pi\sqrt{2} \times 50 \times 240 \times 0.96 \times 0.00291 = 148.94 \text{ V}$$

For the power angle $\delta = 45^0$ or $\delta = 45 \times \pi/180 = 0.7854$ rad, $\cos\delta = \sin\delta \approx 0.707$. The components of the armature current according to eqns (4.17) and (4.18)

$$I_{ad} = \frac{219.4(40.5 \times 0.707 - 4.98 \times 0.707) - 148.94 \times 40.5}{18.5 \times 40.5 + 4.98^2} = -0.68 \text{ A}$$

$$I_{aq} = \frac{219.4(4.98 \times 0.707 + 18.5 \times 0.707) - 148.94 \times 4.98}{18.5 \times 40.5 + 4.98^2} = 3.75 \text{ A}$$

This is an overexcited motor. The *rms* armature current

$$I_a = \sqrt{I_{ad}^2 + I_{aq}^2} = \sqrt{(-0.68)^2 + 3.75^2} = 3.81 \text{ A}$$

The input apparent power

$$S_{in} = 3V_1 I_a = 3 \times 219.4 \times 3.81 = 2507.7 \text{ W}$$

On the basis of the phasor diagram (Fig. 4.5) the following relationship [17] can be obtained

$$I_a \cos\phi = I_{aq}\cos\delta - I_{ad}\sin\delta$$

$$= 3.75 \times 0.707 - (-0.68) \times 0.707 = 3.13 \text{ A}$$

The input active power

$$P_{in} = 3V_1 I_a \cos\phi = 3 \times 219.4 \times 3.13 = 2060.2 \text{ W}$$

The stator winding losses according to eqn (3.6)

$$\Delta P_{1w} = 3I_a^2 R_1 = 3 \times 3.81^2 \times 4.98 = 216.9 \text{ W}$$

Neglecting the stator core losses, the electromagnetic power is

$$P_g \approx P_{in} - \Delta P_{1w} = 2060.2 - 216.9 = 1843.3 \text{ W}$$

The developed torque

$$T_d = \frac{P_g}{2\pi n_s} = \frac{1843.3}{2\pi \times 25} = 11.73 \text{ Nm}$$

The output power

$$P_{out} = P_g - \Delta P_{rot} - \Delta P_{str} = P_g - \Delta P_{rot} - 0.05\Delta P_{out}$$

Thus

$$P_{out} = \frac{1}{1.05}(P_g - \Delta P_{rot}) = \frac{1}{1.05}(1843.3 - 40.0) = 1717.4 \text{ W}$$

The shaft torque

$$T_{sh} = \frac{P_{out}}{2\pi n_s} = \frac{1717.4}{2\pi \times 25} = 10.93 \text{ Nm}$$

The efficiency

$$\eta = \frac{1717.4}{2060.2} = 0.834$$

The power factor

$$\cos\phi = \frac{P_{in}}{S_{in}} = \frac{2060.2}{2507.7} = 0.821$$

4.8 Synchronous reluctance motors

The *synchronous reluctance motor* runs with an unexcited rotor that has unequal reluctance in its d and q axes. Since the rotor has no excitation system, the EMF in eqns (4.5), (4.7), (4.9), (4.11), (4.12), (4.13), (4.16), (4.17) and (4.18) is zero ($E_f = 0$).

The input current I_a of a reluctance motor is higher than that of ordinary synchronous and induction motors since the EMF $E_f = 0$. This correspondingly affects the efficiency, because of the resultant high power losses in the stator winding.

The developed torque (or reluctance torque) is obtained from eqn (4.7), once again by setting $E_f = 0$. The T_{drel} given by eqn (4.10) exists as a result of a change in the energy of the magnetic field in the airgap due to any mismatch between the field and rotor axes. Variation of the reluctance in the motor airgap is afforded by a proper selection of the rotor shape and material (see Fig. 4.8). The developed torque of a reluctance motor can be increased by magnifying the difference in the synchronous reactances in the d and q axes, so as to make the ratio X_{sd}/X_{sq} as high as possible. However, this in turn involves a heavier magnetizing current resulting in a further increase in the input current due to the high reluctance of the magnetic circuit in the q axis. A reluctance motor, like a PM synchronous motor, has good heat exchange properties, since most of its losses are produced in the stator.

The angular characteristic of the reluctance motor obeys the law of magnetic reluctance variation along the stator periphery. The reluctance torque, T_{drel}, corresponding to the fundamental harmonic of the a.c. component of magnetic reluctance can be plotted against δ on the basis of eqn (4.10) (disregarding the stator winding resistance). The torque T_{drel} varies as $\sin 2\delta$ in accordance with line 2 in Fig. 4.2. The steady-state condition of the motor is attained at the particular angle δ at which $T_{drel} = T$, where T is the steady-state external torque on the motor shaft.

If the rotor and the stator rotating field revolve at different speeds, the angle δ becomes a periodic function of time and the average value of the reluctance torque is zero. That is why, during the starting period, reluctance motors run as induction machines. In the course of starting reluctance motors, an a.c. component of magnetic

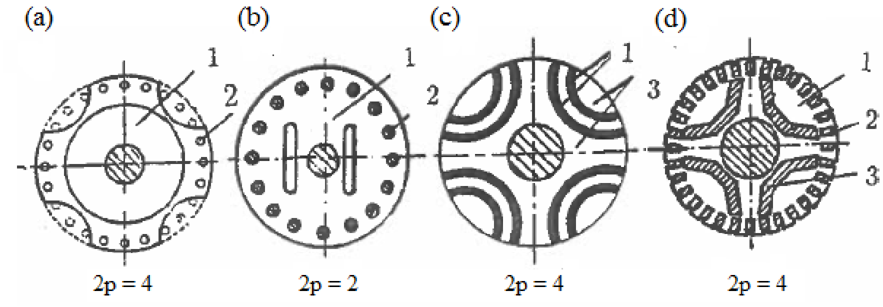

Fig. 4.8. Rotors for synchronous reluctance motors: (a) salient-pole rotor, (b) cylindrical rotor with internal channels, (c) and (d) cylindrical composite rotor (with flux barriers): 1 — ferromagnetic core, 2 — cage winding, 3 — aluminium.

flux appears because of the variations in the reluctance. This induces additional EMF in the stator winding.

The salient-pole rotor of Fig. 4.8a has a laminated core with a starting cage winding. If the laminated core is replaced by a solid steel core, the cage winding is removed because the eddy currents in the solid pole shoes produce an asynchronous starting torque. In practical small synchronous reluctance motors, the rotor *pole-arc–to–pole-pitch ratio* $\alpha = b_p/\tau$ lies in the region of 0.5 to 0.6, and the *maximum–to–minimum airgap ratio* is somewhere between 10 and 12. The internal channels of the cylindrical rotor shown in Fig. 4.8b ensure a variation of the reluctance along the motor periphery. As for the rotor illustrated in Figs. 4.8c and d, this variation is achieved by the use of two materials with different magnetic properties. *Axially laminated rotors* can also be used [45].

It is now easy to draw the equivalent circuit and phasor diagrams along similar lines to Figs. 4.3 and 4.5. The phasor diagrams for reluctance motors are shown in Fig. 4.9, while the equivalent circuit is shown in Fig. 4.10. An a.c. reluctance motor behaves as an inductive load, drawing from mains the reactive power necessary for the magnetization of its magnetic circuit (it is an underexcited motor).

The efficiency and power factor of typical reluctance motors are lower than those of cage induction motors. The low power factor is explained by the fact that the magnetic flux of a reluctance motor is entirely due to the stator magnetizing current. Heavy magnetizing current is the result of high reluctance in the q-axis of the magnetic circuit. The greater the inequality of magnetic reluctances and of inductive reactances X_{sd} and X_{sq}, the higher is the reluctance torque, T_{drel}, and the lower are the motor's power factor and efficiency.

4.9 Hysteresis motors

A *hysteresis motor* is a synchronous motor with its torque produced as a result of the magnetic hysteresis that is encountered at the reversal of the rotor polarity. The rotor of a hysteresis motor is made of a retentive material (such as Co-Va alloy or Al-Ni alloy) which therefore has a wide hysteresis loop. Hysteresis motors are

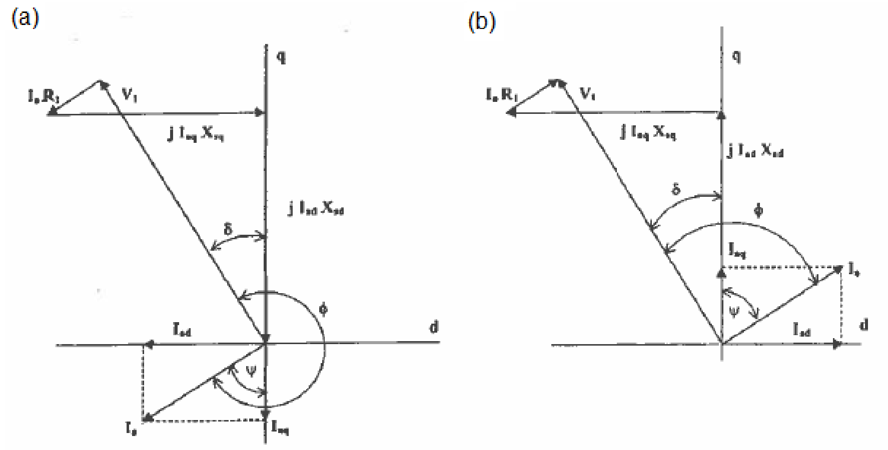

Fig. 4.9. Phasor diagrams for an a.c. reluctance motor: (a) generator arrow system, (b) consumer arrow system.

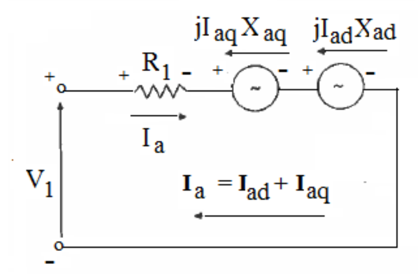

Fig. 4.10. Equivalent circuit per phase of an a.c. reluctance motor.

excellent for applications in audio-visual equipment, clocks, instruments, gyroscope systems, *etc.*

In the early 1980s, the so called *written pole motors* were developed [26, 43] which operate on the similar principle. Written pole motors require a starting current that is less than twice their running current and have a very high efficiency (over 90%) [26].

Problems

1. A three-phase, six-pole, 50 Hz, 380 V (line-to-line), star connected synchronous motor has a synchronous reactance $X_{sd} = X_{sq} = 1.2\ \Omega$ and negligible stator resistance. The motor draws 62.5 kVA at $\cos\phi = 0.8$ (leading). Calculate: (a) the armature current $\mathbf{I}_a$, (b) the excitation EMF E_f (line-to-neutral), (c) the power angle δ and (d) the maximum electromagnetic torque T_{dmax}.

Answer: (a) $\mathbf{I}_a = 94.96\exp(36.87^0)$ A, (b) $E_f = 301.87$ V, (c) $\delta = 17.5^0$, (d) $T_{dmax} = 1581.13$ Nm.

2. A three-phase, four-pole, 15 kW, 460 V (line-to-line), 60 Hz, $\cos\phi = 0.8$ (lagging), $\eta = 0.88$, star-connected, salient pole synchronous motors has the d-axis synchronous reactance $X_{sd} = 11.0\ \Omega$ and the q-axis synchronous reactance $X_{sq} = 6.0\ \Omega$. Find the electromagnetic power, developed torque and its synchronous and reluctance components. The stator winding resistance R_1 can be neglected.

   Answer: $I_{ad} = 0$, $I_{aq} = 26.74$ A, $P_g = 16\,977.8$ W, $T_d = 90.07$ Nm, $T_{dsyn} = 49.13$ Nm, $T_{drel} = 40.94$ Nm.

3. Using the phasor diagram of a salient-pole synchronous motor (Fig. 4.5) prove that $I_a\cos\phi = I_{aq}\cos\delta - I_{ad}\sin\delta$.

   Answer: The above equation has been derived in the book [17], p. 161.

4. A three-phase, six-pole, 346 V (line-to-line), 180 Hz, 160 kW, star connected synchronous motor with a surface-type permanent magnet rotor has the stator winding resistance per phase $R_1 = 0.011\ \Omega$, d-axis synchronous reactance $X_{sd} = 0.335\ \Omega$ and q-axis synchronous reactance $X_{sq} = 0.377\ \Omega$ ($X_{sd} < X_{sq}$). The power angle $\delta = 26^0$, the airgap magnetic flux density $B_{mg} = 0.65$ T, the number of turns per phase $N_1 = 24$, the winding factor $k_{w1} = 0.925$, the effective length of the stator core $L_i = 0.19$ m, the inner stator core diameter $D = 0.33$ m, the rotational losses $\Delta P_{rot} = 1200$ W, the stray losses $\Delta P_{str} = 0.05P_{out}$ and the stator core losses can be neglected. Find the armature current, output power P_{out}, developed torque T_d, shaft torque T_{sh}, efficiency η and power factor $\cos\phi$.

   Answer: $I_{ad} = -191.44$ A, $I_{aq} = 226.7$ A, $I_a = 296.72$ A, $P_{out} = 160\,281.5$ W, $T_d = 449.6$ Nm, $T_{sh} = 425.2$ Nm, $\eta = 0.93$, $\cos\phi = 0.9695$.

5. A three-phase, 4-pole, 380 V (line-to-line), 50 Hz, 5.5 kW, star connected reluctance motor has the stator winding resistance per phase $R_1 = 0.49\ \Omega$, d-axis synchronous reactance $X_{sd} = 15.5\ \Omega$ and q-axis synchronous reactance $X_{sq} = 5.7\ \Omega$. The rotational losses $\Delta P_{rot} = 110$ W, the stray losses $\Delta P_{str} = 0.06P_{out}$ and the stator core losses can be neglected. For the power angle $\delta = 21^0$ find the armature current, output power P_{out}, shaft torque T_{sh}, efficiency η and power factor $\cos\phi$.

   Answer: $I_a = 19.6$ A, $P_{out} = 5160.4$ W, $T_{sh} = 32.85$ Nm, $\eta = 0.84$, $\cos\phi = 0.476$.

5

VARIABLE–SPEED DRIVES

All electrical drives can be divided into constant speed drives, servo drives and variable-speed drives. *Variable-speed drives* have several distinctive features, amongst which are:

- they are economical in terms of energy usage;
- they can be used for accurate velocity or position control;
- when used, they may ameliorate transients (particularly during soft starting, controlled acceleration, *etc.*);
- their fast response offers ease of automatic control;
- many are completely brushless and highly reliable, and therefore require very limited maintenance.

The choice of which drive system to use often depends on even more factors than these. Important considerations might include:

- the costs involved;
- the tradition within the particular industry;
- restrictions imposed by design limitations and the precise motor characteristics that are desired;
- the speed range;
- the maximum power rating.

Progress in power electronics has recently revolutionized electrical drives by replacing electromagnetic methods of speed control by electronic methods. This has come about with the aid of *solid-state converters*. A variable-speed drive system is a system used to control the speed within a certain range, and it consists of the electric motor, a power electronic converter, and a control unit. The various types of power electronic converters used in variable-speed drives can be divided into the following groups:

- controlled rectifiers (a.c. to d.c.);
- choppers (d.c. to d.c.);
- a.c. voltage regulators (a.c. to a.c.);
- inverters (d.c. to a.c.);
- cycloconverters (a.c. to a.c.).

5.1 Power semiconductor devices

Power semiconductor devices or *power semiconductor switches* can be classified into the following three categories according to their degree of controllability [42]:

- diodes, whose on and off states are controlled by the power circuit;
- thyristors, which are turned on by a control signal but must be turned off by the power circuit;
- controllable devices, which are turned on and off by control signals.

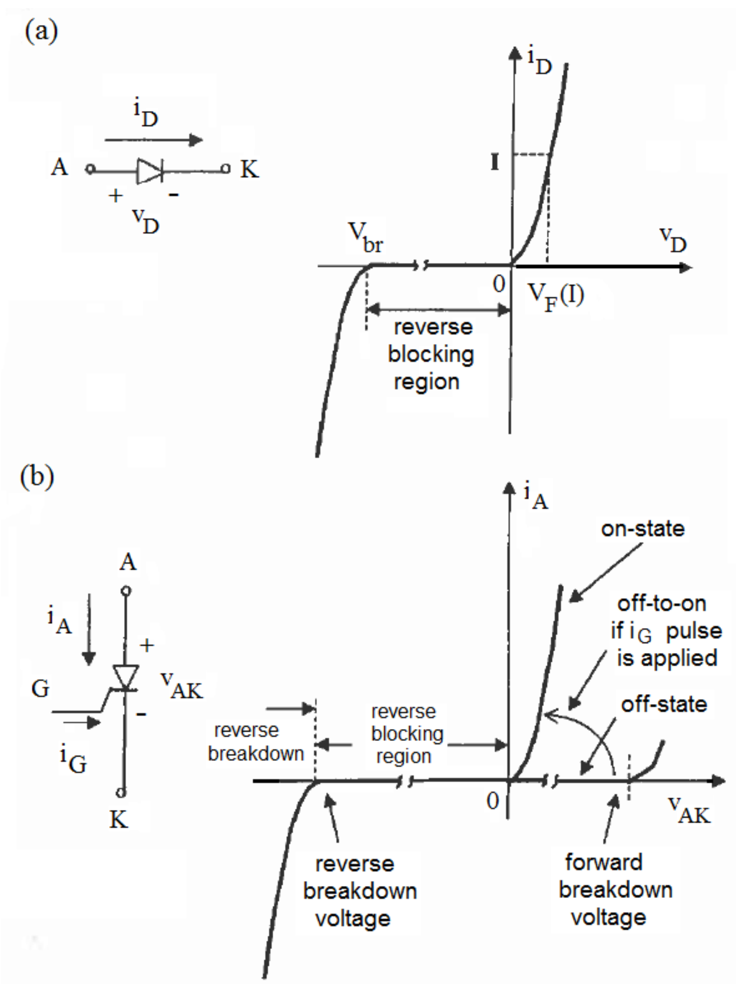

Fig. 5.1. Symbols and characteristics of power semiconductor switches: (a) diode, (b) thyristor.

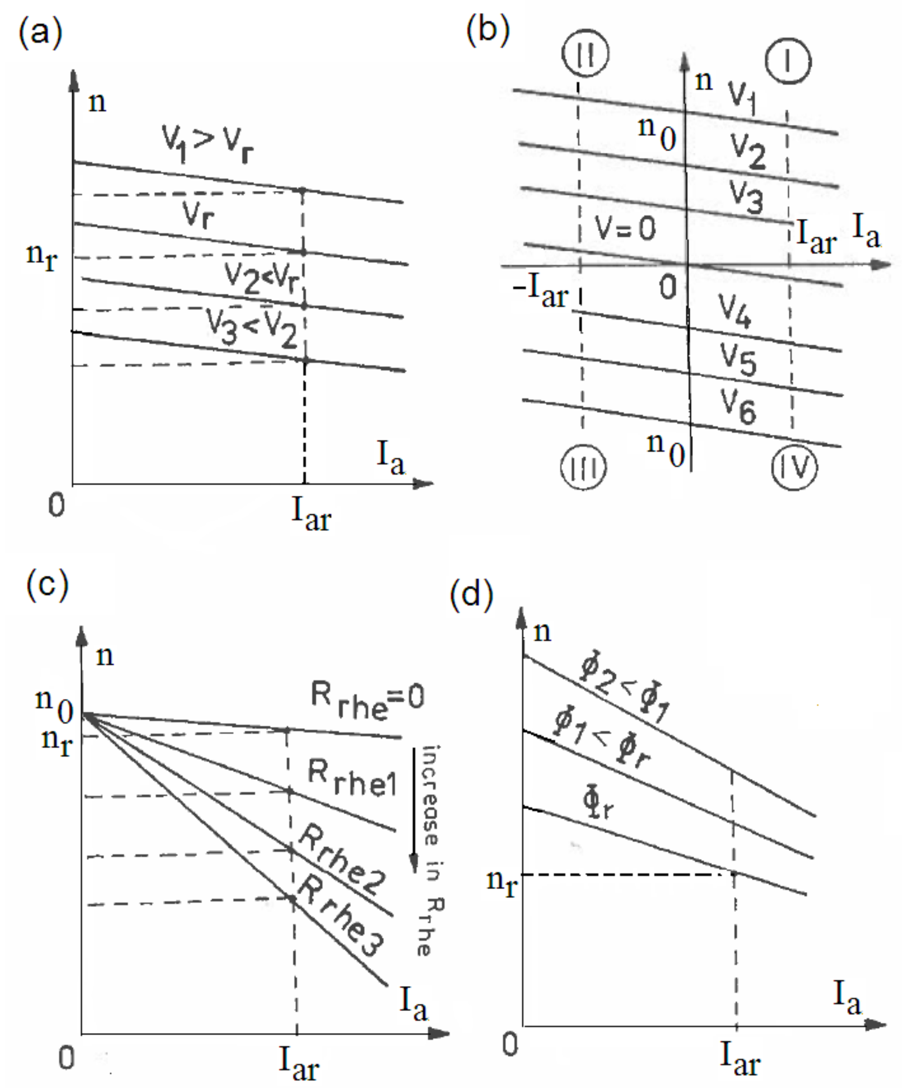

Fig. 5.2. Speed control of d.c. separately-excited and shunt motors using: (a) variable armature-terminal-voltage (separately excited), (b) Ward-Leonard system, (c) armature rheostat (shunt), (d) variable excitation flux (shunt).

The *controllable device group* includes bipolar junction transistors (BJTs), metal-oxide-semiconductor field effect transistors (MOSFETs), gate-turn-off thyristors (GTOs), and insulated gate bipolar transistors (IGBTs).

When a *diode* (Fig. 5.1a) is forward biased, it begins to conduct with only a small forward voltage (of about 1 V) across it. When the diode is reversed biased, only a negligibly small leakage current flows through the device until the reverse breakdown voltage is reached. The reverse bias voltage should not reach the breakdown rating V_{br} under normal operation.

A *thyristor* can be triggered into the on-state by applying a pulse of positive current for a short duration, provided that the device is in its forward blocking state (see Fig. 5.1b). The forward voltage drop is typically from 1 to 3 V. When the thyristor begins to conduct, it is latched on and the gate current can be removed. The thyristor behaves as a diode and cannot be turned off by the gate — it will turn off only when its anode current is negative, under the influence of the circuits in which the thyristor is connected. The gate regains control to turn the thyristor on at some controllable time after it has again entered the forward blocking state.

The mechanism of switching off the thyristor, whereby it ceases to conduct, is termed *commutation*. This can be *natural commutation*, where it ceases to conduct because of a natural decrease of current to zero, or it may be *forced commutation*, which is obtained by applying a reverse voltage across it.

Although *silicon-based devices* are still being developed, the use of other materials such as *silicon-carbide* or *diamond* is predicted for the future.

5.2 D.c. motor drives

5.2.1 Speed control

Eqn (2.46) contains all the relevant information about the speed of a d.c. motor. The speed of a d.c. motor can be controlled by changing: (a) the mains supply voltage V, (b) the armature-circuit resistance $\sum R_a + R_{rhe}$; (c) the field flux Φ.

The speed-torque characteristics for separately-excited and shunt-field motors are shown in Fig. 5.2, and those for series motors are presented in Fig. 5.3.

Substituting T_d of eqn (2.7) into eqn (2.46) and setting $R_{rhe} = 0$, the speed of a separately-excited d.c. motor can be expressed as

$$n = \frac{1}{c_E \Phi}\left(V - \Delta V_{br} - \frac{\sum R_a}{c_T \Phi} T_d\right) \tag{5.1}$$

Eqn (5.1) shows that in a separately-excited d.c. motor both V and Φ can be controlled in order to obtain the desired speed and torque (see Fig. 5.4). To maximise the motor capability, the field current I_f (and hence flux Φ) is kept at its rated value for speeds less than the rated speed n_r. To obtain $T_d = const$ and $I_a = const$ at $I_f = const$, the voltage V must increase linearly from $(\sum R_a)/(c_T \Phi)T_d + \Delta V_{br}$ to its rated value V_r as the speed increases from 0 to its rated value n_r. The region $0 \leq n \leq n_r$ is called the *constant torque region* of the motor. To obtain speeds beyond the rated value n_r, it is necessary to keep $V = V_r = const$ and to decrease Φ by decreasing I_f. When $I_a = I_{ar}$, the torque capability declines, because Φ has been reduced. The region $n > n_r$ is called the *field weakening region* or the *constant*

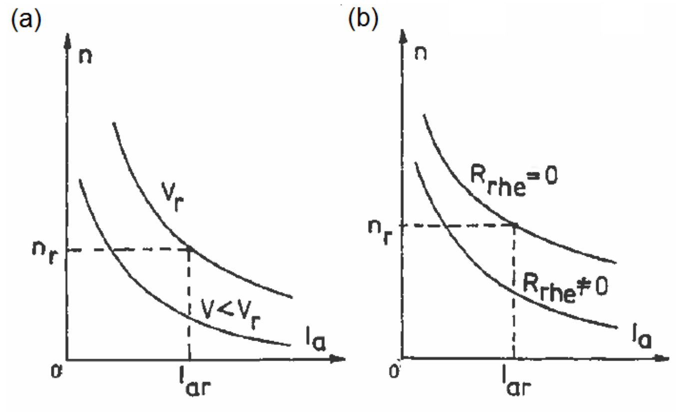

Fig. 5.3. Speed control of d.c. series motors using: (a) variable armature-terminal-voltage, (b) armature rheostat.

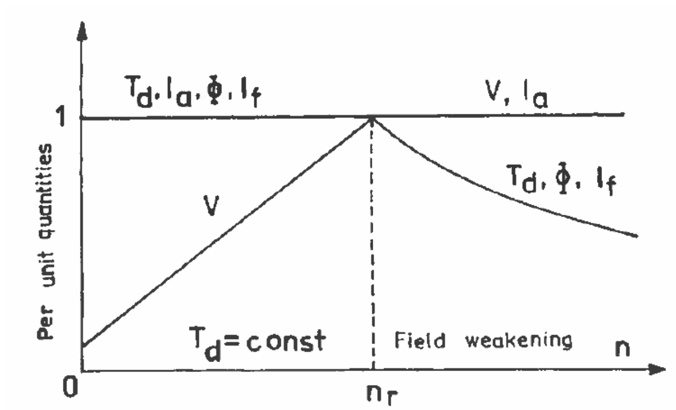

Fig. 5.4. Torque-speed capability of a separately-excited d.c. motor.

power region of the motor (in which $EI_a = 2\pi n T_d$). Any operating point within the regions shown in Fig. 5.4 is permissible, provided that the speed never exceeds the maximum permissible speed for the motor.

Certain motor applications require *four-quadrant operation*, which implies the ability to provide armature current of reversible as well as forward polarity, as in Fig. 5.2b which is called a *Ward-Leonard system*. In the first quadrant, the d.c. separately-excited machine operates as a motor. Reversal of the load torque whilst maintaining the same direction of rotation but at a speed higher than that corresponding to zero torque moves the operating point of the machine into the second quadrant in Fig. 5.5, and represents a change of state for the machine from motoring to generating. This is also known as regenerative braking. Operation in the third and fourth quadrants of the speed–torque plane is achievable in a separately-excited machine by reversing the basic direction of rotation. Two methods of achieving this

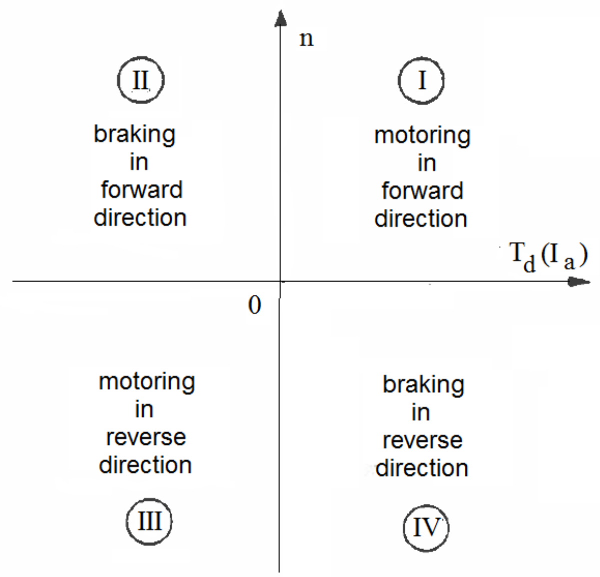

Fig. 5.5. Four-quadrant operation of a d.c. motor.

are available: (a) changing the polarity of the field flux by reversing the field winding connections, and (b) reducing to zero and then reversing the polarity of the armature voltage supply. Alternative (a) is often not practicable since the field would be reduced to zero during the polarity change, so that the transition from first and second to fourth and third quadrants is made via infinite speed rather than via zero speed, as appropriate to armature voltage control. A full four-quadrant drive has the capability of changing state from motoring to generating, or *vice versa*, via torque reversals through zero torque, or speed reversals through zero speed.

A good way to gain a better understanding of four-quadrant motor operation is to imagine a boy pulling, pushing and braking a cart, as shown in Fig. 5.6.

5.2.2 Ward-Leonard system

D.c. commutator motors are still extensively used in many variable-speed drives. If a d.c. machine is used as the variable-voltage source, then the drive system may operate in all four quadrants and as a *Ward-Leonard system* (see Fig. 5.7). The excitation of the drive motor is maintained at its rated value and a controllable voltage is applied to its armature from the generator of a separate motor-generator set. The voltage is controlled by the generator field current using a voltage divider which, when reversible, allows reversal of the field current, the generator voltage, and hence, reversal of the motor speed. With this arrangement, the speed of the motor can be varied from rated speed through zero to rated speed in the reverse direction, with full rated torque capability at all speeds (refer to Fig. 5.2b). Regenerative braking is inherent.

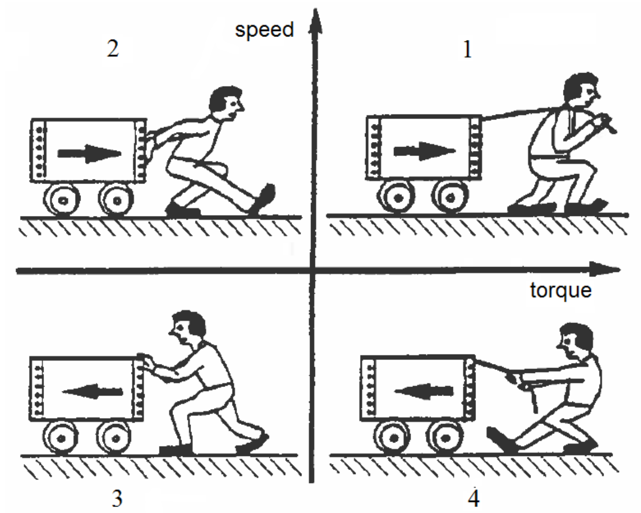

Fig. 5.6. The four-quadrant operation can be visualized by a boy and cart.

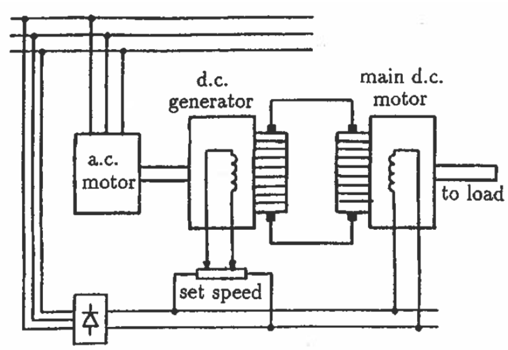

Fig. 5.7. Power circuit of a Ward-Leonard system.

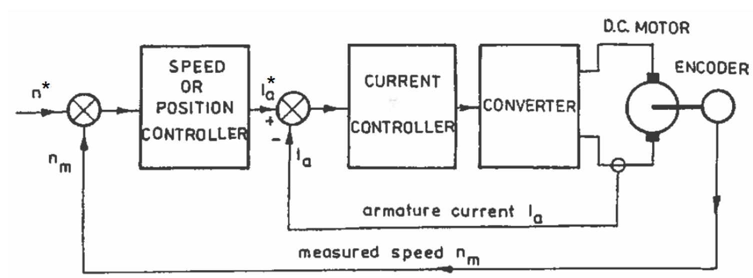

Fig. 5.8. Closed-loop speed control of a d.c. motor with inner current loop.

5.2.3 Closed-loop control system

In a *modern closed-loop system* (Fig. 5.8), the speed can be maintained constant by adjusting the motor's terminal voltage as the load torque changes.

5.2.4 Controlled rectifiers

Power circuits of controlled rectifiers are shown in Fig. 5.9. It is assumed that the instantaneous a.c. input voltage (source voltage) is sinusoidal, i.e.

$$v = V_m \sin \omega t = \sqrt{2} V \sin \omega t$$

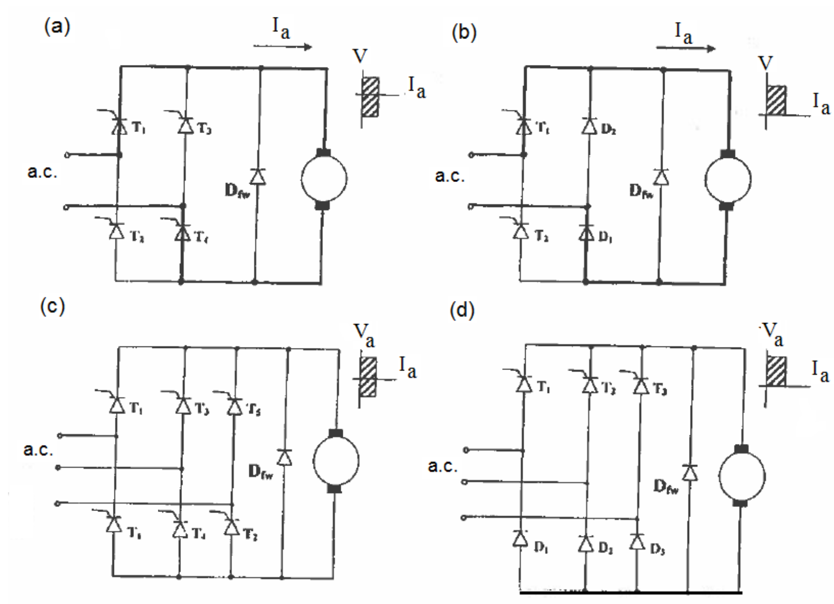

Fig. 5.9. Controlled rectifier circuits: (a) single phase fully controlled (full-wave), (b) single phase half-controlled (half-wave), (c) three phase fully controlled, (d) three phase half controlled. T_1, T_2, ... T_6 — thyristors, D_1, D_2, D_3 — diodes, D_{fw} — free-wheeling diode.

In a cycle of source voltage, thyristors T_1 and T_4 of the single phase fully controlled rectifier (Fig. 5.9a) are given gate signals from α to π and thyristors T_2 and T_3 are given gate signals from $\pi + \alpha$ to 2π where α is the so-called *firing angle*. The *free-wheeling diode* D_{fw} prevents the voltage accross the load from reversing during the negative half-cycle of the supply voltage. The mean converter output voltage accross the motor armature terminals is

$$V = \frac{1}{\pi}\int_{\alpha}^{\pi+\alpha} V_m \sin\omega t d(\omega t) = \frac{2V_m}{\pi}\cos\alpha \tag{5.2}$$

The maximum mean output voltage $2V_m/\pi$ occurs at $\alpha = 0$. Similar equations can be derived for the remaining rectifier circuits, i.e.

- single phase half-controlled rectifier (5.9b)

$$V = \frac{1}{\pi}\int_{\alpha}^{\pi} V_m \sin\omega t d(\omega t) = \frac{V_m}{\pi}(1+\cos\alpha) \tag{5.3}$$

- three phase fully controlled rectifier (5.9c)

$$V = \frac{3}{\pi}\int_{\alpha+\pi/3}^{\alpha+2\pi/3} V_{mL-L} \sin\omega t d(\omega t) = \frac{3V_{mL-L}}{\pi}\cos\alpha \tag{5.4}$$

- three phase half-controlled rectifier (5.9d)

$$V = \frac{3}{\pi}\int_{\alpha+\pi/3}^{2\pi/3} V_{mL-L} \sin\omega t d(\omega t) = \frac{3V_{mL-L}}{\pi}(1+\cos\alpha) \tag{5.5}$$

For three-phase rectifiers V_{mL-L} is the peak value of the line-to-line voltage and $V_{mL-L} = \sqrt{3}V_m$ where V_m is the peak value of the line-to-neutral voltage.

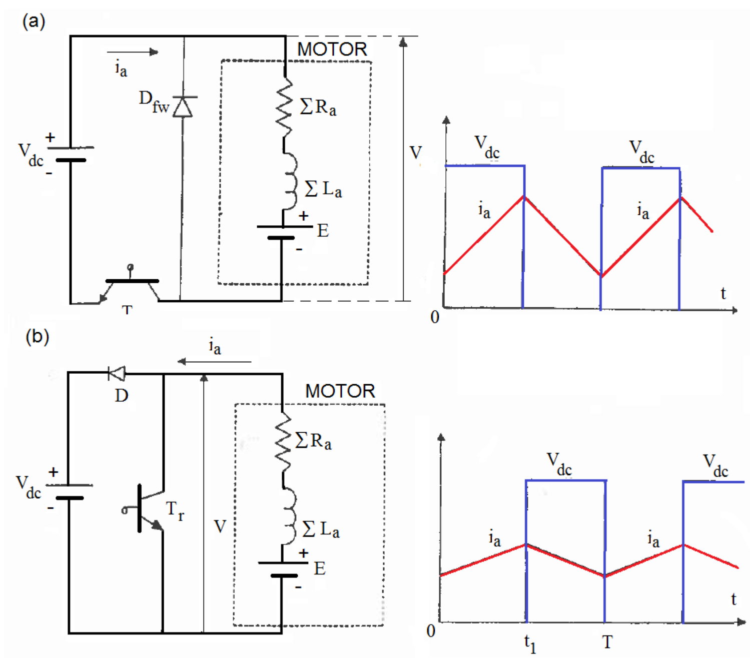

Fig. 5.10. Chopper control of a d.c. separately excited or PM motor: (a) motoring, (b) regenerative braking. Tr — transistor, D — diode, D_{fw} — free-wheeling diode.

5.2.5 Choppers

A *chopper* directly converts a fixed-voltage d.c. supply to a variable-voltage d.c. supply. In applications in which the power source is a battery and where efficiency is an important consideration, various chopper drives provide variable armature terminal voltage to d.c. motors as a means of speed control. Examples are battery-driven automobiles, d.c. urban and suburban trains, d.c. trams, d.c. underground trains, etc. Choppers may employ thyristors or power transistors, and they are essentially switches that turn on the battery for short time intervals. In general, a chopper may be viewed as a d.c. converter without an a.c. link (see Fig. 5.10). Choppers may vary the average d.c. value of the motor's terminal voltage by varying the pulse width (this is called *pulse width modulation* or PWM), or by varying the pulse frequency (*pulse frequency modulation* or PFM), or by varying both.

The operation of a chopper-fed d.c. motor (see Fig. 5.10a) is described by the following equations ($\Delta V_{br} = 0$):

- for current increasing interval $0 \le t \le t_1$

$$\sum R_a i_a + \sum L_a \frac{di_a}{dt} + E = V_{dc} \tag{5.6}$$

- for freewheeling interval $t_1 \le t \le T$

$$\sum R_a i_a + \sum L_a \frac{di_a}{dt} + E = 0 \tag{5.7}$$

where $\sum R_a$ is the armature circuit resistance, $\sum L_a$ is the armature circuit reactance, i_a is the armature instantaneous current, E is the motor back EMF and V_{dc} is the d.c. source voltage. The *duty cycle* of a chopper is defined as

$$\delta = \frac{t_1}{T} \tag{5.8}$$

The mean voltage accross the armature terminals

$$V = \frac{1}{T}\int_0^{t_1} v(t)dt = \frac{1}{T}\int_0^{t_1} V_{dc} dt = \delta V_{dc} \tag{5.9}$$

The steady state armature current ($\Delta V_{br} = 0$)

$$I_a = \frac{V - E}{\sum R_a} = \frac{\delta V_{dc} - E}{\sum R_a} \tag{5.10}$$

For regenerative braking (Fig. 5.10b)

$$\delta = \frac{T - t_1}{T} \qquad \text{and} \qquad V = \frac{1}{T}\int_{t_1}^{T} V_{dc} dt = \delta V_{dc} \tag{5.11}$$

Series motors or separately-excited PM motors (Chapter 2) are often used in these systems.

Example 5.1

A 200 V, 1000 rpm and 190 A separately excited d.c. motor has the armature circuit resistance $\sum R_a = 0.022\ \Omega$ and is fed from a chopper which can provide both motoring and braking operations. The d.c. source voltage is $V_{dc} = 220$ V. Find the duty cycle of the chopper for: (a) motoring at 500 rpm and rated torque and (b) regenerative braking at 300 rpm and rated torque. The brush voltage drop ΔV_{br} and armature reaction is neglected.

Solution

The rated EMF is

$$E = V - I_a \sum R_a = 200 - 190 \times 0.022 = 195.82 \text{ V}$$

For motoring and 500 rpm

$$E_{500} = \frac{500}{1000} 195.82 = 97.9 \text{ V}$$

$$V_{500} = 97.9 + 190 \times 0.022 = 102.1 \text{ V}$$

$$\delta = \frac{V_{500}}{V_{dc}} = \frac{102.1}{220} = 0.464$$

For motoring and 300 rpm

$$E_{300} = \frac{300}{1000} 195.82 = 58.75 \text{ V}$$

$$V_{300} = 58.75 - 190 \times 0.022 = 54.75 \text{ V}$$

$$\delta = \frac{V_{300}}{V_{dc}} = \frac{54.75}{220} = 0.248$$

5.2.6 Switch–mode d.c. — d.c. converters

A full bridge *switch-mode d.c. — d.c. converter* is illustrated in Fig. 5.11a, and it, too, produces a four-quadrant controllable d.c. output. The line-frequency a.c. input is rectified into d.c. by means of a diode rectifier, and it is then filtered by a capacitor. An energy dissipation circuit is included to prevent the filter capacitor voltage from becoming large in the case of braking of the d.c. motor. If reverse speed is not needed but braking is required, then a two-quadrant converter can be used (as in Fig. 5.11b).

5.3 Induction motor drives

5.3.1 Speed control

The *slip* is the ratio of the *slip speed* $(n_s - n)$ to the synchronous speed n_s. Eqn (3.2) is the basis for several methods of speed control of induction motors, i.e.:

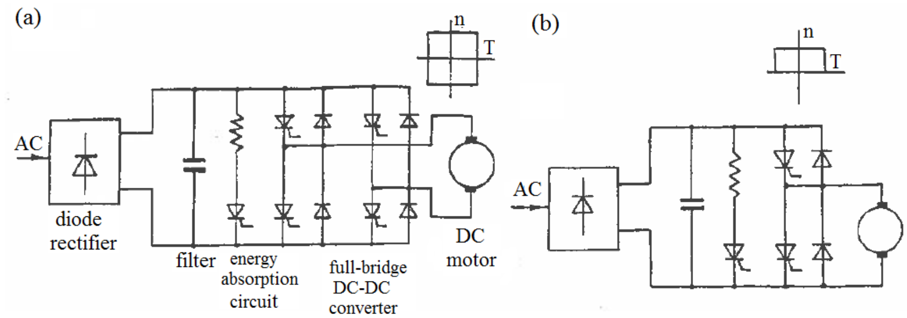

Fig. 5.11. D.c. motors fed from switch mode d.c. — d.c. converters: (a) four-quadrant operation, (b) two-quadrant operation.

- changing the input frequency f (see Figs 3.22 and 3.23);
- changing the number of stator pole pairs p (Fig. 3.27);
- changing the slip s by varying the rotor circuit resistance of wound-rotor induction motors (see Fig. 3.28) or by adjusting the input voltage of cage induction motors (see Fig. 3.6).

With a constant V_1/f ratio (constant magnetic flux Φ), an induction motor develops a constant maximum torque T_{dmax}, except at low frequencies. For a frequency k times the rated frequency 50 Hz and voltage k times the rated phase voltage

$$\frac{V_1}{f} = \frac{kV_{1r}}{k50} = const \tag{5.12}$$

the maximum developed torque according to eqn (3.74) is

$$T_{dmax} = \frac{m_1}{4\pi k n_s(1+\tau_1)} \times \frac{(kV_{1r})^2}{\sqrt{R_1^2 + k^2[X_1 + X_2'(1+\tau_1)]^2} + R_1}$$

$$= \frac{m_1}{4\pi n_s(1+\tau_1)} \times \frac{V_{1r}^2}{\sqrt{(R_1/k)^2 + [X_1 + X_2'(1+\tau_1)]^2} + R_1/k} \tag{5.13}$$

Before the power electronics era, eddy-current couplings were frequently used to build a variable-speed drive with an induction motor fed from a constant-frequency line. Although the dynamic response was poor, sufficient speed stability could be obtained in closed-loop eddy-current coupling drives.

5.3.2 A.c. voltage regulators

Three-phase *a.c. voltage regulators* (see Fig. 5.12) may be used to control the stator voltage, and hence the speed, of an induction motor. Such a voltage regulator allows for power factor control, and hence offers a method of energy saving for induction motors which spend most of their life running at light load. At low speeds, however, the efficiency is very poor because of the high stator and rotor losses that are associated with large slips.

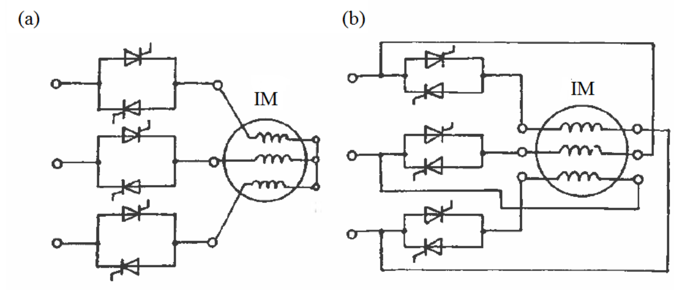

Fig. 5.12. Three-phase a.c. voltage regulators (a) star-connected, (b) delta-connected.

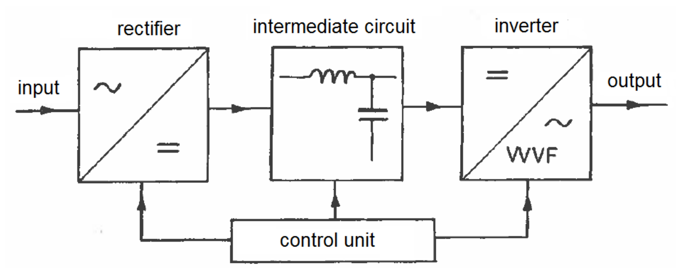

Fig. 5.13. Basic circuitry of a VVVF converter.

There are two thyristors per each phase. The first thyristor is fired at α and the second thyristor at $\pi + \alpha$. The load current builds up at α and decays to zero at β, i.e. the conduction interval is $\alpha < \omega t < \beta$. When the second thyristor turns on at $\pi + \alpha$, a negative current flows in the load.

The load current is sinusoidal if the firing angle $\alpha = \phi$ where the power factor is $\cos\phi$ [49]. Each thyristor conducts for 180^0 and full supply voltage appears across the load.

Analysis of a three-phase star-connected regulator is difficult because operation of one phase affects the operation of the other phases [49]. In a delta-connected regulator each phase is connected across a known supply voltage and the operation can be analysed on a per-phase basis.

5.3.3 A.c. – a.c. converters

An excellent way to control the speed of an induction motor is to vary the input voltage and frequency (VVVF). Fig. 5.13 shows the basic concept of a *d.c. link converter*, which consists of a *rectifier* (a.c. — d.c.), an *intermediate circuit* (or filter), and an *inverter* (d.c. — a.c.) that employs thyristors or other power semiconductor devices. A capacitor or inductor placed between the two converter stages stores the instantaneous difference between the input and output powers. The *rms* inverter output voltage (line-to-line) is equal to $\sqrt{2/3}$ of the d.c. link voltage.

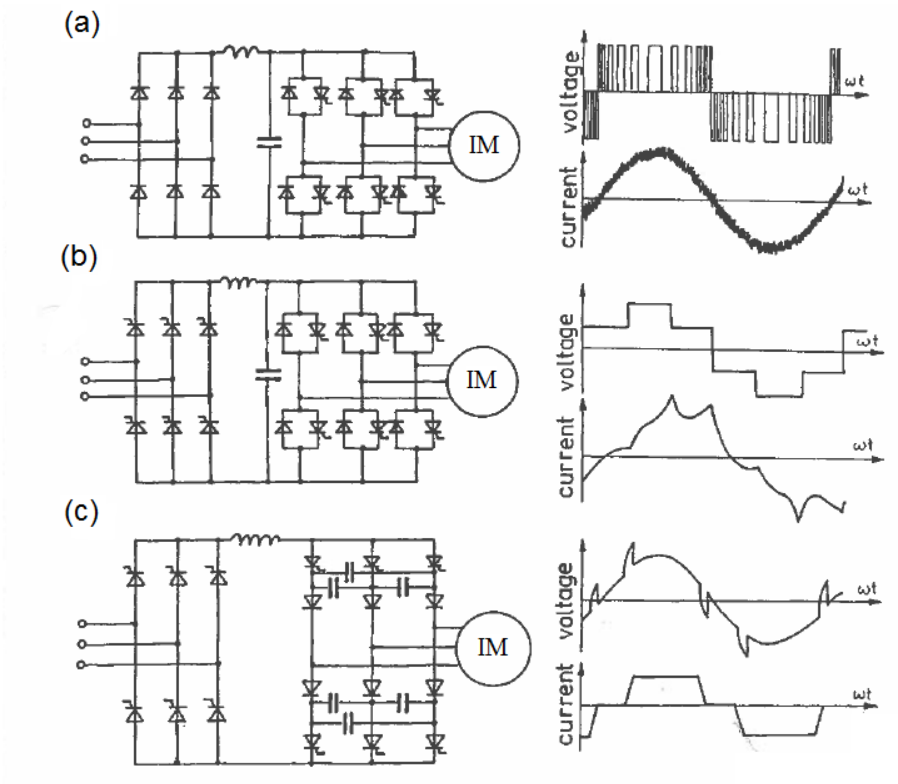

Fig. 5.14. D.c. link converters: (a) PWM VSI with a diode rectifier, (b) square-wave VSI with a controlled rectifier, (b) CSI with a controlled rectifier.

D.c. link converters can be classified on the basis of the type of rectifier and inverter that are used in their manufacture:

- pulse-width-modulated (PWM) voltage-source inverter (VSI) with a diode rectifier (Fig. 5.14a);
- square-wave VSI with a thyristor rectifier (Fig. 5.14b);
- current-source inverter (CSI) with a thyristor rectifier (Fig. 5.14c).

5.3.4 Cycloconverters

In low-speed and large-power a.c. motor drives, it is possible to use a.c. – a.c. converters that provide direct conversion, so called *cycloconverters* (see Fig. 5.15). Cycloconverters utilise line-frequency (natural) commutation. However, their maximum output frequency is limited to about one-third of the input a.c. frequency.

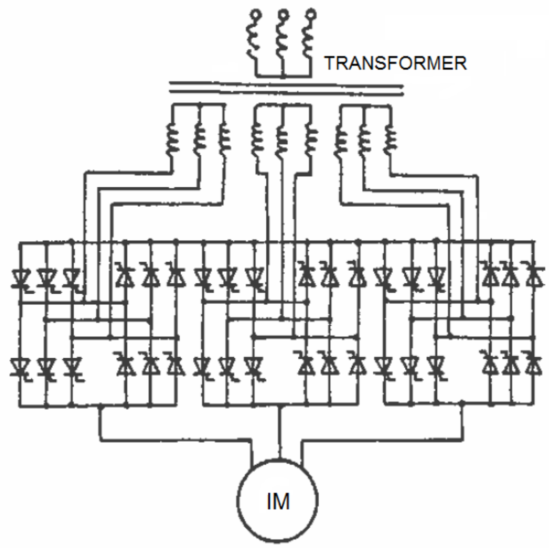

Fig. 5.15. Cycloconverter.

5.3.5 Inverter-fed induction motor capabilities

As it has been discussed, in inverter-fed induction motors the speed can be controlled by varying: (a) input frequency f; (b) input voltage V_1; (c) both input frequency and voltage (VVVF), keeping the airgap magnetic flux constant, i.e. :

$$\pi\sqrt{2}N_1 k_{w1}\Phi \approx \frac{V_1}{f} = const \tag{5.14}$$

Speed control by means of VVVF also allows the motor to operate not only at speeds below the rated speed, but also at above the rated speed (Fig. 5.16). The majority of induction motors can be operated under such conditions without mechanical and thermal problems.

In the region of low speed, below its rated value, the lines in Fig. 5.16a show the electromagnetic (developed) torque T_d versus speed for low slip frequencies sf. The flux Φ is kept constant by controlling V_1/f. The voltage is decreased from its rated value V_{1r} approximately in proportion to f. The developed torque

$$T_d = \frac{P_g}{\Omega_s} = \frac{m_1 E_1 I_2' \cos\Psi_2}{\Omega_s} = \frac{1}{\sqrt{2}} m_1 p N_1 k_{w1} \Phi I_2' \cos\Psi_2 \tag{5.15}$$

is constant if $\Phi = const$, $I_2' = const$ and $\cos\Psi_2 = const$. The angle Ψ_2 between sE_1 and I_2' is approximately constant since

$$\tan\Psi_2 = \frac{sX_2'}{R_2'} \tag{5.16}$$

is very small for a cage rotor ($sX_2' = 2\pi sfL_2 << R_2'$) and $\cos\Psi_2 \approx 1$. The magnetizing current $I_\Phi = const$ and the slip s increases for $sf = const$ as the frequency f decreases.

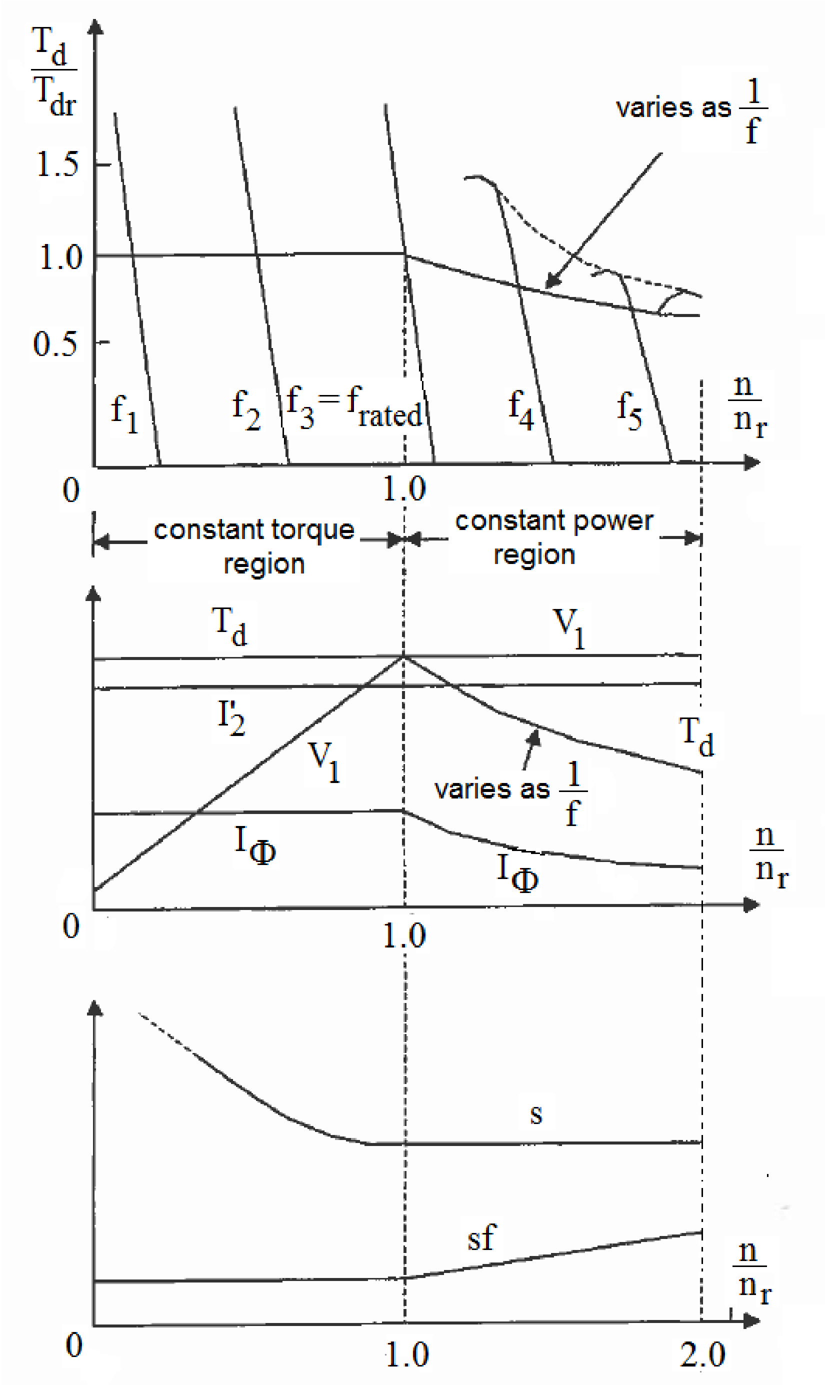

Fig. 5.16. Induction motor characteristics and capabilities.

The speed can be increased beyond its rated value by increasing the input frequency f above its rated value and keeping $V_1 = const$ (very often equal to V_{1r}). According to eqn (5.14) the flux Φ is inversely proportional to the frequency ($\Phi \propto (1/f)$) and at $I_2' = const$ and $\Psi_2 = const$, the electromagnetic torque (5.15) will also be inversely proportional to the frequency. The rotor current I_2' is approximately constant if $V_1 = const$ and $s = const$. Since the frequency increases, the slip frequency sf also increases at $s = const$ and the magnetizing current I_Φ decreases since Φ decreases. The mechanical power $P_m = T_d \Omega$ can be held constant.

Example 5.2

A 3-phase, 7.5 kW, 380 V, 1450 rpm, 50 Hz, Δ-connected cage induction motor has the following equivalent circuit parameters: $R_1 = 2.144\ \Omega$, $R_2' = 1.323\ \Omega$, $X_1 = 2.891\ \Omega$, $X_2' = 5.487\ \Omega$, $X_m = 116.3\ \Omega$. The motor is controlled by a VSI at $V_1/f = const$. The inverter output frequency varies from 5 to 75 Hz. Find: (a) the starting current and starting developed torque at rated frequency, (b) the starting current and starting developed torque at minimum and maximum frequency and (c) the pull-out torque as a function of frequency.

Solution

This is a four pole motor ($2p = 4$). The synchronous speed at rated frequency is

$$n_s = \frac{f}{p} = \frac{50}{2} = 25 \text{ rev/s}$$

The Heyland's coefficient according to eqn (3.66)

$$\tau_1 \approx \frac{X_1}{X_m} = \frac{2.891}{116.3} = 0.0248$$

(a) The starting current and starting torque at rated frequency

$$I_{1st} \approx \frac{V_{1r}}{\sqrt{(R_1 + R_2')^2 + (X_1 + X_2')^2}} = \frac{380}{\sqrt{(2.144 + 1.323)^2 + (2.891 + 5.487)^2}} = 41.91 \text{ A}$$

$$T_{dst} = \frac{m_1 V_{1r}^2}{2\pi n_s} \times \frac{R_2'}{[R_1 + R_2'(1+\tau_1)]^2 + [X_1 + X_2'(1+\tau_1)]^2}$$

$$= \frac{3 \times 380^2}{2\pi \times 25} \times \frac{1.323}{[2.144 + 1.323 \times (1 + 0.0248)]^2 + [2.891 + 5.487 \times (1 + 0.0248)]^2} = 43.06 \text{ Nm}$$

(b) The starting current and starting developed torque for minimum and maximum frequency

For a frequency k times the rated frequency and $V_1/f = kV_{1r}/(k \times 50) = const$ the equations for starting current and starting developed torque are

$$I_{1st} \approx \frac{V_{1r}}{\sqrt{(R_1 + R_2')^2/k^2 + (X_1 + X_2')^2}}$$

$$T_{dst} = \frac{m_1 V_{1r}^2}{2\pi n_s} \times \frac{R_2'/k}{[R_1 + R_2'(1+\tau_1)]^2/k^2 + [X_1 + X_2'(1+\tau_1)]^2}$$

For $f = 5$ Hz or $k = 0.1$

$$I_{1st5} = \frac{380}{\sqrt{(2.144 + 1.323)^2/0.1^2 + (2.891 + 5.487)^2}} = 10.65 \text{ A}$$

$$T_{dst5} = \frac{3 \times 380^2}{2\pi \times 25} \times \frac{1.323/0.1}{(2.144 + 1.323 \times 1.0248)^2/0.1^2 + (2.981 + 5.487 \times 1.0248)^2} = 28.12 \text{ Nm}$$

For $f = 75$ Hz or $k = 1.5$

$$I_{1st75} = \frac{380}{\sqrt{(2.144 + 1.323)^2/1.5^2 + (2.891 + 5.487)^2}} = 43.72 \text{ A}$$

$$T_{dst75} = \frac{3 \times 380^2}{2\pi \times 25} \times \frac{1.323/1.5}{(2.144 + 1.323 \times 1.0248)^2/1.5^2 + (2.981 + 5.487 \times 1.0248)^2} = 31.21 \text{ Nm}$$

The motor is started at the minimum available frequency 5 Hz. Both the starting current and starting torque is lower than that at $V_{1r} = 380$ V and $f = 50$ Hz.

$$\frac{I_{1st5}}{I_{1st}} = \frac{10.65}{41.91} = 0.254$$

$$\frac{T_{dst5}}{T_{dst}} = \frac{28.12}{43.06} = 0.653$$

(c) The pull-out torque as a function of frequency.

According to eqn (5.13)

$$T_{dmax} = \frac{3}{4\pi \times 25 \times (1 + 0.0248)} \times \frac{380^2}{\sqrt{(2.144/k)^2 + [2.891 + 5.487 \times (1 + 0.0248)]^2} + 2.144/k}$$

$$= \frac{1345.549}{\sqrt{4.5967/k^2 + 72.489} + 2.144/k}$$

The pull-out torque for various frequencies at $V_1/f = const$ can be calculated on the basis of the above equation. The results tabulated below show that the pull-out torque decreases as the frequency decreases.

Table 5.1. Pull-out torque versus frequency

$k =$	1.5	1.2	1.0	0.8	0.6	0.4	0.2	0.1	
$f =$	75	60	50	40	30	20	10	5	Hz
$T_{dmax} =$	133.72	128.32	123.17	115.93	105.07	87.26	55.12	30.23	Nm

5.3.6 Vector control method

In the scalar control methods of VSI or CSI drives, the voltage or current and the frequency are the basic control variables of the induction motor. In *vector oriented control* method both the amplitudes and phases of the space vectors of variables are changed. This control method is applicable to both induction and synchronous motors.

In a vector control method, an a.c. motor is controlled like a separately excited d.c. motor. This analogy is explained in Fig. 5.17. In a d.c. motor, neglecting the armature demagnetization effect and magnetic saturation, the torque is given by

$$T_d = c_T \Phi I_a = K_T I_a I_f \tag{5.17}$$

where I_a is the armature or torque component of current and I_f is the field or flux component of the torque. The control variables I_a and I_f can be considered as *orthogonal* or decoupled 'vectors'. In normal operation, the field current I_f is set to maintain the rated field flux and torque is changed by changing the armature current. Since the current I_f or the corresponding field flux is decoupled from the armature current I_a, the torque sensitivity remains maximum for both transient and steady-state operations.

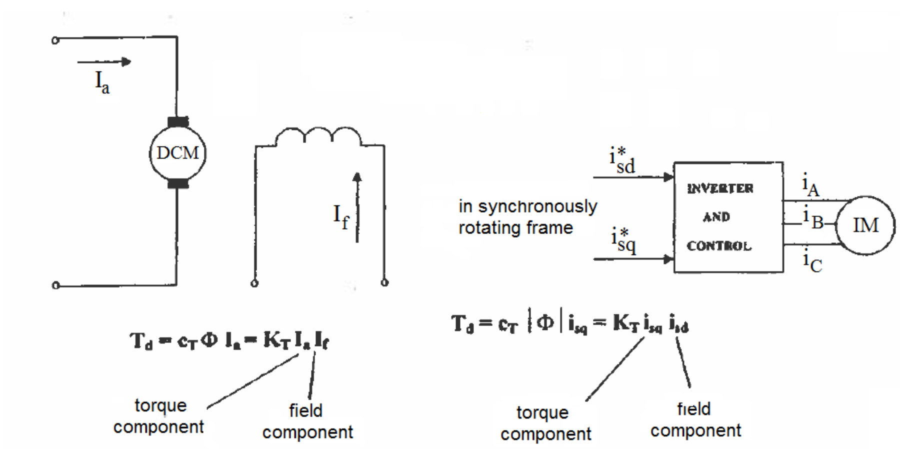

Fig. 5.17. Induction motor and d.c. motor analogy in vector control.

This model of control can be extended to an induction motor also if the machine operation is considered *in a synchronously rotating reference frame d–q where the* *sinusoidal variables appear as d.c. quantities*. In Fig. 5.17 the induction motor with inverter and control is shown with two control inputs i^*_{sd} and i^*_{sq}. The currents i_{sd} and i_{sq} are the direct-axis component and quadrature-axis component, respectively, of the stator current, where both are in a synchronously rotating reference frame.

In dynamic modelling, the time varying parameters are eliminated and the variables and parameters are expressed in *orthogonal* or *mutually decoupled* direct d and quadrature q axes. The $d - q$ dynamic model of machines is usually expressed in a rotating with synchronous speed Ω_s reference frame. In a stationary reference frame, the reference axes α and β are fixed to the stator.

In vector control, i_{sd} is analogous to the field current I_f and i_{sq} is analogous to the armature current I_a of a d.c. motor. Therefore, the torque can be expressed as

$$T_d = c_T|\mathbf{\Phi}|i_{sq} = K_T i_{sq} i_{sd} \tag{5.18}$$

The basic concept of how i_{sd} and i_{sq} can be established as control vectors of the vector control method is explained in Figs 5.18a and 5.18b with the help of phasor diagrams in a synchronously rotating $d - q$ frame.

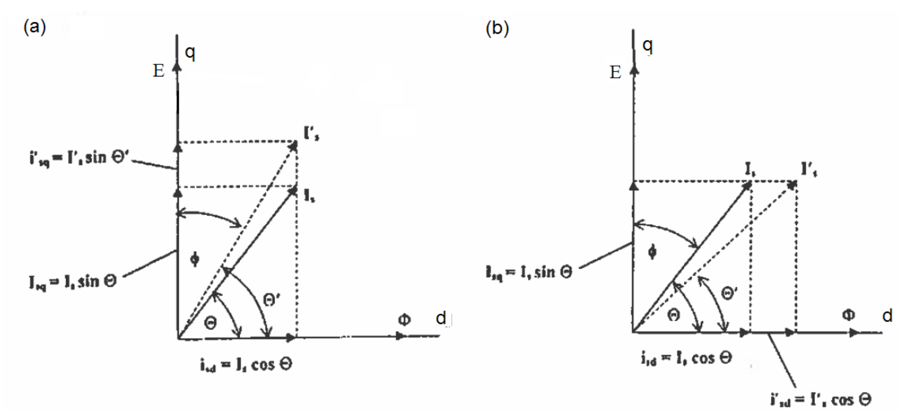

Fig. 5.18. Direct vector control (phasor diagrams in terms of peak values): (a) increase of torque component, (b) increase of field component.

The *direct control method* estimates the flux vector (amplitude and phase) from the measured values of the stator currents and stator voltages [6] (Fig. 5.19). The *indirect control method* calculates only the slip or the integral of the slip from a mathematical model. This method requires a rotor position sensor.

Some of the benefits of the vector controlled drive are:

- it operates using absolutely standard a.c. induction motors;
- it is cost-effective, especially in high power applications;
- it has a wide range of operating speeds, including high speed capabilities;
- it eliminates the maintenance problems associated with d.c. commutator motors or eddy-current couplings.

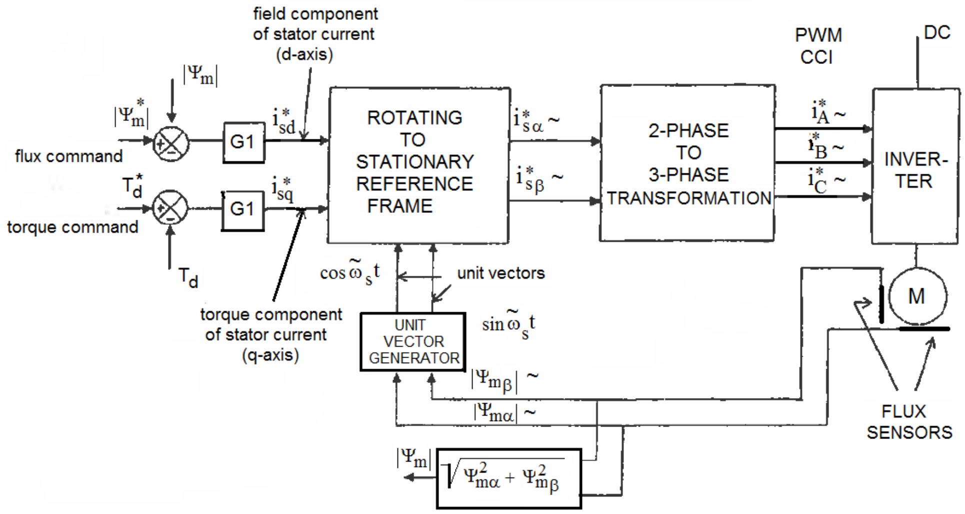

Fig. 5.19. Direct method of vector control of a voltage source current controlled inverter — block diagram.

5.3.7 Energy efficient motors

Nowadays, there is a tendency to use so called *energy-efficient induction motors* in many motor-drive applications, including in variable-speed drives. An energy-efficient motor produces the same shaft output power, but uses less electrical input power than a standard-efficiency motor. Energy-efficient motors are manufactured using the same frame as standard motors, but have:

- more copper in the winding;
- higher quality and thinner steel laminations in the stator;
- a smaller airgap between the stator and rotor;
- reduced ventilation (fan) losses;
- closer machining tolerances.

5.4 Synchronous motor drives

The speed of a synchronous motor is equal to the synchronous speed $n_s = f/p$ of the stator (armature) rotating field. The salient-pole design is the most common (as in Fig.4.1).

As discussed in detail in Chapter 4, synchronous motors are classified according to the mechanical design, construction, and material composition of their rotors into (a) electromagnetically-excited motors, (b) permanent magnet (PM) motors, (c) reluctance motors and (d) hysteresis motors.

A significant feature of the electromagnetically-excited synchronous motor is the controllability of its power factor up to unity or leading values.

The value of the electromagnetic torque T_d developed by a synchronous motor is determined by the airgap power P_g, and by the mechanical angular speed $\Omega_s = 2\pi n_s$ and is given by eqn (4.7).

The most common method of controlling the speed of synchronous motors is through the use of *load-commutated thyristor inverters*. The current commutation is generally provided by the EMFs that are induced in the synchronous motor's windings. At starting and at low speeds, however, these EMFs are insufficient for the task, and so the current commutation is provided instead by the line converter. Load commutation has important advantages over forced commutation, i.e. (a) it does not require commutation circuit, (b) the frequency of operation can be higher and (c) it can operate at power levels beyond the capability of forced commutation. In low-speed applications, *cycloconverters* can also be used to control the speed of synchronous motors.

5.5 Electronically commutated motor drives

Electronically commutated motors are classified into the following categories:

- PM brushless d.c. motors;
- stepping motors;
- switched-reluctance motors.

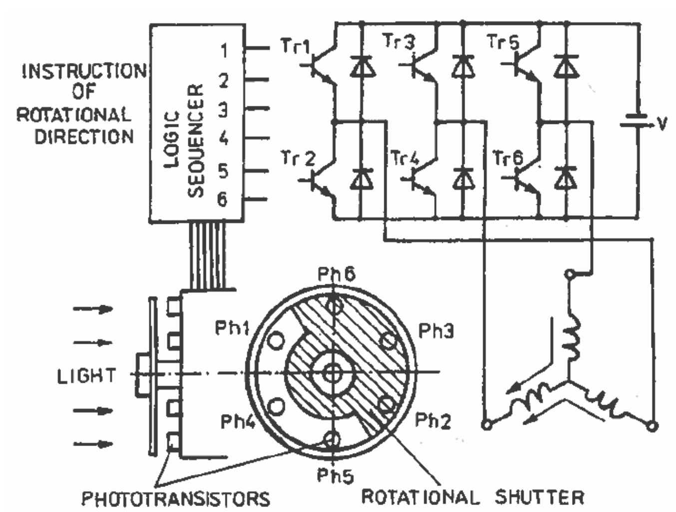

Fig. 5.20. Three-phase brushless motor with optical sensors.

5.5.1 Permanent magnet d.c. brushless motors

The construction of a *PM brushless d.c motor* is very similar to that of a PM synchronous motor. Brushless d.c. motors are different from synchronous motors in the energizing of their armature winding. In PM synchronous motors, the armature winding is fed from an a.c. three-phase power source without any rotor position feedback. Brushless d.c. motors, on the other hand, have a position sensor (which is generally a Hall elements or an optical sensor) that produces signals for controlling the electronic switches in the armature circuits (see Fig. 5.20). The transistors and position sensors thus act as an electronic commutator, replacing the mechanical commutator and brushes. The speed is reversed by an appropriate rearrangement in the logic sequencer.

Servo drives comprising *PM brushless motors* fed from solid-state converters are becoming commercially available on an increasing scale.

5.5.2 Stepping motor

A *stepping motor* is a doubly-salient, singly-excited electric motor which converts a digital electric input into mechanical motion. No feedback (for example using position sensors) is normally required for either position or speed control of these motors. Stepping motors are designed in the following categories as:

- variable-reluctance motors (with no excitation);
- PM motors (with active rotors);
- hybrid motors (which combine the principles of variable-reluctance and PM motors).

A typical control circuit for a stepping motor consists of a *pulse generator*, a *logic circuit*, a *power amplifier*, and a *power source*. Instead of a pulse generator, a microprocessor, microcomputer or A/D converter can be used. A logic circuit forms the pulses, usually of a rectangular shape and distributes them to each of the phase windings (providing the commutation).
The *step* of a rotary stepping motor is the angular displacement of the rotor resulting from a single input pulse. For a variable-reluctance stepping motor, this may be written

$$\alpha_s = \frac{360^0}{s_r m n} = \frac{2\pi}{s_r m_1 n} \tag{5.19}$$

and for a PM stepping motor the step size is

$$\alpha_s = \frac{360^0}{2 p_r m_1} = \frac{\pi}{p_r m_1} \tag{5.20}$$

The number of the rotor pole pairs is p_r, the number of the stator phases is m_1, and the number of the rotor teeth (slots) is s_r. For symmetrical commutation, $n = 1$ and for asymmetrical commutation $n = 2$.

In a *stepping motor with an active rotor*, the rotor's PM produces an excitation flux. The control winding located on the stator's salient poles receives rectangular pulses as input (Fig. 5.21). The *synchronising torque* is produced in a similar way to its production in a synchronous motor. The commutation algorithm is $(+1) \rightarrow$

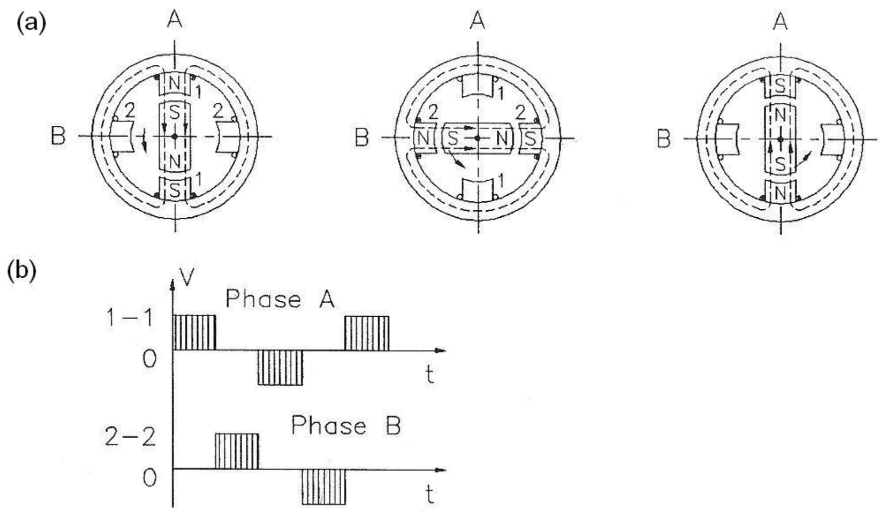

Fig. 5.21. Principle of operation of a stepping motor with active rotor: (a) rotor positions under the action of input pulses, (b) phase voltage waveforms (rectangular pulses).

$(+2) \rightarrow (-1) \rightarrow (-2) \rightarrow (+1) \ldots$. Since the stator control winding consists of two phases, the *value of step* for this motor is $\alpha_s = \pi/(p_r m_1) = \pi/(1 \times 2) = 90^0$. This means that the rotor turns by 90^0 after each input pulse as a result of the synchronising torque.

A stepping motor should meet the following requirements: it should have a very small step, small electrical and mechanical time constants, regular operation without ever missing steps, and a high degree of reliability. Stepping motors provide very high torque at low speeds, offering up to 5 times the continuous torque of a d.c. commutator motor of the same size and double the torque of equivalent brushless motors. This often eliminates the need for a gearbox. Stepping motors are usually used as torque motors with a limited range of speed.

5.5.3 Switched-reluctance motor

The *switched-reluctance motor* (SRM) is a doubly-salient, singly-excited motor (Fig.5.22) which has shaft position sensors for controlling the conduction angle of the phase current. It is designed for efficient power conversion at high speeds. Two main features distinguish the SRM from the reluctance stepping motor:

(a) the conduction angle for phase currents in a SRM is controlled and synchronised with the rotor position, using a shaft position sensor like in a PM brushless d.c. motor;
(b) an SRM is designed for efficient power conversion at high speeds, while the stepping motor is designed as a torque motor with a limited speed range.

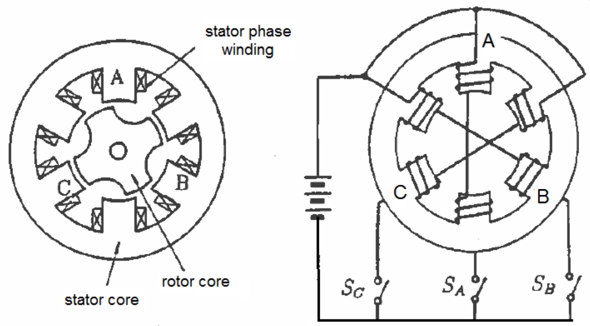

Fig. 5.22. Principle of operation of a switched-reluctance motor.

The advantages of SRMs can be listed as follows [41]:

- the rotor is simple and requires relatively few manufacturing steps;
- the stator is simple to wind;
- the stator winding is robust;
- the stator winding losses are low since the end-turns are short;
- the motor is easy to cool since the majority of losses appear on the stator;
- the maximum permissible rotor temperature may be higher than in PM rotors;
- the torque is independent of the polarity of the phase current;
- the starting torque can be very high without the problem of excessive inrush currents;
- under fault conditions, there would be no problem with locked-rotor overcurrent or open-circuit overvoltage;
- very high speeds are possible.

Since the torque is independent of the polarity of the phase current, the use of unipolar controller circuits with MOSFETs or IGBTs is made possible. The speed is proportional to the switching frequency and can easily be reversed by changing the switching sequence.

On the other hand, a SRM has the following clear disadvantages [41]:

- it suffers from torque pulsation which contributes to acoustic noise;
- the ripple current in the d.c. supply tends to be quite large, making for a large filter capacitance requirement which in turn may cause significant a.c. harmonics;
- an SRM cannot start or run from an a.c. sinusoidal voltage source;
- an SRM requires a power electronic converter, controller circuits, and a shaft position sensor for communication and speed feedback.
- the cabling for SRMs is more complex than that for induction motors — a minimum of four wires and more, usually six, are required for a three-phase motor, in addition to the sensor cabling.

The relationship between speed and fundamental switching frequency follows from the fact that if the poles are wound oppositely in pairs to form the phases, then each phase produces a pulse of torque on each passing rotor pole. The fundamental switching frequency is therefore:

$$f_{sw} = 2p_r n \tag{5.21}$$

where n is the speed in rev/s and p_r is the number of rotor pole pairs. There are $m_1 p_r$ steps per revolution for m_1 phases, and the 'step angle' or 'stroke' is

$$\alpha_s = \frac{\pi}{m_1 p_r} \tag{5.22}$$

The number of stator poles usually exceeds the number of rotor poles.

An SRM can be smaller than an induction motor designed to the same specification. On the other hand the SRM produces more noise and is much more expensive than an induction motor of the same rating. Indeed, neither the SRM nor the induction motor can attain the performance of the brushless PM motor.

Problems

1. A single-phase fully controlled rectifier is used to control the speed of a 4 kW, 110 V, 1200 rpm, 42.5 A separately excited d.c. motor. The armature circuit resistance is $\sum R_a = 0.34\ \Omega$, the shaft torque is $T = 20$ Nm and the speed is $n = 1000$ rpm. The motor armature current is practically ripple free. The brush voltage drop, armature reaction and losses in the rectifier are negligible. The rectifier is connected to a single phase 115 V (rms) power supply. Find: (a) the armature current I_{a20} at $T = 20$ Nm, (b) the firing angle α for motoring mode, (c) the supply power factor for motoring mode, (d) the firing angle for regenerative braking (inverter operation), (e) the power fed back to the a.c. supply for regenerative braking. Calculations for regenerative braking should be performed for the same speed, i.e. 1000 rpm and armature current as for motoring operation.

   Answer: (a) $I_{a20} = 26.9$ A, (b) $\alpha = 30.98^0$, (c) 0.772, (d) $\alpha = 132.9^0$, (e) 1895.9 W.
2. A 200 V, 1000 rpm, 145 A separately excited d.c. motor has the armature circuit resistance $\sum R_a = 0.06\ \Omega$ and is fed from a single phase fully controlled rectifier. The a.c. source voltage is 220 V (rms). Find: (a) the firing angle α at 800 rpm and rated motor torque, (b) firing angle α at -400 rpm and rated motor torque and (c) motor speed at rated torque and $\alpha = 45^0$. The brush voltage drop and armature reaction are neglected.

   Answer: (a) $\alpha = 35.26^0$, (b) $\alpha = 110.02^0$, (c) $n = 320.6$ rpm.
3. A 3-phase, 380 V (line-to-line), 50 Hz fully controlled rectifier feeds a 220 V, 1500 rpm, 50 A separately excited d.c. motor. The armature circuit resistance is $\sum R_a = 0.5\ \Omega$. A star-delta connected transformer is used to obtain the motor terminal voltage equal to the rated voltage when the firing angle $\alpha = 0$. Find: (a) the transformer turns ratio and (b) firing angle at rated torque and 1100 rpm and -750 rpm, respectively.

   Answer: (a) 1.347, (b) 40.22^0, 102.47^0.

4. A 220 V, 1200 rpm and 111 A separately excited d.c. motor has the armature circuit resistance $\sum R_a = 0.105\ \Omega$ and is fed from a chopper which can provide both motoring and braking operations. The d.c. source voltage is $V_{dc} = 220$ V. Find the duty cycle of the chopper for: (a) motoring at 900 rpm and rated torque and (b) regenerative braking at 500 rpm and rated torque. The brush voltage drop ΔV_{br} and armature reaction is neglected.

   Answer: (a) 0.763, (b) 0.341.
5. A three-phase, 10 kW, 380 V (line-to-line), 1450 rpm cage induction motor is fed from a three-phase a.c. voltage regulator. Both the motor and regulator are delta-connected and the motor current is sinusoidal. At rated load the efficiency is $\eta = 0.82$ and the power factor is $\cos\phi = 0.86$. Find: (a) the *rms* current rating of the thyristor, (b) the peak voltage rating of the thyristor, (c) the firing angle α to obtain sinusoidal motor current.

   Answer: (a) 8.8 A, (b) 537.4 V, (c) $\alpha = 30.68^0$.
6. A three-phase, 380 V (line-to-line), 50 Hz, 1450 rpm star-connected cage induction motor is fed from a VVVF three-phase inverter. The maximum input frequency cannot exceed 50 Hz and the maximum to minimum required speed ratio is 10:1. The inverter d.c. input voltage is supplied from a fully controlled three-phase rectifier with three 380 V input. Find the maximum and minimum d.c. link voltage and corresponding firing angles of the rectifier.

   Answer: 465.4 V d.c., $\alpha = 24.9^0$; 46.5 V d.c., $\alpha = 84.8^0$.
7. A three-phase, 3.0 kW, 380 V, 710 rpm, 50 Hz, Δ-connected cage induction motor has the following equivalent circuit parameters: $R_1 = 4.9\ \Omega$, $R_2' = 0.27\ \Omega$, $X_1 = 14.0\ \Omega$, $X_2' = 0.66\ \Omega$, $X_m = 30.0\ \Omega$. The motor is controlled by a VSI at $V_1/f = const$. The inverter output frequency varies from 10 to 100 Hz. Find: (a) the starting current and starting developed torque at rated frequency, (b) the starting current and starting developed torque at minimum and maximum frequency and (c) the pull-out torque as a function of frequency.

   Answer: (a) $I_{1st} = 24.45$ A, $T_{dst} = 5.9$ Nm; (b) $I_{1st10} = 12.8$ A, $T_{dst10} = 8.05$ Nm, $I_{1st100} = 25.53$ A, $T_{dst100} = 3.22$ Nm; (c) $k = 2$, $f = 100$ Hz, $T_{dmax} = 156.55$ Nm; $k = 1$, $f = 50$ Hz, $T_{dmax} = 133.56$ Nm; $k = 0.2$, $f = 10$ Hz, $T_{dmax} = 51.83$ Nm.

6

ELECTRICAL TRACTION

Traction systems can be classified as either *non-electric* or else as *electric*. Non-electric traction does not use electricity at any stage, and would include such drives as steam locomotives and internal combustion engines. Electric traction involves the use of electrical energy.

6.1 Characteristics of traction systems

Driving equipment used for traction purposes should meet the following requirements:

- it should be adaptable to the environment and should afford pollution-free operation;
- the coefficient of adhesion should be high, so that high tractive effort at start-up is possible and so that rapid acceleration of the train can be obtained;
- the wear caused on the wheels, rails and brake shoes should be minimal;
- it ought to be possible to overload the equipment for short periods;
- regenerative braking ought to be built into the system, so that energy may be generated on descents and fed back to the supply system;
- the locomotive or train should be self-contained, so that it could run on any route.

Electric traction satisfies most of these requirements, and one can note that:

- electric traction is the most efficient amongst all of the available systems;
- it does not pollute the natural environtment;
- it offers high starting torque and high acceleration;
- it has simple speed control and braking;
- regenerative braking is definitely possible;
- frequent starting and stopping is not a problem;
- trains may be divided into sections;
- the number of sections of track under operation can be in proportion to the necessary traffic;

- the coefficient of adhesion is high;
- for the same tractive effort, electric locomotives are lighter and hence can achieve higher speeds on gradients;
- an overloading of electric motors is possible for a short time;
- the centre of gravity of electric locomotives is lower than that of steam locomotives and hence electric locomotives can run faster along curved routes.

The major disadvantage of electric traction is its high capital cost. In addition, any power failure even for a short time, may cause complete dislocation of traffic.

6.2 Track geometry

Track geometry is defined in terms of four irregularities consisting of gauge, cross level, alignment and vertical surface profile (Fig. 6.1).

Gauge is the horizontal distance between two rails and is measured between the heads of the rails, in a plane 15.875 mm (5/8 inch) below the top of the rail head, i.e. gauge $= z_l - z_r$. *Cross level* is the difference between the elevations of two rails, i.e. cross level $= y_l - y_r$. *Alignment* is the average of the lateral positions of two rails, i.e. alignment $= (z_l + z_r)/2$ and is often referred to as the centre line. *Vertical surface profile* is the average elevation of the two rails, i.e. vertical profile $= (y_l - y_r)/2$.

Gauge plays an important role in the *lateral stability* of railway vehicles. As the gauge increases the lateral stability of a railcar increases too.

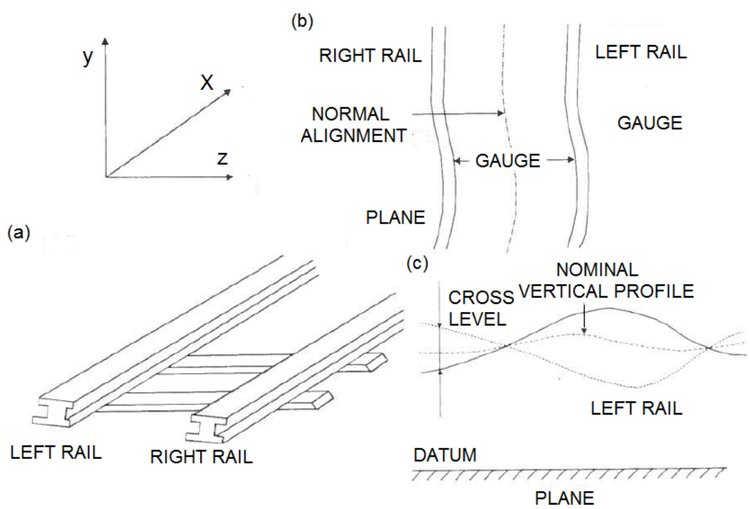

Fig. 6.1. Definitions of track irregularity parameters: (a) track, (b) gauge and alignment, (c) cross level and nominal vertical profile.

The *standard railway track* gauge is 1435 mm and it is used in Argentina, Australia, China, Egypt, Europe (except for Ireland, Portugal and Spain), France (which uses 1500 mm spacing from rail centre to rail centre, but where it is possible to travel with standard gauge wheel sets), Canada, Cuba, Ecuador, Guyana, Iran, Iraq, Israel, Jamaica, Japan, Korea, the Lebanon, Manchuria, Morocco, Mauritius, Mexico, New South Wales, Paraguay, Peru, Saudi Arabia, Tunisia, Turkey, Uruguay and the USA. In other parts of the world, the track gauges range from 500 mm to 1676 mm.

The 1067 mm *Cape track* has been implemented in Angola, Australia, Canada, the Congo, Costa Rica, Ecuador, Ghana, Guatemala, Guyana, Honduras, Indonesia, Japan (except for *Shinkansen* lines), Mozambique, New Zealand, Nicaragua, Nigeria, Norway, the Philippines, Queensland, South Africa, Spain, the Sudan, Sweden, Taiwan, Tasmania, the CIS (where the 1524 mm gauge is marginally predominant), Venezuela and Zimbabwe.

Alignment and cross-level variations are the major causes of *lateral vibration* in railway vehicles, whereas vertical profile has little influence on lateral vehicle dynamics.

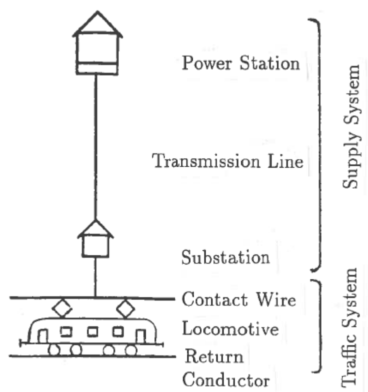

Fig. 6.2. An electric traction system.

6.3 Power supply systems for electric traction

The structure of a system for supplying electric tractive power is shown in (Fig. 6.2). There are three main types of supply system for electric traction:

- d.c. system;
- single-phase a.c. system operating at a low frequency such as 16 2/3 Hz or 25 Hz, or at a standard frequency of 50 Hz or 60 Hz;
- 3-phase a.c. system.

In a *d.c. system*, the energy is obtained from substations which consist of transformers and converting equipment such as rectifiers. In the case of suburban railways (operating usually at 1500 V d.c.) the substations are spaced at a distances of 3

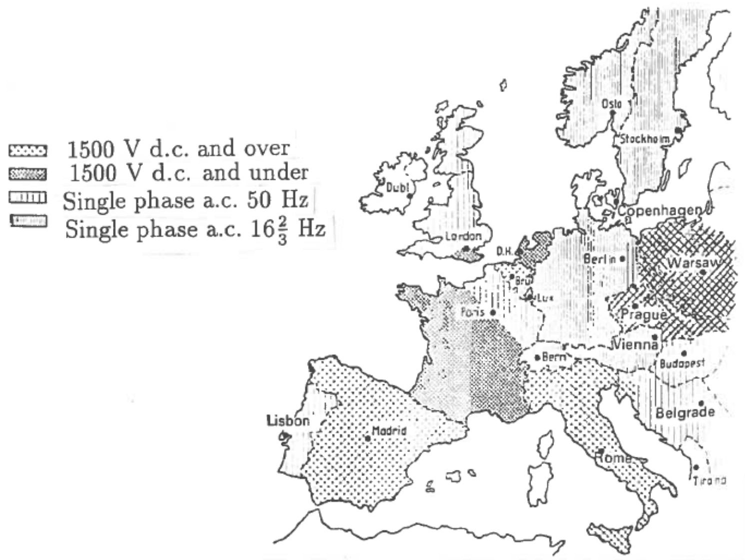

Fig. 6.3. D.c. and a.c. traction systems in Europe.

to 5 kms, but on main lines (which frequently operate at 3000 V d.c.) they are typically spaced at distances of about 40 to 50 kms.

In a *single-phase a.c. system*, the energy for the trains is drawn directly at high voltages (15 to 25 kV) from a generating station when the length of the overhead catenary line is below about 35 km. For longer distances, the economic voltage for power transmission system is higher than the voltage that would be desirable for a traction system, and hence transformer substations are necessary. With a 16 2/3 Hz supply, the first traction motors were of the single-phase commutator series type, and they were supplied by low voltages (of the order of 400 V) from a transformer that was carried on the vehicle.

With both d.c. and single-phase systems, only one contact wire is normally used, and the running rails act as the return conductor. Low frequency operation of the a.c. commutator series motor improves its commutation, power factor, and efficiency. Moreover, since low frequency operation of the overhead line reduces the line reactance, substations can be spaced at relatively greater distances of 50 to 80 km for the same overall voltage drop. D.c. motors have better torque-speed characteristics, lower maintenance costs, smaller weight per unit of output power, better speed control, and more efficient regenerative braking than single-phase a.c. commutator series motors.

If low frequency power is obtained from a dedicated generating station, then there is no problem with frequency conversion, but if the power is to be drawn from an existing industrial electric network, then frequency converters and transformers are required to convert 3-phase 50 Hz (for example) into single-phase 16 2/3 Hz or 25 Hz.

In the case of *3-phase systems*, energy can be drawn from the existing 3-phase electric network or else it can be obtained by using transformer substations when the network is operating at a higher voltage. The efficiency of this system is high because no converting equipment is involved.

The map in Fig. 6.3 shows the distribution of d.c. and a.c. traction systems in Europe.

6.4 Current collection systems

In almost all systems of track electrification, the running rails are used as return conductor, while the 'go' conductor may be either an *overhead wire*, or else a *conductor rail* (third rail) laid alongside the running rails at a distance of about 0.3 to 0.4 m.

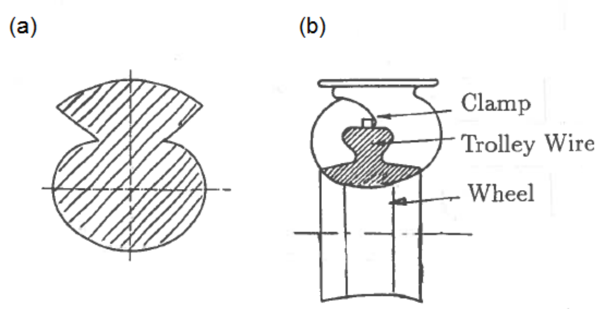

Fig. 6.4. Trolley contact wire: (a) cross section, (b) wire, clamp, and collector wheel arrangement.

For trams, trolley buses and for railways operating at 1500 V and above, overhead contact wire is used. The design of an overhead system is more complex than the design of a conductor rail system because of the greater difficulty of ensuring that the collector and contact wire remain in contact at a fairly even pressure. Hard-drawn copper, cadmium-copper or silicobronze are used for contact wires. In order to facilitate connections to the support, the wire is grooved as shown in Fig. 6.4a. A typical trolley collector wheel is shown in Fig. 6.4b. Although the wheel has a fairly deep groove, there is a danger of its jumping off the wire, especially at points and crossing when the speed exceeds 32 km/h. Trolley collectors must operate in a trailing position, and if the direction of the vehicle is to be reversed then the collector should be rotated through 180^0.

The conductor-rail system is employed at 600 or 750 V for suburban services as it is relatively cheap and the inspection and maintenance are easy. The supporting structures of these rails do not interfere with the visibility of signals, and it is not considered necessary to protect the rail from accidential contact with plate layers etc. except at stations and in sidings. For voltages of 1500 V and above, however, it is always desirable, from the safety point of view, to use an overhead wire as the 'go' conductor.

The conductor rails are placed on insulators. The electrical contact surface is on the upper face of the rail in some cases, but in some others the contact runs along

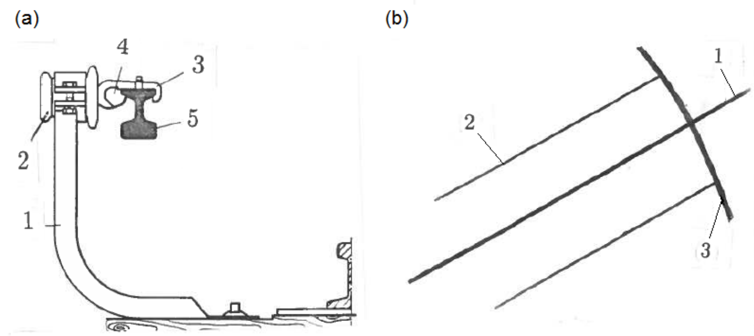

Fig. 6.5. Simple current collectors: (a) conductor rail or third rail (1 — bracket, 2 — insulator, 3 — claw, 4 — wedge, 5 — rail), (b) bow collector (1 — wire, 2 — bow, 3 — metal strip).

the side or even the bottom of the conducting rail. There are various different constructions which are designed to protect against accidential contact and to minimise possible obstruction to the train's movement from ice, snow or leaves. Wear on the conductor rail is due only to the friction of the collector shoes.

For reasons of economy, conductor rails are made from a special steel alloy, which gives high conductivity and at the same time satisfies all of the other requirements. A typical composition is iron 99.63%, carbon 0.05%, manganese 0.2%, phosphorus 0.05%, silicon 0.02% and sulphur 0.05%. In order to reduce the voltage drop at the joints of the conducting rail, short lengths of flexible copper conductor are connected across the rail joints. To accommodate thermal contraction and expansion of the rails, the conductor rail is not fixed rigidly to the insulators. However, to prevent creepage of the rail due to friction between the rail and the collector shoes, it is anchored at intervals of 100 m to 150 m.

Flat steel shoes measuring 0.2 m by 0.075 m are used to collect current from the conductor rail. The necessary contact force of about 150 N is obtained by gravity in the case of a top contact and by means of springs in the cases of side- and underrunning contacts. The current per shoe is of the order of 800 A. Since it is not always possible to have the conductor rail on the same side of the track, it is desirable to provide shoes on both sides of the train. Furthermore, since there are gaps in the rails at points and at crossings, at least two shoes should be provided on each side of the railcar to avoid dicontinuity in the current flow.

The main advantage of the *bow collector* of Fig. 6.5b is that it can be used at high speeds. The bow collector consists of two trolley collector poles at the end of which is placed a light metal strip of about 1 m in length. To avoid the bow jumping off the wire at high speeds, it is desirable that the wire be accurately located above the track, and it is also staggered by about 0.15 m to each side of the centre line to avoid excessive wearing of the groove in the contact strip. The bow collector must always be run in a trailing position, and this means that duplicate bows or reversing bow should be used during a reversal of the direction of motion of the vehicle. The bow collector is made of a relatively soft metal such as aluminium or copper, so that most of the wear will be on the easily-replaceable strip and not on the permanent contact wire. The bow collector has smaller inertia but it is not as readily adaptable to the collection of large currents as the pantograph collector.

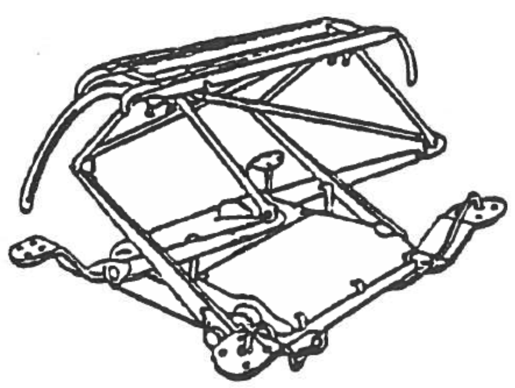

Fig. 6.6. The pantograph collector.

The *pantograph collector* (Fig. 6.6) requires a greater pressure to maintain contact with the wire than a bow collector because of its higher inertia. Both bow collectors and pantograph collectors maintain contact with the overhead conducting wire by means of springs, and any lowering or raising operations are achieved with pneumatics. The pantograph is maintained in its normal, raised position by the use of compressed air, which keeps the central springs under tension. When the air is released from the cylinder, the springs bring the pantograph into the lowered position. A catch or a latch is usually provided to hold the pantograph in the lowered position, to prevent bouncing and to avoid the necessity for a continuous supply of compressed air when the vehicle is out of service. The contact strips are made of copper, steel or carbon and are mounted on a light metal shoe. Current of the order of 1 kA per contact strip may be collected.

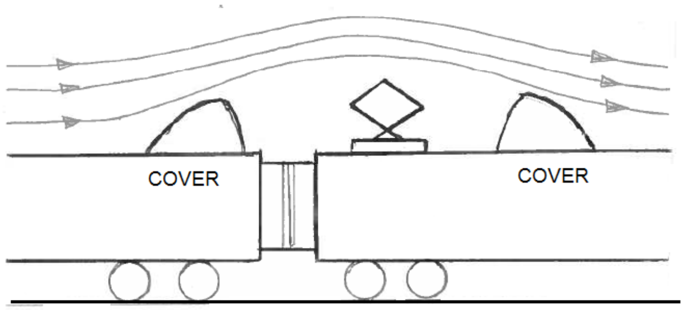

Fig. 6.7. Function of a pantograph cover.

The advantages of the pantograph current collector are as follows:

- because of the absence of sharp points or grooves, the overhead construction at railway points is simplified;
- there is no risk of the collector leaving the wire at junctions;
- the pantograph collector is *reversible*, being quite suitable for operation in either direction of motion;
- speeds as high as 500 km/h can be obtained.

Wind impacting directly on a pantograph is the largest source of noise in trains travelling at speeds above 200 km/h. To reduce the noise, pantographs are equipped with *pantograph covers* (Fig. 6.7). An well-known example of a vehicle with pantograph covers is the *Nozomi Shinkansen* Series 300 superexpress train.

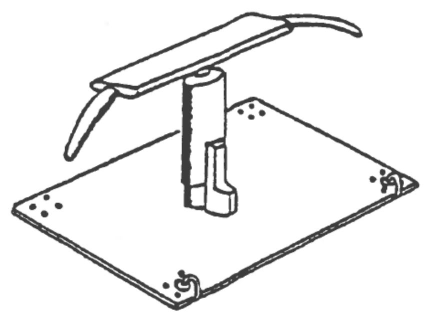

Fig. 6.8. Wing-shaped current collector.

To lower the noise without a cover, a *wing-shaped current collector* (Fig. 6.8) has been developed for the French TGV *Atlantique* superexpress train and for the Japanese prototype train WIN350. Because its contact strip looks like a wing of an airplane, it is called a 'wing-shaped collector'. It provides a great improvement in noise reduction when compared with the conventional pantograph.

6.5 Electrolysis by currents through the earth

If the track is used as the return conductor, then the current passes through the earth as well as through the track. As currents enter the earth, they spread out and follow a large cross section of earth, flowing through any available low-resistance path that might be provided by water-pipes, cable sheaths or other metallic structures. When the currents leave the metallic structures, they corrode the structures at the leaving surface by electrolytic action. In order to reduce such effects, the following methods are suggested:

- low-resistance return paths can be provided;
- insulating joints can be inserted near the pipes or other metallic structures so that the entry of currents into these structures is avoided.

6.6 Train movement

6.6.1 Speed-time curve

A train is to be run between two stations in as efficient a way as possible. To make optimising decisions, it is necessary to know the speed-time curves and the resistance to the motion of the train (in terms of friction and windage). It is then possible to find out what energy must be supplied to the train in order to perform a particular job. The *speed-time curve* is a graph which shows the variation of the train's speed as a function of time. In general, the motion of the train can be classified into the following types:

- acceleration;
- constant free-running speed;
- coasting, i.e. running with the power switched off and therefore there is retardation due to the frictional and windage forces;
- retardation due to braking.

A typical speed-time curve is shown in Fig. 6.9. A main line service is characterised by long periods of free running at high speeds with acceleration periods that are negligibly short as compared with the total running time of the train.

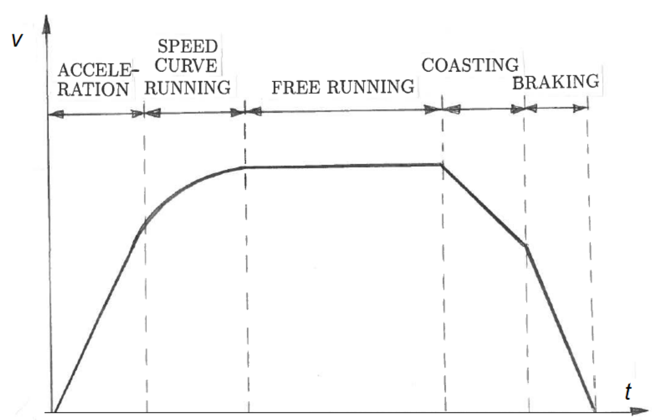

Fig. 6.9. Typical speed-time curve for a train movement.

The duration for which the free-running and coasting periods last on the speed-time curve are determined by the service expected of a train. In the case of an urban service, where the distance between consecutive stops is less than 1 km, the free-running period may be absent. It is desirable to have relatively high average speed so that a good frequency of train service is made available. Therefore, high values of acceleration and retardation are maintained with a short period of coasting in order to obtain reasonable saving on energy consumption. An acceleration up to 4 km/h/s and retardation up to 6 km/h/s is recommended.

Similarly, with suburban services where there are somewhat longer distances between stations, the coasting period is longer but the free-running period is again absent. In this case also, in order to have frequent service of trains, high values of acceleration and retardation are required. Typical values recommended are 2.5 km/h/s and 4 km/h/s, respectively. For suburban trains running on level track the coasting deceleration is approximately 0.16 km/h/s.

6.6.2 Average speed and schedule speed.

The *average speed* v_{av} of a train is defined as the ratio of the distance s between two consecutive stations to the time t_{tr} taken by the train to travel that distance. Thus:

$$v_{av} = \frac{s}{t_{tr}} \tag{6.1}$$

Similarly, the *schedule speed* is defined as the ratio of the distance s between two consecutive stations to the actual time t_{tr} of the run between the stops plus the time t_{st} taken by the stops. So:

$$v_{sch} = \frac{s}{t_{tr} + t_{st}} \tag{6.2}$$

This shows that the schedule speed is always smaller than the average speed. The difference is large in the case of urban and suburban services and is negligibly small in the case of a main line service. This suggests that to have a fairly good schedule speed for urban or suburban services the stop time must be reduced. It is recommended to have stop times less than 30 s for small services.

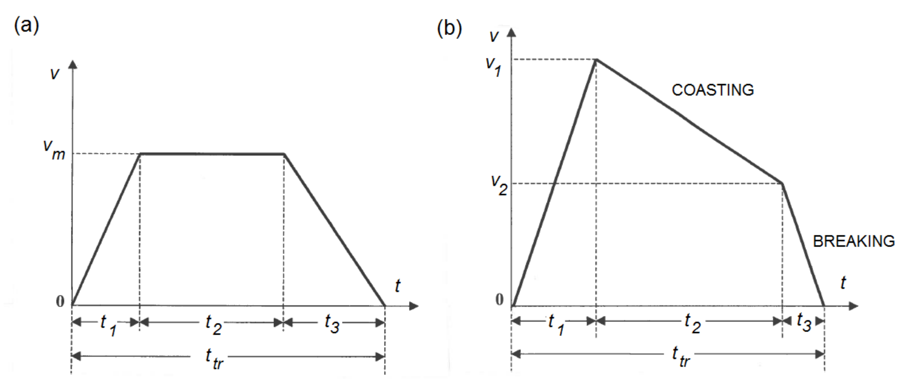

Fig. 6.10. Simplified speed–time curves: (a) trapezoidal, (b) quadrilateral.

6.6.3 Simplified speed–time curves

The movement of the train between two stations can be approximated either by a *trapezoidal* or a *quadrilateral* speed–time curve depending on whether the service is main-line or suburban respectively (Fig. 6.10).

The speed-time curve of a main line service is most often replaced by a trapezoid (Fig. 6.10a). The acceleration time is

$$t_1 = \frac{v_m}{a} \tag{6.3}$$

where v_m is the maximum speed called also *crest speed* and a is the acceleration. Similarly the retardation time is

$$t_3 = \frac{v_m}{d} \tag{6.4}$$

where d is the deceleration. The time for free running t_2 depends both on acceleration and deceleration, i.e.

$$t_2 = t_{tr} - t_1 - t_3 = t_{tr} - v_m\left(\frac{1}{a} + \frac{1}{d}\right) \tag{6.5}$$

The total distance of run can be found as

$$s = \frac{1}{2}v_m t_1 + v_m t_2 + \frac{1}{2}v_m t_3 = v_m t_{tr} - \frac{v_m^2}{2}\left(\frac{1}{a} + \frac{1}{d}\right) \tag{6.6}$$

or

$$kv_m^2 - t_{tr}v_m + s = 0 \tag{6.7}$$

where

$$k = \frac{1}{2}\left(\frac{1}{a} + \frac{1}{d}\right) \tag{6.8}$$

The above quadratic eqn (6.7) allows to find the crest speed as a function of the total time of run, acceleration, deceleration and total distance of run, i.e.

$$v_m = \frac{t_{tr}}{2k} - \sqrt{\left(\frac{t_{tr}}{2k}\right)^2 - \frac{s}{k}} \tag{6.9}$$

For a quadrilateral speed-time curve describing a movement of urban or suburban trains as shown in Fig. 6.10b the times of acceleration, coasting and braking are as follows

$$t_1 = \frac{v_1}{a}, \qquad t_2 = \frac{v_1 - v_2}{d_c}, \qquad t_3 = \frac{v_2}{d_b} \tag{6.10}$$

where d_c is the coasting deceleration and d_b is the braking deceleration. The total distance travelled is

$$s = \frac{1}{2}v_1 t_1 + \frac{1}{2}(v_1 + v_2)t_2 + \frac{1}{2}v_2 t_3 \tag{6.11}$$

Example 6.1

A suburban train runs according to quadrilateral speed-time curve at the average speed $v_{av} = 48$ km/h between two stations 2.4 km apart. The maximum speed is $v_1 = 72$ km/h, acceleration $a = 1.9$ km/h, coasting deceleration is $d_c = 0.16$ km/h/s and braking retardation is $d_b = 3.5$ km/h/s. Find the time of acceleration, deceleration and braking.

Solution

The time of acceleration

$$t_1 = \frac{v_1}{a} = \frac{72}{1.9} = 37.89 \text{ s}$$

The actual time of run

$$t_{tr} = \frac{s}{v_{av}} = \frac{2400}{48} \times 3.6 = 180 \text{ s}$$

The time of coasting

$$t_2 = \frac{v_1 - v_2}{d_c} = \frac{72 - v_2}{0.16}$$

The time of braking

$$t_3 = \frac{v_2}{d_b} = \frac{v_2}{3.5}$$

Since

$$t_{tr} = t_1 + t_2 + t_3$$

or

$$180 = 37.9 + \frac{72 - v_2}{0.16} + \frac{v_2}{3.5}$$

the speed at the end of coasting is

$$v_2 = \frac{307.9}{5.9643} = 51.62 \text{ km/h}$$

Thus

$$t_2 = \frac{72 - 51.62}{0.16} = 127.37 \text{ s} \qquad \text{and} \qquad t_3 = \frac{51.62}{3.5} = 14.74 \text{ s}$$

6.7 Traction effort equation

For a wheel-on-rail vehicle or train, the traction effort equation is

$$F_{te} = (k_r + k_g + k_c + k_a)G \tag{6.12}$$

where k_r is the coefficient of the rolling resistance, k_g is the coefficient the gradient resistance, k_c is the coefficient of the curve resistance, k_a is the coefficient of the acceleration resistance, and G is the weight of the vehicle (train) in Newtons.

The *specific rolling resistance* can be evaluated from the graphs plotted in Fig. 6.11. The *specific gradient resistance* is

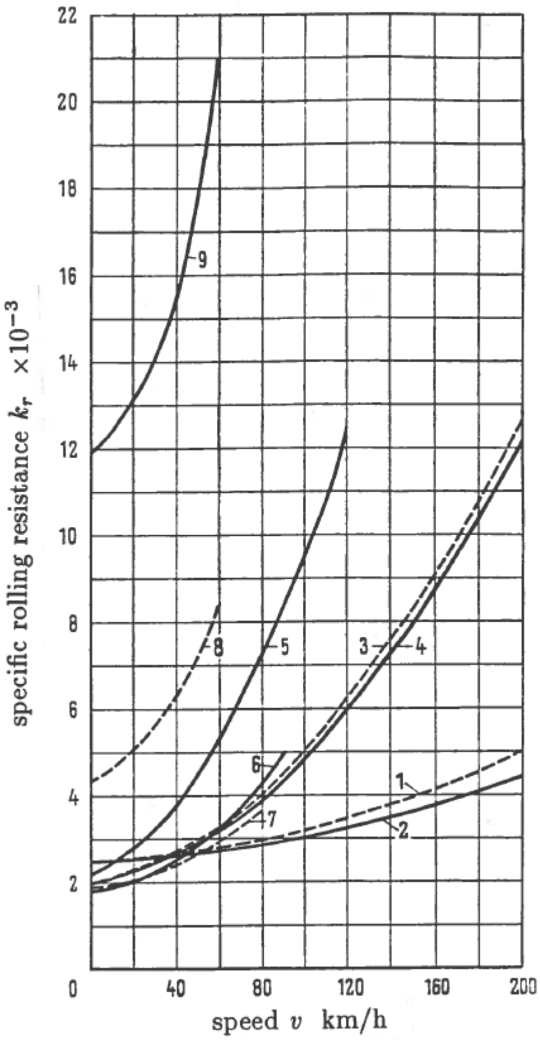

Fig. 6.11. Specific rolling resistance: 1 — four-axled 85 t locomotive (Bo'Bo'), 2 — six-axled 112 t locomotive (Co'Co'), 3 — long-distance 350 t train comprising 7 carriages, 4 — fast 600 t train comprising 13 carriages, 5 — 1200 t freight train, 6 — suburban train with 2/3-unit overhead-wire railcars, 7 — urban fast train with 2/3-unit conductor rail railcars, 8 — tram comprising one motor car and one trailer, 9 — trolley bus. Courtesy of *Siemens*, Germany.

$$k_g = \pm \sin\alpha = \pm \frac{h}{s} \tag{6.13}$$

since the force due to gravity is $G \sin\alpha$. The gradient $\sin\alpha = h/s$ is defined as the *ratio of the rise in elevation to the distance along the track*. The '+' sign is for a train moving up the gradient and the '−' sign is for a train moving down the gradient.

The *specific curve resistance* is

$$k_c = \frac{0.153S + 0.1b}{R_c} \tag{6.14}$$

where S is the running circle distance in m, b is the mean value of all fixed wheel bases with $b < 3.3S$ in m, and R_c is the curve radius in m.

Finally, the *specific acceleration resistance* (derived from $F = m \times a = (G/g)a = Gk_a$, where $k_a = a/g$) is

$$k_a = \frac{(1+\zeta)a}{9.81} \tag{6.15}$$

where ζ is added to take account of any rotating masses on the train and a is the starting acceleration in m/s^2. For a mean increase in acceleration represented by $\zeta = 0.08$, the specific acceleration resistance is $k_a \approx 0.11a$.

For high speed trains the air resistance force

$$F_{air} = 0.5 C \rho v^2 A \qquad \text{N} \tag{6.16}$$

should be added to eqn (6.12). The coefficient $C = 0.2$ for cone or wedge shaped nose, e.g. for *Shinkansen*, $C = 2.1$ for flat fronts of trains and $C = 0.75$ for automobiles. The air density is ρ, the speed is v in m/s and the front surface area is A in m^2. At 20^{0}C and 1 atm the air density is $\rho = 1.21$ kg/m^3.

For example, in the case of TGV *Atlantique* superexpress train (Table 6.1) $A = 4.1 \times 2.814 = 11.537$ m^2, $v = 300$ km/h $= 300/3.6 = 83.33$ m/s, $C = 0.2$ and $F_{air} = 0.5 \times 0.2 \times 1.21 \times 83.33^2 \times 11.537 = 9694.3$ N.

Example 6.2

Calculate the traction effort expended by a 710-t train with a wheel base of $b = 2.5$ m when it accelerates up a gradient of 1:250 with an acceleration of $a = 1.6$ km/h/s $=$ 0.444 m/s^2. The specific rolling resistance is $k_r = 0.01$, the curve radius is $R_c = 1200$ m, and the running circle distance is $S = 5.4$ m (which is equal to $2\pi\times$ the wheel radius).

Solution

The train weight

$$G = m \times g = 710\ 000 \times 9.81 = 6\ 965\ 100 \text{ N}$$

The specific gradient resistance

$$k_g = \frac{h}{s} = \frac{1}{250} = 0.004$$

The specific curve resistance

$$k_c = \frac{0.153 \times 5.4 + 0.1 \times 2.5}{1200} \approx 0.0009$$

The specific acceleration resistance

$$k_a \approx 0.11a = 0.11 \times 0.444 = 0.04884$$

The traction effort according to eqn 6.12 is therefore

$$F_{te} = (0.01 + 0.004 + 0.0009 + 0.04884)6965100 = 443955.47 \approx 444 \quad \text{kN}$$

6.8 Driving mechanisms

Fig. 6.12 shows schematically the essential driving mechanism of an electric vehicle. Some bogies and driving mechanisms of modern motor cars are shown in Fig. 6.13.

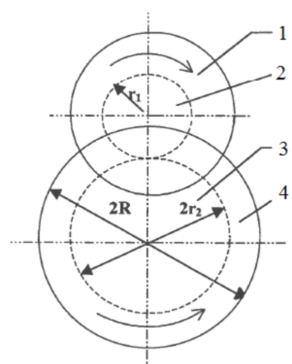

Fig. 6.12. Transmission of tractive effort: 1 — frame of the traction motor, 2 — pinion of the motor, 3 — gear wheel, 4 — driving wheel.

In terms of Fig. 6.12, the traction motor has a pinion meshed with the gear wheel on the driving wheel. If the traction motor exerts a torque T which is transmitted to the driving wheel through the gear, the tractive effort F_1 at the pinion is $F_1 r_1 = T$ where r_1 is the radius of the pinion. According to eqn (1.2) the gear ratio is

$$\gamma = \frac{n_1}{n_2} = \frac{r_2}{r_1} \tag{6.17}$$

where n_1 is the speed of the motor pinion in rpm, n_2 is the speed of the driving wheel in rpm, and r_2 is the radius of the gear wheel that is fixed to the axle.

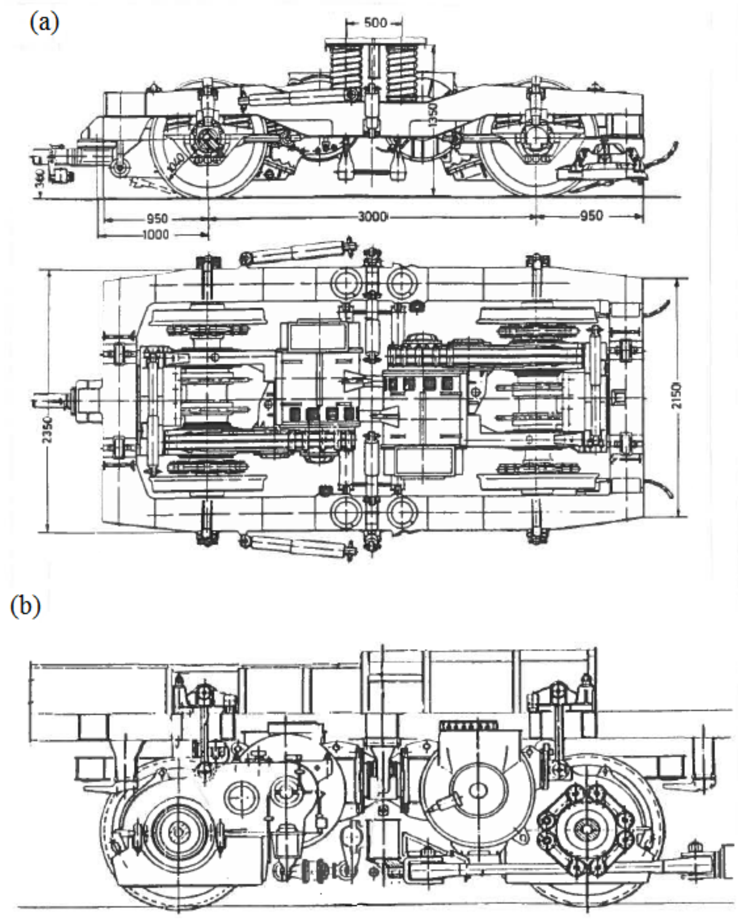

Fig. 6.13. Driving mechanisms of modern cars: (a) InterCity Express (Germany), (b) ETR-500 (Italy).

If F_{te} is the tractive effort at the driving wheel and R is the driving wheel's radius, then

$$F_{te}R = F_1 r_2 \eta_g$$

where η_g is the efficiency of transmission of the power from the motor to the driving axle. Therefore

$$F_{te} = F_1 \frac{r_2 \eta_g}{R} = \frac{T}{r_1} \frac{r_2 \eta_g}{R} = \eta_g T \frac{\gamma}{R} \qquad (6.18)$$

Example 6.3

A 200-t passenger train is pulled by an electric locomotive which has four motors each developing a shaft torque of 5000 Nm during the acceleration period. The gear ratio of the motors is $\gamma = 3.6 : 1$ and the gear efficiency is $\eta_g = 90\%$. The driving wheel diameter is $2R = 0.915$ m, the specific rolling resistance is $k_r = 0.005$ and 10% should be allowed for the effects of rotational inertia. Determine the time taken by the train to attain a speed of 100 km/h starting from rest on a gradient of $h : s = 1 : 200$ on straight track.

Solution

The weight of the train is $G = mg = 200 \times 10^3 \times 9.81 = 1\ 962\ 000$ N.

The torque developed by the four motors $T = 5000 \times 4 = 20\ 000$ Nm.

The total tractive effort available at the tread of the wheel, using eqn (6.12) (with $k_c = 0$) is

$$F_{te} = (k_r + k_g + k_a)G$$

The forces in the above equation are:

- the force due to friction

$$Gk_r = 1\ 962\ 000 \times 0.005 = 9810\text{N};$$

- the force due to gravity acting down the gradient

$$Gk_g = G\frac{h}{s} = 1\ 962\ 000 \times \frac{1}{200} = 9810 \quad \text{N};$$

- the accelerating force (where the rotational inertia allowance is 1.1)

$$Gk_a = \frac{G}{g}a(1+\zeta) = \frac{1\ 962\ 000}{9.81}a(1+0.1) = 220\ 000a$$

The traction effort can be simply calculated as

$$F_{te} = \eta_g T\frac{\gamma}{R} = 0.9 \times 20\ 000 \times \frac{3.6 \times 2}{0.915} = 141\ 639.3 \quad \text{N}$$

and this must be balanced by k_rG, k_gG, and k_aG, so

$$141\ 639.3 = 220\ 000a + 9810 + 9810$$

and the acceleration is now found as

$$a = \frac{122\ 019.3}{220\ 000} = 0.5546 \quad \text{m/s}^2 = (3.6 \times 0.5546) \quad \text{km/h/s} = 1.997 \quad \text{km/h/s}$$

Therefore, the time taken to attain a speed of 100 km/h is

$$t_1 = \frac{100}{1.997} = 50.08 \quad \text{s}$$

6.9 Energy consumption

In order to stick to the speed-time schedule, a suitable amount of electric energy should be fed to the train. If the energy is supplied by a central power station or is tapped from a power grid, it is necessary to predetermine the amount of power required by the train so that the power station equipment, substation feeders and the distributors can be designed optimally. It is to be noted that while designing an optimal electric supply system for the railways the reliability factor is of utmost importance, because a supply breakdown even for a short duration may result in the complete dislocation of all traffic and may sometimes lead to accidents. The degree of accuracy to which the electric energy requirements can be estimated depends upon the exactness of the available knowledge relating to the conditions of operation such as schedule speed, distance between stops, frequency of service, the mass of the train etc., and of course upon the degree of reliability that is required.

The electric energy supplied to the train is spent in:

- accelerating the train on a level track;
- accelerating the revolving parts;
- doing work against gravity if the train is ascending a gradient;
- doing work against the resistance to motion;
- supplying losses to the motors and other electrical equipments.

For urban and suburban services with high schedule speeds, the energy required for acceleration periods forms a large percentage of the total energy required for the propulsion of the train, whereas for main line services on level track at high speeds, the energy spent against the resistances to motion (friction and windage) may be considerably greater than the total energy required during all acceleration periods. The energy supplied during acceleration is stored in the form of kinetic energy. A part of this energy is used during coasting and the remainder is partly dissipated as heat in the brake shoes and is partly, in the case of regenerative braking, fed back to the supply system.

On the basis of a trapezoidal speed-time curve (Fig. 6.10a) the energy output of driving axles to accelerate the train is

$$k_a G\left(\frac{1}{2}v_m t_1\right) = \frac{1}{2}k_a G\frac{v_m^2}{a} \qquad \text{J or Ws}$$

Including the rolling and gradient resistance

$$E_1 = \frac{1}{2}\frac{v_m^2}{a}(k_a + k_r + k_g)G \quad \text{Ws} \tag{6.19}$$

The energy output to run the train at the speed $v_m = const$ against the rolling and gradient resistance

$$E_2 = (k_r + k_g)Gv_m t_2 = (k_r + k_g)Gs_2 \quad \text{Ws} \tag{6.20}$$

where $s_2 = v_m t_2$ is the distance travelled during free run. The total energy output of driving axles

$$E = E_1 + E_2 = \left[\frac{1}{2} v_m^2 \frac{1+\zeta}{g} + (k_r + k_g)(s_1 + s_2)\right] G \quad \text{Ws or } \frac{1}{3.6} \times 10^{-3} \text{ Wh} \quad (6.21)$$

where $s_1 = 0.5 v_m^2 / a$ is the distance travelled during acceleration. The *specific energy output* is defined as the total energy output divided by the mass of the train and total distance of run $s = s_1 + s_2 + s_3$, i.e.:

$$e = \frac{E}{ms} = \frac{1}{2} v_m^2 \frac{1+\zeta}{s} + (k_r + k_g) g \frac{s_1 + s_2}{s} \quad \text{m/s}^2 \text{ or Ws/(kgm)} \quad (6.22)$$

To obtain the specific energy output in Wh/(tkm) it is necessary to multiply eqn (6.22) by 277.78. The *specific energy consumption* is

$$e_c = \frac{e}{\eta} \quad (6.23)$$

where η is the efficiency of motors.

Example 6.4

A 750-t electric train accelerates uniformly from the rest to maximum speed $v_m = 48$ km/h up a gradient of 1:400 in $t_1 = 40$ s. The power is then cut off. First, the train coasts down a uniform gradient of 1:800 and then brakes are applied to bring the train uniformly to the rest on this gradient. The specific rolling resistance is $k_r = 0.004$ and 8% should be allowed for the effect of rotational inertia. Calculate: (a) the maximum power output from the driving axles and (b) the energy taken from the catenary wire, assuming an efficiency of 70%.

Solution

The weight of the train is $G = mg = 750 \times 10^3 \times 9.81 = 7357.5 \times 10^3$ N. The acceleration is $a = v_m / t_1 = 48/40 = 1.2$ km/h/s. The tractive effort required

$$F_{te} = (k_r + k_g + k_a) G = \left(0.004 + \frac{1}{400} + \frac{1.0 + 0.08}{9.81} \frac{1.2}{3.6}\right) \times 7357.5 \times 10^3 = 317.824 \times 10^3 \text{ N}$$

The maximum power output from driving axles

$$P_{outmax} = F_{te} v_m = 317.824 \times 10^3 \times \frac{48}{3.6} = 4237.65 \times 10^3 \text{ W}$$

There is no free run so that the total energy required for the run is

$$E = E_1 = \frac{1}{2} v_m t_1 F_{te} = \frac{1}{2} \frac{48}{3.6} \times 40 \times 317.824 \times 10^3 = 84\,753 \times 10^3 \text{ Ws} = 23.5425 \text{ kWh}$$

The energy taken from the catenary wire is $E/\eta = 23.5425/0.7 = 33.632$ kWh.

6.10 Development of electrical traction drives

Electrical traction drives are classified into drives with

- single-phase a.c. commutator motors (before 1906);
- uncontrolled rectifiers and d.c. motors (since 1906);
- controlled rectifiers and d.c. motors (since 1936);
- choppers and d.c. motors (since 1963);
- inverters and a.c. rotary motors (since 1965);
- inverters and a.c. linear motors (since 1980).

To solve the problem of energy supply, the first electrified railways were supplied with single-phase alternating current. This is why about 50% of today's long-distance electrical traction is the single-phase a.c. traction. D.c. commutator motors were more convenient than a.c. commutator motors, and so with the development of mercury-arc rectifiers attempts were made to convert a.c. drives to d.c. drives. Uncontrolled mercury-arc rectifiers have been in use in traction drives since 1906. The speed control was achieved by means of adjusting transformer taps and resistors.

In 1936, a locomotive with a grid controlled mercury-arc rectifier was equipped by the German Federal Railways on the Höllental part of the network [55]. In 1963, in the USA, railcars with silicon-diode rectifiers and ignitron control were put into service.

In 1964 *Siemens* developed an industrial locomotive for a coal mine, which was equipped with thyristors. The solid-state converter consisted of two half-controlled single-phase bridges connected in series on the d.c. side. In the same year motor coaches with thyristor control were brought into service in Sweden. In Japan the first series of thyristor locomotives was implemented in 1966.

In the converter arrangements described above, the a.c. voltage from the traction supply is used for commutation. When the supply to the traction vehicle is a d.c. voltage, however, it is necessary to use *self-commutated convertors* or *choppers* for control of the motor.

A shunting locomotive in the Siemens Transformer Factory in Nürnberg (Germany), with d.c. chopper control, was put into service in 1963. Since about 1970, chopper control in the armature circuit of traction vehicles used in urban transit systems has been in common use.

From the point of view of dimensioning the chopper circuit itself, the chopping frequency ought to be as low as possible (around 100–300 Hz), but when taking the filter design into account, the chopping frequency should be as high as possible [55]. This problem was solved through a phase shift between several parallel chopper circuits. As an example, the RATP (Régie Autonome des Transport Parisiens) put several subway vehicles into service with power ratings of over 400 kW between 1969 and 1971 [55]. In these systems, the parallel operation of 2,3, and 4 phase-displaced choppers was investigated. Fig. 6.14 shows the principle of a 3-pulse chopper.

In order also to apply chopper controllers to locomotives, the problems involved in connecting several thyristors in series and in handling the surge voltages in traction networks had to be overcome [55]. At first, auxiliary drives with powers below 100 kW, such as the battery chargers of fan motors, were supplied by choppers operating from the normal traction line. Phase-shifted paralled choppers have been installed on locomotives since 1968.

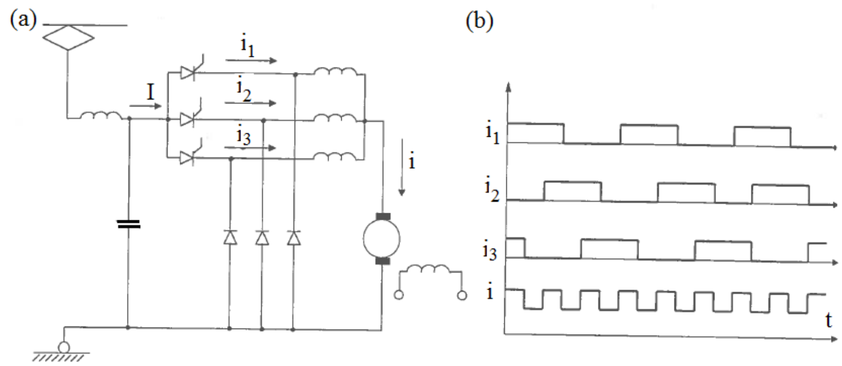

Fig. 6.14. Three-pulse d.c. chopper controllers for traction drives: (a) power circuit, (b) idealised current waveforms with duty cycle of 50%.

Power electronic converters can convert the power from a single-phase overhead supply to multiphase supply, allowing three-phase induction motors or synchronous motors to be driven from a single-phase line.

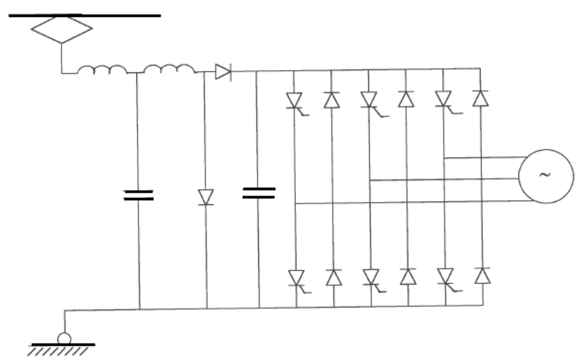

Fig. 6.15. Simplified diagram of main circuit of a locomotive with three-phase a.c. traction motor fed from d.c. overhead supply.

The *first locomotive with a thyristor converter and multiphase a.c. motors* was supplied by the British firm *Brush* in 1965. The converter consisted of a controlled rectifier for feeding the direct voltage link circuit, and also of three forced-commutated inverters for feeding the traction motors from this direct voltage link circuit. The power rating of the inverter was 670 kW and it contained 208 thyristors. Owing to technical problems, this locomotive was never brought into normal service. In the USSR in 1968, a type WL80 locomotive was converted to a multiphase a.c. drive with induction motors as half the drives and synchronous motors as the other half.

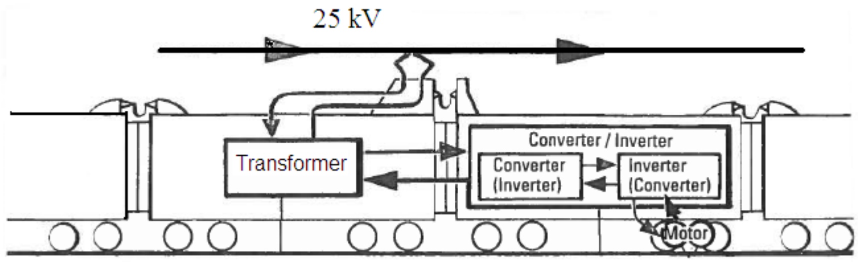

	Transformer	Converter/Inverter		Motor
Powering	→ Steps down the voltage	→ Converter a.c. to d.c.	→ Inverter d.c. to VVVF a.c.	→ Drives the wheels
Regenerative braking	← Steps up the voltage	← Inverter d.c. to a.c.	← Converter a.c. to d.c.	← Operates as a generator

Fig. 6.16. VVVF traction drive with a.c. motors and a.c. regenerative brake system.

In West Germany successful experiments with locomotives DE 2500 were completed in 1971 as a joint effort between *Henschel* and *BBC*. Six cage induction motors were supplied from four parallel forced commutated inverters, feeding onto a busbar. Adjustment of voltage and frequency was obtained through subsynchronous PWM control technology. The technology employed in these locomotives was successfully transferred to locomotives fed from the overhead power supply, and the first application came in 1976 with the construction of six industrial locomotives at *Ruhrkohle AG* [55]. These locomotives could be fed from 15 kV, 16 2/3 Hz or 15 kV, 50 Hz for operation, and they had a power rating of 1.5 MW. This technology was subsequently also applied in locomotives belonging to the railways of Switzerland, Germany, Norway, Denmark and Austria.

Fig. 6.15 shows the fundamental circuit of a traction drive with a three-phase a.c. traction motor fed from a d.c. overhead supply. Fig. 6.16 shows the principle of operation of an a.c. motor fed from an a.c. overhead supply via a transformer and VVVF inverter. This is the system that is implemented, for example, in *Nozomi Shinkansen* Series 300 superexpress train in Japan.

The motivation for introducing a.c. multiphase traction technology into railway systems is different for different applications. Cage induction motors are brushless motors and they are cheaper than d.c. or a.c. commutator motors. Brushless motors are also much more reliable and require much less maintenance than commutator motors. Furthermore, induction motors can operate at much higher speed than d.c. motors, and so they open up the possibility of building much lighter and smaller traction motors. These advantages can be neutralised by the high cost of the inverter required to generate the polyphase a.c. current.

6.11 Survey of modern high-speed trains

High speed railways are becoming the most economical, profitable and sophisticated high speed surface transport systems in the world. The optimum high speed is certainly above 250 km/h, and it is judged by considering such variables as journey time over the travel distance, the operating costs, projected revenue, safety, the vibration and noise produced, and so on. Like highways, a high speed rail network must never cross cities but connections with traditional lines allow direct links between city centres. International airports should be connected to the high speed rail network.

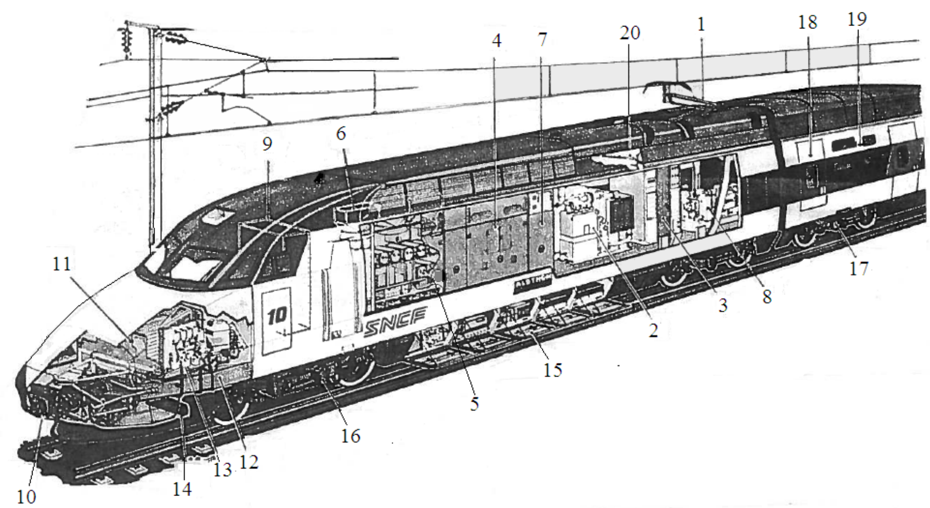

Fig. 6.17. TGV 2400 electric motor car: 1 — wing-shaped current collector, 2 — main transformer, 3 — circuit braker, line filter, 4 — microprocessor-controlled traction motor, 5 — freon cooling for semiconductors, 6 — braking rheostat, 7 — auxiliary power supply, 8 — main compressor, 9 — computer and safety equipment, 10 — automatic coupler, 11 — impact shield, 12 — bodyframe made of high yield point steel, 13 — braking controls, 14 — track circuit code sensors, 15 — equipment housing, 16 — type Y230 A power truck, 17 — type Y237 AB trailing truck, 18 — baggage compartment, 19 — passenger seating, 20 — light alloy roof panels.

6.11.1 TGV superexpress trains

In 1978, GEC Alsthom delivered two pre-production first generation TGV high-speed trains to the French Railways (SNCF). In 1981 a production line TGV trainset set the world speed record of 380 km/h.

The TGV *Atlantique* is the second generation of French high-speed trains, commissioned by SNCF (see Fig. 6.17). TGV *Atlantique* trains speed along at 300 km/h on special newly-laid track, while their ability to run on conventional lines enables

Table 6.1. Characteristics of TGV Atlantique superexpress trains

Configuration	2M10T (2 motor cars, 10 trailers)
Supply voltage	25 kV 50 Hz a.c. or 1.5 kV d.c.
Motors	3-phase 1.1-MW synchronous motors
Number of motors	4 motors per each motor car
Continuous power per trainset at 25 kV	8.8 MW
Continuous power per trainset at 1.5 kV	3.88 MW
Staring tractive effort	210 kN
Converters	Current-source inverters powered from single-phase semicontrolled bridges or d.c. choppers
Braking	Rheostatic braking developing 3/4 of maximum braking power
Additional brake	1 sintered metal shoe per wheel for motor car 4 steel double disks with sintered-metal lining for trailer
Drive system	Motor gearbox, sliding Cardan shaft, and axle-mounted bevel gearboxes
Wheel diameter	0.92 m
Wheel base	3.0 m
Maximum authorized speed	300 km/h
Body length	22.15 m (motor car), 18.7 or 21.845 m (trailer)
Body width	2.814 m (motor car), 2.904 m (trailer)
Maximum height over rail	4.1 m (motor car), 3.48 m (trailer)
Mass	67.8 t (motor car), 475.0 t (trainset)
Length of train	237.59 m
Number of seats	116+11 folding (1st class), 369+26 folding (2nd class)
Current collector	Single arm wing-shaped

operation on existing tracks. A new line from Paris has joined the conventional network already serving western and southwestern France. Although the maximum authorised speed is 300 km/h, the TGV *Atlantique* is the world's fastest train and it set the world rail speed record of 515.3 km/h in May 1990. Specifications of the TGV *Atlantique* train are presented in Table 6.1. The motor cars of the TGV can accept a power supply either 25 kV, 50Hz, single-phase, or 1.5 kV d.c. French Railways has chosen self-commutated *synchronous a.c. drives* for their new generation of high-power motor cars, in which there are four three-phase 1.1-MW synchronous motors. The trainset consists of 2 motor cars and 10 trailers, and the total trainset length is 237.59 m. The use of a *synchronous motor* permits electric safety braking even in the absence of line voltage. Synchronous motors are powered by current-source inverters from single-phase semicontrolled bridges or d.c. choppers.

On the TGV *Atlantique*, all *auxiliary motors*, including variable-speed units, are three-phase induction motors.

French Railways and manufactures have developed *high-power brakes* which incorporate a heat sink, so reducing the aerodynamic drag by some 3%. Use of the new brakes and of microprocessor control prevents axle locking under even the worst conditions, enabling full brake performance to be achieved at all times. Innovative suspension takes advantage of the articulation used between consecutive passenger cars. In particular, the articulation decouples bogie movement from that of the car bodies.

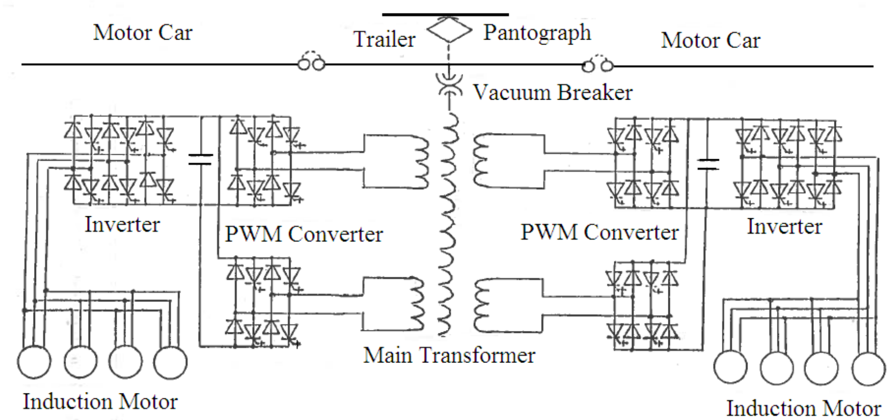

Fig. 6.18. Power circuit of the drive system for *Shinkansen* Series 300 superexpress train.

6.11.2 Shinkansen superexpress trains

The Tokaido-Sanyo *Shinkansen* (Tokyo–Osaka–Fukuoka) trains run on dedicated tracks. The original 4-hour trip (in 1964) between Tokyo and Shin Osaka (on the Tokaido line) was first reduced to 3 hours and 10 minutes (*Kodama Shinkansen*) and then to 2 hours and 53 minutes (*Hikari Shinkansen*). Finally on 14 March 1992, the *Nozomi* or *Hope* began linking Tokyo and Shin Osaka in just two and half hours. The 16-car (10M6T), Series 300, *Nozomi Shinkansen* train was developed by Central Japan Railway Company.

The following improvements have been developed and implemented in the *Nozomi* Series 300 trains:

- the traction motors are 3-phase a.c. cage induction motors fed from VVVF inverters, so that the speed and torque of the motors can be controlled by changing the frequency and voltage of the power supply (smaller and simpler construction of the drive);
- a regenerative brake system returns power to the catenary in the braking mode;
- the cars have low profile styling to decrease air resistance;
- the lightweight and tough body reduces vibration and noise,

Table 6.2. Characteristics of *Shinkansen* superexpress trains

Technical data	*Nozomi* Series 300	Series 100
Configuration	10M6T	12M4T
Supply voltage	25 kV 60 Hz a.c.	25 kV 60 Hz a.c.
Motors	TMT3 (TMT4) 3-phase 300-kW cage induction motors	MT202 230-kW d.c. series motors
Ventilation of motors	Forced	Forced
Number of motors per trainset	40	48
Power per trainset	12 MW	11.04 MW
Auxiliary power source	Stationary voltage stabilizer 100 V a.c. – d.c. auxiliary transformer 100 V a.c. tertiary winding 440 V a.c.	Stationary voltage stabilizer 100 V a.c. – d.c. auxiliary transformer 100 V a.c. tertiary winding 440 V a.c.
Wheel diameter	0.86 m	0.91 m
Wheel base	2.5 m	2.5 m
Bogie	Bolsterless type no end beams	Bolster type with end beams
Gear ratio	1:2.96 (23:68)	1:2.4 (27:65)
Maximum speed	270 km/h	220 km/h
Balancing speed on level line	296 km/h	276 km/h
Starting acceleration	1.6 km/h/s	1.6 km/h/s
Weight of train set	710 t	925 t
Body construction	Aluminium alloy	Steel
Speed control	VVVF	Thyristor continuous phase control
Brake system	A.c. regenerative, air brakes, eddy-current brakes for T cars	Rheostatic, air brakes, eddy-current brakes for T cars
Body length	25.8 m (lead car) 24.5 m (intermediate car)	25.8 m (lead car) 24.5 m (intermediate car) 24.5 m (double decker)
Body width	3.38 m	3.38 m
Body height	3.65 m	4.0 m 4.49 m (double decker)
Total number of seats	1123 ordinary 200 1st class	1153 ordinary 168 1st class
Pantograph	3 pantographs/trainset 2 of 3 used	6 pantographs/trainset 3 of 6 used
ATC	Double-frequency system	Double-frequency system

- the pantograph covers and underfloor equipment covers, help further to reduce air resistance and noise;
- the 'bolsterless bogie' by which the bogie's tractive force is transmitted to the body via special link mechanisms, while air springs are used to support the weight of the body;
- the automatic train control (ATC) signal modified to a double-frequency system helps to maintain safety at higher speeds;
- improvements to the dedicated tracks have been made.

Table 6.2 shows the characteristics of *Shinkansen* trains. The drive system is shown in Fig. 6.18. The Tokaido-Sanyo *Shinkansen* line from Tokyo to Fukuoka (Hakata) via Shin Osaka is 1069.2 km long (1180.3 service kms) and is currently served by *Nozomi*, *Hikari*, and *Kodama* trains. The journey time from Tokyo to Fukuoka by *Nozomi Shinkansen* is 5 hours and 4 minutes (including 6 stops) and an average speed of 211 km/h. A one way ticket costs Yen 23 100.

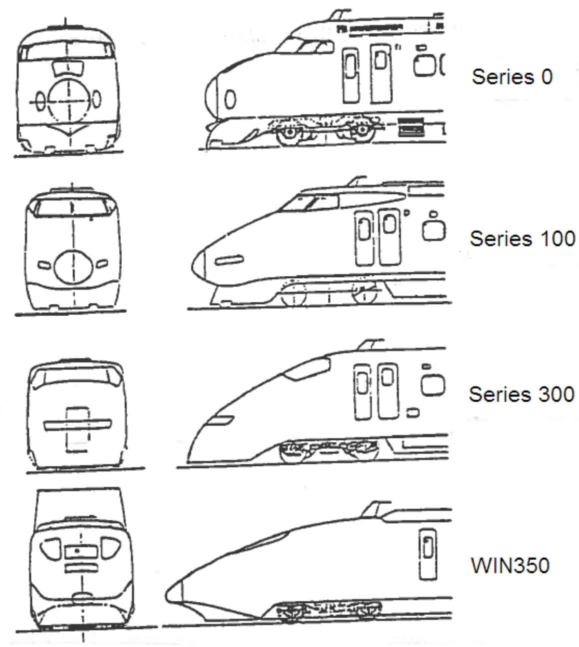

Fig. 6.19. Comparison of front and side views.

To achieve an operational run at over 300 km/h, Japan Railways (Central, West and East) are developing new types of *Shinkansen* trains which are faster, more environment-friendly, more reliable, and more comfortable. Some of the concepts for the new *Shinkansen* trains (Series 500, Series 300X and WIN 350) are listed below:

- they have less influence on environment through complete countermeasures such as their wing-shaped current collectors;

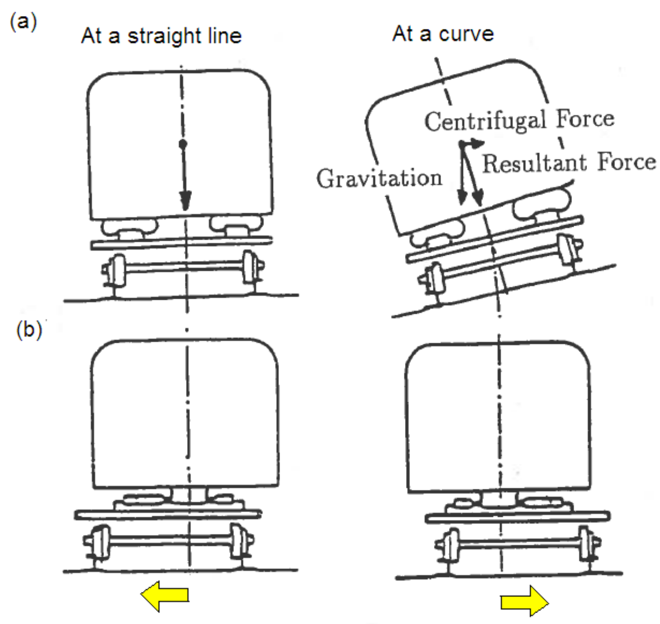

Fig. 6.20. Active suspension system: (a) tilting control using air suspension, (b) active rolling control using hydraulic/pneumatic cylinder.

- there is an improvement of their aerodynamic characteristics by optimizing the front nose and underfloor shapes (see Fig. 6.19);
- there is a thorough reduction in their mass and ground vibration, achieved by adopting aluminium alloy bodies and downsizing certain apparatus;
- they exhibit superior and reliable running performance at over 300 km/h by the use of high-power motors and highly-efficient bogies;
- they offer good riding comfort by using active suspension systems and rigidly structured bodies.

In addition to the *tilting system* for compensation of the centrifugal acceleration at curves (Fig. 6.20a), an *active rolling control system* is used (Fig. 6.20b). It can cut back the level of lateral vibration acceleration to half of its former value. A rubber mat placed between the ballast and the slab to reduce ground vibration has undergone trials as well.

To reduce the noise from the pantograph, which is the largest noise source, Japan Railways West has developed an innovative type of current collector whose top looks like an airplane wing (see Fig. 6.8). New high-tensioned contact wires to reduce the arcing noise have also been tested. A similar current collector is used by TGV *Atlantique* (see Fig. 6.17).

6.11.3 ETR high-speed trains

The ETR 460 (Fig. 6.21) is the third generation of the *Pendolino* train, which has been in service on the Italian State Railway or *Ferrovie dello Stato S.p.A.* (FS) network since 1988. Its electrical traction equipment with continuous power of 6000 kW includes a GTO inverter and 4 three-phase induction motors in each motor coach. The *aerodynamic design* of the trainset has been rigorously tested in a wind tunel to minimise any aerodynamic resistance. The carrying structure is made of a light alloy. The seat arrangements are 2+1 for the the first class and 2+2 for the second class. The characteristics are given in Table 6.3. The *bogie* features innovative aspects, such as the body-to-bogie connection and the arrangement of body actuators on the bogie itself to increase available space inside the passenger compartments. The primary (wheels – bogie) and secondary (bogie – car body) suspensions are helical and guarantee, in addition to the highest possible safety levels against derailment, a high degree of comfort.

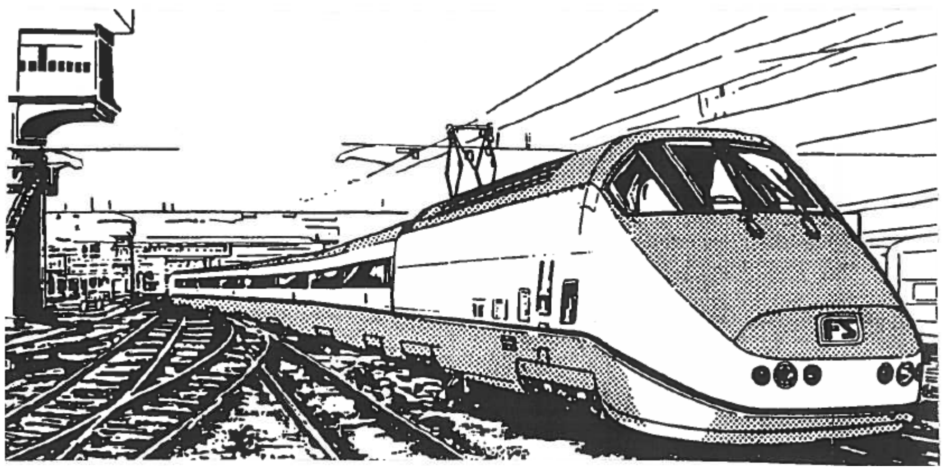

Fig. 6.21. Pendolino ETR 460 high-speed train.

The bogie frame, the suspension, and the axles are perfectly interchangeable, with the sole exception of the driving axle which has a reducer mounted on it. To reduce unsprung masses, the traction motors are installed under the body and are connected to the reducer by a cardan shaft. Each carrying axle has 3 steel disc brakes and each driving axle has 2 steel disc brakes. The motor car bogies are interchangeable, as are the trailer car bogies.

A *tilting system* makes it possible for the ETR to take curves at high speeds without modifying the existing tracks and infrastructures, and whilst guaranteeing the passengers an excellent level of comfort. The car body can be tilted by 8^0, which corresponds to compensating for a centrifugal acceleration of 1.35 m/s^2. This allows the train to run with a non-compensated acceleration equal to 2 m/s^2, but with the centrifugal acceleration affecting passengers reduced to 0.65 m/s^2. The delay in tilting is, for the first vehicle, practically zero, whilst in the later cars the tilt takes effect in real time.

To increase passenger comfort, *Pendolino* has also an efficient *active lateral pneumatic suspension*. This is controlled by a microprocessor and guarantees body truing, even when the body is tilted, thereby allowing the lateral shock absorbers to

Table 6.3. Characteristics of ETR trains

Technical data	ETR 460	ETR 500
Configuration	6M3T	2M10T or 2M14T
Supply voltage	3000 V d.c.	3000 V d.c. or 25 kV 50 Hz single phase
Motors	500 kW induction motors	1.1 MW induction motors
Number of motors	12 motors per train	8 motors per train
Continuous power	6.0 MW	8.8 MW
Gauge	1435 mm	1435 mm
Maximum speed	250 km/h	300 km/h
Mass	433.5 t	640.0 t
Traction effort at rims	207 kN	290 kN
Electric braking effort	—	195 kN
Power/mass ratio	13.84 kW/t	13.75 kW/t
Total length	236.6 m	360.0 m (404.0 m max)
Body width	2.8 m	2.86 m
Total number of seats	400	200 (1st class) plus 476 (2nd class)

work under optimum conditions. This is extremely important because the lateral suspension needs to be very flexible in order to guarantee optimum comfort.

The ETR's *electrical traction equipment* is fitted with inverters supplied by a catenary voltage of 3000 V d.c. The traction motors are three-phase, 380-V, 500-kW *induction motors* (with one motor per bogie, and four bogies per motor coach). The continuous power at rims is 6000 kW, guaranteeing a maximum speed of 250 km/h. The maximum traction effort at the rims with wheels of average wear is about 207 kN. The rheostatic braking force is about 140 kN and is available from the maximum speed down to 40 km/h. If the speed decreases any further than this, only the pneumatic brake system will operate.

It has proved possible to provide trains with traction equipment that can be adapted to meet a variety of service needs. *Pendolino* trains have been developed with electric traction equipment suitable for the following catenary voltages: 3000 V d.c. (the ETR 460), 25 000 V a.c. at 50 Hz, or 3000 V d.c. / 15 000 V a.c. at 16 2/3 Hz.

The latest ETR500 train is especially aimed at using Italian and European high-speed lines. It is designed to run at a top speed of 300 km/h with a very high comfort level, offering up to 700 seats in both 1st and 2nd class cars, with configurations that may vary between 10 and 14 intermediate cars (see Table 6.3).

In each motor car, the main power circuit feeds four three-phase induction motors, and within each power circuit there are two modular units consisting of a converter, filter, and inverter. Inverters have choppers to lower or to rise the voltage in order to maintain a constant value of 2.8 kV. Two inverters use GTO oil cooled thyristors. The electric brake utilises two rheostats and is operated by choppers. The brake is always ready to operate, even in the absence of catenary tension.

6.11.4 InterCity Express train

In 1991, Deutche Bundesbahn (DB) started commercial high-speed travel in Germany using *InterCity Express* trains (ICE). These trains have been derived from the *Intercity Experimental* train which was designed to run at 350 km/h and had set the world speed record of 406 km/h in 1988. ICE services are fully integrated with the *EuroCity* and *InterCity* networks. The first line München – Stuttgart – Frankfurt – Hamburg (Altona) is 750 km long. Owing to heavy populated area and 11 stops the average speed is only 124.5 km/h although on the 107-km distance between Stuttgart and Mannheim ICE trains can achieve an average speed 173.5 km/h (1992). Since 1994 three further routes have been served by ICE trains: (1) Bremen/Berlin – Frankfurt – München, (2) Hamburg – Basel – Zürich, and (3) Hamburg – Würzburg – München. The specification of the ICE train is given in Table 6.4. The electrical subsystems have been developed by AEG Berlin, ABB Henschel Mannheim, and Siemens AG Erlangen.

Table 6.4. Characteristics of ICE, X2000, and AVE trains

Technical data	ICE	X2000	AVE
Configuration	2M11T to 2M14T	1 or 2M, 4 to 12T	2M8T
Supply voltage	15 kV 16 2/3 Hz	15 kV 16 2/3 Hz	25 kV 50 Hz or 3 kV d.c.
Motorized axles	8	4/8	8
Motors	3-phase, 1.25 MW induction motors	3-phase, 825 kW induction motors	3-phase 1.1 MW synchronous motors
Continuous power	9.6 MW	3.3/6.6 MW	8.8 MW at 25 kV
Maximum speed	280 km/h	210 km/h	300 km/h
Train mass	844 t	343 t (1M5T)	393 T
Starting traction effort at rims	400 kN	160 kN	220 kN
Total length	360 m	140 m (1M5T)	200.19 m
Body width	3.02 m	3.08 m	2.814 (motor car) 2.904 m (trailer)
Total number of seats	696 min (2M14T)	254 (1M5T)	321 (2M8T)

The *main circuit* of the ICE motor car (class 401) consists of the vacuum circuit breaker (first vacuum breaker used by DB), the input filter, and the main transformer [12, 51]. In order to have independent operation of all bogies, the 5220 kVA transformer has, on secondary side, four 1430 V, 1127 kVA windings, one for each of the four-quadrant inverters which maintain a constant voltage 2800 V in the intermediate d.c. circuit with a smoothing capacitor. The four 1250 kW, 2050 V, 415 A, four-pole, three-phase *induction motors* with a forced ventilation system have cage rotor windings with trapezoidal copper bars. The motors are fed from VVVF PWM inverters. The inverter output voltage is from 0 to 2200 V (line-to-line) and frequency from 0 to 130 Hz. The *field-oriented control* of induction motors has been implemented. The new version of ICE motor cars uses GTO thyristors rated at 3

MVA with evaporation bath cooling [51]. The solid state converter system permits operation in motoring and regenerative braking without changeover and with high power factor and low interference current. During braking, the three-phase voltage system generated by the motors is rectified and then transmitted to the d.c. link. The four-quadrant converters change the d.c. into a.c. energy and then via a transformer send it to the overhead catenary. The usage of high power GTO technology allows not only to reduce the number of electronic components but also to decrease the mass of the motor car (about 3 t keeping the same rated power) and simplify the control system. Microcomputer technology is extensively used for the open and closed-loop control systems.

6.11.5 X2000 high-speed train

Swedish State Railways (SJ) introduced a commercial operation of high-speed trains X2000 [36, 37] in 1990 (test runs in 1989). These trains run on existing tracks between Stockholm and Göteborg (454 km). The journey time is 2 h and 55 min and the average speed is 155.6 km/h (1994). The high-speed network will also be connecting Stockholm, Göteborg and Malmö/Copenhagen at maximum speed 300 to 350 km/h.

A tilting system has been designed to achieve high speeds on existing tracks (see Fig. 6.22). Resulting from this technology, the intermediate cars can tilt through an angle of maximum 8^0 reducing centrifugal forces by up to 70 %. The *tilting serves only to increase passenger comfort* and not for safety purposes.

The specification of the X2000 train is given in Table 6.4. The train body is made of stainless steel. The specification of the X2000 train is given in Table 6.4.

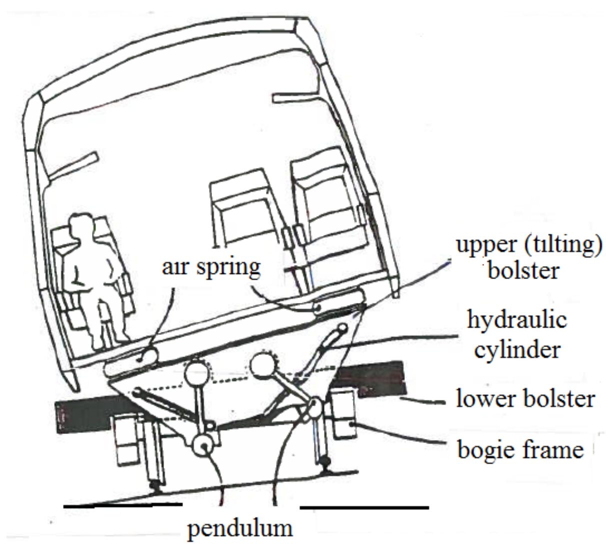

Fig. 6.22. Tilting system of X2000 high speed train.

The new fast train attracted the railways in the world, and was tested in Switzerland and Germany, where it gained its speed record 250 km/h on a straight line. The high speeds on curves (up to 160 km/h) are large due to the usage of radially self-steering wheel axles.

The lightweight motor car has a driver's cab at one end. Its streamlined front and other details have been designed to reduce the aerodynamic resistance and power consumption. Two different types of bogie are used: the driving bogie — for the motor car, and the trailing bogie — for the intermediate cars.

The drive system is divided into two identical modules. Each module consits of four line converters, two intermediate d.c. circuits, two feedback choppers, two inverters and four cage induction motors. The modules are supplied by the same main transformer which is installed under the car body. The line self-commutated converters are fed with 15 kV, 16 2/3 Hz nearly sinusoidal current. The power circuit of each converter has GTO thyristor bridges and works with about unity power factor. The line converters allow for the regenerative braking so that the energy can be recovered and fed back to the catenary. The motors are fed from GTO inverters with fully controllable output voltage within the range from 0 to 1870 V and the frequency from 0 to 120 Hz. In this way the motors can gain the maximum possible torque at each point of the traction drive characteristic.

6.11.6 AVE high-speed train

Spanish National Railways (RENFE) have been developing new Madrid – Seville high-speed rail link since 1989 [2, 4, 46]. The officical Spanish name for this line was originally *Nuevo Acceso Ferroviario a Andalucia* (NAFA) and later has been changed to *Alta Velocidad Espanõla* (AVE). The length of this line is 475 km and its double track has a standard European gauge (1435 mm), not like others Spanish railways (1668 mm). The track has been designed for maximum speed up to 300 km/h (initial maximum speed 250 km/h) for mixed passenger and freight traffic, with a maximum gradient of 1.25 % and the minimum curvature radius of 4000 m.

For high-speed service *Trenes de Alta Velocidad* (TAV) trains (see Table 6.4), which are based on TGV *Atlanitque*, have been designed and supplied by GEC Alsthom. The main difference between the French and Spanish train is its size. The AVE is shorter (200.19 m) than the TGV *Atlantique* (237.59 m) [46]. AVE trains are rated at continuous power of 8.8 MW. All rolling stock is suitable for dual system operation, i.e. 25 kV, 50 Hz on AVE and 3 kV d.c. on other Spanish railway lines. The 25-kV, 50-Hz overhead catenary AVE line with Y-type auxiliary cable and aluminium cantilevers is fed from the public utility system. Twelve traction substations at an average distance of 40 km have been built [7]. The installed capacity of each substation is 2×20 MVA. In order to reduce the unbalance in the power utility system, the substations are connected to the national grid with a cyclic sequence of phases.

Two motor cars, each with two motor bogies, enclose a trainset of eight trailers running on nine bogies. The catering car is located between the three first and four second class cars.

Three-phase *synchronous motors* are fed from CSIs. The two inverter-motor units of each bogie are connected in series [2] . At low speed, a simple auxiliary circuit is used to assist commutation of the thyristors. Each inverter-motor unit is rated at 1.1 MW and weighs only 1600 kg. Voltage regulation of the traction motors at 25 kW uses two mixed rectifier bridges with thyristors and diodes. Each bridge is conenected to a transformer secondary winding and to a circuit ensuring that the power factor is close to unity. A GTO thyristor chopper controls the traction motor voltage when operating under 3 kV catenary. During the rheostatic braking the motors act as generators and the inverters as rectifiers. The power circuit has two braking resistors, one of which is connected in parallel with the chopper used for 3 kV supply. Braking effort is controlled by the excitating current of synchronous motors and by using the chopper to vary the apparent braking resistance. The solid-state devices are cooled by direct freon immersion in hermetically-sealed modules. An emergency disc brake application at 300 km/h brings the AVE to a standstill within 3.6 km on a level track and at 200 km/h within 1.45 km.

The journey from Madrid to Seville takes about 2 h 40 min (the average speed is about of 178.13 km/h).

6.11.7 Eurostar express train

Eurostar services from London to Paris and Brussels via the new Eurotunnel started on 14 November 1994 [23]. The *Eurostar* passenger train (see Table 6.5) is a modified TGV built by GEC Alsthom [47]. Apart from geometric changes, the Eurostar was built to collect a greater variation of electric power than TGV: 750 V d.c. in Great Britain, 25 kV, 50 Hz in France, and 3 kV d.c. in Belgium. The maximum approved speed is 300 km/h. In addition to collecting power from an overhead catenary system, *Eurostar* also collects power from a third rail.

Eurostar consists of 18 passenger cars flanked at each end by a motor car making the train set 400-m long. GEC Alsthom's TGV *Atlantique*, which operates in western France from Paris to Le Mans and Tours, is 237.59 m long and operates with only 10 passenger coaches.

Table 6.5. Characteristics of *Eurostar* train

Trainset configuration	2M18T
Supply voltage	25 kV 50 Hz
	3 kV d.c.
	750 V d.c.
Motor	3-phase, 1.1-MW
	induction motor
Number of motors	6 motors/train
Continuous power	
per trainset	6.6 MW
Converter	1 800 V d.c. link
	$f = 0.6...200$ Hz
	6×4 500 V, 2.5 kA GTOs
	one inverter/motor
Starting tractive effort	54 kN normal
	64 kN boost
Total length	400 m (18 trailers)

On 3 kV d.c. operation in Belgium, the supply current passes via the high-speed circuit breaker and line filter to the series GTO chopper which provides the intermediate 1800 V d.c. link for the range of the catenary voltage from 2 to 4 kV. In France and in the Eurotunnel, on 25 kV 50 Hz operation, the rectifier bridges are connected to the transformer secondary windings and the 1800 V d.c. is kept by the GTO thyristors bridges. The chopper is shorted out to give a two stage filter. For high power factor (over 0.9), additional power factor correction circuits are connected to the secondary windings. In Great Britain, the power is collected from a 750-V d.c. third rail via shoegear. In that case, the 3-kV chopper is shorted, and the link voltage is then simply the filtered line voltage and can vary between 440 and 900 V. At this reduced voltage, the full starting torque can be achieved, but with the increasing speed, the tractive effort is sharply reduced.

The traction motor inverters are a VSIs employing two 2.5-kA, 4.5 kV GTO thyristors and two freewheel diodes per phase. Electronic hardware actively guards against the possibility of 'shoot through' and fast response overload protection unconditionally prevents each of the GTOs from exceedings their specified ratings.

Using a GTO and series resistor, rheostatic braking is employed from maximum speed down to 24 km/h at which the minimum braking effort demand is just equal to that required to supply the auxiliaries and the power circuit losses.

Journey times for the launch service were 3 h or a little more from London to Paris and 3 h 15 min to Brussels. The journey through the Eurotunnel takes about 19 min (50.5 km) [23]. Fares from London to Paris and Brussels are the same despite differences in distance.

6.12 Linear induction motor-driven trains

6.12.1 Light electrical traction

In addition to the specifications listed in Section 6.1, modern urban light electrical traction should meet the following requirements:

- it should have a high level of automation and computerization;
- the propulsion and braking systems must be independent of adhesion, which in turn is primarily affected by the climate and weather;
- the level of noise should fall below 70 dB (A);
- it should have ability to cope with high slopes, at least 6% gradient, and also with sharp bends with radius of curvature less than 20 m;
- it should add no pollution to the natural environtment and landscape;
- it must offer high reliability.

Congestion problems in big cities need to be solved by creating public transport systems that can be implemented without affecting the city adversely. For example, there are many cities in Italy where the historical centre has remained the same since the Renaissance, and where a heavy railway would be a completely wrong solution to the need for public transport and have a most detrimental impact. An adequate solution might be a light railway, designed to be a *people mover* or *automated guided transit* (AGT) system, with transport capacity of 10 to 20 thousand passengers per hour, aiming to replace the traditional transport network and to integrate the existing railway network. All of the above requirements can be met by using linear induction motors (LIMs) as propulsion machines.

6.12.2 Fundamental relationships

Linear electric motors belong to the group of special electrical machines that convert electrical energy into mechanical energy of translatory motion. The most popular are LIMs, which are manufactured commercially in several countries. A LIM can be obtained by cutting a rotary induction motor along its radius from the centre axis of the shaft to the external surface of the stator core and rolling it out flat. The stator becomes the *primary* and rotor becomes the *secondary* (reaction rail). The secondary can be simplified by using a solid steel core and replacing the cage (ladder) or slip-ring winding with a high-conductivity nonferromagnetic plate (aluminium or copper).

The linear velocity of the fundamental harmonic of the MMF travelling wave produced by the primary winding is called the *synchronous velocity*, i.e. :

$$v_s = \frac{2\tau}{T} = 2f\tau = \frac{\omega_s}{\pi}\tau \tag{6.24}$$

where: τ = pole pitch, $f = 1/T$ = input frequency, $\omega_s = 2\pi f$ = angular input frequency. The synchronous velocity of a LIM depends on the frequency of the input current and on the pole pitch. It does not depend on the number of poles $2p$.

The *slip* is defined as:

$$s = \frac{v_s - v}{v_s} \tag{6.25}$$

where v is the linear speed of the movable part. The *electromagnetic power* transmitted from the primary through the airgap to the secondary is

$$P_g = P_m + \Delta P_{2w} = F_d v_s \tag{6.26}$$

where: P_m is the mechanical power, ΔP_{2w} are losses in the secondary winding and F_d is the electromagnetic (developed) force.

The *mechanical* power of a LIM is

$$P_m = P_{out} + \Delta P_m = F_d v \tag{6.27}$$

where P_{out} is the output power and ΔP_m is the mechanical (friction) loss.

The following relationship exists between the electromagnetic force F_d and the *useful force* or *thrust* F_x :

$$F_d = F_x + \Delta F_m = \frac{P_{out}}{v} + \frac{\Delta P_m}{v} \tag{6.28}$$

where ΔF_m is the force proportional to the mechanical losses. Eqns (6.26) and (6.27) give a similar relationship to that of a rotary induction motor — see eqn (3.13), i.e. :

$$P_m = \frac{v}{v_s} P_g = (1 - s)P_g \tag{6.29}$$

If the primary winding resistance is negligible and the magnetic circuit is unsaturated, the electromagnetic force F_d can be expressed as a function of slip, by the Kloss' formula as

$$F_d = \frac{2F_{dmax}}{s/s_{cr} + s_{cr}/s} \tag{6.30}$$

in which s_{cr} = *critical slip* corresponding to the maximum force F_{dmax}. The force F_{dmax} corresponds to the pull-out torque (break-down torque) in a rotary induction motor.

The *efficiency* is

$$\eta = \frac{P_{out}}{P_{in}} = \frac{F_x v}{m_1 V_1 I_1 cos\phi} \tag{6.31}$$

The product *efficiency* $\times$ *power factor* is one of the most important operating parameters of LIMs and usually does not exceed 0.4...0.5. The low product $\eta cos\phi$ of LIMs is mainly due to the large airgap, which is a fundamental disadvantage.

6.12.3 Applications

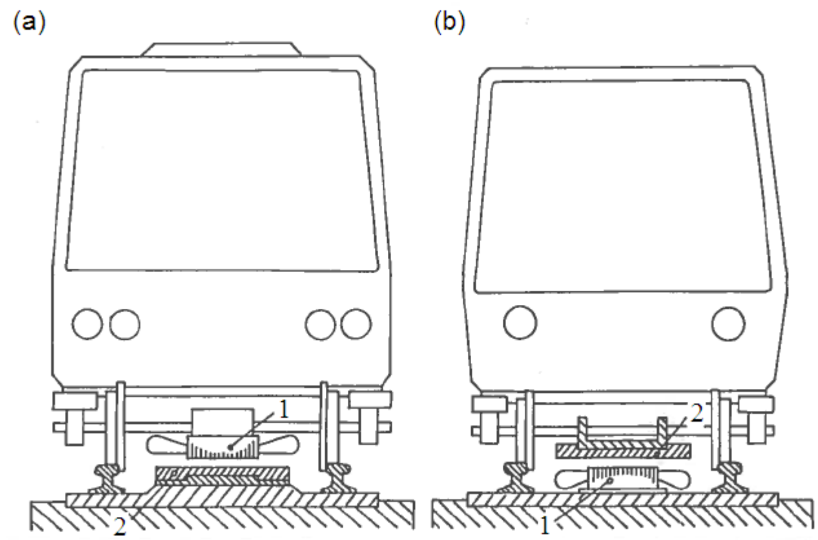

Fig. 6.23. LIM-driven vehicle systems: (a) urban transit, (b) people mover: 1 — primary, 2 — double layer secondary.

Replacing electrical rotary motors with linear motors in traction drives generally does not require new tracks, but only a conversion to linear drives. Single-sided LIMs (Fig. 6.23) are best solution of all, since the normal attractive force of these can strengthen the adhesion of wheels to rails. The airgap is from 10 to 15 mm. Most frequently, the motor car has two LIMs with short primaries assembled in series. The double-layer secondary (Fig. 6.23a) consists of a solid back iron and an aluminum cap, and is located between the rails. Cables for computer communication with the vehicle and, quite often, conductor rails for electrical energy delivery to the vehicle are located along the track. Three-phase LIMs are fed from VVVF VSIs. Furthermore, a linear propulsion system for wheel-on-rail vehicles allows more

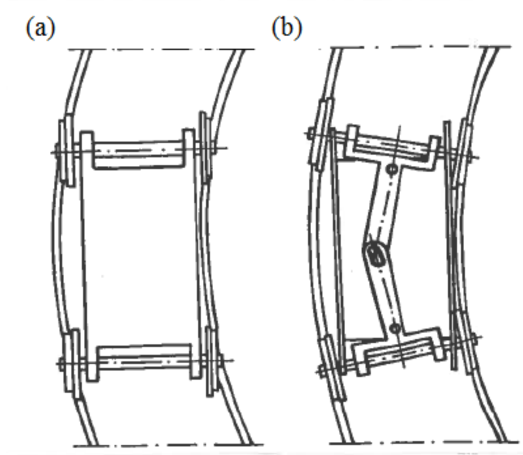

Fig. 6.24. Steerable bogie of a wheel-on-rail vehicle: (a) rotary motor propulsion, (b) LIM propulsion.

flexibility (Fig. 6.24) and reduces noise on the bends and wear on the wheels and rails.

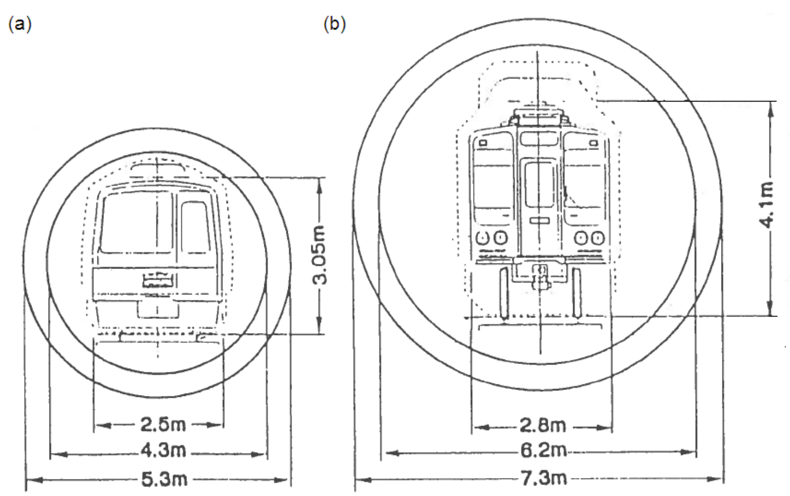

Fig. 6.25. Comparison of tunnel cross sections in Tokyo: (a) Toei No. 12 Line, (b) subway Shinjuku line which uses rotary motors.

LIM-driven wheel-on-rail vehicles are built for low velocities (typically less than 100 km/h) and for short routes (typically less than 50 km). There are ideal for urban transit systems and for short-distance trains. Typical applications of LIMs in passenger transport are the Intermediate Capacity Transportation System (ICTS) in Toronto, Canada (7.1-km line Kennedy–Scarborough–McCowan), the BC Transit in Vancouver, Canada, called Advanced Rapid Transit (ART) MK I *Sky Train* (28.9 km line Waterfront Station–New Westminster, see Table 6.6), the subway Toei Line No. 12 in Tokyo (3.2-km line between Nerima and Hikarigaoka stations), the subway line No. 7 in Osaka, Japan (5.2 km line between Tsurumi-ryokuchi and Kyobashi stations), the Urban Railway in Detroit, USA (5.2 km) and ART MK II LRT System 2 in Kuala Lumpur, Malaysia (29 km line, see Table 6.6. The common feature of these wheel-on-rail systems is a car driven by two single-sided LIMs with a short primary. A car, together with the LIM and the cross-section of the reaction rail, is shown in Fig. 6.25.

Table 6.6. Advanced Rapid Transit Systems in Vancouver and Kuala Lumpur

Technical data	ART MK I *Sky Train* Vancouver	ART MK II LRT Kuala Lumpur
Line length, km	28.9	29.0
Number of stations	20	24
Track gauge, mm	1435	1435
Train control	Fully automated, driverless	Fully automated, driverless
Peak-hour capacity, passenger/h/direction	25 000	30 000
Average speed, km/h	41.0	38.0
Maximum speed, km/h	100.0	90.0
Power supply	600 V d.c. 3rd rail	750 V d.c. 3rd rail
Car length, m	12.7	16.85
Car width, m	2.5	2.65
Car mass (empty), kg	14 370	22 000
Wheel diameter, m	0.47	0.585
Number of LIMs	2 per car	2 per car
Number of inverters	2 per car	2 per car
Braking	Regenerative dynamic + disc brakes	Regenerative dynamic + disc brakes
Seated passengers	33 per car	30 per car
Maximum number of passengers	130 per car	236 per car

Construction costs of new subway lines can substantially be limited by reducing the bore diameter of the subway tunnel. This can be achieved by lowering the floor level of railcars as a result of replacing rotary traction motors by single-sided LIMs. With the aid of LIMs, tunnel diameters have been reduced from 7.3 m in Tokyo and 6.8 m in Osaka to 5.3 m. Each trainset in Tokyo consists of 6 electric motorised units (EMUs) and each trainset in Osaka consists of 4 EMUs with two LIMs per car.

Small car units propelled by LIMs mounted on the track between the rails are used in Disney World (at Orlando, Florida) and at Houston Intercontinental Airport (Texas). There have also been attempts to replace steel wheels and rails with air support pads (Dulles International Airport, Washington; Duke University, Durham; UTDC Kingston, Canada).

Problems

1. An electric train has an average speed $v_{av} = 60$ km/h on a level track between stations 2.8 km apart. The train accelerates at $a = 1.8$ km/h/s and retards at $d = 3.5$ km/h/s. Find the simplified trapezoidal speed–time curve.

   Answer: $t_{tr} = 168$ s, $t_1 = 40.85$ s, $t_2 = 106.15$ s, $t_3 = 21$ s, $v_m = 73.53$ km/h.
2. A train has a schedule speed $v_{sch} = 68$ km/h between stations which are 7.3 km apart. The train accelerates at $a = 1.8$ km/h/s and retards at $d = 3.2$ km/h/s. Duration of stops is $t_{st} = 60$ s. Find the crest speed over the run assuming a trapezoidal speed–time curve.

   Answer: $v_m = 91.66$ km/h.
3. An electric locomotive pulls a train weighting 300×10^3 kg and takes 2500 kW of power from the overhead wire when it accelerates up a gradient of 1:80. The specific rolling resistance is $k_r = 0.005$ and the efficiency of the drive system is $\eta = 0.75$. Calculate the speed at which the train ascends the slope.

   Answer: 130.56 km/h.
4. A suburban train consists of 12 EMU cars and have 12 electric motors. The mass of each car with passengers is 40 t and the driving wheel radius is $R = 0.4$ m. Determine the shaft torque developed by each motor to accelerate the train to a speed of 80 km/h in 45 s up to a gradient 1:200. The rolling resistance is 0.004, the effect of rotational inertia is 19% of the train weight, the gear ratio is 4:1 and gearing efficiency is $\eta_g = 0.85$. What is the output power of each motor if its rotational speed is $n \approx 1000$ rpm ?

   Answer: 3176 Nm; 332.6 kW.
5. A modern high speed 500 t passenger train is driven by 40 three-phase cage induction motors fed from VVVF inverters. The $\eta \cos \phi$ product of each motor is 0.8 and the torque developed during acceleration is 1030 Nm. The motor car bogies are designed with the gear ratio $\gamma = 3$, wheel radius $R = 0.46$ m, wheel base $b = 3.0$ m and gearing efficiency $\eta_g = 3.0$ m. The effect of rotational inertia on the accelerating force has been estimated as 17%. The gradient is 1:250, curve radius $R_c = 5$ km, rolling resistance $k_r = 0.01$ and supply voltage 25 kV a.c. For the train starting from the rest, calculate: (a) the time to reach a speed of 200 km/h, (b) the current drawn from the catenary wire, (c) the air resistance force at 200 km/h if the body width is 3.38 m, body height 3.65 m and the train has a wedge shaped nose.

   Answer: (a) 187.9 s; (b) 671.7 A; (c) 4604.4 N.

6. A suburban passenger electric train has an average speed $v_{av} = 70$ km/h on a level track between stations $s = 4.2$ km apart. It is accelerated at $a = 1.75$ km/h/s and retarded at $d = 3.5$ km/h/s. The rolling resistance is $k_r = 0.005$, efficiency of motors is 91% and 8% should be allowed for the effect of rotational inertia. Assuming a trapezoidal speed–time curve calculate the specific energy consumption.

   Answer: 35.342 Wh/(tkm).
7. A three-phase, 380 V (line–to–line), 165.5 A, Y-connected single-sided LIM has the output power $P_{out} = 40$ kW at the input frequency $f = 28$ Hz and slip $s = 0.2$. The pole pitch is $\tau = 0.261$, efficiency $\eta = 0.655$, mechanical (friction) loss $\Delta P_m = 1.4$ kW and the primary winding resistance per phase $R_1 = 0.06581\ \Omega$. Find: (a) the thrust F_x and the electromagnetic (developed) force F_d, (b) the power factor $\cos\phi$ and the $\eta\cos\phi$ product and (c) the primary winding ΔP_{1w}, secondary ΔP_{2w}, stray ΔP_{str} and primary core losses ΔP_{Fe}.

   Answer: (a) $F_x = 3420.8$ N, $F_d = 3540.6$ N, (b) $\cos\phi = 0.56$, $\eta\cos\phi = 0.3672$, (c) $\Delta P_{1w} \approx 5.41$ kW, $\Delta P_{2w} \approx 10.35$ kW, $\Delta P_{str} + \Delta P_{Fe} \approx 3.91$ kW.

7

DOMESTIC USE OF ELECTRICAL ENERGY

The residential sector uses about 30% of all generated electrical energy, and the following appliances are the main domestic consumers of electrical energy:

- water heaters;
- clothes washers and driers;
- refrigerators and freezers;
- air conditioners;
- cookers;
- dishwashers;
- space heaters;
- lights.

The share of the total residential sector electricity consumption by each of these home appliances in Australia in 1992 is shown in Table 7.1 [40].

7.1 Electric water heating

It is accepted practice in a modern home to supply hot water along with all the cold water taps. No other type of energy offers so many advantages as electricity for this purpose. Electric water heaters are:

- clean, safe, and economical in operation;
- simple to install;
- adaptable both in new buildings and in modernized old houses.

Rule of thumb: 1 kWh heats about 30 l of water to 37^0C or 20 l to 50^0C or 10 l to 85^0C if the cold water temperature is about 12^0C [1].

Water heaters are classified in accordance with their construction as follows [1]:

- continuous storage heaters;
- off-peak storage heaters;
- boilers;
- continuous-flow (instantaneous) heaters.

Table 7.1. Electricity consumption by home appliances in Australia in 1992.

Appliance	Energy consumption in GWh	%
Water heaters	13 379	34.0
Refrigerators and freezers	7 673	19.5
Cookers	3 713	9.4
Clothes washers and driers	3 482	8.8
Lights	3 033	7.7
Air conditioners	1 871	4.7
Space heaters	1 759	4.5
Dishwashers	455	1.2
Other	4 030	10.2
Total	39 387	100%

and, according to their method of operation, into

- non-pressure heaters;
- pressure heaters.

The principle of operation of continuous storage, off-peak storage, and continuous-flow (instantaneous) heaters are explained in Fig. 7.1.

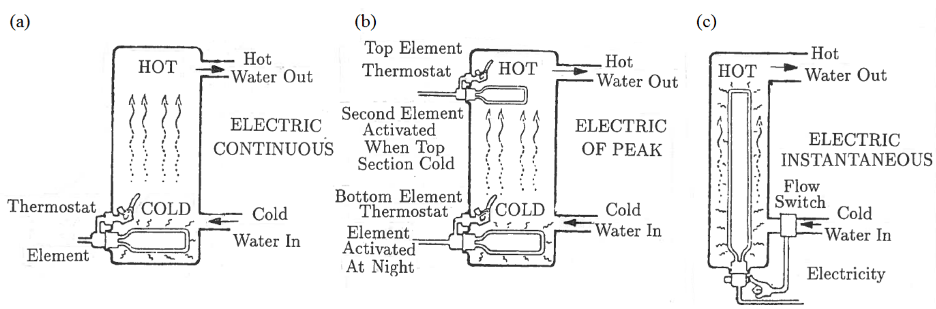

Fig. 7.1. Principle of operation of electric heaters: (a) continuous storage, (b) off-peak storage, (c) continuous-flow (instantaneous).

The *continuous storage heater* (Fig. 7.1a) operates on the same principle as a gas storage water heater. The resistive element heats the water whenever it is colder than the preset temperature. When all of the water is used up, the heater cannot heat the new water quickly enough, so the water at the outlet will be cold.

The tank of water of the *off-peak storage heater* (Fig. 7.1b) is heated at night when electricity is cheaper. There are two kinds of off-peak water heaters: *electric off-peak single element heaters*, in which one element at the bottom of the tank does the heating only at night; and *electric off-peak twin-element heaters*, in which one element at the bottom heats the water at night at cheaper rates, but the second element at the top provides a back-up supply of hot water should the tank be emptied during the day. A small portion of water at the top of the tank is thus kept hot, but the full tank is not reheated until the nighttime.

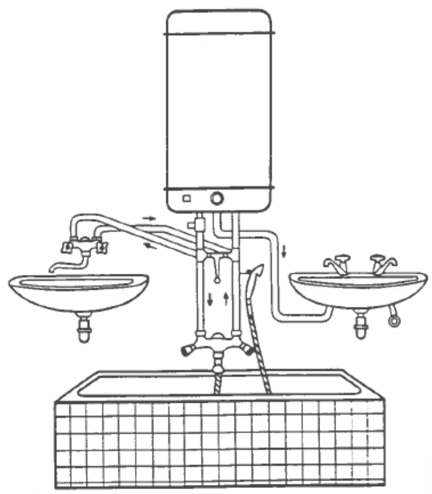

Fig. 7.2. Group supply from a 80-l non-pressure storage water heater. Courtesy of *AEG*, Germany.

The *continuous-flow (instantaneous) heater* can provide hot water around the clock by using an element to heat water as it flows past, but it is limited by its flow rate as to the volume of hot water it can provide at any one time.

The selection of the heater type depends not only on the amount of hot water required, but also on whether decentralized, partially centralized (group supply) or central supply is required and supportable by local conditions. In the case of decentralized supply, each individual supply point is fitted with a non-pressure water heater the size and output of which is matched to the demand. When supply points are close together, it is possible to feed them from one water heater by a partially centralized system. With suitable fittings, this group supply may also be obtained from a non-pressure water heater (Fig. 7.2). A central supply comprises the feeding of all taps in the household from one pressure water heater. However, for reasons of economy, long pipe runs should be avoided and the heater should be installed near the tap which is used most often.

Water heaters, both of the non-pressure and of the pressure type, are thermally insulated devices which are heated independently of the time of withdrawal and which automatically keep the water at the preselected temperature. A high-quality thermal insulation is used in order to ensure minimal heat losses. Under certain conditions, storage water heaters are suitable for the use of *off-peak power*. Table 7.2 shows the recommended size of storage water heaters.

Table 7.2. The size of storage water heaters.

Size required	Number of people in household							
	1	2	3	4	5	6	7	8
Gas storage								
170 l				x	x	x	x	
135 l		x	x	x	x			
90 l	x	x	x					
Electric off-peak storage								
400 l					x	x	x	x
315 l			x	x	x	x		
250 l		x	x	x				
160 l	x	x	x					
Electric continuous storage								
250 l					x	x	x	x
160 l				x	x	x		
125 l			x	x	x			
80 l		x	x	x				

7.1.1 Non-pressure storage heaters

Non-pressure storage heaters are built in sizes from 5 l to 80 l capacity [1]. They are generally used for supplying only one tap near the heater (as in Fig. 7.3a). With a two-way combination fitting (for heaters of 10 l capacity or larger), a second tap next to the heater or on the other side of the wall can also be supplied. In the case of 80 l storage heaters, it is possible to connect a third tap to the built-in unit. Non-pressure water heaters have an inner tank of tinned copper. The heaters are always filled with water and they work on the displacement principle, by which the hot-water tap is in the cold-water supply to the heater. The inner tank is always open to the atmosphere, but, for operation, displacement fittings (such as Fig. 7.3b) should always be used to avoid damage to the tank due to possible excess pressure heads. Depending on the heater capacity, the maximum flow must be adjusted in accordance with the manufacturer's instructions for use.

7.1.2 Pressure heaters

Pressure heaters are built in sizes from 5 l to 400 l capacity. They are used for supplying several taps (see Fig. 7.4). Heaters with a capacity of more than 30 l have an inner tank of galvanized sheet steel or of copper, and copper should be used for preference when the water has corrosive properties. The inner tank is designed for an operating pressure of up to 6 atm (and, with heater of 5 l capacity, up to 10 atm).

All pressure heaters are provided with a temperature limiter that operates independently of the temperature selector. For connection and operation, type-tested fittings are necessary. With water mains pressures over 5 atm, type-tested pressure-reducing valves are also required.

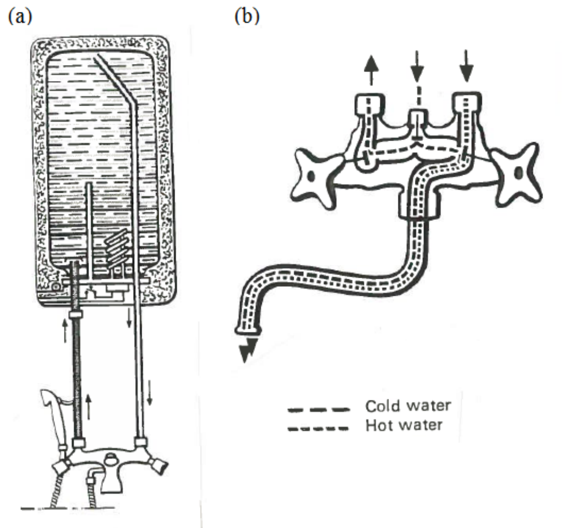

Fig. 7.3. Non-pressure storage water heater: (a) longitudinal section, (b) water flow through a displacement mixing fitting. Courtesy of *AEG*, Germany.

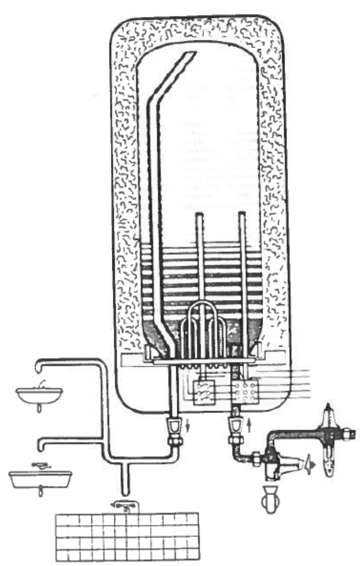

Fig. 7.4. Water connection diagram for a pressure storage heater. Courtesy of *AEG*, Germany.

7.1.3 Boilers

Boilers come with capacities of between 5 l and 80 l [1]. They have a tank of tinned copper which is not thermally insulated. As non-pressure types, they operate on the displacement principle (see Fig. 7.5) and they are used to supply only one tap which sits below the boiler. The water is always heated for a short time before it is required. When the selected temperature is reached, the boiler switches off but it does not switch on again automatically. The water is drawn immediately after heating.

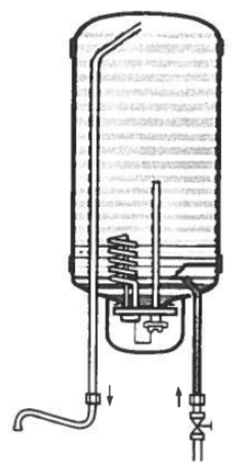

Fig. 7.5. Non-pressure hot-water boiler. Courtesy of *AEG*, Germany.

7.1.4 Continuous-flow (instantaneous) heaters

Continuous-flow heaters heat the water instantly and must be equipped with a very strong heating element (sometimes rated at more than 20 kW). They are sometimes constructed like pressure heaters for supplying several taps. Continuous-flow heaters can be divided into [1]:

- thermally-controlled heaters having a tinned-copper inner container with a capacity of 5 l and thermal insulation (Fig. 7.6);
- two-circuit heaters with thermally-controlled basic heating and flow-controlled supplementary heating, provided with a tinned-copper inner container which has 10 l capacity and thermal insulation;
- flow-controlled heaters without storage capacity.

The selection of the type of continuous-flow heater depends on the regulations of the local electricity supply authority, and the prevailing pressure conditions. Flow-controlled heaters require a minimum flow pressure of 1.1 to 1.5 atm. The thermally

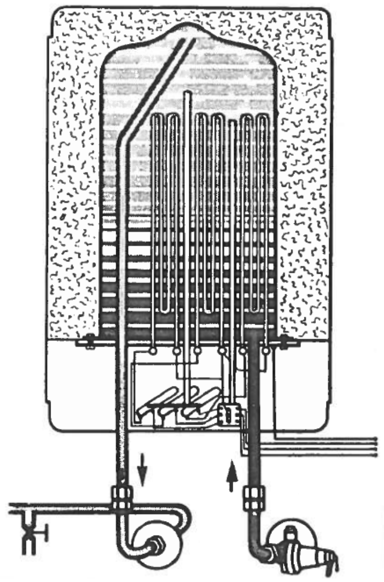

Fig. 7.6. Pressure-type continuous-flow heater. Courtesy of *AEG*, Germany.

controlled continuous-flow heater, on the other hand, is independent of flow pressure. Some heaters operate at up to 15 atm, and where there are higher mains water pressures like these, pressure-reducing valves may be needed. Depending on the size of the element, a continuous flow (instantaneous) heater may fail to perform if, for example, the washing machine and two showers are all going at once.

Example 7.1

Electric boiler draws $I = 15.0$ A of current when connected to a $V = 220$ V supply. A mass of 10 l of water is brought to boiling point with an initial temperature of 12 ^{0}C. The efficiency of the boiler is 70%. Find the time taken for the specified mass of water to be raised to boiling point. Also find the cost of the energy consumed if the charge be \$ 0.15 per kWh.

Solution

Temperature raise

$$\Delta\vartheta = 100^0 - 12^0 = 88^0\mathrm{C}$$

Heat required

$$Q = cm\Delta\vartheta = 1000 \times 10 \times 85^0 = 850\ 000\ \mathrm{kcal}$$

The specific heat of water is $c = 1$ cal/(g^{0}C) $= 1000$ cal/(kg^{0}C). The mass of 1 l of water is 1 kg. The electric power required is

$$P = \frac{Q}{t} = \frac{850\ 000 \times 4.186}{t} = \frac{3.558 \times 10^6}{t}$$

1 cal = 4186 J or 1 kcal = 4.186 kJ. The power supplied as heat (output power of the boiler)

$$P_{out} = VI\eta = 15 \times 220 \times 0.7 = 2310\ \mathbf{W}$$

where the input electrical power is $P_{in} = VI$. Therefore

$$2310 = \frac{3.558 \times 10^6}{t}$$

The time taken is $t = 3.558 \times 10^6/2310 = 1540.26$ s ≈ 25.7 min. Energy required

$$E = VIt = 220 \times 15 \times 1540.26 = 5\ 082\ 858 \text{ Ws} = 1.4119 \text{ kWh}$$

where 1 kWh $= 1000 \times 3600 = 3.6 \times 10^6$ Ws. The cost of energy is $1.4119 \times 0.15 \approx$ \$ 0.21.

7.2 Clothes washers

Electric clothes washers are commonly called *electric washing machines*. They save physical effort and treat the washing more thoroughly and gently than is easily possible by hand. There are three different washing systems[1]:

- drum systems (front loaders);
- blade-agitator systems (top loaders);
- disc-agitator systems, such as twin tubs.

Each of these is shown in Fig. 7.7. The *drum system* of Fig. 7.7a is the most popular of the three. When the drum is turned, the washing is raised from the suds by ribs on the drum and then falls back again. It is thereby squeezed, rubbed together and thoroughly agitated. The washing is also heated in the suds and, after washing, rinsed a number of times and spun, all in the same drum. In order to prevent the washing from tangling and to render the process as gentle as possible, the drum is stopped after a number of rotations and then changes its direction of rotation.

Washing machines are connected to the water mains, and after use the water is drained through a rubber hose into any wash basin or sink. A fixed connection is also sometimes fitted for this purpose. The drum is driven by a special two-speed motor with overload protection. Speeds over 500 rpm are required for spin drying. The a.c. induction or commutator motors in a typical washing machine are rated at 0.75 to 5 kW (single phase or three phase). The drum is flexibly suspended on rubber supports and has smooth walls, so that when the washing is spun at higher speeds of the drum can rotate freely even when it is unevenly loaded. After switch-off, electromagnetic brakes bring the drum to a stop within seconds.

Washing machines are sometimes provided with rollers and can quite easily be placed at the most convenient position by the user. All of the main components, including the tub, the main motor, the suds pump motor and the outlet screen,

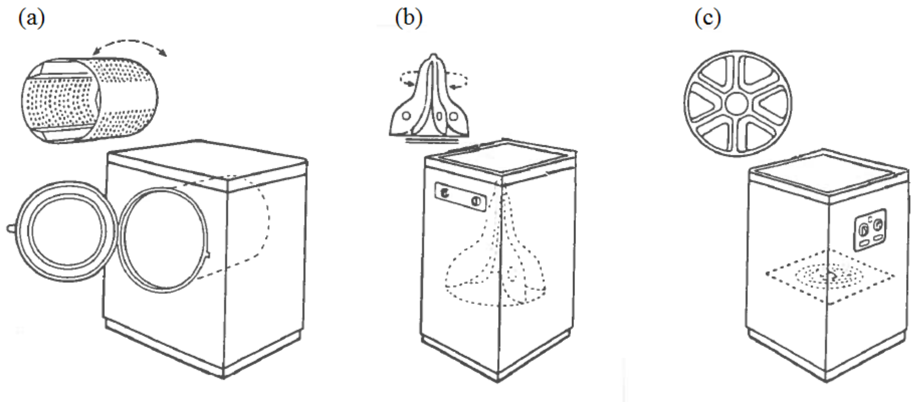

Fig. 7.7. Washing systems: (a) drum system (b) blade-agitator system, (c) disc-agitator systems. Courtesy of *AEG*, Germany.

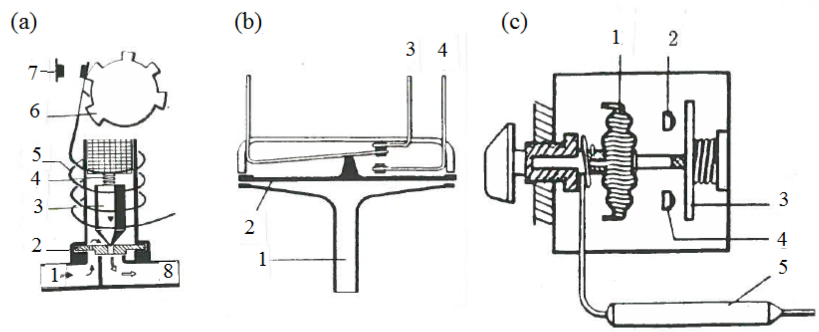

Fig. 7.8. Diaphragm mechanisms in washing machines: (a) inlet valve in close position (1 — water inlet, 2 — diaphragm, 3 — solenoid plunger, 4 — compression spring, 5 — solenoid coil, 6 — programme disc, 7 — contacts of switching mechanism, 8 — water outlet), (b) pressure switch position with tub filled (1 — hose connection, 2 — diaphragm, 3 — thermostat contact, 4 — inlet valve contact), (c) steplessly adjustable thermostat (1 — diaphragm, 2 — connection to heater contactor coil, 3 — contact plate, 4 — connection to pressure switch, 5 — detector tube).

are flexibly mounted so that imbalances are avoided even during high-speed drying. In fact, washing machines for commercial laundries must be anchored to the floor or permanently installed on a bracket. Domestic washing machines are generally designed for a load weight of 5 kg.

The water inlet is controlled by magnetic valves (Fig. 7.8a), and the emptying of water is achieved by a draining pump. The water level is sensed in the tub by a pressure switch in the form of a diaphragm (Fig. 7.8b), in combination with thermostats (Fig. 7.8c) which operate as protection against the machine running dry. Continuously-adjustable or fixed thermostats ensure a definite washing time that is suited to the particular type of laundry that has been loaded, and they provide the feedback necessary to ensure that the laundry stays at the correct temperature, even if the water inlet temperature is low or if the electrical input suffers from under-voltage.

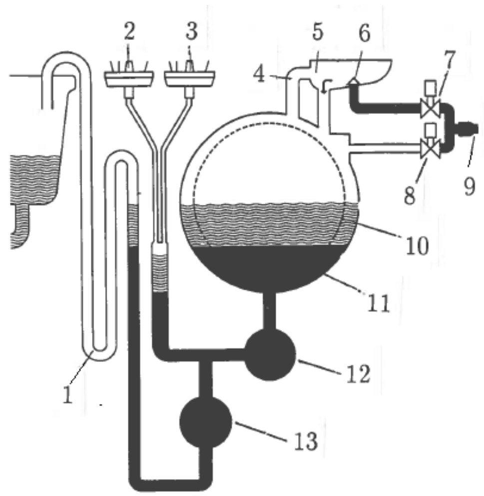

Fig. 7.9. Water flow through fully automatic washing machine: 1 — drain hose, 2 — high-level pressure switch, 3 — normal-level pressure switch, 4 — vent, 5 — detergent container, 6 — spray head, 7 — valve I, 8 — valve II, 9 — inlet hose, 10 — high water level, 11 —normal water level, 12 — screen, 13 — suds pump. Courtesy of *AEG*, Germany.

The programme is controlled by a switching mechanism (timer) with synchronous motor and reversing gear for changing the direction of rotation of the drum. It is possible to select complete fixed programmes for all types of fabrics and all degrees of soiling. The water level and drum movement, timing periods and temperature, number of rinses and, if applicable, spinning operations are exactly fixed for each programme.

A diagram showing the water flow in a fully-automatic washing machine is given in Fig. 7.9. The two suds system is used almost exclusively, in which the laundry is washed twice in clean suds (using fresh water and detergent each time), and this is followed by several rinsing cycles with intermediate spinning before the final spin drying.

7.3 Clothes driers

There are two different clothes-drying systems:

- vented tumble driers;
- condensation driers.

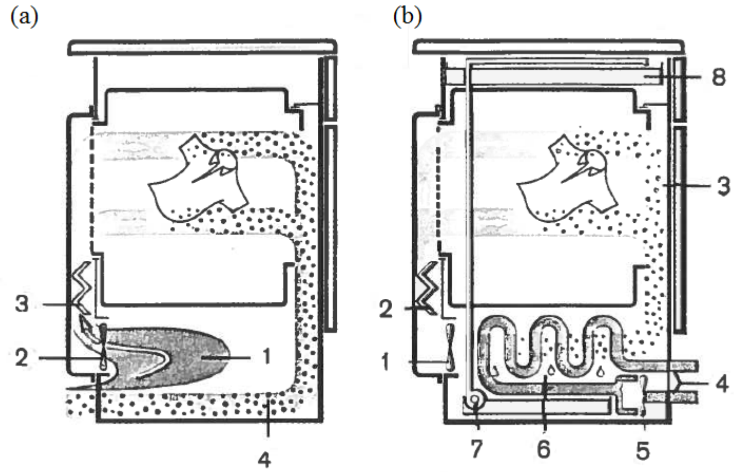

Fig. 7.10. Principle of operation of driers: (a) vented tumble drier (1 — incoming air, 2 — blower, 3 — heater, 4 — outgoing air), (b) condensation drier (1 — blower for drying air, 2 — heater, 3 — drying air, 4 — cooling air, 5 — blower for cooling air, 6 — heat exchanger, 7 — condensate pump, 6 — condensate container).

Vented tumble driers are used in rooms which are easily ventilated, and condensation driers may be used in rooms which have poorer ventilation.

The drying action of both systems is based on the same principle: incoming air is heated up, it is blown through the wet washing, and it removes the moisture. The two systems differ, however, in the details of how the moisture is removed.

The *vented tumble drier*, shown in Fig. 7.10a, lets the moist air out into the surrounding room. This is why the room should be well ventilated. An even better form of venting is to conduct the moist air through an outlet hose to the outside of the building.

This is not necessary, however, when a *condensation drier* (Fig. 7.10b) is used. The condensation drier operates with a *closed* air circuit – in other words, the air is cooled before it goes out into the surrounding room, so that the moisture condenses inside the machine. The condensed water is then collected in a condensate container, which can easily be removed from the control panel. The condensed water can also be pumped off directly into a wash-basin or a drain and in that case it would never be necessary to remove and empty the container.

The drying process is monitored right from the start by an electronic control system. Sensors on the ribs of the drum continuously determine the residual moisture in the drying laundry. The heating is switched off as soon as a preset reduced degree of dampness is reached, which saves electricity and makes the drying process very economical.

During the entire drying process, the drum rotation is continually reversed (from clockwise to anticlockwise and back again). This ensures that the load is dried very evenly and without creasing, so that the wash becomes soft and fluffy.

A cooling-down period automatically follows the end of the drying programme. If the laundry is not immediately taken out of the drum, it will still be gently moved for up to 30 min with a reverse-tumble movement. The washing thus remains smooth and fluffy with no unsightly creasing.

7.4 Refrigeration

The concept of *evaporation* is the key to understanding a cooling effect. Suppose that a boy (his body is normally at about 36.6^{0}C or slightly less) is lying on a lounge chair next to a pool. It is 36.6^{0}C outside with a warm breeze, so he feels quite warm. He jumps into the pool, which also happens to be at 36.6^{0}C, but he does not even feel cooled off because the pool is so warm. When he gets out of the pool, however, he feels quite cool because the warm breeze is causing the 36.6^{0}C water on his skin to evaporate. In order for this evaporation to take place, the water absorbs its latent heat of vaporization before it turns into a vapour. The evaporating water draws its latent heat of vaporization from the boy's body, and this makes him feel cool.

A liquid cannot exist at a temperature higher than its *boiling point* or *saturation point*. An automobile radiator has 110^{0}C water only if the pressure in the radiator system is higher than atmospheric. When at atmospheric pressure, the water cannot exist as a liquid at any temperature higher than 100^{0}C. When the water was pressurized as a 110^{0}C liquid, it was in a saturation condition. If the pressure were to be reduced, boiling and cooling would take place. Sometimes rapid boiling of a saturated liquid is caused by a reduction in pressure, and the liquid is said to be *flashing* into a vapour. The cooling caused by a saturated liquid flashing to a vapour is the same phenomenon that causes cooling to happen in a refrigeration or air-conditioning system.

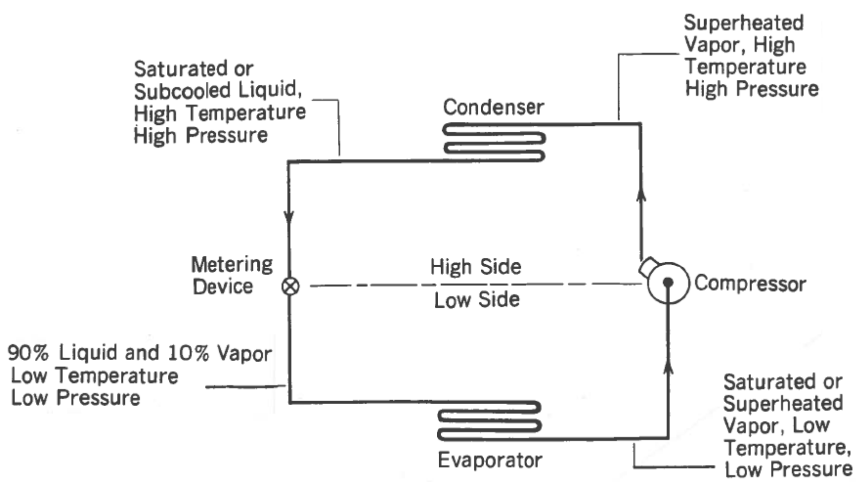

Fig. 7.11. A simple complete refrigeration system.

A *refrigerant* is the fluid that is used inside the refrigeration system to transfer heat. Refrigerants are either natural fluids, such as ammonia, or else they are manufactured chemicals. By far the two most popular refrigerants in use today are *dichlorodifluoromethane* and *monochlorodifluoromethane*, both manufactured substances. Their names are so difficult to say that they are commonly referred to as R-12 and R-22 respectively. The major difference between water and the refrigerants used in vapour compression systems is the difference in their boiling temperatures. At atmospheric pressure, water boils at 100^0C, while R-12 boils at -29.4^0C. If the liquid R-12 is in a pressurized tank and then the pressure is reduced, the refrigerant flashes into vapour. As it flashes, it absorbs its latent heat of vaporization from the remaining liquid, and the liquid that remains becomes cooled to a lower temperature than the external temperature of the surrounding air. If this now cold tank is put inside an insulated box, we will have a refrigerated box, if we used a fan to blow air across this tank, the air would be cooled and we would have a crude form of air conditioner.

A simple refrigeration system is shown in Fig. 7.11. The *compressor* squeezes the refrigerant vapour so that its pressure increases. When any gas is compressed, a lot of work is done on it, and as a result its temperature goes up. The refrigerant leaving the compressor will therefore not only be at a high pressure, but it will also be at a high temperature.

Next, let us run the hot gas through a tube to a coil located outdoors. At the high pressure, high temperature gas passes through this coil, outside air is blown over it. The cooling done to the gas will cause some of the gas to condense into a liquid. As the outdoor coil continues to remove heat from the refrigerant, the refrigerant continues to condense until there is only liquid and no vapour left. This outdoor coil is called the *condenser*, because it removes heat from the refrigerant and causes it to condense. Now there is a liquid refrigerant, and it passes back into the refrigerant tank to replenish the refrigerant supply.

In the complete refrigeration cycle (Fig. 7.11), the *metering device* meters the amount of liquid refrigerant that is allowed to enter from the refrigerant tank to the evaporator. Metering device is actually a general term that is used to describe any of a number of different types of valves or orifices.

The four fundamental components of any refrigeration system are:

- a compressor;
- a condenser;
- a metering device;
- an evaporator coil;

A line is shown in Fig. 7.11 that divides the system into a *high side* and a *low side*. On the high side, both the pressure and the temperature are high. On the low side, there is only low pressure refrigerant at a relatively low temperature. The refrigeration system does not actually eliminate heat. It only moves it around. The refrigerant in the *evaporator* absorbs heat from whatever it is cooled. This heat is then carried around the system by the vaporized refrigerant to a point where one can get rid of it (condenser). The condenser is located in a place where the release of this heat will not be objectionable, such as outdoors. Thus, the point of heat discharge is isolated from the point of heat pickup (which is the point of cooling).

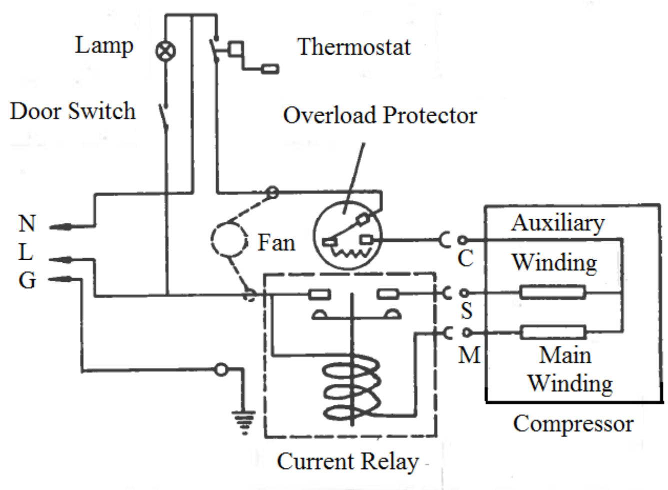

Fig. 7.12. Connection diagram of a single-phase induction motor for a household refrigerator.

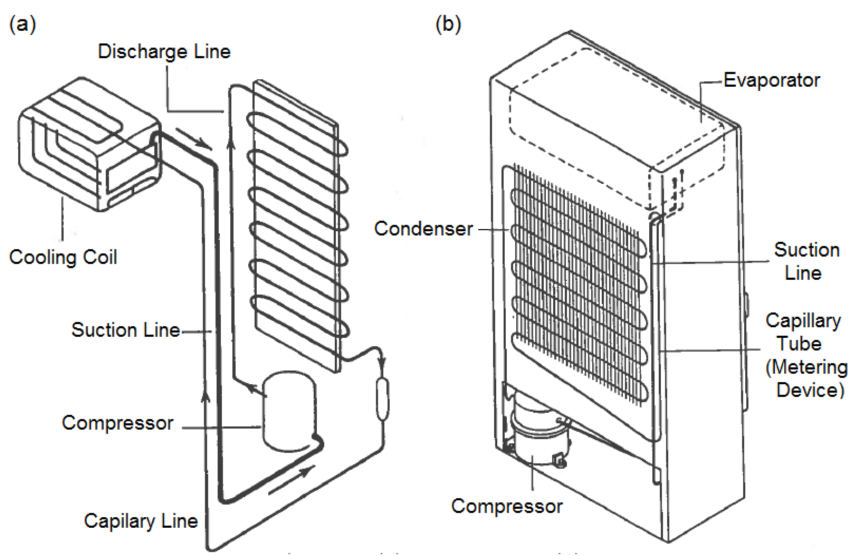

Fig. 7.13. A simple household refrigerator/freezer: (a) arrangement, (b) location of components — the compressor is located below, the condenser is mounted on the back, the metering device consists of a long, small-diameter tube, and the evaporator is located inside the refrigerated space.

There are four common compressor designs in use today:

- reciprocating (piston) compressors;
- rotary compressors;
- screw compressors;
- centrifugal compressors;

Compressors are usually driven by 3000 rpm (or 3600 rpm) cage induction motors, which are either single-phase or three-phase. The connection diagram for a single-phase motor is shown in Fig. 7.12.

The simplest arrangement for a *houshold refrigerator* is shown in Fig. 7.13. The compressor is located under the food storage compartment, and the static condenser is mounted on the back of the box. Air circulates through the condenser by natural circulation, and removes heat as the refrigerant condenses. The metering device is a capillary tube, carrying the refrigerant to the plate-type evaporator inside the box, and the section inside the evaporator box is the freezer. Air that is cooled at the top of the box is allowed to fall down inside the rest of the box. The freezer section is maintained at between -17.8^0C and -23.3^0C, while the refrigerator is kept at between 1.7^0C and 7.2^0C. A *thermostat* to sense the temperature may be located in either the refrigerator or the freezer section. The compressor is cycled on and off to control the temperature in whichever section the thermostat is located. The temperature in the other section is controlled by adjustment of a damper, which regulates the quantity of air that is supplied to the refrigerator section from the freezer section. Refrigerators that have completely separate frozen food sections and refrigerated food sections sometimes use two evaporators. The refrigerant flows first through the freezer evaporator, after which there is sufficient liquid refrigerant remaining to provide cooling to the evaporator in the refrigerator section.

The most common operating pressures for a domestic refrigerator are 0 to 0.14 atm (1 atm = 760 Torr = 760 mm Hg at 0^0C) on the low side, and 6.8 to 8.5 atm on the high side, although some units operate outside these ranges. The refrigerant that returns to the compressor picks up heat from the capillary tube and returns to the compressor at a temperature sufficiently high to prevent the suction line from sweating on the outside surface. Some refrigerators use insulated suction lines to ensure that they will not sweat.

Some compressors used in refrigerators are equipped with two additional connections. These are merely the opposite ends of a tube that runs through the oil reservoir at the bottom of the compressor. They are *oil cooler* connections, and are piped as shown in Fig. 7.14. The hot gas from the compressor discharge flows through an auxiliary condenser, which is sometimes called an oil cooler. From the outlet of the auxiliary condenser, the refrigerant flows through the loop in the bottom of the compressor where it picks up heat from the oil. It then circulates to the main condenser and through the rest of the cycle in the conventional fashion.

The door of the refrigerator has a soft rubberized seal that should be airtight when the door is closed. If it is not, the compressor will have to run for longer than normal to remove the heat that has flowed into the refrigerated box as a result of the air leakage. Under these circumstances, there will be a rapid build-up of frost on the evaporator caused by humidity leaking into the box. Modern refrigerators are equipped with *defrosting devices*.

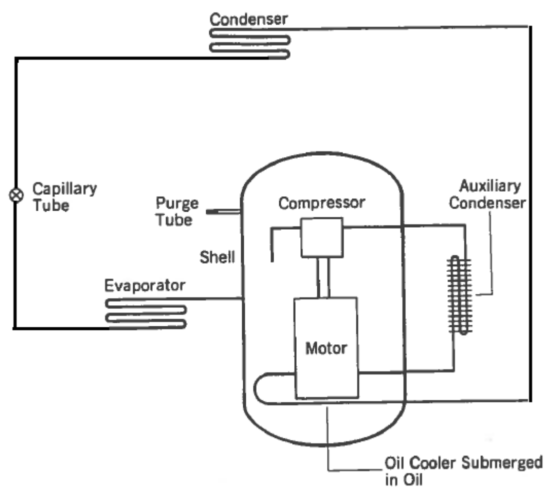

Fig. 7.14. Installation of a compressor with five tubing connections.

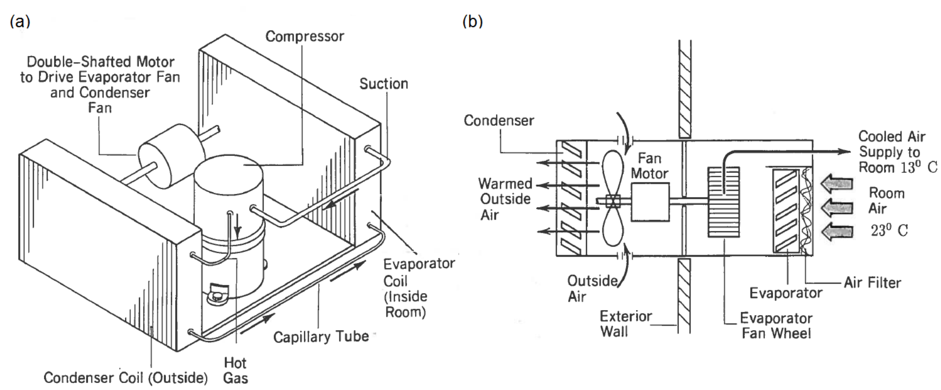

Fig. 7.15. Window (through-the-wall) air conditioner: (a) refrigeration circuit, (b) airflow.

7.5 Air-conditioners

Fig. 7.15 shows a common *window air-conditioner*. All of its components are located in one box, but the box is divided into an outdoor section and an indoor section and it contains one motor which is used to drive both the outdoor condenser fan and the indoor evaporator fan. The outdoor fan draws air through the condenser, where the air picks up heat from the condensing refrigerant. The warmed outdoor air is then discharged back outside the building. The indoor fan draws room air through the evaporator coil where it is made 6.7^0C to 7.8^0C cooler before being discharged back into the room.

The *heat pump* is an air-conditioning system that operates as a heating system. It is sometimes called a *reverse cycle system*, and it is a very efficient system to use whenever electrical energy must be used for heating. It can achieve operating costs comparable to those obtained when gas or fuel oil are used.

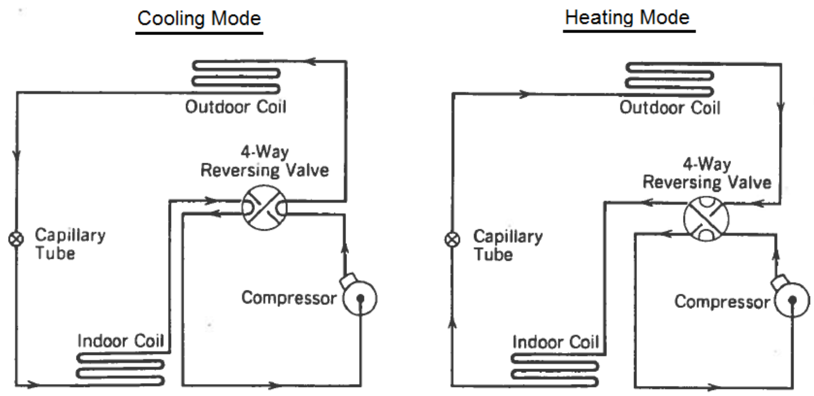

Fig. 7.16. The four-way reversing valve allows the indoor coil to receive the hot gas instead of cold refrigerant during the heating mode.

In practice, air-conditioners use a four-way reversing valve. For normal air-conditioning, the hot gas from the compressor discharge is routed to the outdoor coil and then to the metering device, the indoor coil, and the compressor suction via this four-way valve (see Fig. 7.16). On the heating cycle, the four-way valve changes its position. The hot gas from the compressor discharge is now routed backwards through the indoor coil, the metering device, the outdoor coil (where it picks up heat from outdoor air), and then back to the compressor suction via the four-way valve. A capillary tube is a handy metering device to use with this type of system because it permits flow in either direction. Where thermostatic valves are used as the metering devices, a single thermostat is provided for each coil, and a bypass with a check valve is also fitted.

The *central air-conditioning system* uses the same four basic air-conditioner components (see Fig. 7.17). The condensing unit (comprising a compressor plus condenser) is located outdoors, while the evaporator and the metering device are closer to the area to be air-conditioned. The same fan that provides forced air heating also serves as the evaporator fan. It is important that some distance physically separates the high side from the low side of the system. This arrangement is commonly called a *split system*.

Example 7.2

It is necessary to condition 600 m^3/h (cubic meters per hour) of air from an initial temperature of $+8^0$C to $+22^0$C. In addition, it is necessary to evaporate 0.6 kg of moisture per 100 m^3/h of the air to control humidity. The heat required to raise the

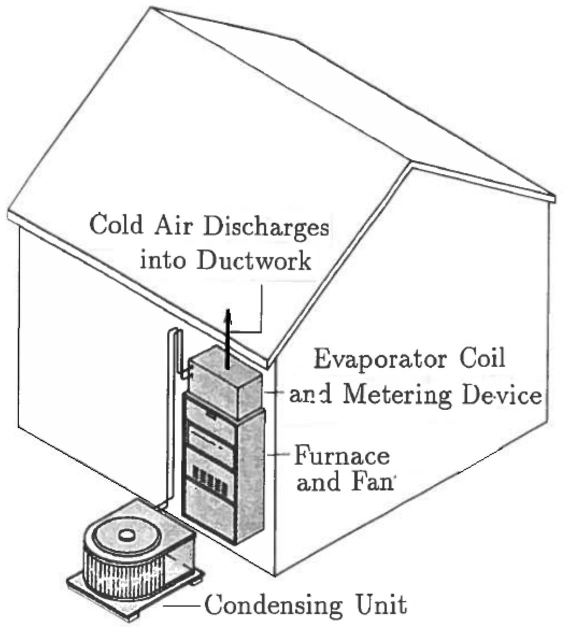

Fig. 7.17. A residential split-system air conditioner.

temperature of 1 m^3 of air through 1^{0}C is $c = 1220$ J/m^3/^{0}C. The heat of vaporisation for water at its normal boiling or condensation temperature is $c_v = 2260$ J/kg. Find the necessary power required.

Solution

The rate of heat required to raise the temperature of air to +22^{0}C

$$H_1 = \frac{Q_1}{t} = cV_{air}\Delta\vartheta = 1220 \times 600 \times (22 - 8) = 10.248 \times 10^6 \text{ J/h}$$

The rate of moisture present in the air

$$m_m = 0.6\frac{600}{100} = 3.6 \text{ kg/h}$$

The rate of heat required to evaporate the moisture

$$H_2 = \frac{Q_2}{t} = c_v m_m = 2260 \times 10^3 \times 3.6 = 8.136 \times 10^6 \text{ J/h}$$

The total rate of heat required

$$H = H_1 + H_2 = (10.248 + 8.136) \times 10^6 = 19.068 \times 10^6 \text{ J/h}$$

Power required

$$P = H = \frac{19.068 \times 10^6}{3600} = 5297 \text{ W} \approx 5.3 \text{ kW}$$

7.6 Cookers

Electric cooking is preferred to other methods because it is quick, clean, economical, and safe. In electric cooking, it is possible not only to control the amount of heat but also to vary the temperature as required. This is an advantage which electric heat has over other types of energy. The operating costs of an electric cooker are best determined by considering the number of people in the household and the amount of food to be prepared, rather than the connected load of the cooker. Table 7.3 shows empirically-established values for the power consumption per month in a fully-electrified domestic kitchen [1].

Table 7.3. Electricity consumption per month in a fully electrified domestic kitchen.

Number of persons	2	3	4	5	6
kWh per months	50 to 60	60 to 72	72 to 90	78 to 105	86 to 117

7.7 Heaters

The following equipment is used for heating of households:

- high temperature radiators,
- convector heaters,
- panel heaters,
- oil radiator heaters,
- floor warming systems.

In a *high temperature radiator* the resistance elements get heated to high temperature 1400 to 1600^0C. Heating elements are wound on a porcelain former and mounted into decorative frames. From 50 to 70% of heat is dissipated by radiation and the remaining amount by convection.

Convector heaters have low temperature (below 100^0C) heating elements mounted in sheet-metal cases. The cool air is admitted from the bottom and after getting heated up, comes out from grills at the top. The front and top are often made of moulded plastic materials to create a nice appearance.

In *panel heaters* resistance elements are embeded in large panels of fire clay or other heat resisting materials. The heat is dissipated by convection and radiation. Panel heaters can be used on walls or ceilling.

In *oil radiator heaters* the oil is heated by resistance elements and circulates in radiators.

A *floor warming system* consists of a number of heating cables made of high resistivity alloys which are embedded in the floor. The loading is usually from 100 to 150 W/m^2 of floor.

Example 7.3

A family room measures $5.5 \times 4.2 \times 3.6$ m. The temperature of the room is to be kept at $+24^0$C when the outside temperature is $+8^0$C. The ventilation is such that the air has to be renewed every 45 min. The heat loss from the wall is $\Delta h = 720$ J/(^{0}C×h). Find: (a) the necessary rating of the heater, (b) the rating of the heater after insulating the walls when the heat loss from the walls drops to $\Delta h = 415$ J/(^{0}C×h), and (c) the cost of electricity per month if the heater operates 300 h/month and 1 kWh costs \$ 0.1.

Solution

The volume of air in the room is $5.5 \times 4.2 \times 3.6 = 83.16$ m^2. The volume of air to be conditioned per hour

$$V_{air} = 83.16 \frac{60}{45} = 110.88 \text{ m}^3/\text{h}$$

The rate of heat required to rise the temperature of air to $+24^0$C

$$H_1 = \frac{Q_1}{t} = cV_{air}\Delta\vartheta = 1220 \times 110.88 \times (24 - 8) = 2.164 \times 10^6 \text{ J/h}$$

The rate of heat loss from the walls

$$H_2 = \frac{Q_2}{t} = \Delta h \Delta\vartheta = 720 \times 10^3 \times (24 - 8) = 11.52 \times 10^6 \text{ J/h}$$

The total rate of heat

$$H = H_1 + H_2 = (2.164 + 11.52) \times 10^6 = 13.68 \times 10^6 \text{ J/h}$$

The rating of heater

$$P = H = \frac{13.684 \times 10^6}{3600} = 3801 \text{ W} \approx 3.8 \text{ kW}$$

After insulation of walls the rate of heat loss from the walls drops to

$$H_2' = 415 \times 10^3 \times (24 - 8) = 6.64 \times 10^6 \text{ J/h}$$

and the total rate of heat required

$$H' = H_1 + H_2' = (2.164 + 6.64) \times 10^6 = 8.804 \times 10^6 \text{ J/h}$$

The rating of heater required

$$P' = H' = \frac{8.804 \times 10^6}{3600} = 2445 \text{ W} \approx 2.5 \text{ kW}$$

The cost of electricity per month before insulating the walls was $3.8 \times 300 \times 0.1 =$ \$ 114. After insulating the cost was reduced to $2.5 \times 300 \times 0.1 =$ \$ 75.

7.8 Lights

Light sources are usually divided into two classes: *incandescent sources* and *luminescent sources*. An incandescent source is one which emits light solely because of its high temperature (for example a tungsten-filament lamp) whereas a luminescent source emits light as a result of ionisation or other types of excitation that are independent of temperature. Mercury vapour lamps, neon lamps, sodium vapour lamps and fluorescent lamps (coated with certain powders) are all examples of luminescent sources. Such sources usually radiate only at certain specific wavelengths.

7.8.1 Tungsten-filament lamps

It is well known that a black body is the most efficient radiator because it emits energy at every wavelength. A black body, when heated to 6250^0C, emits maximum energy within the visible spectrum. Even though it is not possible to realise a perfect black body, the materials used for lamp filaments approach it very closely. Tungsten, with its melting point at 3500^0C, is now universally adopted as a material for incandescent lamps. The safe working temperature of such a filament is about 3000^0C. The cold resistance of the filament is approximately one-sixteenth of its hot resistance, and the filament resistance increases almost instantaneously (after about 0.2 s) when switched on. An inert gas, usually a combination of nitrogen and argon, is used to fill the lightbulb that contains the filament, and this allows the filament to be used at its elevated working temperature without any fear of oxidation. The pressure exerted by the inert gas also helps to prevent any evaporation of the filament.

Since the first use of gas-filled tungsten lamp, improvements have been made in the design of the filament, including the use of a coiled or helical filament instead of a straight wire, and the development of a coiled coil filament in which the single helix is coiled again on itself as shown in Fig. 7.18. The coiled coil filament can be operated at higher temperatures, and as a result the light output per watt increases and the losses due to convection decrease. The *efficacy* in lm/W (lumens per watt) increases as the rated power of the lamp increases. If the working voltage is marginally greater than the rated voltage, more light output is obtained but the life of the lamp is shortened. Operation of the filament at a voltage lower than the rated voltage results in a reduction in the light output.

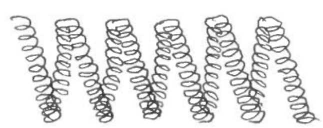

Fig. 7.18. A coiled coil tungsten filament.

7.8.2 Electric discharge in a gas of low pressure

When an electric current flows between two electrodes in tube of gas at an approximate pressure of 1 mm Hg, a cathode glow is produced very close to the cathode, next to which is the cathode dark space and then a bright region sometimes called the negative glow. Beyond this are the Faraday dark space and the luminous positive column (see Fig. 7.19). A decrease in pressure causes the cathode dark space to expand until it can be made to fill the whole tube, while an increase in pressure causes the positive column to expand. In many commercial lamps, the positive column fills almost the whole tube.

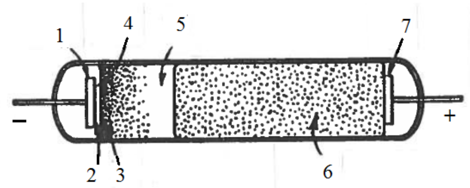

Fig. 7.19. Electrical discharge in a gas at low pressure: 1 — cathode, 2 — cathode dark space, 3 — negative glow, 4 — cathode glow, 5 — Faraday's dark space, 6 — positive column, 7 — anode.

If the cathode is heated so that it gives an adequate supply of electrons, the voltage drop at the cathode is low, and so hot cathode lamps such as the sodium lamp and the mercury vapour lamp (which uses a mercury pool) are essentially low-voltage devices. In cold cathode lamps, the voltage drop at the cathode must be increased to perhaps ten times the ionization potential, in order to accelerate positive ions towards the cathode and to give them sufficient kinetic energy so that when they bombard the cathode they liberate electrons. In order to reduce power loss at the cathode, a long lamp is required, which in turn necessitates a higher operating voltage for these lamps. The bombardment of the cathode also causes its gradual disintegration with a consequent blackening of the tube, and there is a tendency for 'clean up' of the gas which may also reduce the life of the lamp.

7.8.3 Sodium vapour lamps

A *sodium vapour lamp* consists of an inner bulb of special glass containing the sodium and the inert gas, which is either neon or argon at a pressure of 1.5 mm Hg. The inner bulb is fitted with two filaments, and is then enclosed in a larger bulb (Fig. 7.20a) which is evacuated to minimise the escape of heat. The bulb is a highly-effective light source, because the radiation that it emits is that of several yellow sodium lines, which are near the maximum of the visibility curve for the human eye. The normal operating temperature of the tube is at around 300^0C. A small transformer is included in the circuit in order to heat the cathode, and there is a choke for stabilizing the discharge. To begin with, the discharge starts in the inert gas and the temperature of the lamp increases gradually until sufficient metallic vapour is present to conduct the current. Since the ionization potential of the metal vapour is low, it will carry nearly all of the current, and the spectrum of the inert gas will soon practically disappear. Thus the bulb starts as a neon lamp and then gradually changes from red to yellow as the temperature rises. Because their monochromatic yellow light makes objects grey, these lamps are only suitable for street and highway lighting.

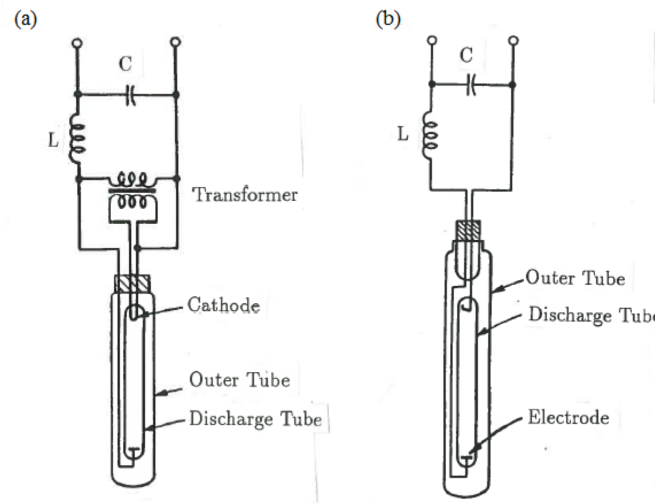

Fig. 7.20. Vapour lamps: (a) sodium lamp, (b) mercury lamp.

7.8.4 Mercury vapour lamps

The *mercury vapour lamp* is similar in construction to the sodium vapour lamp and also consists of a double glass bulb (Fig. 7.20b). Since the cathode is maintained in an incandescent state by ionic bombardment, no heating circuit is required. Operation of the mercury vapour lamp at low vapour pressures gives blue light with a high proportion of the ultra violet rays, and this is unsatisfactory as a source of domestic illumination. A more recent development has been the high-pressure (1 to 2 atm) mercury lamp, in which a small but carefully-measured drop of mercury is introduced into the bulb. On switch-on, the vapour pressure rises until all the mercury is vaporised, after which the light given out is white with a bluish tinge. Here also an inert gas is introduced for initial discharge of the mercury. Whenever the mercury vapour lamp goes out, it will not restart until it has cooled down and the vapour pressure has once again fallen to a value sufficiently low to allow restriking of the discharge in the inert gas. The overall *efficacy* of the bulb is approximately 35 lm/W, and the power factor is 0.65 [56]. A still more recent development in mercury lamps is an ultra-high pressure lamp operating at about 40 atm which has an efficacy comparable with sodium vapour lamps. These lamps are used for outdoor and industrial lighting.

7.8.5 Fluorescent lamp

Mercury vapour lamps operating both at low and high pressures emit radiation in the ultraviolet region, and therefore are of limited use as source of light. However, ultraviolet radiation can be used to excite certain materials. When the excited molecules of these materials return to normal, they emit radiation at a frequency which is different from that which caused the excitation, and therefore the radiation emitted by the material may be within the visible zone. In effect these materials convert ultraviolet radiation to visible light. Materials which possess this property are called fluorescent.

The *fluorescent lamp* takes the form of a tube which is usually 2 to 5 cm in diameter and 0.3 m to 1.5 m long. The tube has electrodes at each end which are in the form of coiled filaments coated with an electron-emitting material. The inside of the tube is coated with fluorescent powder and as the operating temperature of the tube is approximately 50^0C, no outer tube is required. A series choke (inductive ballast) for stabilizing the discharge and a shunt capacitor across the supply terminals for improvement of the power factor are used with the tube. The lagging power factor is only due to the choke. Sometimes a small capacitor of 0.05 μF is connected across the tube as shown in Fig. 7.21 to suppress radio interference because the tube draws non-sinusoidal current from the supply (discharge).

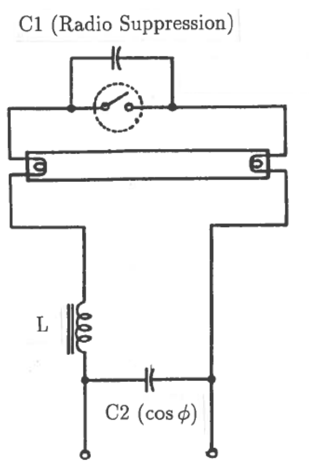

Fig. 7.21. Fluorescent lamp circuit.

When the supply is switched on, the starter provides a path through the electrodes and the choke, which provides preheating. The starter switch then opens automatically, thereby interrupting the current. Since the heating current reduces to zero instantaneously in the choke circuit, the choke field collapses and this releases stored energy and thus produces a high voltage between the electrodes and causes the preionized tube to strike.

There are two main types of starter switches:

- glow starter switches;
- thermal starter switches.

The *glow starter switch* consists of a pair of bimetallic contacts sealed in small glass bulb that is filled with argon gas. When the supply is switched on, the total supply voltage appears across the open contacts, thereby causing an arc discharge to take place between the contacts. The heat from the discharge closes the bimetallic contacts, allowing the preheating current to flow. The closure of the contacts extinguishes the arc, so the bimetallic contacts cool and open, and the lamp strikes. A small capacitor to suppress radio interference is fitted between the contact connections outside the glass bulb. The glass bulb is usually mounted on a plastic base and inserted into a small metal cylinder. The base has metal studs or pins coming out from it, which are connected to the bimetallic contacts. An insulated socket is mounted in the control gear housing to receive the metal studs of the starter switch so that it may easily be connected into the control gear circuit.

A *thermal starter switch* has a very similar appearance to a glow starter switch except that it employs a somewhat larger size of metal cylinder. This starter switch also has a pair of bimetallic strips which are initially closed, rather than open as in the case of glow starter. The contacts, along with the heater coil, are enclosed in a glass bulb, and the bulb is filled with a gas to improve the thermal link between the heater coil and the contacts.

When the supply is switched on, current flows through the choke, the starter heater and the electrodes. The heater coil then raises the temperature of the bimetallic contacts and they separate, interrupting the current through the choke. The resulting voltage pulse of approximately 1000 V causes the tube to strike and once this has happened, the tube current flows through the starter heater and the bimetallic contacts remain open.

The high frequency *electronic ballast* does not require a large inductance. It converts the 50 or 60 Hz input into a high frequency output, usually in the range of 25 to 40 kHz [42]. The electronic ballast consists of a diode rectifier bridge and a d.c. – to – a.c. high frequency inverter. An EMI filter is used before the rectifier to supress higher harmonics. In general, electronics ballasts are more energy efficient compared to the standard ballasts.

Fluorescent discharge lamps may also be operated on a d.c. supply. This requires the use of a resistive ballast for arcing stability in addition to the choke for producing the voltage pulse. The resistive ballast introduces a very high power loss. In addition, the migration of positively-charged mercury ions towards the cathode results in low light output from the anode end of the tube. For this reason, whenever the tube is to be used on d.c. , a reversing switch is normally used in the circuit to change the direction of the current through the tube every few hours.

It is generally preferable to use an inverter circuit for a d.c. power supply (trains, buses and aircrafts).

7.8.6 Compact fluorescent lamps

Compact fluorescent lamps first became popular in 1990 and are designed to fit standard household bulb fittings. The phosphor-containing gas mixture is supposed to produce light of a similar colour to incandescent bulbs. Claims that they use only a fifth of the energy of standard incandescent light bulbs and last eight times as long have helped some consumers to overlook their high purchase price. The ballasts of these lamps have been known to give problems. They often introduce harmonic distortion into the power system, which reduces the efficiency of the system as a whole and can increase interference in nearby wires such as telephone lines.

7.9 Fundamental quantities, units and laws in lighting technology

7.9.1 Luminous intensity

The *luminous intensity* is the *luminous flux*, Φ, radiated in a specific direction from a point source, divided by the solid angle irradiated, ω, i.e.

$$I = \frac{\Phi}{\omega} \qquad \text{cd} \tag{7.1}$$

The base unit *candela* (cd) is defined as the luminous intensity of a surface of 1/600 000 m^2 of a black body at a temperature of 2042 K. The luminous flux is measured in lumen (lm).

If the illuminated area is A and the radius of a sphere is r the solid angle is

$$\omega = \frac{A}{r^2} \tag{7.2}$$

It is measured in steradian (sr). 1 lm = 1 cd × 1 sr.

7.9.2 Illumination

Illumination is the luminous flux, Φ, striking an area of surface, divided by the illuminated area, A, i.e.

$$E = \frac{\Phi}{A} = \frac{I\omega}{A} = \frac{I}{r^2} \qquad \text{lx} \tag{7.3}$$

Illumination is measured in lux (lx).

7.9.3 Luminance

Luminance is the luminous flux, Φ, penetrating a surface in a particular direction, divided by the product of the solid angle ω irradiated and the projection $A\cos\epsilon$ of the surface A onto a plane, perpendicular to the given direction, i.e.

$$L = \frac{\Phi}{\omega A\cos\epsilon} = \frac{I}{A\cos\epsilon} \qquad \text{cd/m}^2 \tag{7.4}$$

where ϵ is the angle of emission between the surface A and its projection A$\cos\epsilon$ (Fig. 7.22a).

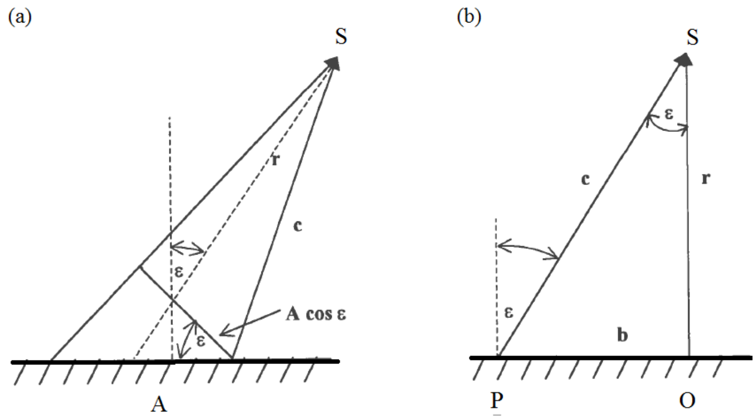

Fig. 7.22. Luminance and illumination: (a) luminance of a surface of area A, (b) illumination of a point on a plane.

7.9.4 Lambert's cosine law

The illuminated surface A is often inclined by an angle ϵ as shown in Fig. 7.22a. The area over which the light is spread is then increased by the ratio $\mathrm{A}/(\mathrm{A}\cos\epsilon) = 1/\cos\epsilon$ and the illumination decreases in proportion to $\cos\epsilon$, i.e.

$$E = \frac{I}{r^2}\cos\epsilon \qquad \mathrm{lx} \tag{7.5}$$

The above equation is known as *Lambert's cosine law*. Illumination at any point on a surface is proportional to the cosine of the angle between the normal at that point and the direction of luminous flux (Fig. 7.22a).

Fig. 7.22b shows a light source at a height r from the plane surface. According to Lambert's cosine law, illumination at a point P on the surface is

$$E = \frac{I}{c^2}\cos\epsilon = \frac{I}{c^3}r = \frac{I}{(b^2+r^2)^{3/2}}r \tag{7.6}$$

where $\cos\epsilon = r/c$ and $c^2 = b^2 + r^2$.

Example 7.4

A bulb rated at 220 V gives a luminous flux of 6400 lm and draws 1.6 A from the mains. Find the luminous intensity and efficiency of the lamp in lm/W (efficacy).

Solution

The input power absorbed by the bulb

$$P_{in} = 220 \times 1.6 = 352 \text{ W}$$

The luminous intensity

$$I = \frac{\Phi}{\omega} = \frac{6400}{4\pi} = 509.3 \text{ cd}$$

The efficiency

$$\eta = \frac{\Phi}{P_{in}} = \frac{6400}{352} = 18.18 \text{ lm/W}$$

since the luminous flux radiated in a specific direction is regarded as a measure of the output power.

Example 7.5

A lamp giving $I = 500$ cd luminous intensity in all direction below horizontal is suspended $r = 2.6$ m above the centre of a square table of $a = 1.2$ m side. Calculate the maximum and minimum illumination on the table.

Solution

Illumination at the centre of the table

$$E = \frac{I}{r^2} = \frac{500}{2.6^2} = 73.96 \text{ lx}$$

Illumination at any corner according to Lambert's cosine law

$$E = \frac{I}{c^2}\cos\epsilon = \frac{I}{(b^2 + r^2)^{3/2}}r = \frac{500}{(0.72^2 + 2.6^2)^{3/2}} \times 2.6 = 63.55 \text{ lx}$$

where $b^2 = (0.5a)^2 + (0.5a)^2 = 0.5a^2 = 0.5 \times 1.2^2 = 0.72$ (see Fig. 7.22b).

7.10 Safety

7.10.1 Electrical shock

The human body will become part of an electric circuit when two or more points on the body are connected to any external source of voltage. The strength of the resultant current flowing between these points will depend on the value of this voltage and on the electrical resistance of the body. Since body tissue contains a high percentage of water and salt, it is a fairly good conductor of electrical current, the passage of which could affect the tissue in two different ways:

- The electrical losses (I^2R) dissipated in the tissue resistance R can cause a temperature increase and thus lead to resultant tissue damage due to burns.
- Local voltages caused by the externally-applied currents could be superimposed on the normal electrochemical action-potentials that the body uses for the transmission of impulses through sensory and motor nerves. If these action-potentials are of sufficiently high intensities, they can stimulate nerves, resulting in tetanus of the muscles, in which all possible fibres are contracted, causing interference with the normal functioning of organs, such as the heart and lungs.

The organ most susceptible to electric current is the heart. A tetanizing stimulation of the heart results in complete myocardial contraction, stopping the heart's pumping action and interrupting the circulation of the blood circulation. Should this condition last for a few minutes, brain damage will occur initially and then death will follow, caused by lack of oxygen in the brain's tissue. At low current intensities, only a portion of the heart's muscle fibre may be affected, and this may change the electrical propagation patterns in the nerves leading to the heart, desynchronizing the activity of the heart and usually resulting in fibrillation.

In the case of the lungs, respiratory paralysis can occur if the muscles of the thorax are tetanized by an electric current flowing through the chest or through the respiratory control centre of the brain.

Cardiac pulmonary resuscitation techniques, consisting of artificial respiration and cardiac resuscitation, are specifically designed for the diagnosis and treatment of respiratory failure and cardiac arrest.

7.10.2 Effect of electrical shock on the body

Medical experts advise that the *killing factor due to electrical shock is the current density in the upper right-hand section of the heart*, which is called the sinoatrial node. Table 7.4 shows some general rules for how current levels at 50 Hz (or 60 Hz) affects a human being who is in limb-contact through intact skin with a voltage source [11].

Table 7.4. Reaction of human organisms to alternating current.

1 — 5 mA	Level of perception
10 mA	Level of pain
25 — 30 mA	Cannot-let-go level
50 mA	Respiratory paralysis
80 mA	Ventricular fibrillation
100 mA	Severe muscular contraction
100 — 300 mA	Electrocution (sustained contraction, burns)

In medical situations, when parts of the body are directly connected, the lethal level of current is in the range between 20 μA and 150 μA, because the current is applied directly in the body where the tissue resistance is in the region of 50 Ω, compared to the normal human skin resistance of 10 to 20 kΩ. Medical instruments must therefore have a high degree of isolation between the patient and nearby a.c. power lines This may be provided by *isolation transformers* which are designed to limit to less than 10 μA the normal leakage current between the a.c. power line carrying the current into the instrument and the instrument chassis. The advantage of using an isolation transformer is illustrated in Fig. 7.23.

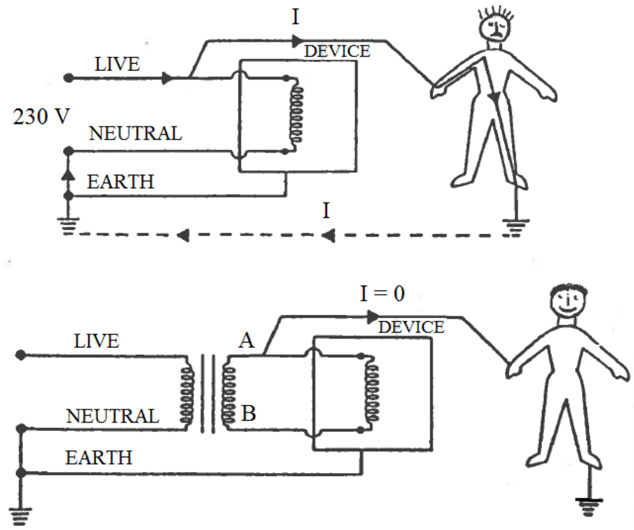

Fig. 7.23. The advantage of using an isolation transformer.

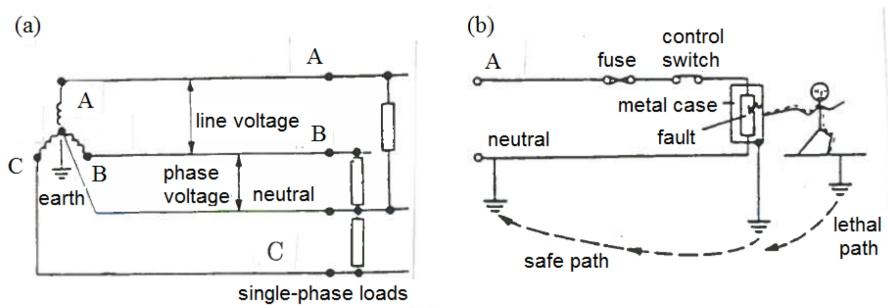

Fig. 7.24. Connection of the star points to the neutral wire and earth: (a) secondary winding of a distribution transformer, (b) earthed neutral wire of a single-phase electric installation.

7.10.3 Earthing the neutral conductor

Distribution transformer secondary windings and alternators are star-connected and their star points are connected to the neutral conductor and also earthed at the supply end, as shown in Fig. 7.24.

The *neutral wire* will only carry current when the load is unbalanced. Thus, if the load is balanced, no current will flow in the neutral wire and the line voltage drop will be a minimum. All metal casings of pieces of equipment are connected to a local earth point, and should one of the live conductors touch such an earthed metal casing, sufficient current would normally be conducted back to the earthed star point at the supply end to blow a fuse or to open an overcurrent trip switch. If a human being touches such a *live metal casing*, a relatively low current will flow through the high resistance of the body, since the greatest portion of the fault current would flow through the low resistance earth path. A high earth-loop resistance, comparable to the human body resistance, could be extremely dangerous, since a larger portion of the fault current would now flow through the body, which could suffer serious injury due to electric shock. If the metal casing is not earthed at all, the total earth fault current will flow through the body with possibly fatal consequences.

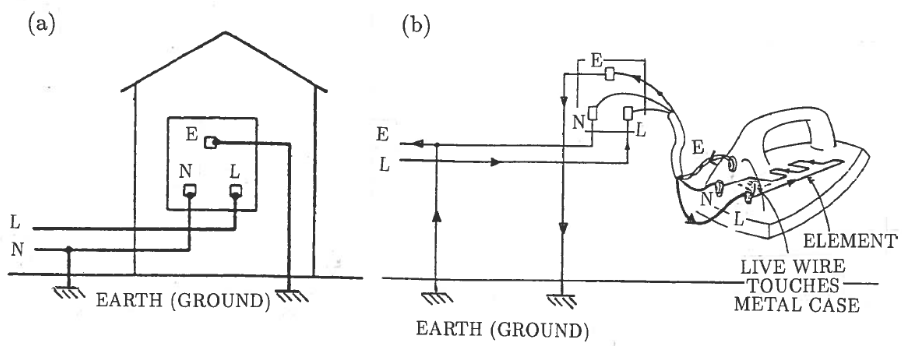

Fig. 7.25. Home electrical installation: (a) connections, (b) current flow due to a fault in an electric iron.

The neutral wire should only be earthed at one point at the supply side of an installation. Failure to adhere to this precaution may prevent the *earth-leakage relay* from functioning properly. The earth connection may be improved by connecting the earth point to the cold water mains. When plastic tubing is installed, a separate earth wire should be drawn through it, together with the live and neutral conductors. This earth wire should be connected to the earth pin of each three-point socket outlet. The live and neutral conductors should be connected to their respective pins, as indicated on the sockets. Care must be taken that the live and neutral conductors of portable equipment are also correctly connected to their respective pins on the plug tops, to prevent swapping of the live and neutral conductors, thereby creating a hazardous situation. All of the above points are illustrated in Fig. 7.25.

7.10.4 Earth-leakage circuit breakers

The action of the fuse protection method relies on a relatively high fault current to clear the line by blowing the fuse. A much better approach is to provide additional protection by including an *earth-leakage relay* in the protection system. The operation of such a relay is based on the fact that current flowing along the live wire of a single-phase system is equal to the current in the neutral wire, unless the circuit has an earth fault. In a healthy three-phase system, the sum of the three line currents is zero, but the system will become unbalanced during an earth fault. Two basic types of earth leakage relays are used: the current-balance type (see Fig. 7.26a) and the voltage-operated type (Fig. 7.26b).

The *current-balance earth leakage relay* (Fig. 7.26a) features live and neutral wires that are passed once or twice around a soft iron core in opposite directions,

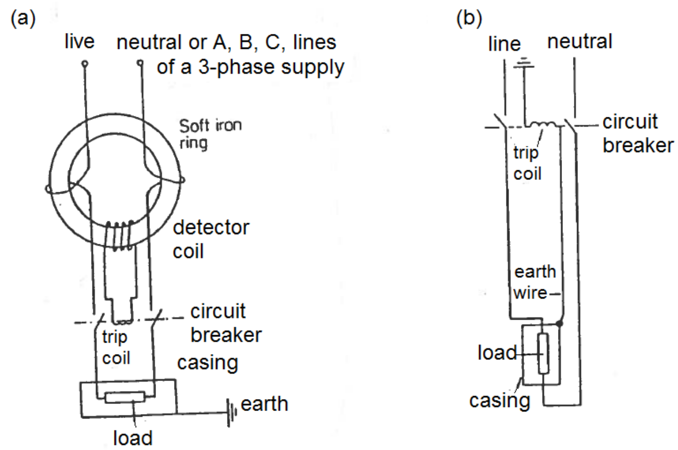

Fig. 7.26. Typical earth leakage relays: (a) current-balance type, (b) voltage-operated type.

so that their respective MMFs will normally cancel each other, and no EMF will be induced in the detector coil. At the occurrence of an earth fault, the live and neutral currents will no longer be equal and the ring will be magnetised. In this case, a voltage is induced in the detector coil, which causes a current to pass through the trip coil, which in turn causes the circuit-breaker to open. This form of relay will obviously work equally well for a three-phase supply. An out-of-balance current of 20 mA will usually be sufficient to trip the circuit breaker.

The *voltage-operated earth leakage relay* (Fig. 7.26b) relies for its action on the potential difference that will occur between the casing and the earth when an earth fault develops, causing a current to flow along the earth wire through the trip coil, and resulting in the opening of the circuit breaker. A potential difference of less than 40 V between case and earth will usually be sufficient to open the circuit breaker.

7.10.5 Installation tests

Before an installation may be connected to the supply authority's mains, the following tests should be performed:

- test of the insulation resistance between live and neutral conductors;
- test of the insulation resistance between live and earth conductors;
- test for the continuity of the earth conductor;
- test for the continuity of the neutral conductor (it must not be swapped with the live conductor);
- test of the polarity of single-switches (only the live conductor is to be switched).

Problems

1. A water tank of a cylindrical shape has its diameter $D = 0.515$ m and height $L = 1.2$ m. It is filled to 90% capacity four times daily. The water is heated from $+12^0$C to $+70^0$C. The losses of tank surface are $\Delta p = 5$ W/(^{0}Cm^2). Find the loading and the efficiency of the tank if the specific heat of water is $c = 4190$ J/(^{0}C kg) and 1 kWh = $3.6{\times}10^6$J.

   Answer: 3.215 kW, 78.73%.
2. Electric kettle draws $I = 3.6$ A of current when connected to a $V = 220$ V supply. A mass of 2 l of water is brought to boiling point with an initial temperature of 15^{0}C. The efficiency of the kettle is $\eta = 75\%$. Find the time taken for the specified mass of water to be raised to boiling point and the cost of energy consumed. The charge is $ 0.2 per 1 kWh.

   Answer: $t = 19$ min and 56 s, cost of energy is $0.0526.
3. An electric hot plate consists of two resistance elements each of 60 Ω. Calculate the power and current drawn from 220 V a.c. mains when the elements are connected in (a) parallel, (b) series.

   Answer: (a) 1613.3 W, 7.33 A; (b) 403.3 W, 1.83 A.
4. An office room measures $8.0 \times 5.5 \times 3.8$ m^3. The temperature of the room is to be kept at $+23^0$C when the outside temperature is -5^0C. The ventilation is such that the air has to be removed every 30 min. The heat loss from the walls is $\Delta h = 780 \times 10^3$ J/(^{0}C $\times$ h). The specific heat of the air is $c = 1220$ J/(^{0}C m^3). Find the necessary rating of the electric heater.

   Answer: 9239.7 W $\approx$ 9.2 kW.
5. Volume of the air to be conditioned is 200 m^3/h from an initial temperature of 5^{0}C to 24^{0}C. In addition, it is necessary to evaporate 0.8 kg of moisture per 100 m^3/h of the air to control humidity. The specific heat of the air is $c = 1220$ J/(^{0}C m^3), the heat of vaporisation for water is 2260 J/kg and the cost of electrical energy is $0.08 per 1 kWh. Find the necessary rating of the electric heater and the cost of electricity consumed per month. The heater operates 8 h per day and 1 month $\approx$ 30 days,

   Answer: 2292.2 W $\approx$ 2.3 kW, $49.68.
6. A 220 V, 0.91 A incandescent lamp emits the luminous flux $\Phi = 3600$ lm. Calculate the efficiency in cd/W and lm/W (efficacy).

   Answer: 1.431 cd/W, 17.98 lm/W.
7. An incandescent lamp hangs from the ceiling of a room. The illumination below the lamp vertically downwards is $E_1 = 100$ lx and at a distance of $b = 2.4$ m is $E_2 = 50$ lx. Find the vertical distance r from the floor and the luminous intensity I of the lamp.

   Answer: $r = 3.1315$ m, $I = 980.64$ cd.
8. The filament of a 40 cd, 110 V incandescent lamp has a length l_1 and diameter d_1. Calculate the diameter d_2 and length l_2 of the filament of a 20 cd, 220 V

lamp operated at the same temperature. The current drawn $I = ad^{1.5}$ where d is the filament diameter and $a = const$.

Answer: $d_2 = 0.3968 d_1$, $l_2 = 1.2596 l_1$.

9. The following measurements have been taken on a d.c. system to determine the insulation resistance of each cable to earth: (i) voltage between earth and the positive line $V_P = 30$ V and (ii) voltage between earth and the negative line $V_N = 90$ V. The internal resitance of the voltmeter is $R_V = 200$ kΩ and the voltage between lines is 220 V. Calculate the insulation resistance R_P and R_N of each cable.

   Answer: $R_P = 222.2$ kΩ, $R_P = 666.7$ kΩ.

Appendix A

Left-hand rule and right-hand rule

According to Ampére's experimental results, the force of translation on a conductor current element $I\mathbf{dl}$ immersed in a magnetic field $\mathbf{B}$ is

$$\mathbf{dF} = I\mathbf{dl} \times \mathbf{B} \tag{A.1}$$

This equation is commonly used in a scalar form and known as Fleming's left-hand rule, i.e.

$$F = BIl \tag{A.2}$$

The direction of the electrodynamic force F can be determined by the so-called *left-hand rule*, i.e. *if the left hand is arranged in the magnetic field so that the lines of magnetic flux are normal to the palm and the four fingers point in the direction of the current, the thumb will indicate the direction of the electrodynamic force* (Fig. A1a).

The EMF produced by motion of a conductor is

$$dE = \mathbf{v} \times \mathbf{B} \cdot \mathbf{dl} \tag{A.3}$$

where $\mathbf{v}$ is the linear velocity of the conductor, $\mathbf{B}$ is the magnetic flux density and $\mathbf{dl}$ is the length of conductor. In a scalar form

$$E = Blv \tag{A.4}$$

The direction of the induced EMF can be determined by the so-called *right-hand rule*, i.e. *if the right hand is arranged in the magnetic field so that the lines of magnetic flux are normal to the palm and the thumb points in the direction of conductor motion the remaining fingers will indicate the direction of the EMF induced in the conductor* (Fig. A1b).

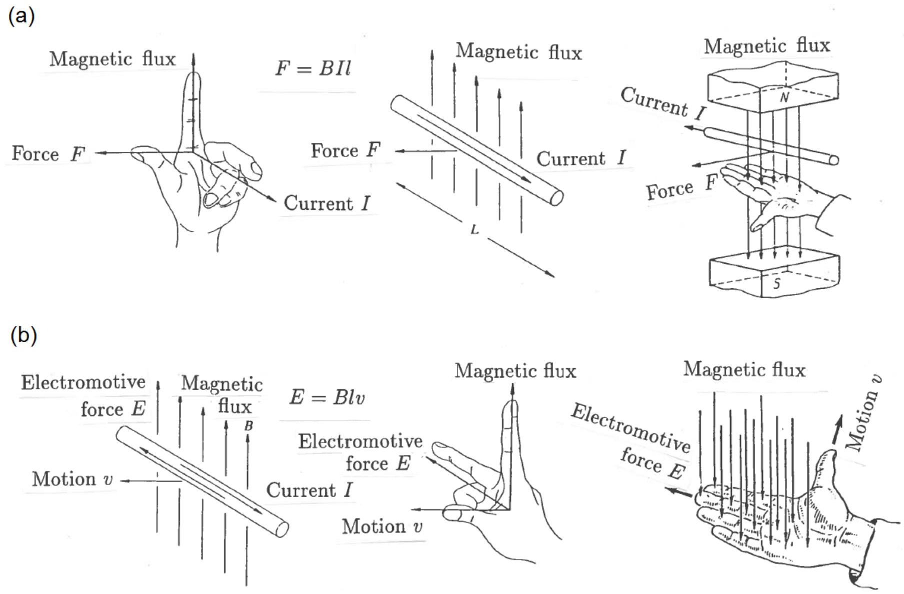

Fig. A.1. Explanation of the (a) left-hand rule and (b) right-hand rule.

Appendix B

Three-phase windings

A simple three-phase armature (stator) winding of an a.c. machine is shown in Fig. B1. There are four poles ($2p = 4$), twelve slots ($s_1 = 12$) and the winding consists of full-pitch coils, i.e. the coil pitch w_c is equal to the pole pitch τ. The winding can be designed as a single-layer winding (one coil in each slots, as shown in Fig. B1a) or double layer winding (two different coils in each slot, as shown in Fig. B1b). The number of slots per pole per phase is $q_1 = s_1/(2pm_1) = 12/(4 \times 3) = 1$.

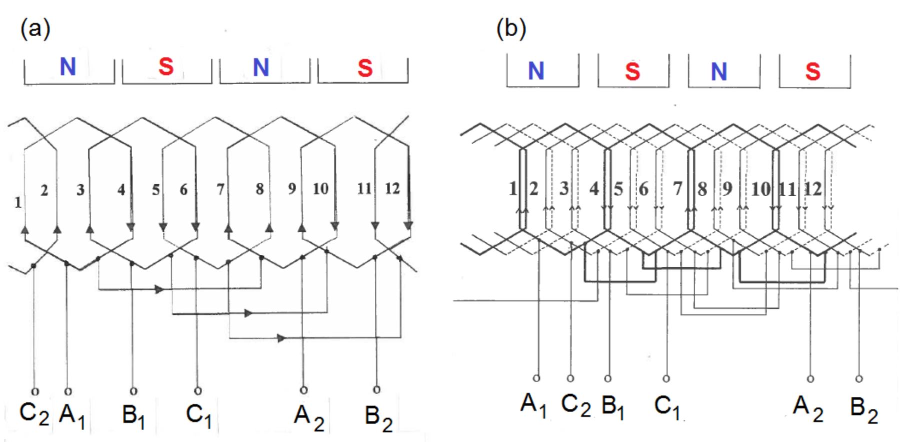

Fig. B.1. Layout of a three-phase winding with $2p = 4$, $s_1 = 12$ and $q_1 = 1$: (a) single-layer winding, (b) double-layer winding.

Appendix C

Rotating magnetic field

How can a rotating field be produced by stationary coils ? This concept is fundamental to the operation of induction (asynchronous) and synchronous motors. It can be explained in terms of the MMF contributed by the three balanced currents in Fig. C.1a. The instantaneous values of the currents are shown in Fig. C.1b and can be described by the following equations:

$$i_A = I_m \cos \omega_s t = \sqrt{2} I \cos \omega_s t$$

$$i_B = I_m \cos(\omega_s t - 120^0) = \sqrt{2} I \cos(\omega_s t - 120^0) \tag{C.1}$$

$$i_C = I_m \cos(\omega_s t + 120^0) = \sqrt{2} I \cos(\omega_s t + 120^0)$$

where I_m is the peak phase current, I is the rms phase current and $\omega_s = 2\pi f$ is the angular frequency. For simplicity, let us assume three windings (coils) with concentrated parameters. Positive currents in the concentrated windings produce MMFs in the directions indicated in Fig. C.1c, i.e.

$$F_A = N i_A \cos\theta$$

$$F_B = N i_B \cos(\theta - 120^0) \tag{C.2}$$

$$F_C = N i_C \cos(\theta + 120^0)$$

where N is the number of turns of a concentrated coil per phase and θ is the space angle. At the instant $\omega_s t = 0^0$, say, i_A is a positive maximum and i_B and i_C are negative and one-half maximum, i.e.

$$i_A = \sqrt{2} I, \qquad i_B = \sqrt{2} I(-0.5) = -\frac{1}{\sqrt{2}} I,$$

$$i_C = \sqrt{2} I(-0.5) = -\frac{1}{\sqrt{2}} I$$

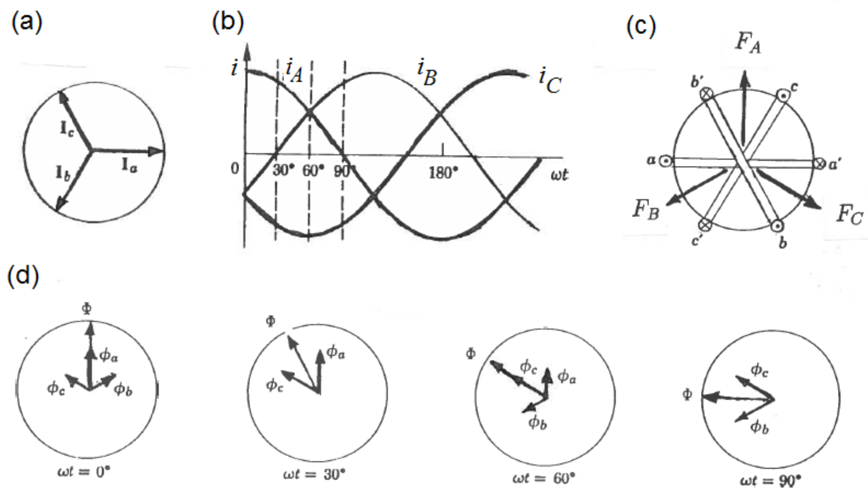

Fig. C.1. Production of the stator rotating magnetic field.

Note that $\sin 30^0 = \cos 60^0 = 0.5$, $\sin 45^0 = \cos 45^0 = \sqrt{2}/2$ and $\sin 60^0 = \cos 30^0 = \sqrt{3}/2$. Assuming a linear magnetic circuit, the principle of superposition applies, and the flux contribution of the three currents are as shown in Fig. C.1d. The stator flux Φ is the vector sum of the three contributions. At $\omega_s t = 30^0$, the relative magnitudes of the three currents have been changed, i.e.

$$i_A = \sqrt{2}I(\frac{\sqrt{3}}{2}) = \sqrt{\frac{3}{2}}I, \qquad i_B = \sqrt{2}I\cos(-90^0) = 0,$$

$$i_C = \sqrt{2}I(-\frac{\sqrt{3}}{2}) = -\sqrt{\frac{3}{2}}I$$

and the position of the resulting stator flux has shifted 30^0. At $\omega_s t = 60^0$ the current magnitudes have changed and the resultant flux vector has shifted another 30^0, i.e.

$$i_A = \sqrt{2}I(\frac{1}{2}) = \frac{1}{\sqrt{2}}I,$$

$$i_B = \sqrt{2}I\cos(-60^0) = \frac{1}{\sqrt{2}}I,$$

$$i_C = \sqrt{2}I\cos(180^0) = -\sqrt{2}I$$

A rotating magnetic field is produced because the position of maximum flux rotates at synchronous speed $\omega_s = 2\pi f$ if the number of pole pairs $p = 1$.

Combining together eqns (C.1) and (C.2) and using the following trigonometric identity

$$\cos A \cos B = \frac{1}{2}\cos(A - B) + \frac{1}{2}\cos(A + B) \tag{C.3}$$

one obtains

$$F(\theta, t) = F_A + F_B + F_C = Ni_A cos\theta + Ni_B \cos(\theta - 120^0) + Ni_C \cos(\theta + 120^0)$$

$$= \frac{\sqrt{2}}{2} NI \cos(\omega_s t - \theta) + \frac{\sqrt{2}}{2} NI \cos(\omega_s t + \theta)$$

$$+ \frac{\sqrt{2}}{2} NI \cos(\omega_s t - \theta) + \frac{\sqrt{2}}{2} NI \cos(\omega_s t + \theta - 240^0)$$

$$+ \frac{\sqrt{2}}{2} NI \cos(\omega_s t - \theta) + \frac{\sqrt{2}}{2} NI \cos(\omega_s t + \theta + 240^0)$$

$$= \frac{3\sqrt{2}}{2} NI \cos(\omega_s t - \theta) = \frac{3}{2} NI_m \cos(\omega_s t - \theta) \tag{C.4}$$

The linear speed of the rotating magnetic field called also the *synchronous speed* is

$$v_s = \omega_s \frac{D}{2} = 2\pi f \tau \tag{C.5}$$

where the distance τ, corresponding to 180^0 electrical degrees, is called the *pole pitch*, and D is the inner diameter of the stator core. For the number of pole pairs $p \geq 1$, the pole pitch is

$$\tau = \frac{\pi D}{2p} \tag{C.6}$$

and the angular synchronous speed is

$$\Omega_s = 2\pi \frac{f}{p} = \frac{\omega_s}{p} \tag{C.7}$$

The rotational synchronous speed in rev/s is

$$n_s = \frac{v_s}{\pi D} = \frac{f}{p} \tag{C.8}$$

Appendix D

Winding factor

The *winding factor* is a product of the distribution factor, k_d, and *pitch factor,* k_p, i.e.

$$k_w = k_d k_p \tag{D.1}$$

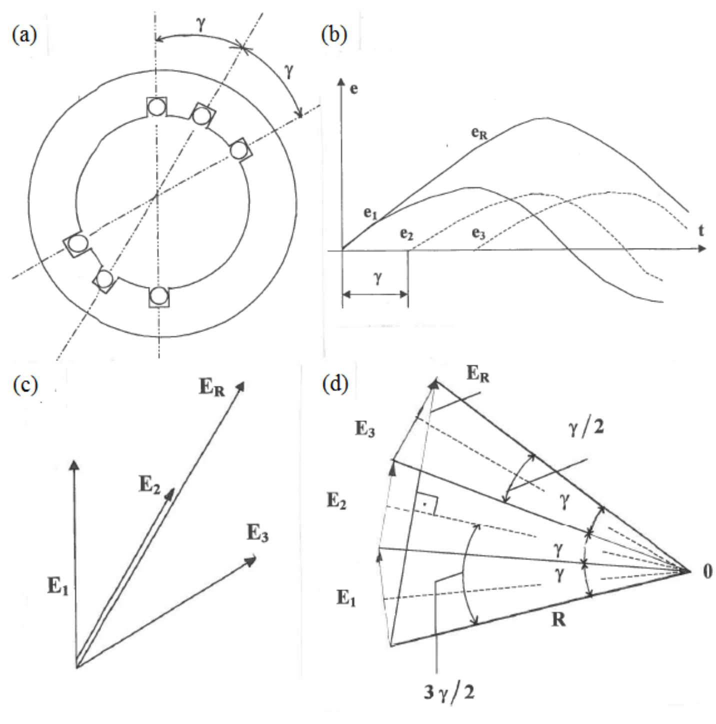

Fig. D.1. Three-coil armature winding of an a.c. machine: (a) arrangements of coils, (b) EMF waveforms, (c) phasor diagram, (d) polygon of EMFs.

D.1 Distribution factor

The ratio *phasor sum—to—arithmetic sum* of EMFs induced in each coil is termed *winding distribution factor*, i.e.

$$k_d = \frac{phasor\ sum\ of\ EMFs}{arithmetic\ sum\ of\ EMFs} \leq 1 \tag{D.2}$$

Let us assume an armature (stator) winding of an a.c. machine consisting of three coils, as shown in Fig. D1. The angle between neighbouring slots, in electrical degrees, is

$$\gamma = \frac{2\pi}{s_1}p \tag{D.3}$$

where s_1 is the number of slots and p is the number of pole pairs. The phase shift between EMFs e_1, e_2 and e_3 induced in each coil is γ, as shown in Fig. D1b. The phasor diagram of EMFs E_1, E_2, E_3 per coil and phasor sum E_R of all EMFs is plotted in Fig. D1c and can be replaced by an equivalent polygon, as in Fig. D1d.

Perpendiculars from the midpoints of E_1, E_2 and E_3 meet at 0 and the radius R is circumscribing a circle. Thus

$$k_d = \frac{E_R}{E_1 + E_2 + E_3} = \frac{2R\sin(3\gamma/2)}{6R\sin(\gamma/2)} = \frac{\sin(3\gamma/2}{3\sin(\gamma/2)} \tag{D.4}$$

In general, the armature has many more than three coils. The total number of coils in one coil group is q_1. Putting

$$q_1 = \frac{s_1}{2pm_1} \tag{D.5}$$

where m_1 is the number of phases and γ according to eqn (D.3), the distribution factor is

$$k_d = \frac{\sin(\pi/(2m_1)}{q_1\sin(\pi/(2m_1q_1)} \tag{D.6}$$

D.2 Pitch factor

To reduce higher space harmonics, armature coils are usually designed as *chorded coils* with coil span $w_c < \tau$ (see Fig. D2). The coil span of a full-pitch coil is τ.

The ratio *phasor sum—to—arithmetic sum* of EMFs per coil side is termed *winding pitch factor*, i.e.

$$k_p = \frac{phasor\ sum\ of\ EMFs\ per\ coil\ side}{arithmetic\ sum\ of\ EMFs\ per\ coil\ side} \tag{D.7}$$

The pitch factor according to Fig. D2c is

$$k_p = \frac{E_c}{E} = \frac{2E\sin(\beta/2)}{2E} = \sin\frac{\beta}{2} \tag{D.8}$$

where E_c is the EMF per coil, E is the EMF per coil side and β is the coil span measured in radians or electrical degrees. The following relationship exists between the coil span β in radians and coil span w_c in meters:

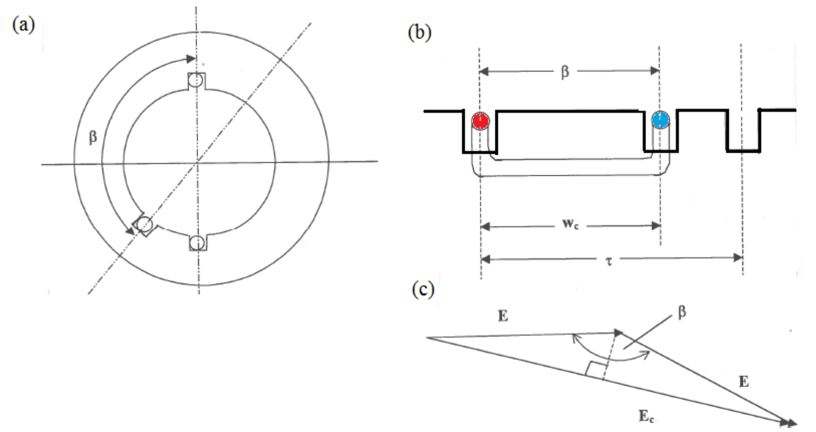

Fig. D.2. A chorded coil: (a) arrangement of coil sides in aramature slots, (b) coil span and pole pitch, (d) phasor diagram.

$$\beta = \pi \frac{w_c}{\tau} \tag{D.9}$$

Thus

$$k_p = \sin\left(\frac{w_c}{\tau}\frac{\pi}{2}\right) \tag{D.10}$$

References

1. **AEG Manual**, 8th Edition, Allgemeine Elektricitäts–Gesellschaft, Berlin, 1966.
2. Arenillas, J.: *Spain's fastest trains to roll in 1992*, **Railway Gazette Int.**, 1990, No. 2, pp. 129–131.
3. Baudot, J.H.: **Les machines électriques and automatique appliquée**, Dunod, Paris, 1967.
4. Behmann, U.: *New Madrid-Seville high speed line for RENFE*, **Elektrishe Bahnen**, 1990, No. 5, pp. 205–214.
5. Boglietti, A., Pastorelli, and Profumo, F.: *High speed brushless motors for spindle drives*, **Int. Conf. on ... Synchronous Machines SM100**, **3**, Zürich, Switzerland, 1991, pp. 817–822.
6. Bose, B.K.: **Power electronics and a.c. drives**, Prentice–Hall, Englewood Cliffs, N.J., 1986.
7. Braun E.: *Powering the new high-speed rail link between Madrid and Seville*, **Elektrishe Bahnen**, 1990. No. 12, pp.3–15.
8. Campbel, P.: *Principles of a permanent-magnet axial field machines*, **Proc. IEE**, **121**, 1974, No. 12, pp. 1489–1494.
9. Casini, C., Cheli, R., and Piro, G.: *ETR 500 and ETR 450/460 high-speed trains of Italian State Railways — main feature and test results*, **Int. Conf. STECH'93**, **1**, Yokohama, 1993, pp. 295–300.
10. Chatenever R.: **Air conditioning and refrigeration for the professional**, Prentice Hall, Englewood Cliffs, 1988.
11. Coetzee, R.J.: *Short lecture on safety for electrical engineering students*, **Southern African Electrical Network**, Newsletter of the Society of EEE Educators, **5**, 1994, No. 2, pp. 6–9.
12. **Class 401 Power cars of the ICE for the Deutsche Bundesbahn**, AEG, ABB, and Siemens, Information pamphlet, 1989.
13. Dote, Y., and Kinoshita, S.: **Brushless servomotors — fundamentals and applications**, Clarendon Press, Oxford, 1990.
14. Dubey, G.K.: **Fundamentals of electrical drives**, Narosa Publishing House, New Delhi, 1995.
15. **Efficient electricity use**, edited by C.B. Smith, Pergamon Press Inc., 1978.
16. Gieras, J.F.: **Linear induction motors**, Clarendon Press, Oxford, 1994.
17. Gieras, J.F. and Wing, M.: **Permanent Magnet Motors Technology: Design and Applications**, Marcel Dekker Inc., New York, 1996.

18. Gieras, J.F., Sone, S., Mizuma T. and Takagi, R.: *Linear Motor Driven Railcars: Subway Lines No. 12 in Tokyo and No. 7 in Osaka*, **Int. Conf. on Modern Electr. Traction MET'97**, Warsaw, 1997.
19. Grumbrecht, P., and Shehata, M.A.: *Comparative study on different high power variable speed drives with permanent magnet synchronous motors*, **Electrical Drives Syposium EDS'90**, Capri (Italy), 1990, 151–156.
20. Gupta, J.B.: **Utilization of electric power & electric traction**, S.K. Kataria & Sons, New Delhi, 1995.
21. Hannah, J. and Stephens R.C. **Mechanics of Machines**, E. Arnold Publishers, London, 1970.
22. Harris, M.R., and Miller, T.J.E.: *Comparison of design and performance parameters in switched reluctance and induction motors*, **4th Int. Conf. on Elec. Machines and Drives**, London, 1989, pp.303–307.
23. Haydock, D. and Fox, P.: *Eurostar — Europe's finest train goes into regular service*, **Today's Railways**, 1994/95, No. 4, pp. 4–7.
24. Heinisch, R.: *High-speed rail transport in Germany — status quo and future developments*, **Int. Conf. Conf. STECH'93**, **1**, Yokohama, 1993, pp. 48–52.
25. Henneberger, G., Schustek, S., and Wirtz, R.: *Inverter-fed three-phase drive for hybrid vehicle applications*, **Int. Conf. on Electr. Machines ICEM'88**, Pisa, Italy, **2**, pp. 293–298.
26. Hoffman, S., Banerjee, B. and Samotyj, M.: *Written–pole revolution*, **IEEE Power Eng. Review**, 1997, No. 12, pp. 6–9.
27. Honsinger, V.B.: *Performance of polyphase permanent magnet machines*, **IEEE Trans. on Power Apparatus and Systems**, vol. PAS–99, 1980, No 4, 1510–16.
28. **Japanese railway engineering**, Special Issue, 1994, No. 131.
29. Jones, B.L., and Brown, J.E.: *Electrical variable-speed drives*, **IEE Proc.**, **131**, Pt A, No. 7, pp. 516–558.
30. Kenjo, T., and Nagamori, S.: **Permanent–magnet and brushless d.c. motors**, Clarendon Press, Oxford, 1985.
31. Kenjo, T.: **Power electronics for microprocessor era**, Oxford University Press, 1990.
32. Kenjo, T.: **Electric motors and their controls**, Oxford University Press, 1991.
33. Kenjo, T.: **Stepping motors and their microprocessor controls**, Oxford University Press, 1985.
34. Kostenko, M., Piotrovsky, L.: **Electrical machines**, **2. A.c. machines**, Mir Publishers, Moscow, 1974.
35. Lawrenson, P.J.: *Switched reluctance motor: a perspective*, **Int. Conf. on Elec. Machines ICEM'92**, Manchester, 1992, **1**, pp. 12–21.
36. Leander, P.: *The Swedish X2000 high-speed train — development, acquisition, and operation experiences* **Int. Conf. Conf. STECH'93**, **1**, Yokohama, 1993, pp. 281–284.
37. Lindwall B.: *X2000 fast train*, **ABB Review**, 1992, No.1, pp. 3–8.
38. Masada, E.: *Electrical drives for traction purposes*, **Electrical Drives Symposium**, Appendix, Capri (Italy), 1990, pp. A1–A8.
39. McNaught, C.: *Running smoothly — making motors more efficient*, **IEE Review**, March 1993, pp. 89–91
40. Michalik, G.: **Energy consumption in the residential sector by introducing minimum energy performance standard**, Reserch Report No. 1994-R-1, Centre for Electrical Power Engineering, Monash University, Australia, 1994.

41. Miller, T.J.E.: **Brushless permanent-magnet and reluctance motor drives**, Clarendon Press, Oxford, 1989.
42. Mohan, N., Undeland, T.M., and Robbins, W.P.: **Power electronics: converters, applications, and design**, John Wiley & Sons, 1989.
43. Morash, R.T., Barber, R.J., and Roesel, J.F.: *Written pole motor — a new a.c. motor technology*, **Int. Conf. on Electr. Machines in Australia ICEMA'93**, Adelaide, Australia, 1993, vol. 2, 379–84.
44. Nasar, S.A.: **Electric machines and power systems**, McGraw-Hill, Inc., New York, 1995.
45. Nasar, S.A., Boldea, I., and Unnewehr, L.E.: **Permanent magnet, reluctance, and self-synchronous motors**. CRC Press, Boca Raton–Ann Arbor–London–Tokyo, 1993.
46. O'Connor, L.: *French TGV making tracks in Spain*, **Mechanical Eng.**, 1992, No. 11, pp. 52–55.
47. O'Connor, L.: *Tunnelling under the channel*, **Mechanical Eng.**, 1993, No. 12, pp. 60–66.
48. Oikawa, Y. and Morokawa, H.: **Shinkansen**, Hoikusha Publishing Co., Ltd, Osaka, 1996.
49. Sen, P.C.: **Principles of electric machines and power electronics**, John Wiley & Sons, NY–Chichester– Brisbane–Toronto–Singapore, 1989.
50. Say, M.G.: **Alternating current machines**, Pitman, 1976.
51. Schmidt D.: *Germany's Intercity Express with ABB three-phase propulsion*, **ABB Review**, 1991, No. 10, pp. 3–10.
52. Shoyama, Y.: *Prototype LIM driven railcar for subways of smaller cross section tunnels*, **Japanese Railway Eng.**, **24**, 1884, pp. 11–15.
53. Szentirmai, L.: *Energy and environment: vision and perspectives of electrical drives*, **Int. Aegean Conf. on Elec. Machines and Power Electronics ACEMP'95**, Kuşadasi, Turkey, 1995, pp. 1–15.
54. **The European variable-speed drive market**, *Frost & Sullivan Market Intelligence*, 1993.
55. Van Wyk, J.D., Skudelny H.Ch., and Müller-Hellmann, A.: *Power electronics, control of the electromechanical energy conversion process and some applications*,**IEE Proceedings Part B**, 133, 1986, No. 6, 369–421.
56. Wadhwa, C.L.: **Generation, distribution and utilization of electrical energy**, John Wiley & Sons, 1989.
57. Wheatley, C.T.: *Drives*, **5th European Power Electronics Conf. EPE'93**, Brighton, UK, vol. 1, pp. 33–39
58. Williams, B.W.: **Power electronics**, MacMillan, 1992.
59. Yamamura, S.: **A.c. Motors for high-performance Applications**, Marcel Dekker Inc, New York and Basel, 1986
60. Yoshie, N., and Yagi, E.: *High-speed testing car WIN 350* **Int. Conf. STECH'93**, **1**, Yokohama, 1993, pp. 275–279.

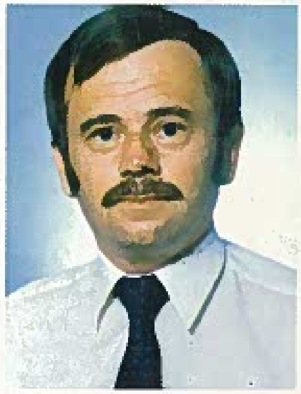

Prof. Jacek F. Gieras – graduated in 1971 from the Technical University of Łódź, Poland. He received his PhD degree in 1975 and DSc (Dr hab.) degree in 1980 from the University of Technology, Poznań, Poland. His research area is electrical machines, drives, electromagnetics and railway engineering.

From 1971 to 1987 he was with Poznań University of Technology, Poznań, and Academy of Technology and Agriculture, Bydgoszcz, Poland. In 1975/76 he was a Visiting Researcher at Czechoslovak Academy of Sciences, Prague, Czechoslovakia. From 1983 to 1985 he was a Research Visiting Professor at Queen's University, Kingston, Ontario, Canada. In 1987 he was promoted in Poland to the rank of Full Professor (life title) in Electrical Engineering. From 1987 to 1989 he was with the Department of Electrical Engineering at Jordan University of Science and Technology, Irbid, the Hashemite Kindgdom of Jordan. From 1989 to 1998 he was with the Department of Electrical Engineering at the University of Cape Town, South Africa. In 1994 he was a Visiting Professor at the University of Rome *La Sapienza*, Italy. In 1996 he was a Japan Railway Central Company Visiting Professor (Endowed Chair in Transportation System Engineering) at the University of Tokyo, Japan. In 1996/1997 he was a Guest Professor at Chungbuk National University, Cheongju, South Korea. He is now involved in high technology research in the United States.

Prof. Jacek F. Gieras authored and co-authored 6 books and about 200 papers and patents. The best known books are *Linear Induction Drives*, Oxford University Press, 1994, U.K. and *Permanent Magnet Motor Technology: Design and Applications*, Marcel Dekker Inc., New York, 1996 (co-author Dr M. Wing).

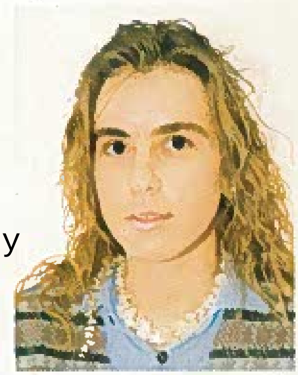

Miss Izabella A. Gieras – is Prof. Gieras' daughter. She received matriculation with exemption in 1993 at Rustenburg High School for Girls in Cape Town. Her interests lie in heavy as well as light current Electrical Engineering with focus on Signal Processing. She is a 4th year undergraduate student in the Department of Electrical Engineering at the University of Cape Town.

wydawnictwo adam marszałek

ISBN 83-7174-199-5